AN NMR INVESTIGATION OF METAL HYDRIDES

MOURAD BELHOUL, D.E.S.

A thesis submitted to the University of Warwick

for admission to the degree of Doctor of Philosophy

Department of Physics

October 1983

Cette these est dediee à tous ceux qui me sont chers

Cette these est dediee à tous ceux qui me sont chers

DECLARATION

This thesis is submitted to the University of Warwick in support of my application for admission to the Degree of Doctor of Philosophy. No part of this work which was carried out in the Department of Physics under the supervision of Dr. G. A. Styles, has appeared in any thesis at this or any other institution. The work reported in this thesis is the result of my own independent research except where specifically acknowledged.

Some parts of the research reported here have been published as follows:

1. Belhoul, M., W. A. Barton: B.R.S.G. Meeting, Nottingham (1981).
2. Belhoul, M., G. A. Styles, E. F. W. Seymour, T-T. Phua, R. G. Barnes, D. R. Torgeson, D. T. Peterson: J. Phys., F12, 2455 (1982).
3. Phua, T-T., R. G. Barnes, D. R. Torgeson, D. T. Peterson, M. Belhoul, G. A. Styles: in Electronic Structure and Properties of Hydrogen in Metals, ed. by P. Jena and C. B. Satterthwaite (Plenum Press, New York, 1983).
4. Phua, T-T., R. G. Barnes, D. R. Torgeson, D. T. Peterson, B. J. Beaudry, M. Belhoul, G. A. Styles, E. F. W. Seymour: in press Phys. Rev., B (1983).

It is anticipated that a full report of the investigation of the hydrogen dependence in the yttrium dihydride system will be published. The results of the study of the titanium-manganese hydride system and a more complete report of the palladium-yttrium hydride system will also be published.

M. Belhoul

Acknowledgements

I wish to express my sincere gratitude to my supervisor, Dr. G. A. Styles, who through his patient guidance, criticism, friendship has made this work possible and very rewarding.

I would like to thank Professor E. F. W. Seymour for the many fruitful discussions which have been most useful for the completion of this work.

Special thanks are due to all the members of the Nuclear Magnetic Resonance Group, Physics Department, University of Warwick for helpful discussions and companionship, and particularly Mr. T. B. Sheffield who has provided an excellent technical support during the course of this study.

The collaboration with Professor R. G. Barnes, Ames Laboratories, USA, who provided some of the samples, is particularly acknowledged.

I am most grateful to the Ministry of Higher Education, Algeria, for the financial support.

Finally I would like to thank Miss S. Callanan for her accurate and speedy typing of this thesis.

CONTENTS

ABSTRACT

Pulsed nuclear magnetic resonance has been used for the investigation of YH_x where x = 1.72, 1.81, 1.92 and 1.98, $YD_{1.88}$, $YH_{1.98}$ doped with 20, 50, 100, 200 and 915 ppm Gd, $TiH_{1.74}$ doped with 150, 500 and 10^4 ppm Mn and $[Pd_{0.92}Y_{0.08}]H_{0.51}$. The proton relaxation times T_1 and T_2 have been measured for most of the samples at the resonance frequencies 7 and 45 MHz and for the range of temperature 120 K to about 1300 K. Measurements of the diffusion coefficient have also been performed at 7 MHz for $YH_{1.98}$ and $[Pd_{0.92}Y_{0.08}]H_{0.51}$.

T_1 and T_2 data for YH_x show that the activation energy for hydrogen diffusion decreases by about a factor of two as the hydrogen concentration increases from x = 1.72 to x = 1.98. This is interpreted as due to the result of a large H-H repulsive interaction which increases with hydrogen concentration. The electronic contribution to T_1 clearly indicates that the d-density of states at the Fermi energy remains constant in the β-phase of yttrium hydride. The anomalous behaviour observed for both T_1 and T_2 at temperatures above 800 K is interpreted in terms of a highly correlated hydrogen motion at these temperatures. The behaviour of T_1 for $YD_{1.88}$ may be accounted for by some 20 ppm residual Gd impurity present in the sample.

T_1 data for $YH_{1.98}$ doped with Gd show that an additional relaxation time arises from dipolar coupling between the proton nuclear spin and the local magnetic moment of the impurity. This process shows an effect on the observed T_1 at concentrations of Gd as low as 2 ppm.

The spin-lattice relaxation data for $TiH_{1.74}$ doped with Mn reveal that the hydrogen diffusion is much faster in the vicinity of Mn than it is in the bulk and also shows that $[Ti_{1-y}Mn_y]H_x$ is a bottlenecked system.

The activation energy deduced from the direct diffusion coefficient measurements in $[Pd_{0.92}Y_{0.08}]H_{0.51}$ is consistent with a partially ordered sample. The much lower activation energy deduced from the T_1 minimum indicates that the main contribution to T_1 is due to paramagnetic impurity induced relaxation.

CHAPTER I: METAL HYDRIDES

1.1. Introduction

Since the historical discovery by Thomas Graham in 1866, of the ability of the metal palladium to absorb large amounts of hydrogen, forming non stoichiometric alloys, many transition metals and intermetallic compounds have been found readily to absorb hydrogen. In such systems, customarily called hydrides although this term should strictly be reserved for stoichiometric compounds, the hydrogen atoms occupy interstitial sites of the metal lattice and diffuse through the metal lattice with a characteristic self diffusion coefficient D . The large interest shown in these systems, which has been enhanced by the possible use of hydrogen as a synthetic fuel for the future and by the superconducting properties of palladium hydride (Skoskiewicz (1972)) and Thorium hydride (Satterthwaite and Toepke 1970), stems not only from the basic science involved, but is also motivated by their potential applications.

The unique properties of hydrogen in its reaction with neutrons (i.e. low thermal-neutron absorption cross-section and high scattering cross-section), in combination with the strength and stability of those metals such as yttrium and zirconium which are characterised by a low thermal-neutron absorption cross-section, make metal hydrides excellent contenders for use as moderators in high temperature fission nuclear reactors (Mueller et al 1968).

Owing to the large hydrogen permeability of some metal-hydrides, they find applications as purification membranes. For instance Pd and

$[Pd_{1-y}\ Ag_y]$ which offers better mechanical and permeability characteristics, are now being used as purification membranes in ultra-pure hydrogen systems. $[Pd_{1-y}\ Y_y]$ which allies the mechanical properties of $[Pd_{1-y}\ Ag_y]$ with better permeability characteristic is a potential improved hydrogen purification membrane [Hughes et al 1980]. Furthermore because of the isotope-dependent properties of metal hydrides, these compounds have potential applications both as commercial isotope separators (Wiswall and Reilly 1972) and in fusion reactors (Evans et al 1983) .

Among the large number of other possible applications of metal hydrides there is their potential use to store hydrogen as an important alternative to the bulky and somewhat unsafe high pressure gas cylinders. Intermetallic compounds such as $LaNi_5$ (Van Vucht et al (1970)) can store hydrogen (i.e. as $LaNi_5H_6$) at a greater density than that of liquid hydrogen and through the reversible absorption desorption process may be used as a means of supplying fuel which can be used for automotive propulsion (Meijer 1970) for example. The absorption of hydrogen by metals is generally an exothermic reaction and since the process is reversible, metal hydrides can be used to store energy, as cooling systems and as heat pumps (Alefeld 1975).

1.2. Properties of metal-hydrides

1.2.a. Metal hydride formation and phase diagram

Measurement of equilibrium hydrogen pressures as a function of hydrogen content and of temperature are most useful in determining the thermodynamic properties of a metal-hydrogen system. From the pressure-composition isotherms, shown in fig. 1.1 which illustrate the phase diagram of a hypothetical dihydride, it can be seen that

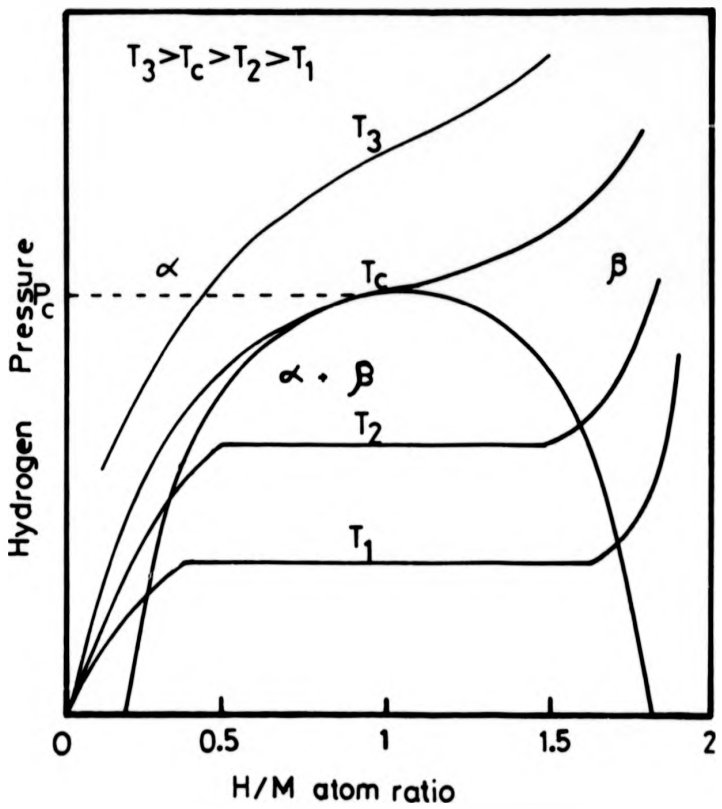

Fig. 1.1: Typical pressure-composition isotherms for a hypothetical dihydride.

the compounds formed are non-stoichiometric and, in this case, there are two phases. The α phase which is characterised by a strong dependence of pressure on composition, refers to the disordered phase in which hydrogens are randomly distributed in the metal lattice (i.e. solid solution). The β phase refers to a high density phase in which the probability of occupation of a site is not the same for all sites (non-random distribution). The constant-pressure plateaux correspond to the region where the two phases α and β coexist. Above a critical temperature T_c and pressure P_c a single solution is expected.

To a good approximation in the α phase the pressure-composition isotherms are expressed by Sieverts' law (Speiser 1968) which states that the solubility of hydrogen in a metal is proportional to the square root of the hydrogen pressure.

$$P_{H_2}^{\frac{1}{2}} = K \frac{c}{1-c} \qquad (1.1)$$

where K is Sieverts' constant and c is the fractional concentration of hydrogen atoms. The region of two condensed phases is important in determining the enthalpy of formation of the hydride which can be considered as a measure of its stability. In this region, with the condition $T << T_c$ the equilibrium pressure can be approximated by

$$\mathrm{Ln}P_{H_2} = - \frac{\Delta S^o}{R} + \frac{\Delta H^o}{RT} \qquad (1.2)$$

where ΔS^o and ΔH^o are the entropy and enthalpy of formation per mole of H_2, respectively. From the slope of $\mathrm{Ln}P_{H_2}$ versus the reciprocal temperature (Van't Hoff isochore) the enthalpy of formation of a given hydride can be calculated. The β phase is again characterised by Sieverts' law.

In the theoretical approach to an explanation of the phase diagrams most macroscopic models are of the lattice-gas type (see for instance, Manchester (1976)). In this model the particles are confined to sites but can jump freely from site to site. Only one particle is allowed per site. This type of model gives rise to equation (1.1) and does not predict phase-changes. Assuming nearest neighbour attractive interactions between hydrogen atoms Lacher (1937) was able to predict a phase transformation characterised by a transition temperature $T_c = \frac{W_{NN}}{4k}$ where W_{NN} is the energy of the attractive interaction and, as in the ideal solution saturation occurs for $c \to 1$. In order to account for the saturation concentration $c < 1$ of some systems for example $c = {}^1/6$ in NbH, Oates et al (1969) applied the so-called "blocking" model. This assumes that a hydrogen atom prevents a certain number of its nearest neighbour sites from being occupied. Assuming that the interaction is repulsive they were able to account for the saturation concentration $c = {}^1/6$ in NbH. However, these models do not exhibit phase transitions. Wagner (1971) pointed out that the distortion of the lattice when hydrided should influence the interactions between hydrogens (elastic interaction). Hall and Stell (1975) were able qualitatively to explain the appearance of α and ordered β phases assuming both long-range attractive and short-range repulsive interactions. The model was able to reproduce the phase diagrams for hydrogen in Nb, Pd, Ta and V and they concluded that the electronic repulsive interactions are responsible for the appearance of ordered β phases at high concentration and that the long-range attractive elastic interactions lead to the disordered α, α' transitions. Hall (1983) indicates that if alloying with another metal results in an expansion of the lattice (e.g. $[Nb_{1-y}V_y]$, $[Pd_{1-y}Ag_y]$, $[Pd_{1-y}Y_y]$) the

critical temperature T_c is reduced and the solubility of hydrogen is increased. This is in agreement with the experimental evidence (Pick and Welch (1979), Evans et al (1983)).

1.2.b. Electronic structure

Generally, hydrides are classified, according to the electronic affinity of the elements as covalent, ionic or metallic. The covalent hydrides, where the valence electrons are equally shared between the elements forming the bond do not exhibit large electric charge differences andconsequently in the absence of strong intermolecular electric forces are characterised by a high degree of volatility and low melting points. These hydrides are formed by elements to the right of the periodic table. The strongly electro-positive alkali metals (to the left of the periodic table) form ionic hydrides. The very strong electrostatic forces existing between the two ions result in high heats of formation and high melting points in the hydrides. They crystallise with the NaCl structure. The transition metal and rare earth hydrides are metallic in nature and exhibit the normal metallic properties (i.e. high thermal conductivity, high electrical conductivity, hardness ... etc). Whereas the two first classes of hydrides are well defined with regard to bonding, the metallic-hydrides have been the subject of some controversy.

The rigid band model (Mott and Jones 1936) was used to explain the decrease of the magnetic susceptibility of Pd to essentially zero at the concentration $PdH_{0.6}$ in analogy with PdAg. It is assumed that the shape and position of the band is not altered on alloying and that the hydrogen contributes one electron to the d band, the system becoming diamagnetic when the postulated 0.6 holes in the d-band are filled. The protonic model has been used very extensively

to explain the changes of magnetic susceptibility in V_2H (Zanowick and Wallace (1962), Childs et al (1960)) Ta_2H and Ta_4H_3 (Stalinski (1954)), Nb hydride (Trzebiatowski and Stalinski 1953) and TiH_2 (Trzebiatowski and Stalinski 1953) compared to the elemental metal. Schreiber and Cotts (1963) and Merriam and Schreiber (1963) made use of the protonic model to explain the loss of metallic character of lanthanum hydride as hydrogen is added until it reaches LaH_3 which is a semiconductor. The protonic model was assumed in order to account for the fact that since no proton Knight shift was observed, the hydrogen had to be a bare proton (i.e. no electron density around the proton). In their model they assumed a splitting of the d band, with the lower energy subband capable of accommodating a maximum of 4 electrons and the upper subband able to accommodate the remaining 6 electrons. For the concentration LaH_3 the lower subband is completely filled up and the splitting in the d band accounts for the semiconducting gap. Schreiber (1965) indicates that this model can be generalised to transition metals and explains why d^1, d^2 and d^3 transition metals can accommodate a maximum of 3, 2 and 1 hydrogens per metal atom (this is not exactly the case as discussed in section 1.2.d.).

Early studies of magnetic properties of rare-earth hydrides (Stalinski 1959) led to the anionic model in which H^- anions are formed as the result of electron capture from the conduction band and consequently the conduction band is depopulated as the concentration of hydrogen is increased. This results in the formation of saline hydride (i.e $R^{3+}(H^-)_3$) and can explain the large increase in resistivity in CeH_3 and LaH_3, but conflicts with the protonic model used by Schreiber. In general the magnetic properties of rare earths

favour the anionic model (see for instance Wallace (1978), (1982)) which is also supported by heat capacity measurement (Van Diepen et al (1971), Bieganski and Stalinski (1970)). However the failure of both the protonic and anionic models to explain how the hydrogen atom interacts electronically when introduced into a metal lattice, is clearly exemplified by the magnetic susceptibility results of Nagel and Goretzki (1975) on $Ti_{1-y}V_y H_2$ and the experimental result of Vuillemin and Priestly (1965) and the theoretical calculations of Mueller et al (1970) which show that palladium has only 0.36 holes in the d band.

Friedel (1953, 1972) first studied the behaviour of a proton in a simple metal, introducing the concept of screening whereby the electron density in the vicinity of an occupied site is higher than that around an unoccupied site. This shows clearly that the idea of a bare proton is impossible. However it was not until the early 1970's that the details of metal-hydrogen interactions were considered in the context of band structure (Switendick (1970), (1971)) and it was shown that the rigid band model is inadequate. Switendick (1971) in carrying out band calculations for yttrium metal, yttrium hydride, yttrium dihydride and yttrium trihydride, showed the importance of the hydrogen potential (M-H interaction) in determining and altering the electron properties.

In the mono-hydrides PdH_x and YH_x Switendick (1971, 1972, 1978) showed that the hydrogen potential strongly influences the lower states in the band structure and, more specifically, alters states which have substantial real-space charge distributions near the proton site resulting in mixing between the H 1s-states and the extended states which have the correct symmetry. Some empty states of the metal are lowered below E_F (M-H interactions) and are occupied.

To account for the excess of electrons added over the number of states lowered there is a shift of the Fermi level. These theoretical predictions are in good agreement with photoemission experiments (Eastman et al 1971) and optical spectroscopy studies (Frazier and Glosser 1982) .

In the dihydride there are two hydrogen atoms in the cell resulting in derived charge distributions around the hydrogens which can be written as the bonding and antibonding combinations of hydrogen 1s orbitals where the H-H separation ($\sim$ 2.5 Å) determines the energy separation of these states. Switendick (1971) showed that in metal-dihydrides with the CaF_2 structure, the extended metal states which are affected by the hydrogen potential can hybridize with the antibonding states (if they have the right symmetry) and are lowered in energy by several electron volts. The derived localized d-states are unchanged. Photoemission spectra for ScH_2, YH_2, LuH_2 (Weaver and Peterson 1980) and more recently for LaH_2, PrH_2 and NdH_2 (Weaver et al 1983) clearly show the formation of the bonding hybridized s-p-d states in a region ($\sim$ 5 eV below the Fermi energy) where nothing is observed in the elemental metals. Excellent agreement for the position and width of the different bands observed experimentally, has been obtained with the more recent and more sophisticated band calculations (Peterman et al (1979), Gupta (1978), Gupta (1979)).

In the trihydride the addition of an extra hydrogen to the unit cell results in the hybridisation of yet more metal and hydrogen states. This is due to the additional symmetries of the H-1s states which can mix with states above and near the Fermi energy and lower these states well below E_F. Photoemission spectra (Weaver et al 1983) show these features and indicate diminished emission from states near

E_F in $LaH_{2.89}$. This is expected from band calculations (Kulikov 1982) which indicate that the additional coupling of hydrogen states with metal states which are well above E_F in the LaH_2 results in a shift of E_F to accommodate the 6 electrons per unit cell which falls in a gap. This results in a narrow-gap semiconductor.

The band calculations are not only in good agreement with spectroscopic measurements but also explain unambiguously results obtained from NMR, resistivity, magnetic susceptibility and heat capacity measurements. This emphasizes the fact that the rigid band model is inadequate and that detailed calculations for each system are necessary. Fig. 1.2 indicates the trend in the density of states for the pure metal and hydrided metal, which is expected from the discussion given above.

1.2.c. Magnetic properties

From the temperature dependence of the magnetic susceptibility for the transition metal hydrides, it is clear that their paramagnetism does not have its origin in the formation of a local moment. These systems are all Pauli paramagnets. The magnetic susceptibility of all the transition metals except Ti and Cr decreases on hydrogenation. The magnetic susceptibility is the result of several contributions i.e. $\chi = \chi_{orb} + \chi_{dia} + \chi_L + \chi_p$ where χ_{orb} is the Van Vleck susceptibility, χ_{dia} is the core electron diamagnetic susceptibility, χ_L is the Landau diamagnetic susceptibility of the conduction electrons ($\chi_L \simeq -\chi_p/3$) and $\chi_p = 2\mu_B^2 N(E_F)\ (1+\lambda)$ is the Pauli susceptibility where $N(E_F)$ is the density of states at the Fermi level and λ is an enhancement factor resulting from the interactions of the conduction electrons. Although one cannot therefore

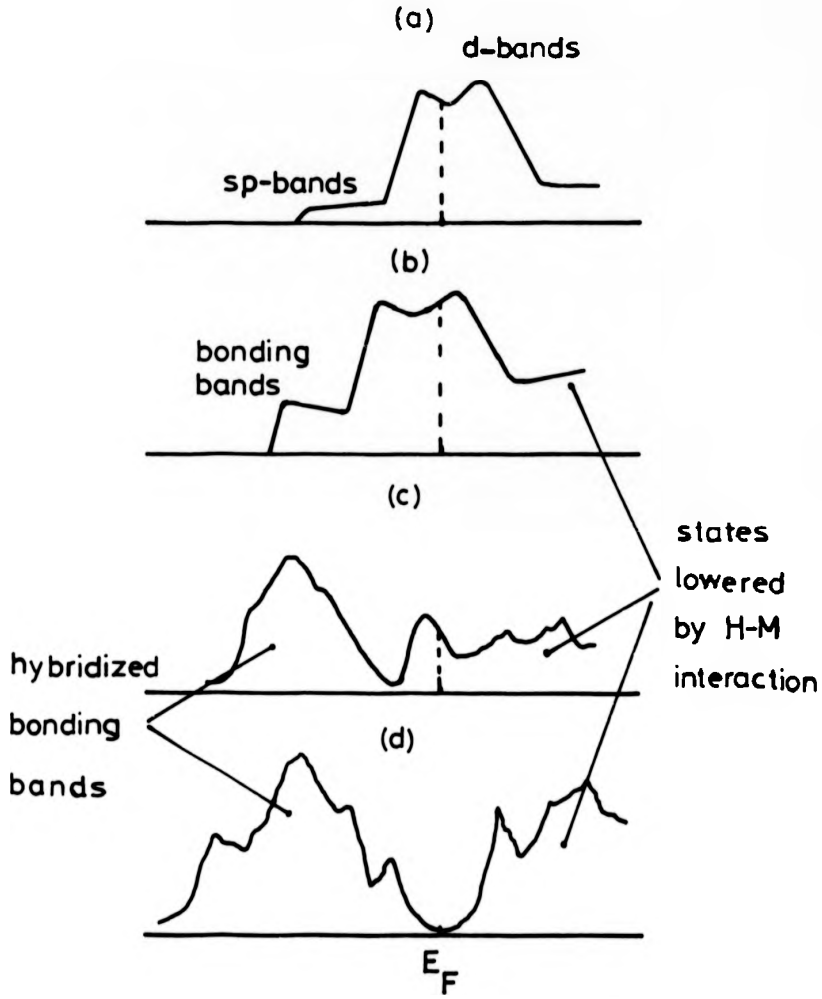

Fig. 1.2: Schematic diagram of the density of states of
(a) a d-band metal
(b) a monohydride
(c) a dihydride
(d) a trihydride

assume that $\chi = \chi_p$ the decrease in susceptibility may be nevertheless, understood in terms of a decline in the density of states. The increase in χ on hydrogenation shown by Ti and Cr is expected from band calculations (Gupta (1979), Switendick (1978)) which predict an increase in the density of states at the Fermi level for TiH_2 compared to the elemental metal.

The rare earths which are characterised by a 4f inner shell (except La) have been shown from magnetic susceptibility measurements (Stalinski 1959) to retain an unchanged paramagnetic moment on hydriding. This clearly indicates that the 4f band remains localised and therefore, in view of the discussion of the previous section, is not affected by the hydrogen potential and is not liable to participate in the formation of hybridized states with the 1s-hydrogen states. This is indeed observed from photoemission spectroscopy (Weaver et al 1983). Since the f electrons centered on adjacent rare earth atoms are too localised to appreciably overlap, direct exchange is negligible and the alignment of the moments is due to the indirect RKKY interaction through the conduction electrons. Thus as the metallic character of the rare earth-hydrides decreases (RH_3 are non-conducting) the ordering temperature is expected to decrease. This is indeed observed (see for example, review by Wallace (1978)) i.e. the fully hydrogenated rare earths do not form a cooperative magnetic phase at temperature down to 4 K.

The magnetic properties of rare earth intermetallic compounds are also changed by hydrogenation. However as opposed to the rare earth hydrides where a general trend is predicted the compounds produce a variety of behaviours. For instance $PrCo_2$ and $NdCo_2$ when contaminated with hydrogen become ferromagnetic at 45 and 116 K respectively (Deenadas et al 1972) while the degassed materials

fail to show a magnetic phase down to 4 K Titcomb et al (1972) . This is interpreted as due to the loss of magnetisation of cobalt on removal of hydrogen. In contrast in the RCo_5 compounds studied by Kuijpers (1972), the Co moments, the exchange interactions and Curie temperatures are all reduced by hydriding. The RFe_2 compounds (Gualtieri et al (1976), Buschow and Van Diepen (1976)) show a reduced Curie temperature when hydrided excepting $CeFe_2H_4$ where Ce is thought to have a different valence state to that in $CeFe_2$. Similarly the RFe_3 compounds show a weakening of exchange upon hydriding (Malik et al 1976), however they all seem to show a rise in Fe moment on hydriding. The results of the studies of hydrogenated Y_6M_{23} and Th_6Mn_{23} by Malik et al (1977) are somewhat surprising. Y_6Mn_{23} is a ferromagnet, with T_c = 500 K which when hydrided (i.e. $Y_6Mn_{23}H_{25}$) behaves like a paramagnet. On the other hand the isostructural Th_6Mn_{23} compound is a paramagnet but becomes ferromagnetic at $T_c \sim 329$ K when hydrided (i.e. $Th_6Mn_{23}H_{30}$). These puzzling results have not yet found a proper explanation and underline the need for detailed band calculations to fully explain some of the experimental observations which show clearly that no one model can fit all the observed behaviour.

1.2.d. Structure and stoichiometry of metal hydrides

As indicated in section 1.1.a. the phase transformations which are often accompained by changes of metal crystal structure and hydrogen site occupation, are the result of both short-range repulsive interactions of electronic origin and long-range attractive elastic interactions. It is therefore expected that the H-H distance and the cell size play an important role in the structures and stoichiometries of metal hydrides.

Hauck (1979) has shown that the most important factor determining the site occupation in transition and rare earth metal hydrides is the metal-hydrogen M-H interaction. He states that because of the change of the effective charges at the H and M atoms to $M^{\delta+}$ $H^{\delta-}$ or $M^{\delta-}$ $H^{\delta+}$ during the hydriding process and since the electron density of the metal d-orbitals is higher at octahedral than tetrahedral sites (Hauck and Schenk 1977) the octahedral sites are preferred by $H^{\delta+}$ and the $H^{\delta-}$ are repelled to tetrahedral sites. Correlating the electronegativity to the partial enthalpy of dilute H solution (i.e. enthalpy obtained from the region of Sieverts' law) he is able, as indicated in fig. 1.3, to separate the transition metal hydrides into two distinctive groups and predict octahedral site occupation for the group to the right of the figure and tetrahedral site occupation for the remainder. Although as clearly indicated by the band calculations of Switendick (1971) there exist no such charges associated with either the metal or hydrogen atoms, Hauck's qualitative model is in excellent agreement with experimental evidences as shown in table 1.2 which summarized the limiting compositions and structures of the known binary metal hydrides.

Swintendick (1979) has demonstrated the importance of the H-H distance on the position of the hybridized states below E_F which are formed on hydriding and which play an important role in accommodating the added electrons to the unit cell. From a survey of the stable hydrides of seven transition metals, he concludes that there may be a universal minimum H-H distance of 2.1 Å. This is substantiated by a more recent and much wider survey of the hydrides of metals and intermetallic compounds by Westlake (1983).

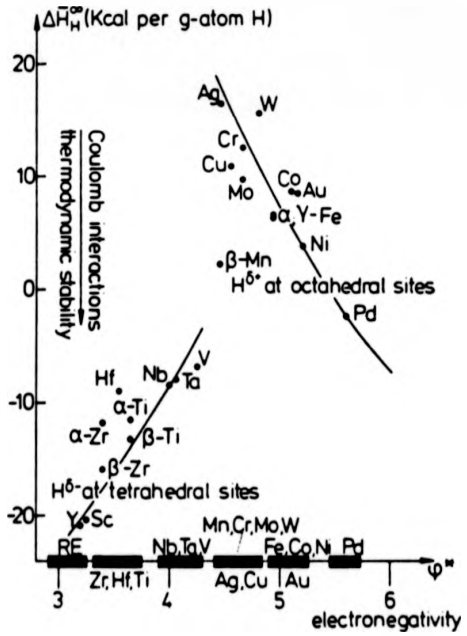

Fig. 1.3: Correlation between electronegativity and relative partial enthalpy of dilute H solutions (Hauck (1979)).

This concept of a minimum distance is very useful in qualitatively understanding why some of the transition and rare-earth metals form a trihydride phase unlike others. In table 1.1 the distance between O and T-sites is calculated from the lattice parameter of the dihydrides which for all the elements listed have the CaF_2 structure. The correlation between T-O distance and the formation of a trihydride is most clearly seen. Furthermore it can also be seen that only the element having a T-O distance greater than d > 2.35 Å retain the same metal structure in the trihydride phase. The structures of hydrided intermetallic compounds are in general much more complex than those of the binary hydrides. In these compounds, hydrogen atoms occupy interstitial sites which do not necessarily have octahedral or tetrahedral symmetries. Numerous attempts to predict the structure, stability and stoichiometry of these compounds can be found in the literature.

Regarding the stability of ternary intermetallic hydrides, it has been suggested by Van Mal et al (1974) that the more stable the binary intermetallic compound, the less stable is its hydride. From values of the enthalpy of formation of the binary hydrides and binary intermetallic alloys it is possible to estimate the enthalpy of formation of ternary hydrides. For instance

$$\Delta H_f\ (AB_5H_6) = \Delta H_f\ (AH_3) + \Delta H_f(B_5H_3) - \Delta H_f(AB_5) \qquad (1.3)$$

While the rule has been shown to hold for numerous systems (AB_5 and AB_2 compounds), its validity is not universal (it fails in the case of AB compounds).

In considering the preferential interstitial site occupation and stoichiometry, Shinar et al (1978) have attempted to rationalize the observed preferences for H occupation of particular interstitial sites in intermetallic compounds, using calculated enthalpies of

Table 1.1: Interstitial spacings in the metal dihydride phase (CaF_2) of some transition and rare-earth metals

Metal	Dihydride		Trihydride
	a (Å)	T-0 distance (Å)	Structure
Sc	4.738	2.05	-
Ti	4.437	1.92	-
Y	5.204	2.25	H.C.P.
Zr	4.603	1.99	-
La	5.661	2.45	F.C.C.
Ce	5.575	2.41	F.C.C.
Pr	5.515	2.39	F.C.C.
Nd	5.469	2.37	F.C.C.
Sm	5.374	2.33	H.C.P.
Gd	5.303	2.30	H.C.P.
Tb	5.246	2.27	H.C.P.
Dy	5.201	2.25	H.C.P.
Lu	5.033	2.18	H.C.P.
Hf	4.710	2.04	-

IA	IIA								
LiH (N)									
NaH (N)	MgH_2(T)	III B	IV B	V B	VI B	VII B	VIII B		
KH (N)	CaH_2(O)	ScH_2(C)	TiH_2(T)	VH (BT) VH_2 (C)	CrH (H) CrH_2(O)				NiH (N)
RbH (N)	SrH_2(O)	YH_2 (C) YH_3 (H)	ZrH_2(T)	NbH (O) NbH_2(c)					PdH (N)
CsH (N)	BaH_2(O)	LaH_2(C) LaH_3(B)	HfH_2(T)	TaH (O)					
		AcH_2(C)							

CeH_2(C) CeH_3(B)	PrH_2(C) PrH_3(B)	NdH_2(C) NdH_3(B)		SmH_2(C) SmH_3(H)	EuH_2(O)	GdH_2(C) GdH_3(H)	TbH_2(C) TbH_3(H)	DyH_2(C) DyH_3(H)	HoH_2(C) HoH_3(H)	ErH_2(C) ErH_3(H)	TmH_2(c) TmH_3(H)
YbH_2(O) YbH_3(B)	LuH_2(C) LuH_3(H)										

KEY

N:NaCl (f.c.c.)
C:CaF_2 (f.c.c.)
B:BiF_3 (f.c.c.)
H:Hexagonal
T:Tetragonal(f.c.t.)
BT:Tetragonal(b.c.t.)
O:Orthorhombic ($PbCl_2$)

Table I.[2] :Limiting compositions of some binary metal hydrides and their structures.

formation of elemental hydrides. In this model a hydrogen atom in a particular site is considered to be equally associated with each of its nearest-neighbour metal atoms and the elemental hydride formed at the site is made up of one H atom and fractional parts of A and B atoms.

More recently Westlake (1980) proposed a qualitative geometrical model based on the minimum H-H distance and the minimum hole size of the interstitial sites. The former is taken as d = 2.1 Å and the latter, based on evidence reported by Beck (1961) and Oesterreicher (1981) that the hole size has an indisputable effect on the stoichiometry and site occupation of the compound considered, is taken as 0.4 Å. This very simple model was used to predict the stoichiometry and site occupation in ZrNiH and $ZrNiH_3$ giving excellent agreement with experiment (Westlake et al 1982). The model also gave satisfactory agreement (Westlake 1983) with the site occupancy deduced from neutron and X-ray diffraction (Percheron-Guegan et al 1980) in $LaNi_5H_x$.

1.3. Diffusion of hydrogen in metals

Hydrogen in metals has a large diffusion coefficient compared to other interstitials. Furthermore the three isotopes of hydrogen, namely ^2D, ^3T and the positive muon (light isotope of the proton $m_\mu/m_H \sim 9$), have large mass ratios, and allow the possibility of studying isotope effects. Kehr (1978) showed that the diffusion processes can be separated into the following three principal regimes owing to the low mass of the hydrogen interstitial which makes quantum mechanical effects possible.

(i) At low temperature ($T \sim 0K$), in a fixed ideal lattice, since the proton has a large tunneling probability it is expected to be completely delocalized and form a band. A finite diffusion constant results from the interaction with thermal phonons and static defects. This process is known as "coherent tunneling" (Kagan and Klinger 1974). It can be seen that large concentrations of defects or host lattice vibrations, result in localization of the proton and inhibit the coherent tunneling.

(ii) At higher temperatures, the lattice vibrations result in the localization of the interstitial at or about a specific site. The interstitial can jump to a neighbouring site either by tunneling or by hopping over the potential barrier. Both processes are thermally activated.

(iii) Finally at very high temperature the interstitial will be mainly in states above the potential barrier and the dwell time at a site is comparable to the time taken to jump from one site to another. The diffusion can be thought of that of a dense gas or liquid. Some anomalies observed at high temperatures in Nb (Lottner et al 1979) may be ascribed to this type of diffusion process.

1.3.a. Classical rate theory

In the classical approach originated by Eyring (1932) and applied to solids by Wert and Zener (1949) and Vineyard (1957), it is assumed that all energy values of the system occur with probabilities deduced from the Boltzmann statistics. The transition rate ν is calculated by evaluating the probability of finding the system in a saddle point configuration and the current over the saddle point. This results in the Arrhenius relation

$$\nu = \nu_o \exp\left[-\frac{E_a}{kT}\right] \qquad (1.4)$$

where ν_o is the normalised attempt frequency: $\nu_o = \nu_{oo}\, z(1-c)$ where (1-c) is the probability that a neighbouring site is unoccupied, z is the number of possible jump paths and ν_{oo} the vibration frequency about its equilibrium position. E_a is given to a good approximation by the difference between potential energy at the top of the barrier (saddle-point) and the minimum.

The classical theory predicts an isotope dependence of the prefactor since $\nu_{oo} \propto (\frac{1}{m})^{\frac{1}{2}}$ where m is the mass of the interstitial but does not predict an isotope effect for the activation energy. This treatment cannot correctly describe the large amount of existing diffusion data (Völkl and Alefeld 1978) which shows an isotope effect for both the prefactor and activation energy. Hydrogen is a light particle compared to the atom forming the host lattice. Consequently the hydrogen vibrations are well decoupled from those of the lattice (i.e. hydrogen can perform localised vibrations with widely separated energy levels $\hbar\omega_o$). In order to account for the discreteness of the energy levels, Le Claire (1966) and Ebisuzaki et al (1967) have modified the classical theory. Two limiting cases can be considered.

(i) In the limit $\hbar\omega_o \ll kT$ one expects to obtain similar results to those obtained from the classical theory. Indeed, in this limit which is relevant to fcc metals, a classical isotope effect for the prefactor is expected $\frac{\nu_o^H}{\nu_o^D} = \left(\frac{m_H}{m_D}\right)^{\frac{1}{2}}$ (Katz et al 1971). In this treatment the activation energy is slightly different from that derived previously. Here $E_a = (E_s + \hbar\omega_s) - (E_m + 3/2\,\hbar\omega_m)$ where E_s and E_m are the energies in the saddle-point and minimum configuration respectively and $\hbar\omega_s$ and $\frac{3}{2}\hbar\omega_m$ are the zero point vibration energies in the respective configurations. The difference in the factors $\frac{2}{2}$ and $\frac{3}{2}$ results from the different degrees of freedom. The normal

isotope effect for the prefactor has indeed been observed experimentally for f.c.c. metals (Völkl and Alefeld (1978), Kaltz et al (1971)), however the observations have shown a reverse isotope effect for the activation energy, i.e. the lowest activation energy for the heaviest isotope. Jost and Widman (1940) show that a reverse isotope effect may be explained by the assumption of higher frequencies ω_s for the localised vibration in the saddle-point configuration, compared to the frequencies ω_m in the minimum configuration i.e. $(\hbar\omega_s)^{2D} - (\frac{3}{2}\hbar\omega_m)^{2D} < (\hbar\omega_s)^{1H} - (\frac{3}{2}\hbar\omega_m)^{1H}$. Kehr (1983) pointed out that although the physical origin of this phenomenum is not well understood, the modified classical theory describes the diffusion processes in f.c.c. metals very well.

(ii) In the limit $\hbar\omega_o \gg kT$, relevant to b.c.c. metals Katz et al (1971) showed that

$$\nu = \frac{kT}{2\pi\hbar} \exp\left|-\frac{(E_s + \hbar\omega_s) - (E_m + \frac{3}{2}\hbar\omega_m)}{kT}\right| \qquad (1.5)$$

This treatment predicts an isotope effect only for the activation energy. Indeed above room temperature where the above condition is fulfilled all group VB-metals have the same prefactor, within experimental error, independent of the isotope (Völk and Alefeld 1978). Furthermore if one assumes $\omega_s = \omega_m = \omega_o$, $E_a^D - E_a^H = \Delta E$ can be estimated as: $\Delta E = \frac{1}{2}(\hbar\omega^H - \hbar\omega^D) = \frac{1}{2}\hbar\omega^H (1-1/\sqrt{2})$, using $\hbar\omega^H = 150$ meV (Springer 1978), one obtains $\Delta E \sim 22$ meV. This value is in excellent agreement with those obtained experimentally for b.c.c. metals. However, Kehr (1983) pointed out that there are serious objections to such a simple interpretation of the b.c.c. results. The main one being that at $\sim$ 400 K the jump rate, in b.c.c. metals, is of the order of 10^{12} s^{-1}, which is comparable to typical lattice vibration frequencies. Thus memory effects are expected (i.e.

correlated motion) since the lattice cannot relax quickly enough to justify the assumptions used in deriving equation (1.5).

1.3.b. Quantum mechanical rate theory

Even when localized, the light hydrogen interstitial has a large transfer tunneling matrix and it exerts forces on the neighbouring metal atoms which lead to a relaxation of the lattice around it resulting in trapping energy of the order of 100 meV. A thermally activated process can result in a configuration where the site occupied and a neighbouring unoccupied site coincide energetically, allowing the possibility of a tunneling process as shown in fig. 1.4. This diffusion process which is known as small polaron diffusion has been applied to the case of hydrogen in a metal by Flynn and Stoneham (1970). The predictions of the theory are :

(i) in the high temperature limit $kT > \hbar\omega_D$ where ω_D is the Debye frequency of the host lattice

$$\nu = \left(\frac{\pi}{4E_a kT\hbar^2}\right)^{\frac{1}{2}} J^2 \exp\left(-\frac{E_a}{kT}\right) \qquad (1.6)$$

where J is the tunneling matrix element (a measure of the tunneling probability) and E_a is the activation energy required to create the configuration shown in fig. 1.4(b). E_a is determined by the coupling between the host lattice and the proton and by the force constant of the host lattice i.e. by the host phonon frequencies (Kehr 1978). Kehr (1983) shows that standard small-polaron theory cannot describe the experimental results for hydrogen diffusion in either the f.c.c. and b.c.c. metals above room temperature. Equation (1.6) predicts a strong isotope effect in the prefactor whereas experimental results show only a classical isotope effect in f.c.c. metals and no isotope

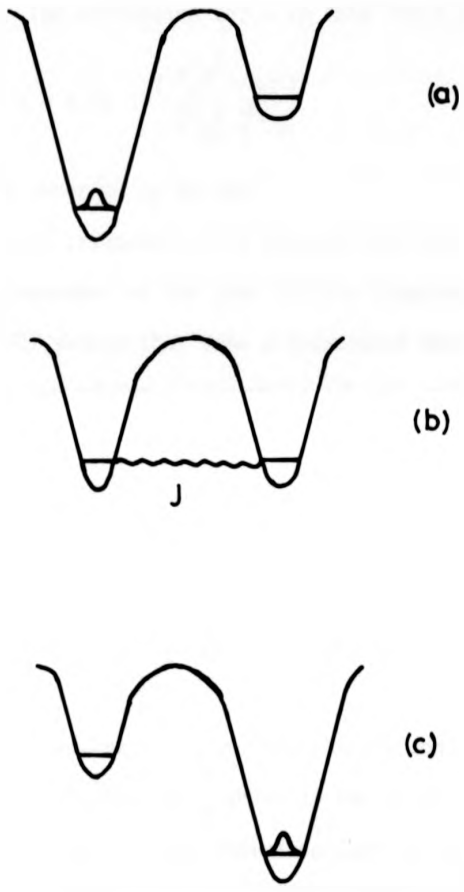

Fig. 1.4: Small-polaron process.

(a) the occupied site has a lower energy because of lattice relaxation

(b) thermal fluctuations have produced a coincidence, allowing tunnelling

(c) the lattice has relaxed about the new equilibrium position.

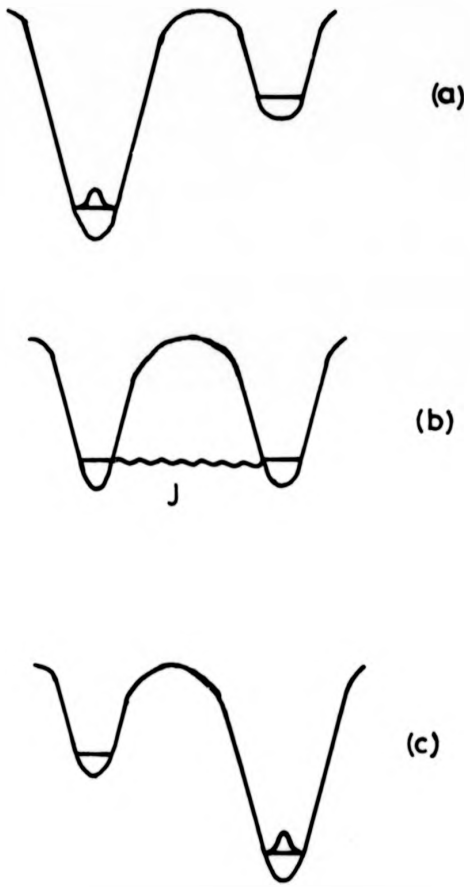

Fig. 1.4: Small-polaron process.

(a) the occupied site has a lower energy because of lattice relaxation

(b) thermal fluctuations have produced a coincidence, allowing tunnelling

(c) the lattice has relaxed about the new equilibrium position.

effect in b.c.c. metals.

(ii) in the low temperature limit $kT < \hbar\omega_D$, energy coincidence is obtained via a two phonon process. One phonon is absorbed and creates a virtual coincidence, tunneling occurs, and then a phonon is emitted at the end. The expression for ν in this limit is

$$\nu = 5.76\ 10^5 \frac{E_a^2 J^2}{\hbar^4 \omega_D^3} \left(\frac{kT}{\hbar\omega_D}\right)^7 \qquad (1.7)$$

No such T^7 law has been observed up to now.

In the development of this treatment it is assumed that the tunneling matrix element J is independent of the host lattice displacement. Flynn and Stoneham (1970) showed that some displacement modes contribute to the trapping energy of the proton while others can greatly increase the matrix J enhancing the overlap of proton wave functions. They were able to derive an expression for f.c.c. lattices where the so called "lattice-activated processes" are important giving

$$\nu = \frac{J_{lim}^2}{4\hbar(E_a E_L)^{\frac{1}{2}}} \exp(-(E_a+E_L)/kT) \qquad (1.8)$$

where E_L is the energy necessary to create the lattice configuration (displacement modes) so as to have J_{lim} which is the enhanced tunneling matrix element. Kehr (1983) indicates that it is unlikely that the hydrogen diffusion data in f.c.c. metals can be explained by this extension. However, it should be particularly relevant to b.c.c. lattices where the estimated tunneling transfers are much larger than in f.c.c. metals if only a fixed host lattice is considered. Emin et al (1979) obtained qualitative agreement with experiment in b.c.c. metals and were able to reproduce the decrease in activation energy of H below room temperature in niobium. In their approach they considered both the "lattice-activated process" and the possibility of direct tunneling from excited states. Kehr (1983)

concludes that the diffusion process in b.c.c. metals is well described by the extention of the small polaron theory.

1.3.c. Coherent diffusion

As seen above at absolute zero the particle would spread over the whole crystal and at finite temperature a diffusion constant results from the scattering by thermal phonons and, in an imperfect crystal, by defects. Kagan and Klinger (1974) and Kehr (1980) derived a T^{-9} behaviour for the diffusion coefficient from scattering processes with phonons. Coherent tunneling has not yet been observed for hydrogen. However positive muons offer the opportunity to study diffusion in metals in the dilute limit and at very low temperatures. In very pure Al (Hartmann et al 1980) and Nb (Niinikoski et al 1979) there is evidence of muon mobility down to 30 mK and 1 K respectively. Since at these temperatures thermal activation is very unlikely this can be regarded as evidence for coherent diffusion.

A full quantitative description of the diffusion of hydrogen in metals is still far from being achieved. This is mainly due to the lack of knowledge of the potentials involved in the interactions between hydrogens and metals and between the hydrogens themselves which prevent rigorous computations of the activation energies describing the different regimes. This is also especially true where considering the tunneling matrixes which depend greatly on the form of the potential used. However, from a literature survey one can conclude that for f.c.c. metals the hydrogen diffusion process is best described by the modified classical theory (jump over barrier) while for b.c.c. metals, the "higher excited states" and "lattice-activated" processes (incoherent tunneling) are expected to be dominant.

1.3.d. The tracer correlation factor

The diffusion coefficient for three dimensional motion is related to the microscopic diffusion parameters and is given from the random walk model (Le Claire 1973) , which is only valid for simple hopping, by

$$D = f_T \frac{\langle \ell \rangle^2}{6} \nu \qquad (1.9)$$

where $\langle \ell \rangle$ is the mean jump distance (generally first nearest neighbour distance) ν is the jump rate as defined in previous subsections and f_T is the self spatial or tracer correlation factor. This is a measure of correlation for successive jumps, where $f_T = 1$ in the ideal case of an infinitely dilute solution and may be written more generally (Sankey and Fedders 1977) as

$$f_T = 1 - AC/(2-C) + BC(3C-2)/(2-C)^2 \qquad (1.10)$$

where for a simple cubic lattice A = 0.419 and B = 0.088 (i.e. tetrahedral sites in an f.c.c. host lattice) for an f.c.c. A = 0.245 and B = 0.030 (i.e. Octahedral sites in an f.c.c. host metal) and where C is the site occupancy factor. In the case of tetrahedral sites in an f.c.c. lattice C = X/2 where X is the hydrogen to metal atom ratio, while for octahedral site in an f.c.c. lattice C = X. This value of f_T will be used to analyse our diffusion coefficient data.

1.4. Nuclear magnetic resonance studies of hydrogen diffusion in metal hydrides

Besides the valuable information that nuclear magnetic resonance (NMR) can provide concerning electronic structure, atomic locations and crystallographic structures, it is also a powerful tool for the study of translational atomic diffusion in solids and liquids. The

very favourable magnetic resonance properties of protons make metal hydrides excellent candidates for the investigation of hydrogen diffusion by NMR. Cotts (1978), Barnes (1981) and Seymour (1982) have given comprehensive surveys of the potential of NMR in the investigation of the properties of metal hydrides and it is proposed here to emphasize, with illustrated examples from the literature, the application of NMR to the study of hydrogen diffusion in metal hydrides. This can be performed by investigating the line narrowing behaviour as a function of temperature using steady-state methods, by measuring one or more of the several spin system relaxation times using pulse methods or by direct diffusion coefficient measurements using the pulsed field gradient technique (see Chapter III, IV and VI). From the two first methods, values of the mean residence time $\tau_D = 1/\nu$ for a proton on a lattice site are calculated from theory, allowing the computation of the activation energy E_a. The steady-state experiment yields somewhat unreliable values of these parameters since it can only be performed over a limited temperature range due to magnet inhomogeneities and thus the pulsed NMR experiment is preferred. Values of τ_D ranging from about 10^{-3} to 10^{-10} s can be determined by this technique. The pulsed gradient technique which yields values of the diffusion coefficient is model-independent and is thus certainly the most reliable method of obtaining the diffusion coefficient and thus the activation energy for diffusion.

One of the first studies of hydrogen translational diffusion by NMR was conducted by Stalinski et al (1961). From line narrowing measurements in the γ-phase of titanium hydrides (CaF_2 structure), they deduced the activation energy for hydrogen diffusion and found that E_a increased with hydrogen concentration and that the diffusion rate was proportional to the vacancy concentration. To explain the decrease in activation energy they based their interpretation on the

electrostatic model developed by Coogan and Gutowsky (1962) who suggested that the hydrogen jump path is along the hydrogen cube diagonal through the octahedral site. This corresponds to the hydrogen atom jumping from one tetrahedral interstitial position to a third nearest neighbour position. Schreiber and Cotts (1963), from both line narrowing and T_1 measurements, found a large decrease in the activation energy for hydrogen diffusion as the hydrogen concentration is increased in the β-phase of LaH_x (CaF_2 structure). This was thought to support the rigid band model (protonic model) and was interpreted in terms of the electrostatic model. Korn and Zamir (1970) performed an extensive set of T_1 measurements for a wide range of temperature and for several different hydrogen concentrations in the γ-phase of TiH_x. In contrast to the results of Stalinski et al, Korn and Zamir found an activation energy for hydrogen motion independent of hydrogen concentration. On comparing their NMR data to inelastic neutron scattering data (Pan and Webb 1965) they proposed that the M-H bonding has a strong covalent character (Korn and Zamir 1973) . More recent measurements of the relaxation times in the γ phase of TiH_x have confirmed that the activation energy is independent of hydrogen concentration (Schmolz and Noack (1974), Bustard (1979), Bowman et Rhim (1981), Pope et al (1980), (1981)).

By combining direct diffusion and relaxation time measurements it is possible to estimate the jump path. This has been applied to $NbH_{0.6}$ (Zogal and Cotts 1975) who deduced that the diffusion of hydrogen is limited to sites having nearest neighbour sites unoccupied, indicating that short range repulsive interactions between H atoms are important. This is confirmed by measurement of D and T_1 in α-TaH_x where $0.1 < x < 0.8$ (Mauger et al 1981) . The measurements were combined so as to obtain (D/T_1) for a temperature on the high

temperature side of $(T_1)_{min}$ ($\omega_o\tau_D << 1$, see Chapter II). For this temperature the ratio (D/T_1) is independent of τ_D and depends only upon the distribution of hydrogen atoms in the metal and the jump process. Comparing their experimental data to theoretical calculations (Sankey and Fedders 1980), which, assuming no H-H interactions and hence random occupation of the tetrahedral sites, predicts a large increase of (D/T_1) as a function of hydrogen content, they concluded that short range H-H repulsive interactions are very important.

Combining measurements of D and τ_D deduced from T_1 measurements, Seymour et al (1975) and Davis et al (1976) show that the results obtained for palladium hydrides and Pd-Ag hydrides respectively are consistent with random jumps between nearest-neighbour octahedral sites. This was latter confirmed by Sankey and Fedders (1979) who, in a similar test of site occupancy, compared theoretical and experimental values of (D/T_1) for $PdH_{0.7}$ with good agreement for octahedral site occupation and no strong evidence for a repulsive interaction.

Bustard, Seymour and Cotts (1980) measured T_1 and D in γ-$TiH_{1.55}$ and γ-$TiH_{1.71}$. Two possible diffusion paths were tested i.e. third nearest neighbour and first nearest-neighbour jumps respectively, and it was found that H atoms hop to the nearest neighbour vacancy on the s.c. lattice formed by the tetrahedral hydrogens. This is in agreement with the calculation of Bisson and Wilson (1976) who predicted that the lowest migration energy is given for hydrogen motion to the first nearest-neighbour position via a parabolic path through the octahedral site. They showed that the highest activation energy was for direct T-T jumps. It is interesting to note that Bowman, Attalla and Maeland (1978) who

performed relaxation time measurements on TiCuH report an activation energy of 0.8 eV compared to 0.51 eV in TiH_x. This is in agreement with Bisson and Wilson prediction since in TiCuH consists of alternating layers of copper and titanium atoms in which the H atoms are arranged as in TiH_x. Hydrogen motion is therefore limited to a two-dimensional plane so that passage into octahedral positions is not possible.

The different theories which allow the computation of τ_D assume a pairwise interaction. That is the dipolar Hamiltonian is deduced from the summation over all pairs of spins (see section 2.2.a.1.) and consequently the hydrogen motion is included as that of one spin relative to another. Characteristically for such interactions (Picton et al 1982), the relaxation time T_1 as a function of temperature which goes through a minimum at $\omega_o\tau_D \sim 1$, where ω_o is the operating frequency, is perfectly symmetric about the minimum. It is thought that the inclusion of repulsive interactions (unless they are temperature dependent) would not result in an asymmetric minimum. This seems to be confirmed by the calculations of Fedders (1982) who included repulsive H-H interactions and found that T_1 was symmetric about the minimum. However, there are a large number of examples in the literature which deviate from symmetrical behaviour or even show a subsidiary minimum. These have been often interpreted in terms of multiple diffusion processes which under certain conditions may result in an asymmetric T_1 (see section 4.1.f.). Some typical examples are shown in fig. 1.5.

Weaver (1972) from T_1 measurements on ScH_2 found two activation energies resulting from the asymmetric T_1. He suggests that at high temperature the higher activation energy obtained characterises the hopping process taking a hydrogen from a T site to an O site (ScH_2 has the CaF_2 structure). Similar behaviour was reported by Weaver

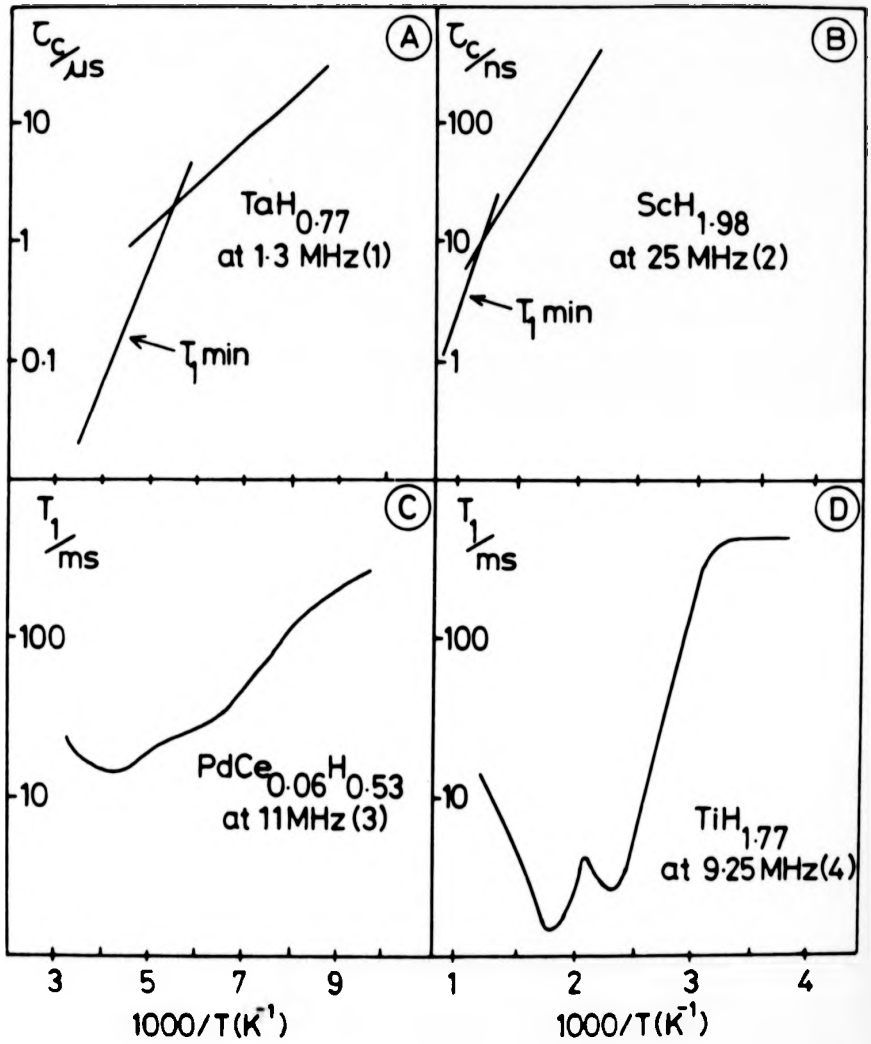

Fig. 1.5: Variations of τ_c (A and B) and T_1 (C and D) with temperature in some metal hydrides.

(1972) for $YH_{2.83}$ which forms a hexagonal structure and where the hydrogens occupy both octahedral and tetrahedral site and was again interpreted in terms of independent diffusion processes.

Anderson et al (1980) have measured the proton relaxation times for YH_x where x = 1.63, 1.92, 1.98. Yttrium dihydride has the CaF_2 structure, but octahedral site occupation occurs before the hydrogen to metal atom ratio reaches 2 (see next subsection). They found three regions in which a plot of $Ln\tau_D$ against reciprocal temperature could be fitted to a straight line. They suggested that the lower activation energy corresponded to hydrogen diffusion on the f.c.c. lattice formed by the octahedral sites while the higher activation energy characterised hydrogen diffusion on the tetrahedral sites. A double minimum in T_1 is also reported by Kashaev et al (1980) and again interpreted as due to independent motion on the two sublattices formed by the octahedral and tetrahedral sites.

Lowe and Karlicek (1980), using a new pulsed-gradient technique which overcomes the problems of background gradient enountered in metal hydrides (see Chapter III), have studied diffusion in $LaNi_5H_6$ and found a single activation energy E_a = 0.42 eV which is considerably larger than that deduced from T_1 measurements (Halstead et al (1976), Bowman et al (1979)). It should also be noted that the reported T_1 data showed a marked asymmetry from which two activation energies can be deduced.

As a result of a study of the proton relaxation times in the intermetallic hydrides $Hf_2RhH_{2.2}$ and $Hf_2CoH_{3.8}$, Jones, Halstead and Buschow (1980) proposed a frequency temperature superposition technique to obtain an empirical spectral density function of the form $J(\omega\tau_c) = A(\tau_c)B(\Omega)F(\omega\tau_c)$ where $A = (\tau_c)^{1-m}$, $F(\omega\tau_c << 1) = 1$, $F(\omega\tau_c >> 1) = (\omega\tau_c)^{n-2}$ and $B(\Omega)$ is a factor independent of ω and τ_c. Whereas the

theory predicts m = n = o, they obtained m = 0.36 and 0.14 and n = 0.87 and 0.53 for the Rh and Co samples respectively. This leads to a low temperature frequency dependence $J(\omega\tau_c >> 1) \alpha \omega^{-1.13}$ and $\omega^{-1.47}$ respectively when ω^{-2} would be expected from simple theory. It should be noted that the ω dependence on the low temperature side of the T_1 minimum follows from their data analysis and is not derived from direct measurements which are not reported. Furthermore the technique relies heavily on the assumption that the observed T_1 is due to dipole-dipole interactions only.

Chang et al (1981) measured the relaxation time in $LaNi_5H_6$. The asymmetry observed for T_1 and $T_{1\rho}$ gives rise to an apparent activation energy E_a = 0.42 eV on the high temperature side of the T_1 minimum, and E_a = 0.21 eV on the low temperature side. They interpreted their result as due to an anomalous spectral density function. Using the model derived by Jones et al, they were able to fit their $T_{1\rho}$ data using n = 0.65, m = 0.08 and E_a = 0.42 eV. It is interesting to note that m is nearly equal to zero.

The results of this investigation which aims also, at explaining some of the anomalies discussed above, show that very small amount of paramagnetic impurities (i.e. 2 ppm Gd in YH_2) can contribute a very effective relaxation mechanism that could cause weakened temperature dependences on the low temperature side of the T_1 and $T_{1\rho}$ minima and warn that care must be taken if the shape of the relaxation times are to be analysed.

1.5. Structures of the hydrides studied in the present investigation

1.5.a. Yttrium dihydrides

Yttrium reacts exothermically with hydrogen to form hydrides with a maximum hydrogen to metal atom ratio of three. The solid

solution α-YH_x which ranges from $x = 0$ to $x \sim 0.3$ at room temperature, has the hexagonal close packed structure of the elemental metal. The β-phase which exists over the range of concentrations $1.8 \leq x \leq 2.05$, has the CaF_2 structure. In the trihydride phase which exists for $x > 2.8$, the structure reverts to hexagonal where both octahedral and tetrahedral sites are occupied. The intermediate regions $0.3 \leq x \leq 1.8$ and $2.05 < x < 2.8$ are mixed α and β, and β and trihydride phases respectively. All the yttrium hydride samples studied here are single β-phase. Tetrahedral sites are predominantly occupied, however there is evidence that a substantial occupation of octahedral sites occurs before the limiting, YH_2, composition is reached (Anderson et al (1980), Khatamian et al (1980), Venturini et al (1980)). It is assumed that for the series of $YH_{1.98}$ doped with Gd yttrium is substituted by Gd^{3+} and that the lattice parameter remains unchanged. This is reasonable considering the very low concentrations of Gd involved.

1.5.b. Titanium dihydrides

Below 370 K titanium dissolves negligible amounts of hydrogen in its h.c.p. structure. Above 370 K the solubility increases to a maximum hydrogen to metal atom ratio of about 0.09. This is referred to as the α-phase. The β-phase which is b.c.c. exist only above 590 K. This phase, at $T \simeq 1100$ K, extends across the range of concentrations $0 \leq x \leq 1$. The dihydride region between $x = 1.5$ and $x = 2.0$ has two crystallographic forms: the γ-phase with the CaF_2 structure, exists for the range of concentrations $1.5 < x < 2.0$ for temperatures above 315 K, and for the range of concentrations $1.5 < x < 1.8$ for temperatures below 315 K and a second form, referred to as the tetragonal δ-phase, which has a tetragonally distorted f.c.t. structure with $c/a < 1$ and exists below 315 K for $1.8 < x < 2.0$. All the titanium hydrides studied

in this investigation are single γ-phase samples.

1.5.c. Palladium yttrium hydride

In the $[Pd_{0.92}\ Y_{0.08}]$ sample it has been shown that Pd is not obviously substituted for Y. This is discussed in detail in Chapter VI. However, the presence of yttrium in palladium closes the (α + β) miscibility gap for temperatures below room temperature. The addition of yttrium does not affect the structures of the α and β phases observed in palladium hydrides. Thus the $[Pd_{0.92}\ Y_{0.08}]\ H_{0.51}$ sample studied is single β phase, the hydrogens occupying the octahedral interstitial sites of the host f.c.c. lattice.

REFERENCES

Alefeld, G: Energie, 27, 180 (1975).

Anderson, D. L., R. G. Barnes, T. Huang, D. T. Peterson, D. R. Thorgeson: J. Less-Common Met., 73, 243 (1980).

Barnes, R. G: in Nuclear and Electron Resonance Spectroscopies Applied to Materials Science, ed. by E. N. Kaufmann and G. K. Shenoy (North Holland, New York 1981).

Beck, R. L.: Report Number LAR-55 (1961).

Bieganski, Z, B. Stalinski: Phys. Stat. Sol., 2, K161 (1970).

Bisson, C. L., W. D. Wilson: Moran, Wyoming (1976).

Bowman, R. C., W-K Rhim: Phys. Rev., B24, 2232 (1981).

Bowman, R. C., D. M. Gruen, M. H. Mendelsohn: Sol. St. Comm., 32, 501 (1979).

Bowman, R. C., A. Attalla, A. J. Maeland: Sol. St. Comm., 27, 501 (1978).

Buschow, K. H. J., A. M. Van Diepen: Sol. St. Comm., 19, 79 (1976).

Bustard, L. D : Ph.D. Thesis, Cornell University (1979).

Bustard, L. D., R. M. Cotts, E. F. W. Seymour: Phys. Rev., B22, 15 (1980).

Chang, H., I. J. Lowe, R. J. Karlicek: in Nuclear and Electron Resonance Spectroscopies Applied to Materials Science, ed. by E. N. Kaufmann and G. K. Shenoy (North Holland, New York, 1981).

Childs, B. G., W. E. Gardner, J. Penfold: Phil. Mag., 5, 1267 (1960).

Coogan, C. K., H. S. Gutowsky: J. Chem. Phys., 36, 110 (1962).

Cotts, R. M: in Hydrogen in Metals I, ed. by G. Alefeld and J. Völkl (Springer Verlag, Berlin 1978).

Davis, P. P., E. F. W. Seymour, D. Zamir, W. D. Williams, R. M. Cotts: J. Less-Common Met., 49, 159 (1976).

Deenadas, C., R. S. Craig, N. Marzouk, W. E. Wallace: J. Sol. St. Chem., 4, 1, (1972).

Eastman, D. E., J. K. Cashion, A. C. Switendick: Phys. Rev. Lett., 27, 35 (1971).

Ebisuzaki, Y., W. J. Kass, J. O'Keeffe: J. Chem. Phys., 46, 1373 (1967).

Emin, D., M. I. Baskes, W. D. Wilson: Phys. Rev. Lett., 42, 791 (1979).

Evans, J., I. R. Harris, D. K. Ross: J. Less. Common. Met., 89, 407 (1983).

Eyring, H: J. Chem. Phys., 3, 107 (1932).

Fedders, P. A: Phys. Rev., B25, 78 (1982).

Flynn, C. P., A. M. Stoneham: Phys. Rev., B1, 3966 (1970).

Frazier, G. A., R. Glosser: Sol. St. Comm., 41, 245 (1982).

Friedel, J: Phil. Mag., 43, 153 (1953): Ber. Buns. Ges., 76, 828 (1972).

Gualtieri, D. M., K. S. V. L. Narasimhan, W. E. Wallace: A. I. P. Conf. Proc., 34, 219 (1976).

Gupta, M: Sol. St. Comm., 27, 1355 (1978): Ibid, 29, 47 (1979).

Hall, C. K., G. Stell: Phys. Rev., B11, 224 (1975).

Hall. C. K: in Electronic Structure and Properties of Hydrogen in Metals, ed. by P. Jena and C. B. Satterthwaite (Plenum Press, New York, 1983).

Halstead, T. K., N. A. Abood, K. H. J. Buschow: Sol. St. Chem., 19, 425 (1976).

Hartmann, D., E. Karlsson, L. D. Norlin, T. O. Nünikoski, K. W. Kehr, D. Richter, J. M. Welter, A. Youanc, J. Lehericy: Phys. Rev. Lett., 44, 337 (1980).

Hauck, J., H. J. Schenk: J. Less-Common Met., 51, 251 (1977).

Hauck, J: Z. Phys. Chem., 114, 165 (1979).

Hughes, D. T., J. Evans, I. R. Harris: J. Less-Common Met., 74, 255 (1980).

Jones, T. C., T. K. Halstead, K. H. J. Buschow: J. Less-Common Met., 73, 209 (1980).

Jost, W., A. Widman: Z. Phys. Chem., B45, 285 (1940).

Kagan, Y., M. J. Klinger: J. Phys., C7, 2791 (1974).

Kashaev, R. S., E. F. Gudmidullin, A. N. Gilmanov, M. E. Kost: Sov. Phys. Solid St., 22, 530 (1980).

Katz, L., M. Gwinan, R. J. Borg: Phys. Rev., B4, 330 (1971).

Kehr, K. W: in Hydrogen in Metals I, ed. by G. Alefeld and J. Völkl (Springer Verlag, Berlin, 1978): Suppl. Trans. Japan Inst. Met. 21, 181 (1980): in Electronic Structure and Properties of Hydrogen in Metals, ed. by P. Jena and C. B. Satterthwaite (Plenum Press, New York, 1983).

Khatamian, D., R.G. Barnes, D.T. Peterson: Phys. Rev., B21, 2622 (1980).

Korn, C., D. Zamir: J. Phys. Chem. Sol., 31, 489 (1970): Ibid, 34, 725 (1973).

Kuijpers, F. A: J. Less-Common Met., 27, 27 (1972).

Kulikov, N. I: J. Less-Common Met., 88, 307 (1982).

Lacher, J. R: Proc. Roy. Soc., 161, 525 (1937).

Le Claire, A. D: Phil. Mag., 14, 1271 (1966); Fast Ion Transport in Solids, ed. by W. Van Gool (North Holland Press, London, 1973).

Lottner, V., U. Buchenau, W. J. Fitzgerald: Z. Phys., B35, 35 (1979).

Lowe, I. J., R. F. Karlicek: J. Mag. Resonance, 37, 75 (1980).

Malik, S. K., T. Takeshita, W. E. Wallace: Mag. Lett., 1, 33 (1976): Sol. St. Comm., 23, 599 (1977).

Manchester, F. D: J. Less-Common Met., 49, 1 (1976).

Mauger, P. E., W. D. Williams, R. M. Cotts: J. Phys. Chem. Sol., 42, 821 (1981).

Meijer, R. L: Philips Techn. Rev., 31, 169 (1970).

Merriam, M. F., D. S. Schreiber: J. Phys. Chem. Sol., 24, 1375 (1963).

Mott, N. F., H. Jones: Theory of the Properties of Metals and Alloys (Oxford University Press 1936).

Mueller, W. M., J. P. Blackledge, G. G. Libowitz: Metal Hydrides (Academic Press, New York, 1968).

Mueller, W. M., A. J. Freeman, J. O. Dimmock, A. M. Furdyna: Phys. Rev., B1, 4617 (1970).

Nagel, H. H. Goretzki: J. Phys. Chem. Sol., 36, 431 (1975).

Niinikoski, T. O., O. Hartmann, E. Karlsson, L. O. Norlin, K. Pernestal, K. W. Kehr, D. Richter, E. Walter, K. Schulze: in Proceeding of the First International Topical Meeting on Muon Spin Rotation, ed. by F. N. Gygaz, W. Kündig and P. F. Meier (North Holland, Amsterdam 1979).

Oates, W. A., J. A. Lambert, P. T. Gallagher: Trans. Met. Soc., 245, 47 (1969).

Oesterreicher, H: Appl. Phys., 24, 169 (1981).

Pan, S. S., F. J. Webb: Nucl. Sci, Eng., 23, 194 (1965).

Pick, M. A., D. O. Welch: Z. Phys. Chem. (N.F), 114, 37 (1979).

Picton, D. J., R. A. Bond, B. S. Bowerman, D. K. Ross, D. G. Witchell, I. S. Anderson, C. J. Carlile: J. Less-Common Met., 88, 133 (1982).

Percheron-Guegan, A., C. Lartigue, J. C. Achard, P. Germi, F. Tasset: J. Less-Common Met., 74, 1 (1980).

Peterman, D. J., B. N. Harmon, J. Marchiando, J. H. Waver: Phys. Rev., B19, 4867 (1979).

Pope, J. M., K. R. Doolan, P. P. Narang: J. Phys., F10, 2073 (1980): J. Chem. Sol., 42, 519 (1981).

Sankey, O. F., P. A. Fedders: Phys. Rev., B15, 3586 (1977): Ibid, B20, 39 (1979): Ibid, B22, 5135 (1980).

Satterthwaite, C. B., I. L. Toepke: Phys. Rev. Lett., 25, 741 (1970).

Schmolz, A., F. Noack: Ber. Bun. Phys. Chem., 78, 339 (1974).

Schreiber, D. S., R. M. Cotts: Phys. Rev., 131, 1118 (1963).

Schreiber, D. S: Phys. Rev., A137, 860 (1965).

Seymour, E. F. W., R. M. Cotts, W. D. Williams: Phys. Rev. Lett., 35 165 (1975).

Seymour, E. F. W: J. Less-Common Met., 88, 323 (1982).

Shinar, J., I. Jacob, D. Davidov, D. Shaltiel: in Hydrides for Energy Storage, ed. by F. Andressen and A. J. Maeland (Pergamon, New York, 1978).

Skoskiewicz, T: Phys. Status Solidi, 11a, K123 (1972).

Speiser, R: in Metal Hydrides, ed., by W. M. Hueller, J. P. Blackledge and G. G. Libowitz (Academic Press, New York, 1968).

Springer, T: in Hydrogen in Metals I, ed. by G. Alefeld and J. Völkl (Springer Verlag, Berlin, 1978).

Stalinski, B: Bull. Acad. Polon. Sci., C1 III, 2, (1954): Ibid, 7, 269 (1959).

Stalinski, B., C. K. Coogan, H. S. Gutowsky: J. Chem. Phys., 34, 1191 (1961).

Switendick, A: Sol. St. Comm., 8, 1463 (1970): Int. J. Quantum Chem., 5, 459 (1971): in Hydrogen in Metals I (1978): Z. Phys. Chem., 117, 89 (1979).

Titcomb, C., R. S. Graig, W. E. Wallace: Phys. Lett., 39A, 157 (1972).

Trzebiatowski, W., B. Stalinski: Bull. Acad. Polon. Sci., 1, 317 (1953), Ibid, 1, 131 (1953).

Van-Diepen, A. M., R. S. Graig, W. E. Wallace: J. Phys. Sol., 32, 1853 (1971).

Van-Vucht, J.H.N., F. A. Kuijpers: Philips Res. Repts., 25, 133 (1970).

Van-Mal, H. H., K. H. J. Buschow, A. R. Miedema: J. Less-Common Met., 35, 65 (1974).

Venturini, E.L., P.M. Richards: Phys. Let., 76A, 344 (1980).

Vineyard, G. H: J. Phys. Chem. Sol., 3, 121 (1957).

Völkl, J., G. Alefeld: in Hydrogen in Metals I, ed. by G. Alefeld and J. Völkl (Springer Verlag, Berlin 1978).

Vuillemin, J. J., M. G. Priestly: Phys. Rev. Lett., 14, 307 (1965).

Wagner, C: Acta Met., 19, 843 (1971).

Wallace, W. E: in Hydrogen in Metals I, ed. by G. Alefeld and J. Völkl (Springer Verlag, Berlin 1978): J. Less-Common Met., 88, 141 (1982).

Weaver, H. T: Phys. Rev., B5, 1663 (1972): J. Chem. Phys., 56, 3193, (1972).

Weaver, J. H., D. T. Peterson: J. Less-Common Met., 74, 207 (1980).

Weaver, J. H., D. J. Peterman, D. T. Peterson: In Electronic Structure and Properties of Hydrogen in Metals, ed. by P. Jena and C. B. Satterthwaite (Plenum Press, New York, 1983).

Wert, C., C. Zener: Phys. Rev., 76, 1169 (1949).

Westlake, D. G: J. Less-Common Met., 75, 177 (1980): in Electronic

Structure and Properties of Hydrogen in Metals, ed. by P. Jena and C. B. Satterthwaite (Plenum Press, New York, 1983).

Westlake, D. G., H. Sttaked, P. R. Mason, B. R. McCart, M. H. Mueller, T. Matsumoto, M. Amano: J. Less-Common Met., 88, 17 (1982).

Wiswall, R. H., J. J. Reilly: Inorg. Chem., 11, 1691 (1972).

Zanowich, R. L. W. E. Wallace: J. Chem. Phys., 36, 2059 (1962).

Zogal, O. J., R. M. Cotts: Phys. Rev., B11, 2443 (1975).

CHAPTER II: NMR THEORETICAL BACKGROUND

2.1. Introduction

Nuclear magnetic resonance is the study of dynamic magnetic and electric effects associated with the spin angular momenta and quadrupolar moments of nuclei respectively. The first NMR signal was observed independently by Bloch and Purcell in 1946 and since the basic theory of NMR has been well documented since then (Abragam (1961), Slichter (1963)), in this chapter only the relevant parts of the NMR theory will be discussed.

The Hamiltonian describing the interaction of a nuclear magnetic moment $\vec{\mu}$ with an external applied field H_o is given by

$$\mathcal{H}_z = - \vec{\mu}.\vec{H}_o \qquad (2.1)$$

where $\vec{\mu} = \gamma\hbar\vec{I}$, γ is the gyromagnetic ratio and $\hbar\vec{I}$ is the spin angular momentum of the nucleus and where the subscript z refers to the Zeeman interaction. Since $\vec{I}$ commutes with I_z by choosing H_o to be along the z direction the energy levels derived from equation (2.1) are

$$E = -\gamma\hbar H_o m$$

where m is one of the (2I+1) eigenvalues of I_z. In NMR, transitions between adjacent levels (selection rule gives $\Delta m = \pm 1$) are stimulated by electromagnetic radiation of frequency ω_o (the Larmor frequency) which satisfies the condition,

$$\omega_o = \gamma H_o \qquad (2.2)$$

This picture assumes that the spins do not interact with each other. In solids however, the coupling of spins ($\sim 10^{23}$) with one another is important. The time evolution of measurable macroscopic quantities associated with the spin system may only be predicted if the Schrödinger equation for the wave function of each individual spin is solved. This many-body problem can be simplified by knowing that before a disturbance of the thermal equilibrium between spin system and 'lattice' the entire system was in a state of macroscopic equilibrium. This enables one to describe the entire system statistically. Moreover the density of nuclear spins is usually low enough to make quantum-statistical effects due to the overlap of different spin wave functions negligibly small so that the nuclear spin system can be described by Maxwell-Boltzmann statistics introducing the concepts of a spin temperature which characterises the degree of preferential spin alignment parallel to H_o.

The assignment of a spin temperature T_s to a disturbed spin system is equivalent to saying that the ratio of the probabilities of finding spins with energy E_n and E_m is

$$\frac{P(E_n)}{P(E_m)} = \frac{\exp(-E_n/kT_s)}{\exp(-E_m/kT_s)} \tag{2.3}$$

where k is the Boltzmann constant. When the spin system is in equilibrium with the lattice the ratio of populations is equal to the Boltzmann ratio

$$\frac{P(E_n)}{P(E_m)} = \frac{\exp(-E_n/kT_L)}{\exp(-E_m/kT_L)} \tag{2.4}$$

where T_L is the lattice temperature. The disturbance of this equilibrium, by applying an r.f. pulse at the frequency ω_o, results in an increase

of the spin temperature due to a promotion of spins from E_m to E_n. To reach its equilibrium value ($T_s = T_L$) there must be a transfer of energy from the spin system to the lattice. The rate of cooling of the spin system is characterised by the spin lattice relaxation time or longitudinal relaxation time T_1. In order to be able to talk about a spin temperature the spin system must reach a internal thermal equilibrium. This is achieved through spin-spin interactions with a characteristic time T_2 called the spin-spin or transverse relaxation time. During the time T_2 information is passed through the spin system making the temperature of the spin system uniform.

For reference only two other relaxation times $T_{1\rho}$ and T_{1D} may be mentioned. The former refers to the spin lattice relaxation time in the rotating frame which is measured in the applied r.f. rotating field,first introduced by Redfield (1955) while the latter is measured in the local dipolar field.

2.2. Relaxation theory

Any fluctuating local magnetic field or, when $I > \frac{1}{2}$, any fluctuating local electric field gradient having a component at a frequency close to the Larmor frequency of the nucleus provides a relaxation mechanism. The transverse component of the fluctuating field is associated with T_1 which can be described as the characteristic time of the magnetization growth along the H_o direction after disturbance. The relaxation time T_2 which characterises the decay of the magnetization in a plane (x,y) perpendicular to H_o is the result of both the dephasing of the precessions of individual spins in the (x,y) plane and the relaxation of the magnetization out of the (x,y) plane. Therefore,T_2 is associated with both the longitudinal and transverse components of the fluctuating field. The time average component of the fluctuating field along the H_o direction introduces

a shift of the resonance frequency and will not be discussed in this chapter.

In metal hydrides/deuterides the investigation of the relaxation times T_1 and T_2 as a function of temperature may yield information on the hydrogen/deuterium diffusion and on the electronic structure of the compound studied.

We now discuss the specific time varying magnetic/electric interactions which produce relaxation.

2.2.a. Relaxation mechanisms associated with atomic diffusion

The Fourier spectrum of the time-dependent component of an interaction with a nucleus may contain a non-vanishing intensity at the Larmor frequency ω_o and at frequencies related to ω_o capable of producing transitions with finite probability between adjacent levels of the nuclear spin system. This can be described by defining an auto-correlation function

$$G(\tau) = \overline{F(t)\ F^*(t+\tau)} \qquad (2.5)$$

where F(t) is the component of the fluctuating field at time t and the sign '*' denotes the complex conjugate. The functional form of $G(\tau)$ can only be determined in very few cases but can always be characterised by a correlation time which expresses the duration of a correlation between two configurations of a nuclear environment at two different times. In the case of fluctuations induced by atomic diffusion the correlation time is directly related to the dwell time τ_D which is temperature dependent.

The power spectrum or spectral density $J(\omega)$ is expressed as the Fourier transform of $G(\tau)$

$$J(\omega) = \int_{-\infty}^{+\infty} G(\tau) \exp(-i\omega\tau)d\tau \qquad (2.6)$$

and similarly

$$G(\tau) = \frac{1}{2\pi} \int_{-\infty}^{+\infty} J(\omega) \exp(i\omega\tau)d\omega \qquad (2.7)$$

it follows that if τ=o

$$G(o) = \frac{1}{2\pi} \int_{-\infty}^{+\infty} J(\omega)d\omega = \overline{F(t)^2} \qquad (2.8)$$

where the quadratic component $G(o) = \overline{F^2(t)}$ which is proportional to the energy corresponding to the component F(t), is a constant independent of the correlation time and therefore, the area under $J(\omega)$ is also independent of the correlation time. Fig. 2.1 shows the typical behaviour of $J(\omega)$ versus ω for different values of the correlation time or the temperature (i.e. the correlation time decreases with increasing temperature). It can be seen from the diagram that for a given frequency, labelled ω_o on the graph, the value of the spectral density goes through a maximum which in fact, is obtained for $\omega_o\tau_c \sim 1$.

In the following sections we discuss specific forms of the interaction, relevant to the present experiments, which induce relaxation through a time dependence arising from atomic diffusion.

2.2.a.1. Nuclear dipole-dipole relaxation

An interaction common to all nuclear spins in solids or liquids and which is particularly relevant to metal hydride systems (i.e. proton spin I = ½) is the nuclear dipole-dipole interaction. The Hamiltonian describing this interaction between two spins takes the form

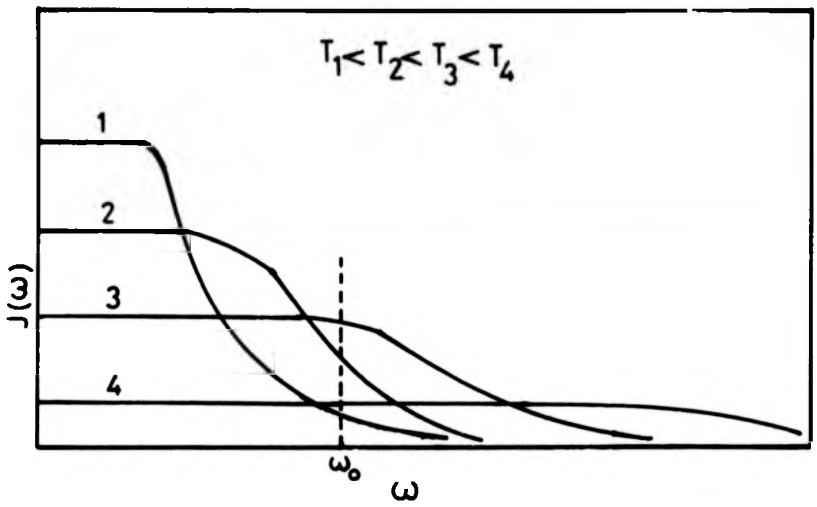

Fig. 2.1: Typical behaviour of the spectral density $J(\omega)$ for various temperatures.

$$\mathcal{H}_d = \frac{\hbar^2 \gamma_1 \gamma_2}{r_{12}^3} \left[\vec{I}^{(1)} \vec{I}^{(2)} - \frac{3 (\vec{I}^{(1)} \vec{r}_{12})(\vec{I}^{(2)} \vec{r}_{12})}{r_{12}^2} \right] \qquad (2.9)$$

where γ_1 and γ_2 are the gyromagnetic ratios of the nuclei, $\vec{I}^{(1)}$ and $\vec{I}^{(2)}$ the spin operators and $\vec{r}_{12}$ the position vector from spin 1 to spin 2. In metal hydrides the interaction between hydrogen and metal spins cannot always be neglected and therefore this should be taken into account when expressing the hydrogen nuclear Hamiltonian describing the Zeeman and dipole-dipole interactions. However in our case the interaction between unlike spins can always be neglected and is not included in the expression for the Hamiltonian. Thus

$$\mathcal{H} = \mathcal{H}_z + \mathcal{H}_d = -\hbar \gamma_I H_o \sum_j I_z^{(1)} + \mathcal{H}_d^{I.I} \qquad (2.10)$$

where $\mathcal{H}_d^{I.I}$ describes the dipole-dipole interaction between like spins. A useful form for $\mathcal{H}_d^{I.I}$ which was suggested by Van Vleck (1948) gives

$$\mathcal{H}_d^{I.I} = \sum_{j<k} \frac{\hbar^2 \gamma_I^2}{r_{jk}^3} (A^{jk} + B^{jk} + C^{jk} + D^{jk} + E^{jk} + F^{jk}) \qquad (2.11)$$

where

$$A^{jk} = (1-3\cos^2\theta) I_z^j I_z^k$$

$$B^{jk} = -\frac{1}{4} (1-3\cos^2\theta)(I_+^j I_-^k + I_-^j I_+^k)$$

$$C^{jk} = -\frac{3}{2} \sin\theta\cos\theta \exp(-i\phi)(I_z^j I_+^k + I_z^k I_+^j)$$

$$D^{jk} = -\frac{3}{2} \sin\theta\cos\theta \exp(+i\phi)(I_z^j I_-^k + I_z^k I_-^j)$$

$$E^{jk} = -\frac{3}{4} \sin^2\theta \exp(-2i\phi) I_+^j I_+^k$$

$$F^{jk} = -\frac{3}{4} \sin^2\theta \exp(2i\phi) I_-^j I_-^k ,$$

θ and ϕ are the polar and azimuthal angles for r_{jk} relative to the z axis of quantisation parallel to H_o and I_+, I_- are the raising and lowering operators. Atomic diffusion results in a time dependence of the parameters r_{jk}, θ and ϕ and thus modulates the dipolar interaction. If the local dipolar field is small compared with the applied field H_o, the interaction can be treated as a time-dependent perturbation. In the motionally narrowed regime the relaxation rates $^1/T_1$ and $^1/T_2$ are expressed in terms of power spectra of the randomly varying dipolar fields (Abragam 1961)

$$\frac{1}{T_{1d}} = \frac{3}{2}\gamma_I^4\hbar^2 I(I+1)[J^{(1)}(\omega_o) + J^{(2)}(2\omega_o)] \tag{2.12}$$

$$\frac{1}{T_{2d}} = \frac{3}{8}\gamma_I^4\hbar^2 I(I+1)[J^{(o)}(o) + 10J^{(1)}(\omega_o) + J^{(2)}(2\omega_o)] \tag{2.13}$$

where

$$J^q(\omega) = \int_{-\infty}^{+\infty} G^q(\tau)e^{-i\omega\tau}d\tau \tag{2.14}$$

$$G^{(q)}(\tau) = \sum_j \langle F_{ij}^{(q)}(t).F_{ij}^{(q)*}(t+\tau)\rangle \tag{2.15}$$

$$F_{ij}^{(q)}(t) = d_q \frac{Y_{2,q}(\Omega_{ij})}{r_{ij}^3} \tag{2.16}$$

$$d_o^2 = \frac{16\pi}{5} \qquad d_1^2 = \frac{8\pi}{15} \qquad d_2^2 = \frac{32\pi}{15} \tag{2.17}$$

In which $Y_{2,q}$ are normalised spherical harmonics. One can recognise from equation (2.12) and (2.13) that the terms at frequency ω_o and $2\omega_o$ come from the C, D and E, F terms respectively of equation (2.11) since the former induce transition of only one spin at ω_o and the latter, transitions of both spins at $2\omega_o$. The term at zero frequency

arises from A which leaves the two spin states unchanged.

The simplest form of the auto-correlation function $G^{(q)}(\tau)$ was suggested by Bloembergen, Purcell and Pound (1948). It is assumed that the dipolar field correlations decay exponentially as

$$G^{(q)}(\tau) = G^{(q)}(0) \exp-\tau/\tau_c$$

Abragam (1961) showed that this form of correlation function in the case of rotation in liquids is a consequence of the diffusion equation. The corresponding spectral density is

$$J^{(q)}(\omega) = G^{(q)}(0) \frac{2\tau_c}{1+\omega^2\tau_c^2}$$

and typically for H-H interactions in metal-hydrides $\tau_c = \tau_D/2$. If the motion is thermally activated τ_c is expected to follow an Arrhenius relation. $\tau_c = \tau_{co} \exp(E_a/kT)$ where E_a is the activation energy describing the diffusion process. Making use of this spectral density form in equation (2.12), a minimum in T_1 is predicted when $\omega_o\tau_c = 0.616$. In metal hydrides where the hydrogen diffusion is characterised by typical values of τ_{co} and E_a of the order of $\sim 10^{-13}$s and ~ 0.5 eV respectively the condition $\omega_o\tau_c \sim 0.616$ is obtained for relatively low temperatures. Therefore, a study of T_1 and/or T_2 as a function of temperature yields values of the activation energy and preexponential dwell time. The BPP theory is independent of the microscopic jump mechanism but the summation (equation 2.15) conceals some association with lattice sites. Several models based on a random walk to nearest-neighbour sites have been developed to introduce the microscopic features of the diffusion mechanism. In these models the time average of equation (2.15) is replaced by an ensemble average.

Torrey (1954) and later Resing and Torrey (1963) assumed that isotropic jumps of equal length from a lattice site to all points on a surface of a sphere are possible. This assumption leads to the need to introduce a parameter which depends on the structure of the lattice in order to adequately normalise the value of $G^{(q)}(0)$. The accuracy of Torrey's isotropic diffusion model is expected to decrease as the nearest-neighbour coordination number decreases. For instance if the nuclei (i.e. Hydrogens) diffuse between sites on a cubic lattice, Torrey's prediction should be less accurate as one goes from a fcc lattice to a bcc to a simple cubic lattice.

Sholl (1974) and Wolf (1975) have extended Torrey's theory by describing the diffusion mechanism in a more rigorous manner. In Sholl's theory the assumption of isotropic diffusion for polycrystalline samples is replaced by the orientational averaging of the auto-correlation function explicitly summed over all lattice sites. Wolf in his model, expressed the correlation function of translational random walk diffusion by the product of a simple exponential decay with a series expansion in increasing powers of time. From the spectral densities calculated for a single crystal the average over all crystallographic orientations is calculated for polycrystalline samples. The difference between these two models lies mainly in the orientational averaging for polycrystalline samples. The result is an average of the relaxation rate in Sholl's model (Barton and Sholl 1976) as opposed to an average of the magnetisation in Wolf's model. But for a simple cubic polycrystalline sample the deviation of the magnetisation from an exponential decay characterised by $\langle T_1^{-1} \rangle$ (the brackets indicate the average) is less than 10% and has never been seen experimentally. In all the models reviewed up to now the effect of correlation due to blocking of sites is not included. This is shown by the fact that in all three calculations one spin is

permanently placed at the origin and the second spin is allowed to hop with twice the jump frequency. This is equivalent to having $\tau_c = \tau_D/2$ in the BPP model (H-H interaction). Therefore these theoretical predictions should be less accurate in describing systems (e.g. metal hydrides) characterised by a high occupation factor c (in the limit where $c \to 1$).

For monovacancy diffusion Wolf (1974) applies the encounter model first suggested by Eisenstadt and Redfield (1963). In this model the temporal description during an encounter is assumed to be of such high frequency that it may be neglected compared to the frequencies describing the occurences of encounters. Following this argument this model may be described as a 'random walk of encounters' with correlation time τ_c being the time between encounters. This limits the applicability of the encounter model to the case where the vacancy concentration c_v is less than approximately 10^{-4}.

Fedders and Sankey (1978) calculate the correlation function taking into account the spatial correlation effects due to occupied sites (blocking factor). They developed a reciprocal-space formalism to evaluate the correlation functions within the mean-field and multiple scattering approximations. They give assymptotic values of T_1 in the low and high temperature limits for fcc and sc lattices. They concluded that the 'random walk' model could be in error by as much as 100% at high temperature and 18% at low temperature. Barton and Sholl (1980) extended the calculation to bcc lattices within the mean-field approximation which is an exact formalism in the low temperature limit except for $c \to 1$. They give numerical values of T_1 for the entire temperature range for sc, fcc and bcc lattices. Bustard (1980) developed the 'independent spin-pair' model in which the statistical description of a spin-pair's motion includes, spatial temporal and pair correlation effects. He gives values of T_1 for vacancy concentrations of 0.15 and 0.225, for the entire temperature range in

the case of a sc lattice.

A comparison of some of the different theoretical predictions in the high and low temperature limits is given in table 2.1. Table 2.2 gives the predicted value of T_1 at the minimum together with the value of $\omega_o\tau_D$. As commented by Sankey and Fedders, the value of T_1 at the minimum is very insensitive to the model used therefore it should give a good idea of the jump mechanism involved in the diffusion process, namely in the case of metal hydrides, the interstitial position of the hydrogen atoms and, if the diffusion coefficient is available at the temperature of $(T_{1d})_{min}$, the jump length. The activation energy deduced from the different theoretical models (except in the case of the BPP model), varies by less than 5% from model to model although the high temperature limit predictions and the shape of T_1 near the minimum (fig. 2.2) are sensitive to the model used. In view of this small variation the calculations of Barton and Sholl (1980) although not exact in the high temperature limit, will be used in the course of this investigation.

Fedders (1978) has obtained expressions for the distinguishable particle correlation functions for a system of atoms hopping among inequivalent sites in a three dimensional lattice. This model is applied specifically to the hopping of atoms among the octahedral sites of a body-centered tetragonal lattice with the sites along the c axis taken to be preferentially occupied. A quantitatively crude estimate of T_1 which on the low temperature side may be characterised by an apparent change in activation energy, is obtained. With the condition $\partial_{up} > \omega_o > \partial_u > \partial_{pu}$

$$\frac{1}{T_1} \alpha \exp[-(E_p+E_c)/kT]$$

Table 2.1: High and low temperature assymptotic limits of the spin lattice relaxation rate ($^1/T_1$) in polycrystalline samples with the definition: $\alpha = \frac{\gamma^4\hbar^2 I(I+1)}{b^6} c$ where c is the site occupation factor and b the length of one side of the unit cell.

Theory	S.C. lattice ($^1/T_1$)		F.C.C. lattice ($^1/T_1$)	
	$\omega_o\tau_D<<1$	$\omega_o\tau_D>>1$	$\omega_o\tau_D<<1$	$\omega_o\tau_D>>1$
B.P.P.	$8.4\alpha\tau_D$	$13.44^\alpha/\omega_o^2\tau_D$	$115.6\alpha\tau_D$	$185.0^\alpha/\omega_o^2\tau_D$
Random Walk				
Torrey	-	-	$213.1\alpha\tau_D$	$158.5^\alpha/\omega_o^2\tau_D$
Barton & Sholl	$17.9\alpha\tau_D$	$10.4^\alpha/\omega_o^2\tau_D$	$217.6\alpha\tau_D$	$156.5^\alpha/\omega_o^2\tau_D$
Wolf	$17.9\alpha\tau_D$	$10.4^\alpha/\omega_o^2\tau_D$	$184.3\alpha\tau_D$	$156.6^\alpha/\omega_o^2\tau_D$
Bustard ($c \to 0$)	$17.3\alpha\tau_D$	-	-	-
Mono Vacancies				
Wolf	$28.54\alpha\tau_D$	$4.2^\alpha/\omega_o^2\tau_D$	$306.6\alpha\tau_D$	$81.64^\alpha/\omega_o^2\tau_D$
Fedders & Sankey ($c \to 1$)	$30.86\alpha\tau_D$	$4.37^\alpha/\omega_o^2\tau_D$	-	-
Bustard ($c \to 1$)	$26.72\alpha\tau_D$	-	-	-
Multiple Scattering				
Fedders & Sankey				
$c = 0.20$	$20.29\alpha\tau_D$	$8.76^\alpha/\omega_o^2\tau_D$	$232.0\alpha\tau_D$	$143.7^\alpha/\omega_o^2\tau_D$
$c = 0.60$	$22.84\alpha\tau_D$	$8.76^\alpha/\omega_o^2\tau_D$	$250.2\alpha\tau_D$	$143.7^\alpha/\omega_o^2\tau_D$
$c = 0.90$	$25.17\alpha\tau_D$	$8.76^\alpha/\omega_o^2\tau_D$	$285.0\alpha\tau_D$	$143.7^\alpha/\omega_o^2\tau_D$
Independent 'spin pair'				
Bustard				
$c = 0.775$	$21.41\alpha\tau_D$	-	-	-
$c = 0.85$	$22.35\alpha\tau_D$	-	-	-
Mean Field				
Barton & Sholl	$19.9\alpha\tau_D$	$8.76^\alpha/\omega_o^2\tau_D$	$229.6\alpha\tau_D$	$143.7^\alpha/\omega_o^2\tau_D$

Table 2.2: Theoretical predictions of the relaxation rate $(^1/T_1)$ at the maximum together with $(\omega_o\tau_D)_{max}$ for polycrystalline sample. The coefficient c is defined in Table 2.1 and $\alpha = \frac{\gamma^4 \hbar^2 I(I+1)}{\omega_o b^6} c$.

Theory	S.C. lattice		F.C.C. Lattice	
	$(\omega_o\tau_D)_{max}$	$(^1/\alpha T_1)_{max}$	$(\omega_o\tau_D)_{max}$	$(^1/\alpha T_1)_{max}$
B.P.P.	1.23	4.78	1.23	65.71
Random Walk				
Barton & Sholl	0.92	4.34	1.04	60.52
Wolf	0.91	4.32	1.00	64.00
Bustard	0.90	4.34	-	-
(c → o)				
Mono Vacancies				
Wolf	0.38	4.15	0.54	64.00
Bustard	0.44	4.34	-	-
Independent 'spin pair'				
Bustard				
c = 0.775	0.70	3.97	-	-
c = 0.85	0.61	3.97	-	-
Mean Field				
Barton & Sholl	0.77	4.38	0.95	60.80

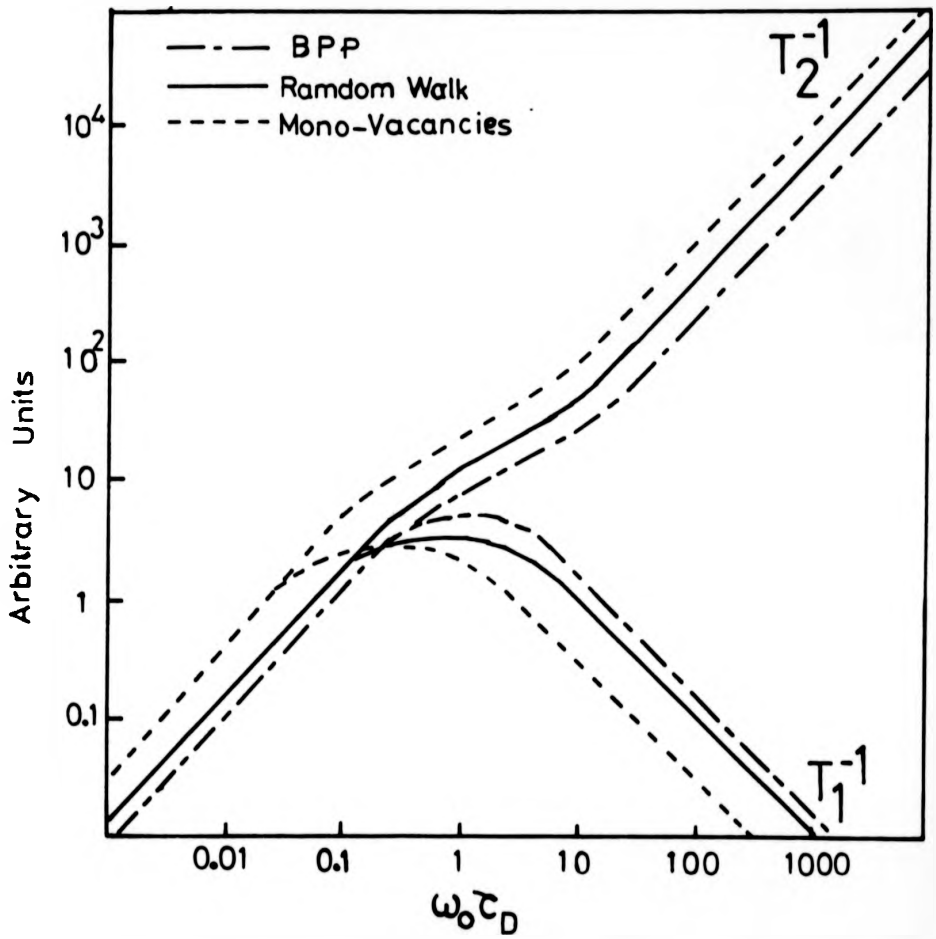

Fig. 2.2: Theoretical predictions of $(^1/T_1)$ and $(^1/T_2)$

and with $\omega_o > \partial_{up} > \partial_u > \partial_{pu}$

$$\frac{1}{T_1} \alpha \exp[-(E_p-E_c)/kT]$$

where ∂'s are the hopping rate and the subscript u and p refer to unpreferred and preferred sites respectively. E_p is the activation energy among preferred sites and $2E_c$ is the energy difference between preferred and unpreferred sites. Fedders argues that since the form of the correlation functions is largely determined by the fact that preferred sites have only unpreferred nearest neighbours this model could describe other systems.

2.2.a.2. Nuclear Quadrupolar relaxation

In general for nuclei having a nuclear spin $I > \frac{1}{2}$, the nuclear charge distribution $\rho(r)$ around the centre of gravity of a nucleus is not spherically symmetric and so gives rise to a nuclear quadrupolar moment Q

$$Q = \frac{1}{2} \int_V (3z^2-r^2)\rho(r)d^3r$$

where Q represents a measure of the deviation of the nuclear charge distribution from sphericity, the z direction is defined by the nuclear spin and the integral extends over the nuclear volume. The classical quadrupole energy resulting from the interaction between an electric field gradient (E.F.G.) and the quadrupole moment can be written in terms of quantum mechanical raising and lowering operators (Cohen and Reif 1957).

$$\mathcal{H}_Q = \sum_{p=-2}^{2} Q^{(p)} F^{(-p)} \qquad (2.18)$$

where

$$Q^{(0)} = \beta[3I_z^2 - I(I+1)] \tag{2.19}$$

$$Q^{\pm 1} = \frac{\beta\sqrt{6}}{2}[I_z I_\pm + I_\pm I_z] \tag{2.20}$$

$$Q^{(\pm 2)} = \frac{\beta\sqrt{6}}{2} I_\pm^2 \tag{2.21}$$

with $$\beta = eQ/2I(2I-1) \tag{2.22}$$

and $$F^{(o)} = \tfrac{1}{2}(V_{zz} - \tfrac{1}{3}\nabla^2 V) \tag{2.23}$$

$$F^{(\pm 1)} = 6^{-\frac{1}{2}}(V_{xz} \pm iV_{yz}) \tag{2.24}$$

$$F^{(\pm 2)} = \tfrac{1}{2}6^{-\frac{1}{2}}(V_{xx} - V_{yy} \pm 2iV_{xy}) \tag{2.25}$$

In the above equations I is the nuclear spin ($I \geq 1$), $V_{ij} = \frac{\partial^2 V}{\partial x_i \partial x_j}$ is the second derivative of the potential at the nucleus with respect to a set of orthogonal axis. The E.F.G. is due to external charges associated with the surrounding ions. A complication may arise due to the distortion of the charge cloud of the complete inner shells (ideally isotropic) resulting in an enhancement of the external field gradient $(V_{ij}^{ext})_{eff} = (1+\gamma)V_{ij}^{ext}$. γ is known as the 'anti-shielding factor' or 'Sternheimer factor' (Sternheimer 1956). When γ is governed by external charges alone it becomes independent of the distance from the nuclear centre ($r \to \infty$) and is referred to as γ_∞. The E.F.G. components at a nucleus can be expressed as the sum over all other particles of the second derivatives with respect to x,y,z, of the potential $v(r_i)$ at the nucleus due to particle ar r_i. The form of the potential will depend, in the case of a metal, on the screening of the bare potential by the conduction electrons. Equations (2.23) to (2.25) may then be written (Barton 1982)

$$F^{(p)} = \sum_i U_p(r_i) \qquad (2.26)$$

where in the case of a central potential $v(r)$

$$U_p(r_i) = \left(\frac{4}{45\pi}\right)^{\frac{1}{2}} \sigma\, v_2(r_i)(-1)^{(p+|p|)/2}\, Y_{2p}(\Omega_i) \qquad (2.27)$$

and

$$v_2(r_i) = r\{\frac{d}{dr}\,[\frac{1}{r}\,\frac{dv(r)}{dr}]\} \qquad (2.28)$$

Y_{2p} are the spherical harmonics normalised to unity and Ω_i is the direction of r_i relative to the z axis. The factor σ includes the Sternheimer antishielding factor. The time varying quadrupolar interaction resulting from the E.F.G. fluctuations induces relaxation.

Among the various cases of E.F. G. fluctuations induced by translational diffusion one is of particular importance to our investigation. This is when the E.F.G. fluctuations are due to the diffusion of both the surrounding charged particles as well as the nucleus in question. It should be noted that although all the components of the E.F.G. tensor vanish in the case of a cubic crystal (e.g. YD_2), the E.F.G. components at a given time are likely to be non-zero due to distortion of cubic symmetry in non stochiometric metal deuterides where the deuterons randomly occupy the cubic interstitial sites. The concept of relaxation described in sections 2.2 and 2.2.a.1 is only valid in the limiting case where the magnetisation recovery can be described by a single exponential. In the case of quadrupolar interactions which connect states $\Delta m = \pm 2$ (equation 2.21) resulting in non-single-exponential behaviour these concepts are only applicable in some restricted conditions. Firstly when the spin value is I = 1 (e.g. Deuterium) the relaxation can always be expressed by a single exponential. Secondly, this is also the case if the extreme narrowing condition is fulfilled, that is if the frequency

characterising the fluctuations of the E.F.G. is much larger than the Larmor frequency (Abragam 1961) and finally in the case where the spin lattice relaxation is much slower than the spin-spin relaxation, if the dipolar linewidth is broader than the splitting energy due to quadrupolar interactions; the concept of spin temperature is applicable and the spin-lattice relaxation can again be described by a single exponential (Abragam (1961), Andrew and Tunstall (1961)). If one of these conditions is fulfilled and if the fluctuating quadrupolar interactions can be regarded as a perturbation on the nuclear Zeeman energy the concept of relaxation may be applied. The associated relaxation times due to quadrupolar interactions are expressed in terms of the spectral density functions (Abragam (1961), Wolf (1979)) by

$$\frac{1}{T_{1Q}} = \frac{3}{20}\left(\frac{eQ}{\hbar}\right)^2 \frac{2I+3}{I^2(2I-1)} \left[J^{(1)}(\omega_o) + 4J^{(2)}(2\omega_o)\right] \qquad (2.29)$$

$$\frac{1}{T_{2Q}} = \frac{3}{40}\left(\frac{eQ}{\hbar}\right)^2 \frac{2I+3}{I^2(2I-1)} \left[3J^{(0)}(0) + 5J^{(1)}(\omega_o) + 2J^{(2)}(2\omega_o)\right] \qquad (2.30)$$

The similarity of the relaxation rate equations for nuclear dipole-dipole and quadrupolar interactions stems from the fact that both interactions involve the spin operator in the same way (Wolf 1979). The quadrupolar relaxation is induced by the fluctuation of E.F.G. which does not depend on the spin states of the surrounding nuclei but depends on the distribution of charged particles. In that case the three particle term, which is diagrammatically represented in fig. 2.3(b), can be described, if the particle at the origin is considered to be stationary by the motion of a particle initially at r_k from the origin to a site at r_j which was initially occupied by a particle which has diffused to site r_ℓ. This term should be very important in the case of quadrupolar relaxation. In the case

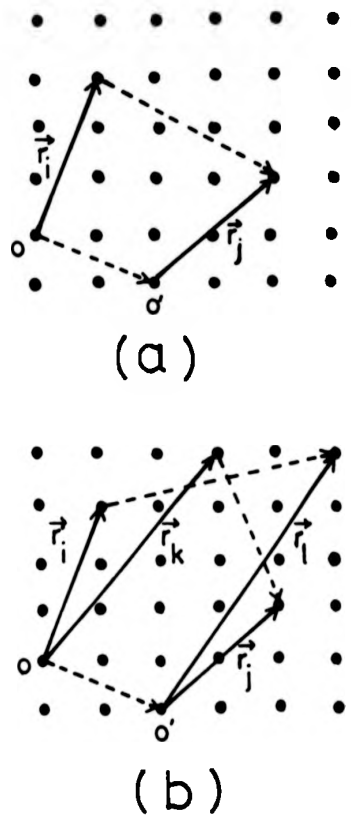

Fig. 2.3: Diagrammatic representation of the relative motions of particles on a two-dimensional lattice. The full arrows indicate the positions of particles relative to the origin (0 or 0′) at a given time and the broken arrows represent the particle displacements in time t.
(a) Illustrates the two-particle function which is the diffusion of a particle from $\vec{r}_i$ to $\vec{r}_j$ relative to the particle at the origin.
(b) Illustrates the three particle function which describes the diffusion of a particle initially at $\vec{r}_i$ to any site of the lattice except $\vec{r}_j$ or the origin and some other diffusing particle to $\vec{r}_j$.

of dipole-dipole interactions, the dipolar field at a given nucleus depends on the spin state of the surrounding nuclei and provided that the difference in the populations of the spin states is small (high temperature limit) and that the state of spin is not correlated to the atomic diffusion, the three particle term averages to zero (Titman 1973) (e.g. in the case $I = \frac{1}{2}$ the probability of having a spin up is equal to that of having a spin down). The three particle function produces terms in the relaxation equations which tend to cancel the two-particle terms. Sholl (1967,1974) and (Titman 1977) showed the importance of the three particle term in the case of liquids.

A recent treatment of the quadrupolar nuclear relaxation by translational diffusion in solids within the mean field formalism has been developed by Barton (1982). The three particle term is included and as expected is shown to play a very important role particularly at concentration higher than $c = 0.5$. The spectral density function is expressed as

$$J^{(p)}(\omega) = c(1-c)\, J_1^{(p)}(\omega) + c^2\, \Delta J_2^{(p)}(\omega) \qquad (2.31)$$

where $J_1^{(p)}(\omega)$ is the two particle spectral density and $\Delta J_2^{(p)}(\omega)$ is a spectral density describing the three particle term. The first term of equation (2.31) is the result of both the two particle term $c\, J_1^{(p)}(\omega)$ and the part of the three particle terms $- c^2 J_1^{(p)}(\omega)$ which can be expressed in terms of a two particle spectral density. The second term describes the other part of the three particle term. If an unscreened central potential is assumed: $v(r) \propto r^{-1}$, the resulting E.F.G. at the nucleus is proportional, as with the dipolar magnetic field, to r^{-3}. This results in an identical expression for $J_1^{(p)}(\omega)$ to that calculated in the case of a dipole-dipole interaction.

In the dilute limit (c→o) equation (2.31) reduces to

$$J^{(p)}(\omega) = c\, J_1^{(p)}(\omega)$$

In that limit the quadrupolar relaxation can be derived from existing calculations of $J_1^{(p)}(\omega)$ (e.g. Barton-Sholl 1980). As the concentration increases to c = 0.5, since c(1-c) goes through a maximum at c = 0.5, the first term in equation (2.31) decreases in magnitude and the second term of equation (2.31) becomes more important. But in the limit where $c^2 \Delta J_2^{(p)}(\omega)$ can still be neglected compared to c(1-c) $J_1^p(\omega)$ and assuming an unscreened central potential at the nucleus one can see that the quadrupolar relaxation rates are proportional to the corresponding dipolar rates. In the light of the importance of the three particle function particularly when c→1 the danger of using existing models which take into account only the two particle term should be pointed out.

2.2.b. Relaxation due to conduction electrons

Metal hydrides and deuterides exhibit relaxation processes due to the interaction of the nuclei with the conduction electrons. This interaction commonly called the hyperfine interaction should reflect the electronic structure of the M-H alloy. The hyperfine interaction between an electronic spin and a nuclear spin can be expressed by the Hamiltonian (Abragam 1961)

$$\mathcal{H}_{hyp} = -\gamma_I \gamma_S \hbar^2 \left\{ \left[\frac{\vec{I}.\vec{S}}{r^3} + \frac{3(\vec{I}.\vec{r})(\vec{S}.\vec{r})}{r^5} \right]_{dip} + \left[\frac{\vec{I}.\vec{l}}{r^3} \right]_{orb} + \left[\frac{8\pi}{3} \vec{I}\vec{S}\, \delta(r) \right]_{cont} \right\} \qquad (2.32)$$

where $\vec{r}$ is the vector joining the nuclear and electronic spins, $\vec{I}$ is

the electron orbital moment and γ_I and γ_S the gyromagnetic ratios of the nucleus and electron respectively. The first term is the dipole-dipole interaction between unlike spins I and S, the second term represents the orbital interaction and the last term is the Fermi contact interaction. Equation (2.32) can be written in a simpler way as

$$\mathcal{H}_{hyp} = -\gamma_I \hbar \vec{I} \cdot \vec{H}_{eff}$$

The time average component of the hyperfine field $\vec{H}_{eff}$ parallel to H_o produces the shift of the Larmor frequency known as the Knight shift (Knight 1949) which, as can be seen from equation (2.32), will in general contain orbital, dipolar and contact interaction contributions. If the symmetry at the nuclear site is cubic, the three components of the diagonalized dipolar tensor are equal and since the dipolar interaction is traceless the interaction disappears. The time dependence of the transverse components of the hyperfine fields provides a relaxation mechanism and contributes a conduction electron component $(1/T_{1e})$ to the total spin-lattice relaxation rate. It should be noted here that even for a site with cubic symmetry a dipolar contribution exists in contrast with the shift associated with dipolar interactions. In transition metals which are of particular relevance to our investigation a complication arises owing to the presence of d-electrons in the conduction band. The d electrons are able to polarise the inner s electron shell (and also the s conduction electrons) via an electrostatic exchange interaction resulting in an indirect contact hyperfine interaction. This effect contributes to both the Knight shift and the relaxation processes and is called the core polarisation contribution. Among all the processes described, in transition metals the three processes that are usually predominant are the contact interaction for s electrons

and the orbital and core polarisation interactions for d electrons (Winter (1971), Narath (1967)). Assuming that the electrons occupy two sub-bands, having respectively, densities of states at the Fermi level $N_s(E_F)$ and $N_d(E_F)$, the relaxation rate dut to the three contributions described can be expressed as (Obata (1963), Yafet and Jaccarino (1964), Korringa (1950)).

$$\frac{1}{T_{1e}} = 4\pi\hbar\gamma_I^2 k T \{[(H_{hf}^{(s)} N_s(E_F))^2 + (H_{hf}^{(d)} N_d(E_F))^2 q + [H_{hf}^{(o)} N_d(E_F)]^2 p\} \quad (2.33)$$

where $H_{hf}^{(s)}$, $H_{hf}^{(d)}$, $H_{hf}^{(o)}$ are s electron contact, d electron core polarisation and orbital hyperfine fields respectively. These are given by $H_{hf}^{(s)} = \frac{8}{3}\pi\beta \langle|\psi_s(o)|^2\rangle$, $H_{hf}^{(d)} = \frac{8}{3}\pi\beta \langle\psi_{cp}(o)^2\rangle$ and $H_{hf}^{(o)} = 2\beta \langle r^{-3}\rangle$ where β is the Bohr magneton and the averages are taken over all states at the Fermi level for s electrons, d electrons and for the orbital angular momentum respectively. p and q are band reduction factors related to the d wave functions symmetries at the Fermi surface. For cubic symmetry and pure d functions if f is the fractional Γ_5 symmetry of d orbitals at the Fermi surface

$$q = \frac{1}{3} f^2 + \frac{1}{2} (1-f)^2 \text{ and } p = \frac{2}{3} f(2 - \frac{5}{3} f)$$

The factor kT of equation (2.33) is associated with the fact that only electrons within kT of the Fermi level contribute to the relaxation i.e. in the presence of a static magnetic field only the electrons within kT of E_F are found unpaired. Equation (2.33) which is derived for a transition metal nucleus does not obviously describe the conduction electron contribution to the total relaxation rate of protons or deuterons which occupy interstitial sites of the host metal in transition metal hydrides. At the interstitial site position the d-conduction electronic wave function may have an s character

(Kazama, Fukai 1977). Therefore the first term of equation (2.33) should strictly be replaced by $H_{hf}^{(SL)} N_{SL}(E_F)$ where the subscript (SL) stands for s-like electron. The electronic relaxation rate which is related to the density of states at the Fermi level can provide information on the electronic structure of metal hydrides but one can only be definite about the contribution which is predominant in very few cases. For instance NMR studies of several Ti-based hydrides combined with band calculations have indicated that the main contribution to the proton spin relaxation rate due to the conduction electrons arises from the core polarisation term (Bowman et al (1981), Goring et al (1981), Nowak et al (1979), Korn (1983)). Equation (2.33) may usefully be written as $T_{1e}T = K$ where K is a constant. This relation is often referred to, loosely as the Korringa product or Korringa relation which strictly speaking is not correct since the Korringa relation relates $T_{1e}T$ and the Knight shift K with the restriction that the s contact interaction is the only contribution to the hyperfine interaction. When paramagnetic impurites with localised f or d electrons are present (e.g. Mn^{2+}, Gd^{3+}), the local magnetic moment can polarise the conduction electrons via an effective exchange interaction $J_{\sigma-\varepsilon} \vec{S}.\vec{\sigma}$. Here $J_{\sigma-\varepsilon}$ are the effective σ-ε exchange constants, $\vec{\sigma}$ refers to the s, p and d conduction electron spin and ε refers to the local moment arising from f or d electrons of spin $\vec{S}$. This exchange interaction creates an inbalance of the conduction electron spins which is large in the vicinity of the magnetic impurity, but decreases in an oscillatory fashion as the distance from the ion increases. This interaction can provide a coupling between magnetic ions which may result in magnetic ordering but even in the absence of ordering the polarised conduction electrons interact with the nuclear spin of the non magnetic ions via the contact, core polarisation and orbital terms. This indirect interaction is

called the R.K.K.Y. interaction (Ruderman and Kittel (1954), Kasuya (1956), Yoshida (1957)). Fradin (1970) derived an expression for the relaxation time in the case of an indirect contact interaction due to R.K.K.Y. interactions

$$\frac{1}{T_{1e}} = \eta \left(\frac{T}{T-\theta}\right) + \frac{1}{T_{1K}} \qquad (2.34)$$

where η is a constant and θ is the Curie-Weiss temperature. In the case of a dilute random distribution of impurities with localised magnetic moments Giovannini and Heeger (1969) used second-order perturbation theory to derive an expression for $\frac{1}{T_{1e}}$, in the case of an exchange R.K.K.Y. interaction giving rise to an indirect interaction. The resulting value of $\frac{1}{T_{1e}}$ is expressed as

$$\frac{1}{T_{1e}} = \frac{1}{T_{1K}} \{1 + C\alpha J^2 << s_z >>\} \qquad (2.35)$$

Here C is the mole fraction of impurities having a local moment, α is a constant, T_{1K} is defined as $T_{1K}T = K$ where K is a constant and $<<s_z>>$ is the thermal average of the localized spin. When $<<s_z>>$ follows a Curie law the additional term in $\frac{1}{T_{1e}}$ is temperature-independent. This is to be expected from equation (2.34) since in the low concentration limit the interaction between impurities can be neglected and the temperature-dependence is removed by putting θ equal to zero.

Both treatments neglect the effect of spin and atomic diffusion. Bernier and Alloul (1973) developed a qualitative expression for the spin lattice relaxation taking into account the spin diffusion to account for the results obtained in the case of CuMn where no atomic diffusion is present. It should be noted that the expression for T_1 can be generalized to the case where atomic diffusion is present which

is the case of metal-hydrides. This will be only briefly discussed in the following section since this type of interaction is thought to be negligible in our case.

2.2.c. Relaxation caused by paramagnetic impurities

The effect of paramagnetic impurities on relaxation times has been known for a long time. As early as 1949, Bloembergen investigated this effect in insulating solids. In earlier measurements in metal hydrides these effects have been neglected because they have been thought to be insignificant for concentrations of impurities in the ppm range. However the present investigation has unequivocally demonstrated their importance for concentration as low as 20 ppm and a detailed discussion of the theory is therefore presented in this section.

Two important situations can be distinguished. The first is where one has a dilute random distribution of paramagnetic impurities which do not interact with each other and the second where one has a large concentration of paramagnetic impurities which is characterised by the fact that the ions interact with one another. Only the former case will be discussed here since it is the only one relevant to the present investigation.

When the paramagnetic ions are stationary and the nuclei under study are diffusing two important parameters must be considered. These are the probability per unit time that a nucleus changes its spin state and the average time of encounter with a paramagnetic impurity. The first is related to the time-dependent interaction between the nucleus and the ion. This involves the strength of the interaction and a correlation time characterising the fluctuations. The second parameter is related to the spin diffusion coefficient or atomic diffusion coefficient whichever is the fastest. Spin diffusion arises

from the nuclear dipole-dipole spin flip term which is described by the B^{jk} term of equation (2.11) and by analogy with atomic diffusion can be pictured as the diffusion of spin magnetization. The correlation time τ_i^* characterising the time dependence of the interaction between the nucleus and the ion has two different origins. One is associated with the dwell time τ_D of the moving nucleus and the other is associated with the time τ_i characterising the dynamical fluctuations of the paramagnetic impurity electron spin. τ_i^* is the fastest of these two times. In a metal for instance τ_i is expected to follow a Korringa relation, that is, τ_i is inversely proportional to the temperature (Barnes (1981), Taylor (1975)) or in the case of a non metal τ_i is the result of interaction with lattice vibrations (phonons). In metal hydrides or deuterides, in general, the protons or deuterons are coupled to the paramagnetic ions both by direct dipole-dipole interactions and indirectly through the conduction electrons via the R.K.K.Y. interaction discussed in the previous paragraph. Both type of interactions are relatively long range compared to the transferred contact interaction encountered for example in PbF_2 (Vernon et al 1981). It is thought that in the systems under investigation here, the dipole-dipole coupling is the dominant interaction (see next chapter) but for the sake of completeness and understanding both types of interaction namely the short-range contact interactions and the long-range dipole-dipole interaction are discussed in what follows. The indirect R.K.K.Y. interaction is also briefly mentioned in the discussion of the latter interaction since there are some similarities.

2.2.c.1. Short-range contact interaction

If a transferred contact interaction is assumed, of the form $\vec{I}.\vec{A}.\vec{S}$, in the nearest neighbour (NN) position to a paramagnetic ion a nucleus experiences a hyperfine field

$$H_{hf} = \frac{|A|S}{\gamma}$$

where γ is the gyromagnetic ratio of the nucleus, s the spin of the paramagnetic impurity (e.g. for Gd^{3+}, $S = \frac{7}{2}$ and for M_n^{2+}, $S = \frac{5}{2}$) and $\vec{I}.\vec{A}.\vec{S}$ is the hyperfine interaction which here for simplicity is described by the constant $|A|$ (isotropic interaction). The probability of a given nucleus being in the NN position to an impurity is zc where z is the coordination number and c the fractional paramagnetic ion concentration. The average encounter rate with paramagnetic ions is given by zc/τ_D where τ_D is the nuclear dwell time. In the limit where the duration of the encounter is sufficiently long so that the nuclear spin is fully relaxed during this time, the spin-lattice and spin-spin relaxation times are the same and are simply equal to the average rate of encounter with a paramagnetic impurity so that

$$\frac{1}{T_{1p}} = \frac{1}{T_{2p}} = \frac{zc}{\tau_D} \qquad (2.36)$$

In this limit $(\Delta\omega_{hf}^2\tau_i)\tau_D >> 1$ where $\Delta\omega_{hf}^2 = \langle\gamma H_{hf}\rangle^2$ and τ_i is the time describing the time dependent fluctuations of the electronic spins of the magnetic ion (i.e τ_i = the electronic relaxation time). This is equivalent to saying that the probability per unit time η_α of the nuclear spin being relaxed is much greater than the probability per unit time of a spin diffusing away from the NN position (i.e.: $\frac{1}{\tau_D}$). At the other extreme many encounters are required to effect relaxation of the nucleus and under this weak interaction condition the relaxation

times are given by

$$\frac{1}{T_{\alpha p}} = zc\ \eta_\alpha \qquad (2.37)$$

where α is either 1 or 2 so that the equation may be applied to either T_1 or T_2. Since we are dealing with an interaction which can be written as $\mathcal{H}_{hf} = \sum_{ab} \vec{I}_a \vec{A}_{ab} \vec{S}_b$ which for an isotropic hyperfine tensor can be simplified to $\mathcal{H}_{hf} = A[I_z S_z + \frac{1}{2}(I_+ S_- + I_- S_+)]$ where $I_\pm = I_x \pm iI_y$ and $S_\pm = S_x \pm iS_y$, the relevant transition frequencies are $(\omega_e - \omega_o)$ in the case of the longitudinal relaxation rate $\frac{1}{T_1}$ and $(\omega_e - \omega_o)$ and 0 in the case of the transverse relaxation rate $\frac{1}{T_2}$. Here ω_o is the Larmor frequency of the nuclear spin and ω_e is the electron Larmor frequency. Since generally $\omega_e >> \omega_o$ the expression $(\omega_e - \omega_o)$ will be taken as ω_e. One may consider the two limiting cases where

$$1/\tau_i^* >> \omega_e \quad \text{and} \quad 1/\tau_i^* << \omega_e$$

where τ_i^* is defined by $\frac{1}{\tau_i^*} = \frac{1}{\tau_i} + \frac{1}{\tau_D}$. In the first limit $\frac{1}{\tau_i^*} >> \omega_e$ $\eta_1 = \eta_2 \sim \Delta\omega_{hf}^2 \tau_i^*$ (Slichter 1963) in analogy with motional narrowing. In the limit where $\omega_e >> 1/\tau_i^*$, $\eta_2 \sim \Delta\omega_{hf}^2 \tau_i^*$ but, here η_1 is characterised by a different expression, $\eta_1 \sim \Delta\omega_{hf}^2 \left[\frac{\tau_i^*}{\omega_e^2 \tau_i^{*2} + 1}\right]$ (Abragam 1961) and in this case $\frac{1}{T_{1p}} \neq \frac{1}{T_{2p}}$. For simplicity one can assume that $\frac{1}{\tau_i^*} = \frac{1}{\tau_D}$ and $\omega_e \tau_D << 1$. With these conditions expression (2.37) can be rewritten as

$$\frac{1}{T_{1p}} = \frac{1}{T_{2p}} = zc\ (\Delta\omega_{hf})^2\ \tau_D \qquad (2.38)$$

This case is equivalent to $\Delta\omega_{hf}\ \tau_D << 1$ (weak collision). It can be

seen from equations (2.36) and (2.38) that as τ_D decreases with temperature $^1/T_{1p}$ and $^1/T_{2p}$ pass through a maximum when $\Delta\omega_{hf}\tau_D \sim 1$. The maximum is due to the transition from the strong to weak collision case. This is true as well if $\tau_i^* = \tau_i$ and $\omega_e\tau_i << 1$, but in that case the temperature dependence of $^1/T_{\alpha p}$ would be that of τ_i and the maximum in the rate is characterised by $(\Delta\omega_{hf})_{eff}$ $\tau_D \sim 1$ where $(\Delta\omega_{hf})_{eff} \cong (\Delta\omega_{hf})^2\tau_i$. At low temperatures spin diffusion takes over from atomic diffusion as the agent of relaxation when $T_{2RL} \leq \tau_D$ where T_{2RL} is the rigid lattice spin-spin relaxation time due to the spin-spin nuclear dipole interaction. Thus equation (2.36) becomes $^1/T_{\alpha p} \sim zc/T_{2RL}$ and is independent of temperature. It should be noted that this can only be true if the spin diffusion barrier radius b defined as the minimum distance which still enables the spin to communicate via dipole-dipole interaction is small enough so that the spin diffusion is effective in transporting the magnetization to a nearest neighbour site to the paramagnetic impurity.

Richards (1978) using a perturbative treatment found that the relaxation rates $^1/T_{1p}$ and $^1/T_{2p}$ could be expressed as

$$\frac{1}{T_{\alpha p}} = (1-\langle f_\alpha \rangle)\ \frac{zc}{\tau_D} \qquad (2.39)$$

If $\tau_i << \tau_D$ and $G_\alpha(0)\tau_i\tau_D >> 1$ or $\tau_i >> \tau_D$ and $G_\alpha(0)\tau_D^2 >> 1$ then $\langle f_\alpha \rangle << 1$ and expression (2.39) reduces to $\frac{1}{T_{\alpha p}} = \frac{zc}{\tau_D}$ as predicted by the simple model. $G_\alpha(0)$ is defined by $G_\alpha(0) = 2/3\ \mathbf{S}(\mathbf{S}+1)\ A^2$ for an isotropic transferred contact interaction. At the other extreme for $\tau_i >> \tau_D$ and $\begin{cases} G_\alpha(0)\tau_D^2 << 1 \\ \omega_e\tau_D << 1 \end{cases}$, equation (2.39) reduces to $\frac{1}{T_{\alpha p}} =$ $zc\ G_\alpha(0)\tau_D$. The case where $\tau_i << \tau_D$ and $G_\alpha(0)\ \tau_i\tau_D << 1$ is considered

as well. In this limit $\frac{1}{T_{\alpha p}} = zc\ \eta_\alpha$ where $\eta_2 = \frac{1}{3} A^2 \$(\$+1)[\tau_i + \frac{\tau_i}{1+\omega_e^2\tau_i^2}]$ and $\eta_1 = \frac{2}{3} A^2 \$(\$+1)\ [\frac{\tau_i}{1+\omega_e^2\tau_i^2}]$.

Vernon et al (1981) have developed the so-called 'impact' model. In the strong collision limit (i.e. $G_\alpha(0)\tau_D\tau_i >> 1$ if $\tau_i << \tau_D$ or $G_\alpha(0)\tau_D^2 >> 1$ if $\tau_D << \tau_i$) unlike Richards model, the method does not rely on a perturbative treatment. Moreover the statistics of the motion are derived in a more rigorous manner leading to better agreement with experiment. The general form of $\frac{1}{T_{\alpha p}}$ is the same as that derived by Richards except for a factor u which depends on the structure of the crystal and

$$\frac{1}{T_{\alpha p}} = (1 - \langle f_\alpha \rangle)\ \frac{zc}{u\tau_D} \qquad (2.40)$$

In the case of PbF_2, which forms the CaF_2 structure $u \sim 4$. If allowance is made for the factor u in the treatment developed by Richards, the two models agree very well in both the strong and weak collision limits. The main difference lies in the value of $T_{\alpha p}$ where the rate goes through the maximum.

2.2.c.2. Dipole-dipole interactions

The differences between the treatments of the contact and dipole-dipole interactions come essentially from the fact that the volumes over which the impurity is active, in the former case, it is constant and equal to $\frac{4\pi}{3} a_o^3$ where a_o is the nearest neighbour distance while in the latter case, due to the longer range of the interaction, this volume is much larger and varies as τ_i and τ_D change with temperature. Therefore the distance characterising this volume is a variable parameter of the problem. A simple qualitative picture can be drawn in a similar way to that in the previous paragraph. In the slow hopping limit (strong collision)

the relaxation times are the average time required for a diffusing spin to first encounter an impurity. Similarly to the previous case, it is assumed that relaxation effectively takes place instantly once the impurity is encountered. If one imagines that there is one impurity in the volume $\frac{4\pi}{3} R^3 = v$ and that $\Delta v = \frac{4\pi}{3} \beta^3$ is the volume over which a paramagnetic impurity is active (β will be defined more rigorously later) then if the spin is not in the region Δv, it is not relaxed but it is relaxed once it diffuses into Δv. If the time $\langle\tau\rangle$ is defined as the time a diffusing particle spends in Δv, the effective dwell time is $\langle\tau\rangle \sim \beta^2/D$ and the probability of finding a spin in the volume Δv is $\frac{\Delta v}{v}$. So the average paramagnetic encounter rate is $\frac{\Delta v}{v\langle\tau\rangle} = \frac{4\pi}{3} N \beta D$ where $N = \frac{1}{v}$ is the concentration of paramagnetic ions per unit volume. Since the limit of the slow hopping regime occurs when the probability per unit time of a spin being relaxed is equal the reciprocal of the average dwell time of a spin in the volume Δv, the size of the volume Δv is determined by $\langle\tau\rangle = \frac{1}{\eta_\alpha(\beta)}$. For the dipolar interaction $\eta_\alpha(r) = C_\alpha/r^6$ and therefore the relaxation times can be written as $1/T_{\alpha p} \cong \frac{4\pi}{3} N D (C_\alpha/D)^{1/4}$ where C_α represent the strength of the dipolar interaction (defined rigorously later). The strength of the dipolar interaction can be written in the limit where $\tau_i \ll 1/\omega_o, 1/\omega_e$ as $C_\alpha \sim c' \tau_i$ where c' is a constant. If for simplicity one assumes that $\tau_i \ll \tau_D$ and is inversely proportional to the temperature then as the temperature is increased D increases and the volume Δv decreases. When for a given temperature the condition $\beta \ll a_o$ which is equivalent to $\eta_\alpha(a_o)\ \tau_D \ll 1$, is reached many encounters with a paramagnetic impurity are required to produce relaxation and the relaxation rate becomes $\frac{1}{T_{\alpha p}} = \frac{\Delta v}{v} \eta_\alpha(a_o)$. This expression is similar to the one derived in the same limit for the short-range contact interaction

(equation 2.37). Here $v = \frac{4\pi}{3} R^3 = \frac{1}{N}, \Delta v = \frac{4\pi}{3} a_o^3$ and $\eta_\alpha(a_o) = \frac{C_\alpha}{a_o^6}$. In the limit where $\tau_i \ll \tau_D$ and assuming a Korringa relation $\tau_i = K/T$, then $\frac{1}{T_{\alpha p}}$ decreases with increasing temperature. Therefore $\frac{1}{T_{\alpha p}}$ goes through a maximum at the temperature for which $\tau_D \eta_\alpha(a_o) = 1$. The same argument can be applied if $\tau_D \ll \tau_i$. The maximum in $\frac{1}{T_{\alpha p}}$ is again the result of the transition from the strong collision to the weak collision cases. The only assumption made regarding the specific interaction is $\eta_\alpha(r) = \frac{c}{r^6}$ for the case of a dipolar interaction (i.e $\eta(r) \alpha H_d^2(r)$ where $H_d(r) \alpha \frac{1}{r^3}$). Therefore this qualitative argument can be generalised to different types of relatively long range interactions. For instance in the case of an indirect R.K.K.Y. interaction the local field is given by $H_{RKKY}(r) = \frac{\pi E_F}{2\mu_B} K J_{\sigma\epsilon} \rho(E_F) \langle \$_z \rangle \frac{\cos 2k_F r}{(K_F r)^3}$ where E_F is the Fermi energy of the host metal, K the Knight shift, $J_{\sigma\epsilon}$ the exchange integral between σ and ϵ electron; $\rho(E_F)$ the density of state at the Fermi level and $\langle \$_z \rangle$ the mean value of the z component of the impurity spin. This expression which can be simplified to $H_{RKKY}(r) = A \frac{\cos 2K_F r}{r^3}$ resembles that for the dipolar interaction and except for the oscillatory behaviour the same qualitative results should be expected. For a quantitative argument the geometry of the compound investigated has to be taken into account together with the shape of the Fermi surface.

In this development no assumption on the nature of D has been made. The nuclear dipole-dipole coupling between diffusing spin also provides a means whereby the relaxation effects produced in the neighbourhood of an impurity may be transferred to more distant nuclei. Thus the spin diffusion coefficient D_s is particularly relevant at low temperature where the atomic diffusion coefficient, which is

generally thermally activated, becomes much smaller than D_s. Following the formulation of Rorschach (1964) which applies to this particular region, the expression for the relaxation time is derived from the steady state solution of the total rate of change of the magnetization given by

$$\left.\frac{\partial M}{\partial t}\right)_{total} = \left.\frac{\partial M}{\partial t}\right)_{p} + \left.\frac{\partial M}{\partial t}\right)_{d} \tag{2.41}$$

where $\left.\frac{\partial M}{\partial t}\right)_{d} = D_s \nabla^2 M$ in the case of a continum medium (Bloembergen 1949) and $\left.\frac{\partial M}{\partial t}\right)_{p} = \eta_\alpha(r)(M-M_o)$. The parameter $\eta_\alpha(r)$ which is the relaxation rate a nucleus would have if held at a fixed distance r from the paramagnetic ion is expressed as

$$\eta_\alpha(r) = \frac{C_\alpha}{r^6} \tag{2.42}$$

where C_α is the constant defined earlier which is a measure of the strength of the interaction between an ion and a nucleus and is given (Bloembergen 1949) for a powder sample, averaged over all orientation, by

$$C_1 = \frac{2}{5}\gamma_p^2\gamma_n^2\hbar^2 J(J+1)\left[\frac{\tau_i}{1+\omega_o^2\tau_i^2} + \frac{7\tau_i}{3(1+\omega_e^2\tau_i^2)}\right] \tag{2.43}$$

$$C_2 = \frac{2}{5}\gamma_p^2\gamma_n^2\hbar^2 J(J+1)\left[\frac{2}{3}\tau_i + \frac{\tau_i}{2(1+\omega_o^2\tau_i^2)} + \frac{13\tau_i}{6(1+\omega_e^2\tau_i^2)}\right] \tag{2.44}$$

where the subscripts 1, 2 correspond respectively to η_1 and η_2 and where J, γ_p, τ_i, ω_e are the angular momentum, gyromagnetic ratio, spin lattice relaxation time and Larmor frequency of the ion respectively and γ_n is the gyromagnetic ratio of the diffusing nuclear spin. Since generally $\omega_e >> \omega_o$, ω_e^2 has been written for $(\omega_e \pm \omega_o)^2$ in the

last term of equations (2.43) and (2.44). These terms result from the non-secular part of the dipolar interaction which involves the transverse component of the electronic spin since that is the only component rotating at ω_e. In these terms τ_i should therefore be the time which is associated with changes of that component namely τ_i should be replaced by the electronic transverse relaxation time of the ion. But if there is no interactions between paramagnetic impurities (dilute solutions) and because in the case of a metal τ_i is expected to follow a Korringa relation which implies that the correlation rate involved in such interactions is generally much shorter than the characteristic frequencies ω_o and ω_e, the transverse and longitudinal relaxation times are equal.

The coefficient D_s was first derived by Bloembergen (1949) for a simple-cubic lattice and estimated to be $D_s \sim a_1^2/50\ T_{2RL}$ where T_{2RL} is the dipole-dipole rigid lattice spin-spin relaxation time for the diffusing nuclei and a_1 is the nearest-neighbour distance between diffusing nuclei. However a more rigorous treatment developed more recently by Lowe and Gade (1967) gives $D_s = 0.15\ \gamma_n^2 \hbar / a_1$ for the same structure, in the case of isotropic diffusion (i.e. the diffusion tensor is replaced by a constant). This value is usually about 4 times larger than that derived by Bloembergen. In the spin diffusion limit the pseudo-potential radius β is given by

$$\beta = \left[\frac{C_\alpha}{D_s}\right]^{1/4} \qquad (2.45)$$

This radius, is essentially the distance at which the rates for direct relaxation $\eta_\alpha(\beta)$ and for spin diffusion β^2/D_s are equal. Another parameter which must be defined is the barrier radius within which spin diffusion is inhibited because the time averaged field produced by the impurity at nearby nuclear sites has a gradient such that the

frequencies of adjacent nuclei are sufficiently different that mutual spin flips cannot occur anymore. The barrier radius has been discussed by Bloembergen (1949) and is given to first order by

$$b = (3 \langle \mu_p \rangle / \mu_n)^{1/4} a_1 \tag{2.46}$$

where μ_n is the nucleus moment and $\langle \mu_p \rangle$ the effective static component of the ion moment given by

$$\langle \mu_p \rangle = \gamma_p \hbar J [B^2(x) + \frac{\partial B(x)}{\partial x} \frac{2}{\pi} \tan^{-1} \frac{2\pi\tau_i}{T_2}]^{\frac{1}{2}} \tag{2.47}$$

here $B(x)$ is the Brillouin function with $x = \gamma_p \hbar J H_o / kT$, and H_o is the static applied field. This definition of the barrier radius implies that there is a sharp transition corresponding to the passage from a region where the spin diffusion occurs to a region where spin diffusion can no longer occur. However, Horwitz (1971) showed that some spin diffusion can occur within the radius b which is equivalent to a small reduction of b.

In the limit where $R >> b, \beta$. From the steady state solution of equation (2.41), Rorschachfinds the relaxation rate is given by

$$\frac{1}{T_{\alpha p}} = 8\pi N D_s \beta \frac{\Gamma(3/4)}{\Gamma(1/4)} \frac{I_{3/4}(\delta)}{I_{-3/4}(\delta)} \tag{2.48}$$

where $I_m(\delta)$ is the modified Bessel function of fractional order with $\delta = \beta^2 / 2b^2$ and $\Gamma(3/4)$ and $\Gamma(1/4)$ are gamma functions. From equation (2.48) two limiting cases can be considered. In the case where $\delta >> 1$, since $I_{3/4}(\delta) = I_{-3/4}(\delta)$ and $\Gamma(3/4)/\Gamma(1/4) = 0.338 \sim 1/3$ equation (2.48) reduces to

$$\frac{1}{T_{\alpha p}} \sim \frac{8\pi}{3} N D_s^{3/4} C_\alpha^{1/4} \tag{2.49}$$

This expression has the same structural form as the expression derived earlier in the development of the simple argument (slow hopping limit). Equation (2.49) was first derived by Khutsishvili (1962) and De Gennes (1958) and describes the regime commonly referred to as the slow spin diffusion limit. In the case where $\delta << 1$, $I_m(\delta) = \frac{1}{\Gamma(m+1)} (\delta/2)^m$, and equation (2.48) reduces to

$$\frac{1}{T_{\alpha p}} = \frac{4\pi}{3} \frac{NC_\alpha}{b^3} \tag{2.50}$$

This characterises the fast diffusion regime and was first dervied by Blumberg (1960).

As the temperature is increased atomic diffusion eventually becomes faster than spin diffusion and provides a more efficient means of transferring relaxation effects in the vicinity of the impurity to the rest of the sample. Shen (1968) first suggested replacing D_s by the atomic diffusion coefficient D_a when the condition $D_a >> D_s$ was fulfilled. Richards (1978) showed that under this condition the replacement of spin diffusion by atomic diffusion could be extended to Rorschach's general equation. In that limit the relaxation rate is written as

$$\frac{1}{T_{\alpha p}} = 8\pi N D_a \beta' \frac{\Gamma(3/4)}{\Gamma(1/4)} \frac{I_{3/4}(\delta_a)}{I_{-3/4}(\delta_a)} \tag{2.51}$$

where $\delta_a = \beta'^2/2a_o^2$ with a_o defined as the closest distance of approach of a diffusing nucleus to a paramagnetic ion and where $\beta' = (C_\alpha/D_a)^{1/4}$. In equation (2.43) and (2.44) τ_i should be replaced by τ_i^* defined by $\tau_i^{*-1} = \tau_i^{-1} + \tau_D^{-1}$. As the temperature is further increased D_a increases and the value of β' decreases until eventually $\beta' << a_o$. In this fast atomic diffusion limit equation (2.51) reduces to

$$\frac{1}{T_{\alpha p}} = \frac{4\pi}{3} N a_o^3 \eta_\alpha(a_o) \qquad (2.52)$$

This expression is identical to the equation derived earlier in the weak collision limit. The transition from the strong to weak collision case is achieved for either $\beta' = a_o$ or $\beta = a_o$ which ever occurs first. This is equivalent to $\tau_D = {}^1/\eta_\alpha(a_o)$ or $T_{2RL} = {}^1/\eta_\alpha(a_o)$ respectively. This corresponds to the temperature for which $\frac{1}{T_{\alpha p}}$ goes through a maximum. It should be noted that even though the condition $\delta << 1$ may be realised in the spin diffusion regime, leading to an expression for the relaxation rate ${}^1/T_{\alpha p}$ independent of the spin diffusion coefficient, one cannot assume that this will necessarily result in a relaxation rate independent of the diffusion coefficient in the atomic diffusion regime which would give an expression for ${}^1/T_{\alpha p}$ that does not go through a maximum. As has been stressed earlier the maximum in ${}^1/T_{\alpha p}$ is the result of the transition from the strong to the weak collision limit and the only case for which no maximum in ${}^1/T_{\alpha p}$ will be obtained is when the condition $\beta < a_o$ is satisfied in the spin diffusion regime.

Richards (1978) has also treated the intermediate case where D_s and D_a are comparable and has derived a general expression covering the entire range of temperature ($D_s >> D_a$, $D_s \sim D_a$, $D_a >> D_s$). Equations (2.51) and (2.48) are in fact limiting cases of this more general expression which can be written as

$$\frac{1}{T_{\alpha p}} = 8\pi N \beta(D_a + D_s) \frac{\Gamma(3/4)}{\Gamma(1/4)} \frac{q I_{3/4}(\delta) - I_{-1/4}(\delta)}{q I_{-3/4}(\delta) - I_{1/4}(\delta)} \qquad (2.53)$$

where $q = \frac{\beta_1^2}{\beta'^2}\left[1 + \frac{D_s}{D_a}\right]\frac{K_1}{K_2}$

with

$$K_1 = I_{-1/4}(\delta') - \frac{I_{3/4}(\delta_a)}{I_{-3/4}(\delta_a)} I_{1/4}(\delta')$$

$$K_2 = I_{3/4}(\delta') - \frac{I_{3/4}(\delta_a)}{I_{-3/4}(\delta_a)} I_{-3/4}(\delta')$$

in which $\beta_1 = \left(\frac{C_\alpha}{D_a + D_s}\right)^{1/4}$ $\beta' = \left(\frac{C_\alpha}{D_a}\right)^{1/4}$

and

$$\delta = \beta_1^2/2b^2, \ \delta' = \beta'^2/2b^2 \ \text{ and } \ \delta_a = \beta'^2/2a_o^2$$

The rate $(^1/T_{1p})$ has been calculated using equation (2.53) and the results are shown in fig. 2.4. In the calculation which does not apply to a particular system the concentration of paramagnetic ions has been kept constant for the three curves (a), (b) and (c). The only parameter which has been changed is the prefactor of equation (2.43), which affects the stength of the interaction only, making possible an illustration of the transition from strong to weak collision cases-curves (a), (b) and (c). Curve (a) shows clearly the maximum which occurs for $\tau_D = \eta_1(a_o)$ or $\beta \sim a_o$. The high temperature side of the maximum reflects the temperature dependence of τ_i which has been arbitrarily chosen to follow a Korringa relation and which is always shorter than τ_D. As expected a frequency dependence occurs only for $\tau_D < {}^1/\eta_1(a_o)$ and results from the terms involving ω_e in equation (2.43). As the strength of the interaction is reduced by a factor of 3 in curve (b) the condition $\beta \leq a_o$ is nearly realised in the spin diffusion regime. The maximum can still be seen but is shifted to lower temperature. Curve (c) for which C_1 has been reduced by a further

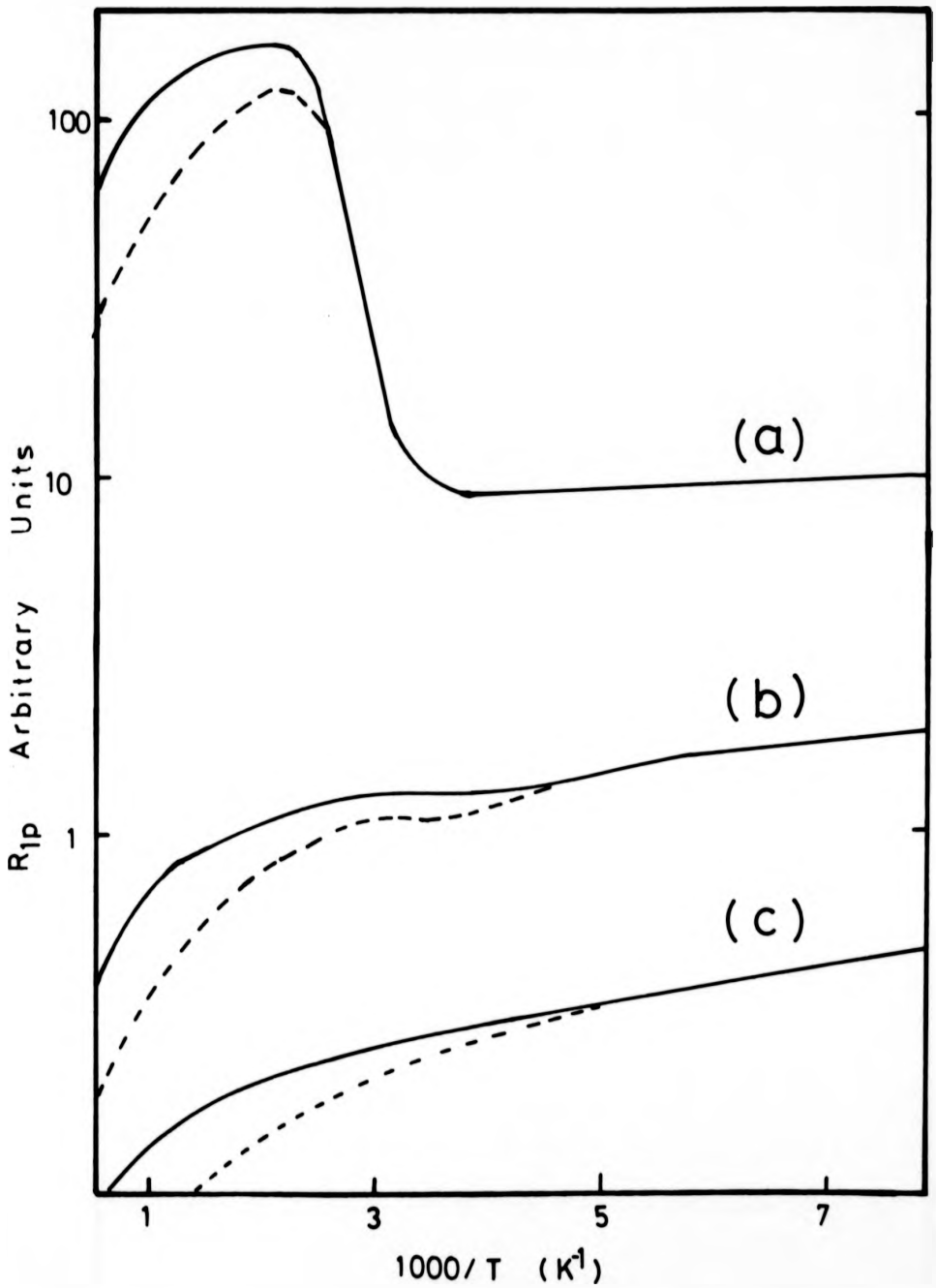

Fig. 2.4: Relaxation rate due to dipolar interactions between paramagnetic ions and diffusing nuclei. The full curves are calculated for the Larmor frequency ν_0 = 7 Mlz and the broken curves for ν_0 = 45 Mlz. Details of the various curves are given in the text.

factor of 2 shows clearly that no maximum occurs. This results from the fact that β is always less than a_o over the complete range of temperature (weak collison) and curve (c) now reflects the temperature and frequency dependence of C_1 (equation 2.43).

The predictions of the temperature dependence of the relaxation rates in the case of the two different types of interactions discussed here can be summarized as :-

(a) spin diffusion regions: assuming that $b < a_o$ the short-range contact interaction is characterised by a constant rate independent of the temperature while the dipolar interaction shows a temperature dependence arising from $C_\alpha^{1/4}$.

(b) Slow atomic diffusion: if the diffusion processes can be described by an Arrhenius relation, the former interaction gives rise to a $T_{\alpha p}$ temperature dependence which can be characterised by the activation energy of the diffusion process (i.e. $T_{\alpha p} \propto \tau_D$) while for the latter interaction the temperature dependence of $T_{\alpha p}$ is that of $\tau_D^{3/4}$ (in the case where C_α is not temperature dependent or only weakly so).

(c) Fast atomic diffusion: the temperature dependence of $T_{\alpha p}$ arises from that of $1/\eta_\alpha$ which in the case of both types of interaction depends on $\tau_i^{*-1} = \tau_i^{-1} + \tau_D^{-1}$.

2.2.d. Other relaxation mechanisms

The relaxation mechanisms discussed in the previous paragraphs are the most relevant processes as far as this investigation is concerned, but it should be noted that there are other possible sources of relaxation. For instance in diamagnetic substances the second order magnetic effects due to the polarisation of the electron cores by the applied field H_o is generally anisotropic giving rise

to an interaction which can be expressed by the Hamiltonian

$$\mathcal{H} = -\gamma\hbar \sum_{n=1}^{N} \vec{H}_o \hat{A}_n \vec{I}_n \qquad (2.54)$$

where $\hat{A}_n$ is a second-rank tensor $\hat{A} = [a_{ik}]$. This interaction can be written in term of lowering and raising operators as (Wolf 1979)

$$\mathcal{H} = -\hbar\omega_o \sum_{n=1}^{N} \sum_{q=-1}^{q=+1} I_n^{(q)} L_n^{(q)} \qquad (2.55)$$

where $I_n^{(0)} = I_{nz}$; $I_n^{(\pm 1)} = I_n^{\pm}$ and $L_n^{(0)} = (a_{33})_n$;

$$L_n^{(\pm 1)} = \frac{1}{2}\{(a_{13})_n \mp i(a_{33})_n\}$$

The form of the Hamiltonian indicates that the non secular term ($q=\pm 1$) may give rise to spin lattice relaxation if the terms $L_n^{(q)}$ are time dependent. That is if the tensor $\hat{A}_n$ varies in time. In molecular crystals this time dependence may originate from rotation of molecules for instance. In metals showing electron paramagnetism the first order magnetic effects due to the contact term (see equation 2.32) may not be solely due to s electrons giving rise to an anisotropic Knight shift. This can be described by

$$\mathcal{H} = \sum_i \sum_m \gamma_n \gamma_e \vec{S}_m \hat{K} \vec{I}_i$$

where $\tilde{K}$ denotes the 'Knight shift anisotropy tensor'. In addition to the spin lattice relaxation associated with the isotropic Fermi contact interaction, a time dependence of the individual element of $\tilde{K}$ gives rise to another spin lattice relaxation mechanism. An other relaxation mechanism is associated with the rotation of molecules which if a localised distribution of electric charges is present, produces a magnetic field at the nucleus. The time fluctuations of this field produce what is called the 'spin-rotation' relaxation.

REFERENCES

Abragam, A: The principles of Nuclear Magnetism (Oxford University Press, New York, 1961).

Andrew, E. R., D. P. Tunstall: Proc. Phys. Soc., 78, 1 (1961).

Barnes, S. E : Advances in Phys., 30, 801 (1981).

Barton, W. A., C. A. Sholl: J. Phys. C, 9, 43151 (1976).

Barton, W. A., C. A. Sholl: J. Phys. C, 11, 4405 (1978).

Barton, W. A., C.A. Sholl: J. Phys. C, 13, 2579 (1980).

Barton, W. A: J. Phys. C, 15, 5123 (1982).

Bernier, P., H. Alloul: J. Phys. F, 3, 869 (1973).

Bloch, F: Phys. Rev., 70, 460 (1946).

Bloembergen, N., E. M. Purcell, R. V. Pound: Phys. Rev., 73, 679 (1948).

Bloembergen, N : Physica, 15, 386 (1949).

Blumberg, W: Phys. Rev., 119, 79 (1960).

Bowman, R. C., Jr., W-K. Rhim: Phys. Rev., B24, 2232 (1981).

Bustard, L. D: Phys. Rev., B22, 1 (1980).

Cohen, M. H., F. Reif: Solid State Phys., 5, 322 (1957).

De Gennes, P: Phys. Chem. Solids, 7, 345 (1958).

Eisenstadt, M. A. G. Redfield: Phys. Rev., 132, 635 (1963).

Fedders, P. A: Phys. Rev., B18, 1055 (1978).

Fedders, P. A., D. F. Sankey: Phys. Rev., B18, 5938 (1978).

Fradin, F. Y: J. Phys. Chem. Solids, 31, 2715 (1970).

Giovannini, B., A. J. Heeger: Solid State Commun., 7, 287 (1969).

Goring, R., R. Lukas, K. Bohmhammel: J. Phys., C14, 5675 (1981).

Horvitz, E. P: Phys. Rev. B3, 2868 (1971).

Kazama, S., Y. Fukai: J. Phys. Soc. Japan, 42, 119 (1977).

Kasuya, T: Prog. Theor. Phys., 16, 45 (1956).

Khutsishvili, G: Soviet Physics J.E.T.P., 15, 909 (1962).

Knight, W. D: Phys. Rev., 76, 1259 (1949).

Korn, C: Phys. Rev. B. (1983).

Korringa, J: Physica, 16, 601 (1950).

Lowe, I.J., S. Gade: Phys. Rev., 156, 817 (1967).

Narath, A: In Hyperfine Interactions (Academic Press, New York 1967).
Nowak, B., D. J. Zogal, M. Minier: J. Phys., C12, 4591 (1979).
Obata, Y: J. Phys. Soc. Japan, 18, 1020 (1963).

Resing, H. A., H. C. Torrey: Phys. Rev., 131, 1102 (1963).

Redfield, A. G: Phys. Rev., 98, 1787 (1955).

Richards, P. M: Phys. Rev., B18, 6358 (1978).

Rorschach, H. Jr: Physica, 30, 38 (1964).

Ruderman, M. A., C. Kittel: Phys. Rev., 96, 99 (1954).

Sankey, O. F., P. A. Fedders: Phys. Rev., B20, 39 (1979).
Shen, L: Phys. Rev., 172, 259 (1968).
Sholl, C. A : Proc. Phys. Soc., 91, 130 (1967).

Sholl, C. A : J. Phys. F., 4, 1556 (1974).

Sholl, C. A : J. Phys. C., 7, 3378 (1974).

Slichter, C. P : Principle of magnetic resonance (Harper and Row, New York, 1963).

Slichter, C. P : Principle of magnetic resonance (Springer Verlag, Berlin, 1978).

Sternheimer, R. M : Phys. Rev., 102, 731 (1956).

Taylor, R. H: Advances in Physics, 24, 681 (1975).

Titman, J. M: J. Phys. C, 6, 2417 (1973).

Titman, J. M: Phys. Rep., 33C, 1 (1977).

Torrey, H. C.: Phys. Rev., 96, 690 (1954).

Van Vleck, J. H : Phys. Rev., 74, 1168 (1948).

Vernon, S. P. Thayamballi, R. Hogg, D. Hone, V. Jaccarino: Phys. Rev., B24, 3756 (1981).

Winter, J: Magnetic Resonance in Metals (Clarendon Press, Oxford, 1971).

Wolf, D: Phys. Rev., B10, 2710 (1974).

Wolf, D: J. Magn. Res., 17, 1 (1975).

Wolf, D: J. Phys. C, 10, 3545 (1977).

Wolf, D: Spin Temperature and Nuclear Spin Relaxation in Matter (Clarendon Press, Oxford, 1979).

Yafet, Y., V. Jaccarino: Phys. Rev., A133, 1630 (1964).

Yoshida, K: Phys. Rev., 106, 893 (1957).

CHAPTER III : EXPERIMENTAL

3.1. The pulsed NMR spectrometer and magnet

Measurements were performed using a modified triple frequency Polaron spectrometer operating at 7,11 and 45 MHz. A block diagram of the spectrometer and peripherals is shown in fig. 3.1. The spectrometer consists of four main items: the pulse programmer, the transmitter, the receiver and the probe.

3.1.a. The pulse programmer

This unit built at Warwick University, is a slightly modified version of the digital pulse programmer designed by Conway (1974). The pulse programmer is a modular unit which consists of a 10 MHz clock module used to time four different channel modules. Provision of a 1 MHz clock output is available and is used to time the pulse gradient circuitry which is fully described in section 3.2. A block diagram of the pulse programmer is shown in fig. 3.2. The clock module also determines the repetition rate of a given pulse sequence (with repetition times selectable from 1 μs to 999 s) by providing clear and start pulses which are used to reset and trigger respectively the first of four channel modules connected in series. Each of these can supply up to 999 output pulses of continuously variable width and switchable time separation. Each succeeding channel module is reset and triggered in turn by a time delayed clear and start pulses supplied by the previous channel module. These occur either after each output pulse or after the last output pulse of the sequence. Independent time delayed output pulses of fixed width are also available from each channel module. These pulses which we call "trigger pluses" are used to externally trigger measuring devices such as oscilloscope, averager

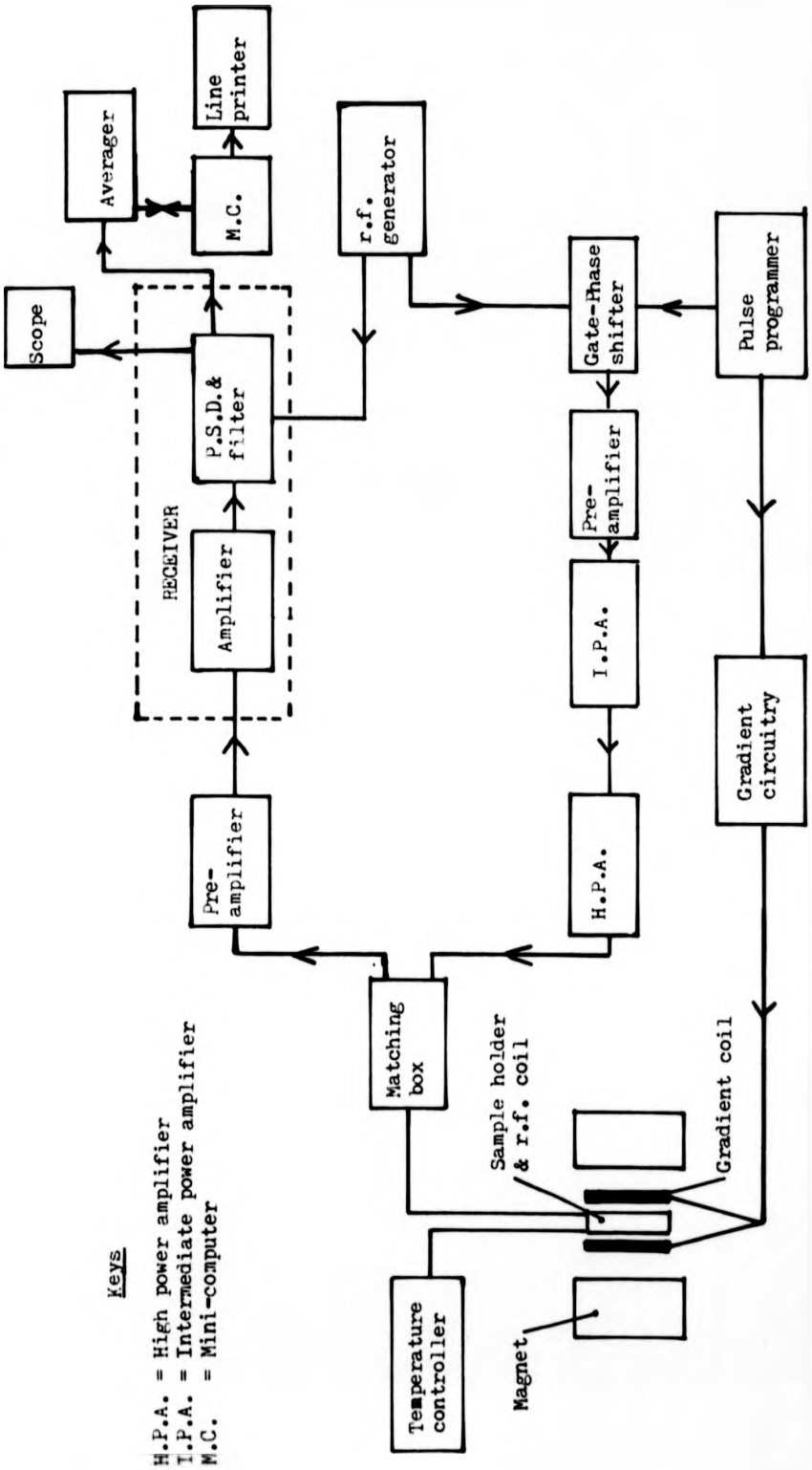

Fig. 3.1: Block diagram of the pulsed NMR spectrometer.

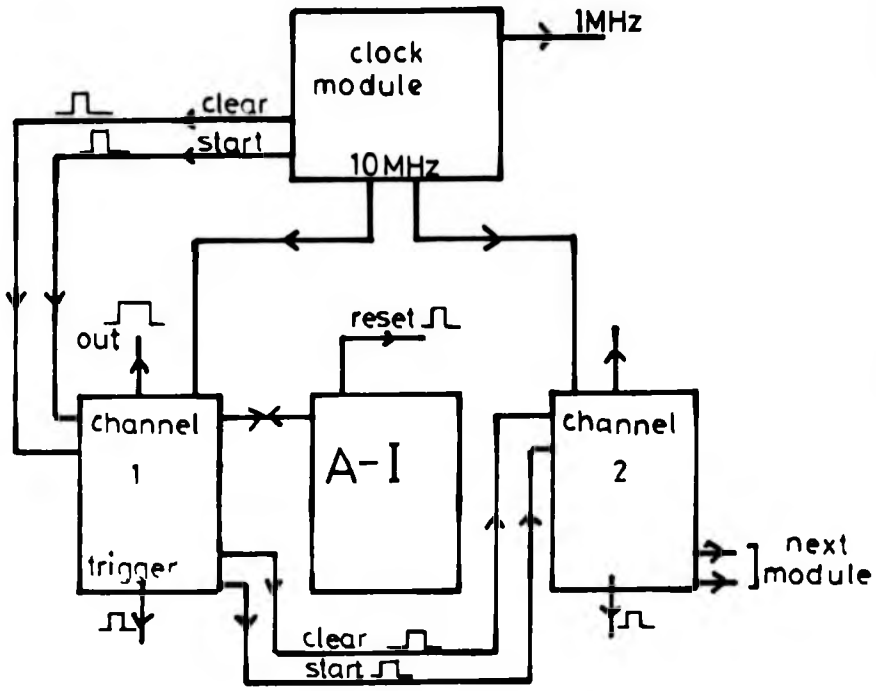

Fig. 3.2: Block diagram of the modular pulse programmer.

integrator and/or to synchronise the pulse sequence used with the gradient circuitry. Again trigger pulses can be selected to be output either after each main output pulse or after the last main output pulse of the sequence.

Two auto-increment modules based on the design of Adducci et al (1977) were added to the basic pulse programmer. These provide the facility of automatically incrementing the start pulse delay in a given channel module between preselected initial and final delays. The increment time can be selected to be either 1, 2, 4 or 8 times the time base set on the channel module. The sequence of increments can either be stopped after the final delay or indefinitly repeated. When used in the latter mode, an output pulse is provided after each final delay. This output pulse is used to reset the averager to the first channel (see section 3.4).

3.1.b. The transmitter

The radio-frequency signal was generated by a Marconi TF 2016 continuously variable signal generator locked to a Marconi TF 2173 digital synchronizer which delivered a 2 vpp signal divided into three outlets. One was used as reference for the phase sensitive detector (P.S.D.) in the receiver while the two others were fed to two independent phase shifters. Each phase-shifted continuous wave signal was then passed through gates controlled by the output pulses from the pulse programmer. The r.f. pulses thus produced were fed to a 10 W Marconi TF 2167 wide band amplifier followed by a two stage tunable high power amplifier. The transmitter was able to deliver approximately 1 kW of r.f. power into a 50 Ω load thus meeting the experimental requirements.

3.1.c. The probe system

A good probe system should not only be able to efficiently transfer energy from the transmitter to the coil and from the coil to the receiver, but should also protect the transmitter from possible reflected waves as well as the receiver against overloads. To perform ideally the probe should be connected to the transmitter only for the duration of the r.f. pulse and should present a pure resistive impedence equal to the transmitter output impedance while at the same time it is disconnected from the receiver. Following the transmitter pulse the coil should be connected to the receiver for signal reception while disconnected from the transmitter. To fulfil these requirements fast switching diodes and transmission lines were used. Fig. 3.3. shows the duplexer circuit used. The set of diodes D_1 and D_2 are effective short circuits in the transmission mode connecting the transmitter to the probe and disconnecting the receiver which is seen as a high impedance at the probe due to the transformer action ($z_I z_0 = z^2$) of the $\lambda/4$ transmission line. During signal reception the two set of diodes are open circuit disconnecting the transmitter from the probe and connecting the probe to the 50 Ω input impedance of the receiver. To cover the temperature range used in the experiments which extended from $\sim$ 100 K to $\sim$ 1300 K two different probe configurations were used. A low temperature (100 K to 500 K) probe based on a double coil system and a high temperature (300 K to 1300 K) single coil were used.

3.1.c.1. Low temperature probe

The matching box and probe circuitry are shown in fig. 3.4. The capacitors C_1 and C_2 were made from two concentric brass cylinders insulated by P.T.F.E. The inner cylinder could be continuously moved

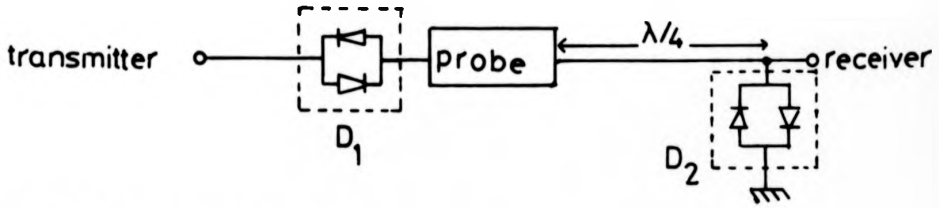

Fig. 3.3: Duplexer circuit used

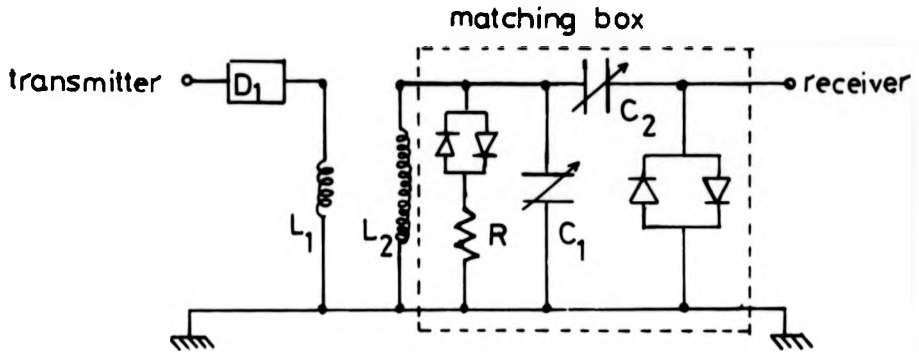

Fig. 3.4: Low temperature matching box and probe circuitry

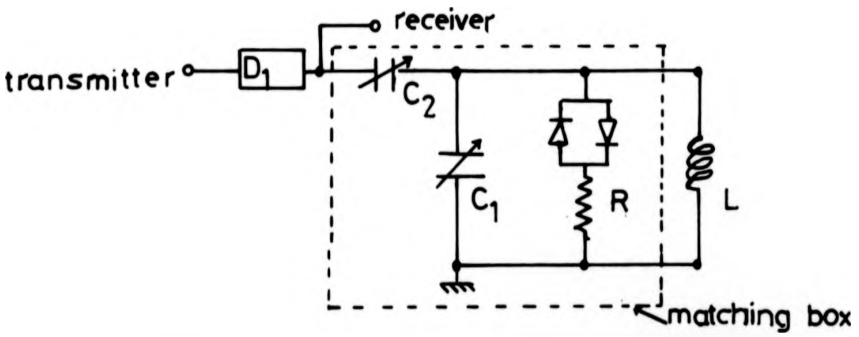

Fig. 3.5: High temperature matching box and probe circuitry

back and forth to give capacitances ranging from 30 pf to 90 pf. The resistor R, by determining the Q of the circuit, sets the ring down time following the transmitter pulse $t = \frac{2Q}{\omega_o} = \frac{2L}{r}$ where r is the equivalent series resistance of R. R was removed when operating at 45 MHz. The coils L_1 and L_2 were coaxial 10 mm diameter solenoids having a turn ratio of 1 to 3. At 45 MHz the coils consisted of 1 turn and 3 turns respectively of 16 gauge flattened bare copper wire while at 7 MHz, coils containing 10 and 30 turns respectively of 32 gauge bare copper wire were used. The tuning condition which in fact corresponds to proper matching of the probe to the characteristic impedance of the transmitter and receiver (50 Ω), was obtained by adjusting C_1 and C_2. An aerial signal was monitored and maximised to effect this tuning. The typical width of a 90° pulse for protons was ∿ 4 to 5 μs at 45 MHz and ∿ 2 μs at 7 MHz.

3.1.c.2. High temperature probe

The matching box and probe circuitry are shown in fig. 3.5. The different components used for the matching box were essentially the same as those described above. The single coil L was a simple solenoid of 9 mm diameter containing 8 turns of 0.3 mm O/D platinium wire for operation at 45 MHz and 22 turns for operation at 7 MHz. Typical width of a 90° pulse for protons was ∿ 5 μs at 45 MHz and ∿ 2 μs at 7 MHz. The poorer performance at 45 MHz compared to that at 7 MHz with both high and low temperature probe was in fact due to the lower power of the high power amplifier in the transmitter chain at the higher operating frequency.

3.1.d. The receiver

The r.f. NMR signal induced in the sample coil was amplified

and detected in the receiver system. The signal was amplified in a video preamplifier (gain = 60 dB) which is tuned to the operating frequency, enabling spurious signals to be eliminated, before being further amplified (gain = 50 dB) and phase sensitive detected with an ajustable bandwidth variable from 5 kHz to 1 MHz. The output signal was continuously monitored on an oscilloscope. The total dead time after a 90° pulse (receiver and probe ringdown) was $\sim$ 10 μs at 45 MHz and $\sim$ 20 μs at 7 MHz.

3.1.e. The magnet

The static magnetic field was supplied by a Varian Associates electromagnet having 9" diameter poles and a $1^3/4$" magnet gap. The magnet was stabilized by a Fieldial Hall Effect regulator capable of stabilities of 1 in 10^6 over periods of several hours. The maximum field obtainable was 13 kG with a homogeneity over the sample volume of better than 1 in 10^6.

3.2. Pulsed gradient field system

Generation of two identical magnetic field gradient pulses was obtained by using a current pulser designed and built in the laboratory by Cotts. The d.c. current is supplied to the current pulser by a bank of ten, 12 volt heavy duty accumulators connected in series. The width of the pulsed d.c. current could be adjusted from 0.1 ms to 9.9 s. The design of the two different quadrupole gradient coils used to generate the magnetic field gradient followed the descriptions of Webster and Marsden (1974).

The maximum value of the current used in the course of this study was 50 A. This corresponded to a rise time $t_r < 4\,\mu s$

3.2.a. Low temperature quadrupole gradient coil

The cylindrical gradient coil former was made of P.T.F.E. with four longitudinal channels of length 5 cm equally spaced round the circumference. Each of these had a further pair of channels on either side at an angle $\theta = 23°$ (see fig. 3.6). Enamelled copper wire, 0.37 mm in diameter was wound so that the direction of the d.c. current flow was opposed in each adjacent quadrant. The number of turns of wire as defined in fig. 3.6 was $N_0 = 10$ and $N_1 = 7$. The contours of percentage deviation from uniformity for a quadrupole coil of radius r is shown in fig. 3.7. In our case r = 9.5 mm and the radius of the sample was 3.2 mm thus no portion of the sample resided in a region where the deviation was greater than 1%.

3.2.b. High temperature quadrupole gradient coil

The high temperature quadrupole gradient coil was made by cutting four 5 cm long vertical channels in a 29 cm O/D pyrophillyte tubing. The four channels were symetrically placed at a 90° interval on the circumference of the former. Six windings of gold wire were placed on the former with neighbouring channels having opposite current flow. Insulation was accomplished by placing alternating windings inside thin thermocouple alumina tubing. The coil was fixed in position using Saureisen cement and thoroughly dried before usage. Fig. 3.8 shows the contour of precentage deviation from uniformity for this type of coil of radius r. In our case r = 14.5 mm and since the sample radius did not exceed 3.2 mm the maximum deviation from linearity was less than 1%.

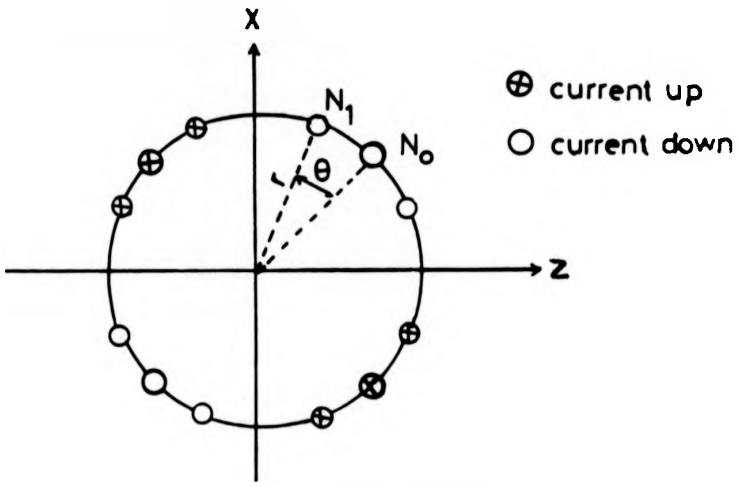

Fig. 3.6: Transverse cross-section of the low temperature quadrupole gradient coil. The windings are distributed on a cylindrical surface according to $N_1 = N_o \cos 2\theta$.

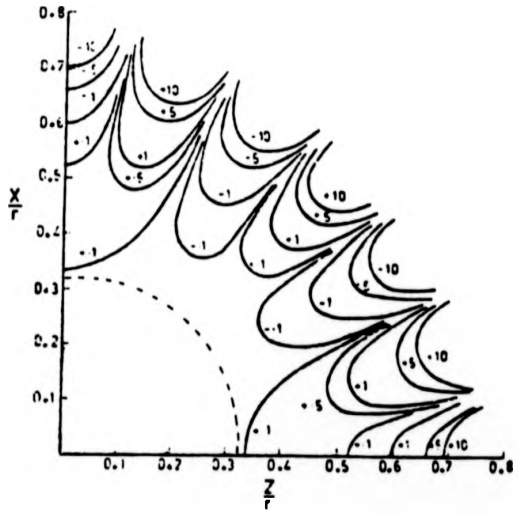

Fig. 3.7: Contour lines representing percentage deviation from uniformity near the centre for the low temperature gradient coil.

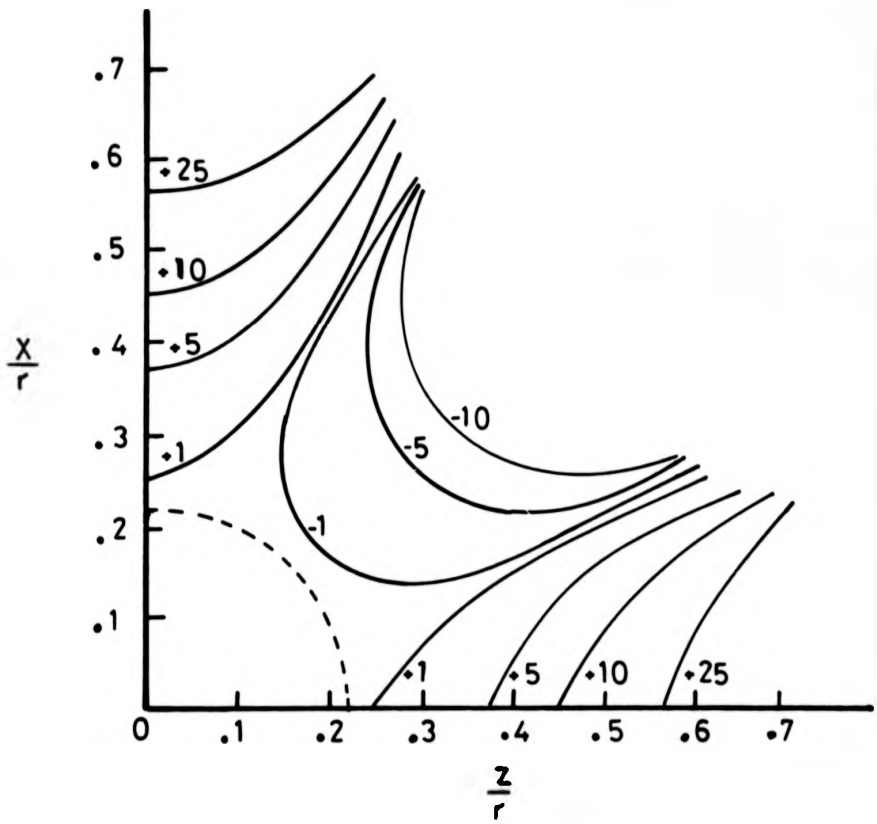

Fig. 3.8: Contour plot illustrating the percentage deviation from uniformity of the high temperature quadrupolar field gradient coil of radius r. The dotted line indicates our sample radius (after Webster and Marsden 1974).

3.3. Coil assembly and temperature controller

The employment of two different probe systems to cover the range of temperature investigated means that two different coil assembly designs were used in the course of this study.

3.3.a. Low temperature coil assembly

Fig. 3.9 illustrates the arrangement used. The copper block contained a 25 watts heater element and a sensing thermocouple (copper-constantan) connected to the temperature controller. The gradient coil was mounted inside a copper can which was tightly fitted to the copper block, allowing very good thermal and electrical contact. The temperature of the sample was measured with a calibrated copper-constantan thermocouple sitting at the base of the sample vial. A liquid nitrogen bubble pump was used to obtain temperatures ranging from room temperature down to liquid nitrogen temperature. The bubble pump which is shown schematically in fig. 3.10 consisted of a glass tube with a funnel - shaped end containing a heater element immersed in liquid nitrogen. Pulses of current supplied by the temperature controller were fed to the heater element which vaporised the liquid nitrogen surrounding the heater forming a bubble which pushed the liquid nitrogen enclosed in the glass tube upwards. The pulses of current in the heater caused a sequence of such bubbles to be produced which continuously pumped the liquid nitrogen out of the storage vessel. The rate at which the bubbles of liquid nitrogen were produced was controlled by adjusting the times for which the pulses of current were on and off. In order to achieve good temperature stability the level of liquid nitrogen in the bubble pump storage vessel had to be kept constant.

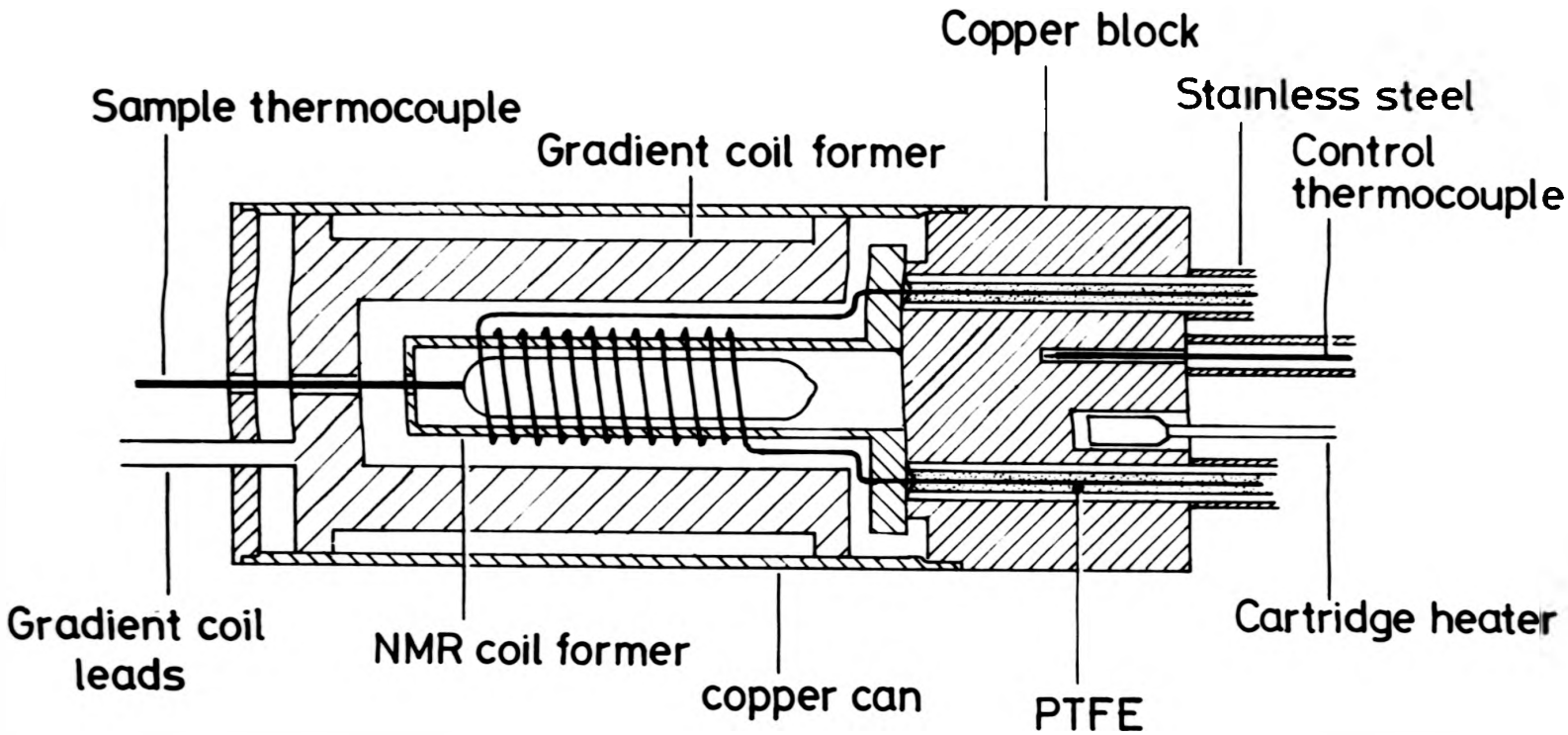

Fig. 3.9: Low temperature probe assembly.

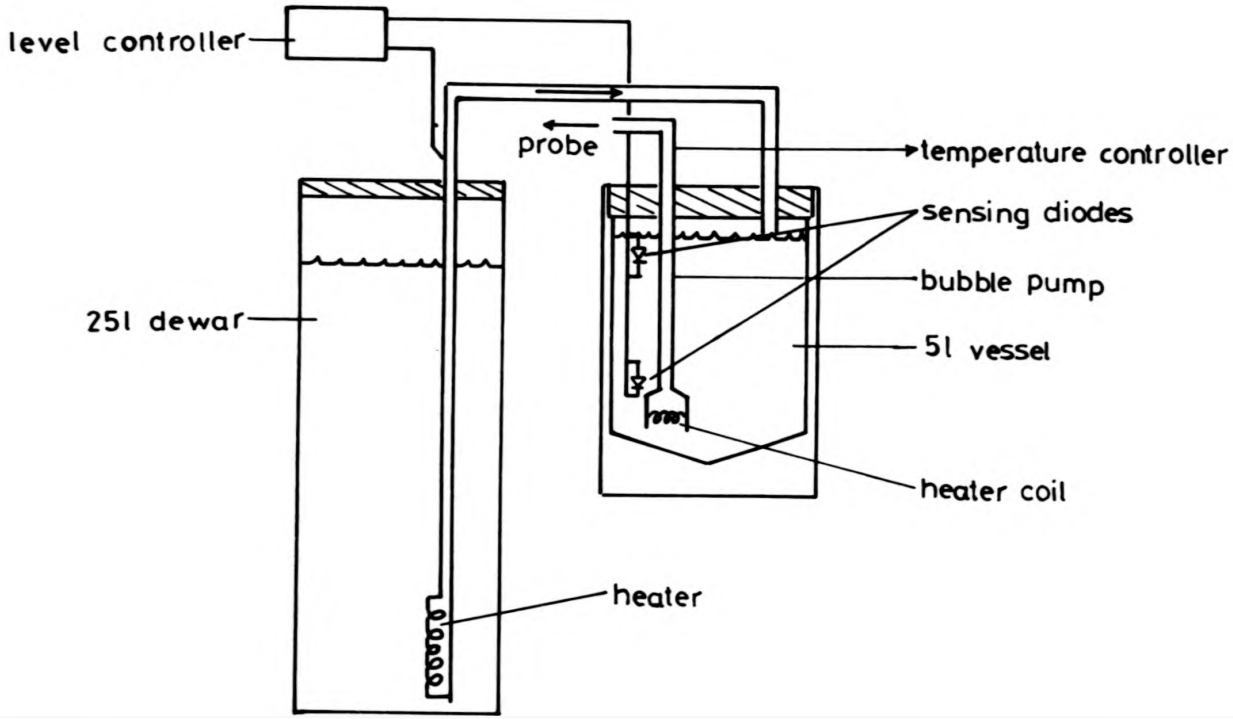

Fig. 3.10: Bubble pump arrangement.

A sensing diodewas therefore used to control the transfer of liquid nitrogen from a 25 litres storage dewar to the bubble pump vessel. Temperatures above room temperature were obtained using the heater element only. The maximum temperature of 500 K obtained was limited by the thermal stability of the P.T.F.E. used in the construction. The whole coil assembly was surrounded by a glass dewar vessel. The sample temperature-stability and homogeneity achieved was approximately ± 0.5 K.

3.3.b. High temperature coil assembly

In order to achieve high temperatures (up to ∿ 1300 K) a furnace constructed of refractory material was used. The coil assembly is illustrated in fig. 3.11. The water cooled jacket housing was made of a double walled brass cylinder providing good shielding from unwanted r.f. signals. The heater consisted of a nichrome non inductive winding mounted on the inside of a pre-threaded pyrophillyte cylinder. The heater was centred inside the pyrophillyte former of the high temperature gradient coil which was positioned and fixed in place by adequately filling the space of the housing with Zircar insulation felt and board. The housing was attached to the NMR coil support plate. The temperature of the sample was measured using a platinium platinium - 13% rhodium thermocouple in contact with the base of the sample tube. Two Farnell B30/10 power supplies (30V-10A) connected in series were used to provide the heater current. The e.m.f. of the thermocouple was continuously monitored with a digital microvoltmeter. Temperature stability was better than ± 0.5 k over the entire range.

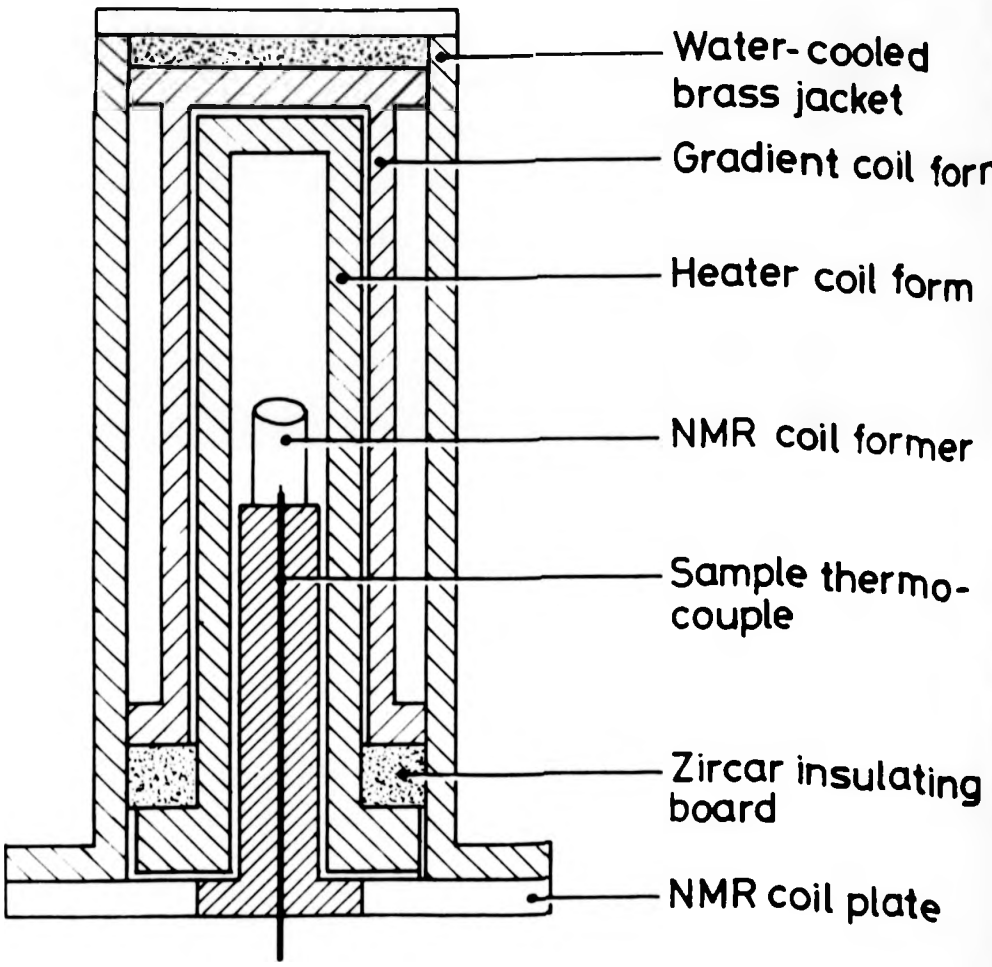

Fig. 3.11: The high temperature probe holder and oven assembly.

3.4. Experimental procedures and data aquisition

In a typical pulsed NMR experiment a d.c. magnetic field H_o ($H_o \sim 10^3$ to 10^4 G) is applied to polarise the spin system defining at the same time the z axis. In thermal equilibrium at temperature T the net magnetization of the spin system M_o is parallel to the z direction and can be expressed as

$$M_o = \langle M_z \rangle = \frac{N \gamma^2 \hbar^2 I(I+1) H_o}{3 kT} \quad \text{and} \quad \langle M_x \rangle = \langle M_y \rangle = 0$$

Here N is the number of spin per unit volume, γ the gyromagnetic ratio, I the spin of the nuclei and k Boltzmann constant. The pulsed NMR experiment is best described using a coordinate system (x′, y′, z′) rotating about the z axis (z′ parallel to z) at the frequency of the r.f. field, $H_1(t) = 2H_1 \cos \omega t$ applied along x and which can be described as the sum of two components one rotating at the frequency $\vec{\omega}$ while the other rotates at $-\vec{\omega}$. The first component appears stationary in the frame rotating at $\vec{\omega}$ and since the second rotates at $-2\vec{\omega}$, it is of no consequence in the following description. The classical equation of motion

$$\frac{d\vec{M}}{dt} = \vec{M} \wedge \gamma[\vec{H}_o + \vec{H}_1(t)]$$

becomes in the system of axis (x′, y′, z′)

$$\frac{\partial \vec{M}}{\partial t} = \vec{M} \wedge \gamma[\vec{k}(H_o - \frac{\omega}{\gamma}) + \vec{i}\, H_1]$$

where $\vec{k}$ and $\vec{i}$ are unit vectors along the z′ and x′ directions respectively. At the resonance frequency $\omega = \omega_o = \gamma H_o$ the effective field becomes $\vec{i}\, H_1$. Therefore the magnetization initially parallel to H_o (when $\omega << \omega_o$ and $H_1 << H_o$) precesses about the H_1

field with the angular frequency $\omega_1 = \gamma H_1$. If H_1 is switched on for a time t for which $\gamma H_1 t = \frac{\pi}{2}$ the magnetization is tipped into the (x′, y′) plane and induces, in the coil aligned in the direction perpendicular to the z′ axis, a voltage at the frequency ω_o. This signal which decays with a characteristic time T_2^* is known as the free induction decay (F.I.D.)

3.4.a. T_1 measurements

The recovery of the magnetization in the z direction is characterised by the spin lattice relaxation time T_1. During the experiment the principal axis of the sample coil is in the (x,y) plane and T_1 is measured by sampling the growth of the magnetization along the direction of the applied field H_o using a 90° sampling pulse applied at time τ after an initial disturbing pulse. The growth of magnetization M_z according to Bloch (1946) is expressed by

$$\frac{dM_z}{dt} = (M_o - M_z)/T_1 \qquad (3.1)$$

From the various pulse sequences designed to measure T_1, the accurate and widely used 180° - τ - 90° sequence was chosen for the present experiments. The 180° pulse rotates the magnetization into the -z direction and following a time τ a 90° pulse is applied to sample the value of the magnetization. The experiment is repeated for a number of different values. Under these limiting conditions

$$M_z\ (\tau=0) = -M_o \quad \text{and} \quad M_z\ (\tau=\infty) = M_o$$

The magnetization recovery is described by

$$M_z = M_o\ [1 - 2\ \exp(-\tau/T_1)] \qquad (3.2)$$

This method also has the advantage of enabling one to rapidly estimate

T_1 since $\tau = T_1$ Ln 2 for $M_z = 0$. When signal averaging is necessary, the magnetization must be allowed to return to its equilibrium value before the sequence is restarted. In order to fulfil this condition the time between a 90° pulse and the 180° pulse of the following sequence (180° - τ - 90°) was set to at least $6T_1$. The experiments were conducted on resonance and the magnetization was sampled for each value of the time separation between the 180° pulse and 90° pulse which could either be automatically or manually incremented. In most T_1 measurements τ was automatically incremented using the auto-increment module described earlier (section 3.1.a.). In all the measurements performed the signal to noise ratio was never adequate to allow an accurate measurement of T_1 in a single sequence of increments and signal averaging was performed using a Nicolet 1170 digital signal averager. The averager which contained 1024 channels could be used either in the internal address advance mode, where the internal clock of the averager was used to automatically advance the sampling window of the averager to successive channels or in the external address advance mode where an external TTL pulse was required. The sampling window of the averager was less than 1 μs however and therefore a very small portion of the F.I.D. would be sampled by each channel in either internal or external address modes. To alleviate this difficulty a linear intergrator, designed and built in the laboratory was connected between the receiver and averager and the latter used in the external address mode. In this system a sampling gate, triggered externally, was opened for a time comparable with T_2^* (see next section). The time for which the gate was open could be continuously varied from 1 μs to 300 ms. The integrator produced a d.c. signal directly proportional to the integrated F.I.D. as well as a TTL pulse used to externally address advance the averager. The

integrator was then automatically reset to zero d.c. volts ready for the next F.I.D. sample. For the T_1 measurements the averager was used in the external mode, the integrator was connected between the receiver and the averager and the auto-increment module was set to the repeat mode (i.e. at the end of the sequence of increments the auto-increment module sends a reset pulse to the averager and resets itself automatically to the initial delay τ_i before repeating the sequence). The integrator was triggered by a delayed pulse following the sampling 90° pulse. The time delay was set to be slightly larger than that of the dead time of the receiver and probe system. The sequence of increments was started manually and stopped automatically when the number of averages reached a preset value on the averager. The resultant signal on the averager was a curve which was described by equation (3.2). The number of data points describing this curve varied from 35 to 80 and the number of averages, which dependent on the operating frequency and temperature , was 8 to 32 at 7 MHz and 8 to 16 at 45 MHz. For analysis the data were then transferred to a Superbrain mini-computer which was interfaced with the Nicolet 1170. This method had the advantage of considerably reducing the averaging time since high frequency noise (compared to the characteristic frequency of the F.I.D.) was averaged out by the integrator. Fig. 3.12 a, b, show the arrangement used and the time sequence of events.

3.4.b. T_2 measurements

The precessing magnetization, in the laboratory frame following a 90° pulse decays with a charateristic time T_2 known as the spin-spin or transverse relaxation time. But due to static field inhomogeneities the experimental characteristic exponential decay time of the F.I.D. T_2^* is shorter than T_2 and can be expressed as:-

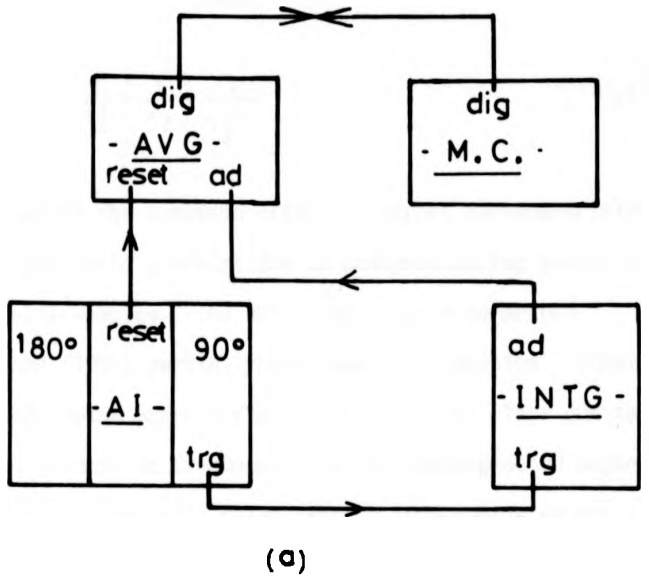

(a)

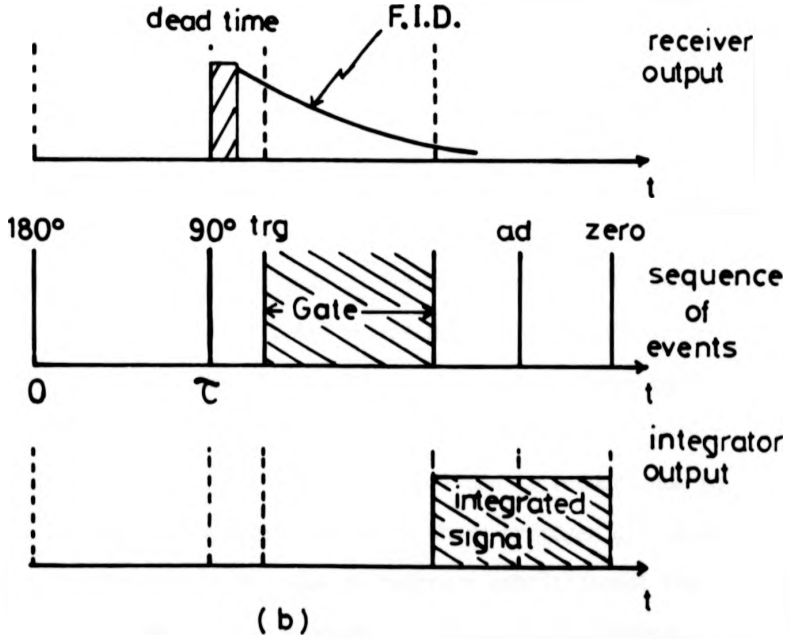

(b)

Fig. 3.12: (a) block diagram of the integrator, (b) timing sequence of events.

Keys: AVG = Averager, M.C. = Mini-computer, AI = Auto-increment, INTG = Integrator, dig = digital, RS232 input/output, trg = trigger pulse, ad = address advance pulse.

$$\frac{1}{T_2^*} = \frac{1}{T_2} + \frac{1}{T_2^{(1)}} \tag{3.3}$$

where $T_2^{(1)}$ is due to the combined effect of magnet inhomogeneities and the background field gradient due to demagnetizating fields in the powdered metal samples. The 90°-τ-180° spin echo method developed by Hahn (1950) partially overcomes this problem. After the 90° pulse the spins start dephasing in the (x,y) plane due to their different precession frequencies in the inhomogeneous magnetic field. Applications of a 180° pulse after a time τ rotates the spins by 180° and since the spins are still precessing in the same direction they will rephase and produce an echo at time τ after the 180° pulse whose amplitude depends only on T_2 if diffusion is negligibly small. The amplitude of the echo at time 2τ after the 90° pulse is expressed as

$$M(x,y) = M_o \exp\left(-\frac{2\tau}{T_2} - \frac{2\gamma^2 D\tau^3 G_o^2}{3}\right) \tag{3.4}$$

where D is the diffusion coefficient, G_o the magnitude of the field gradient and γ the gyromagnetic ratio of the nuclei. It can be seen from equation (3.4) that if the diffusion coefficient is large enough so that during the time 2τ a given spin is transported to a different part of the inhomogeneous field, the echo amplitude is reduced due to incomplete rephasing. In hydrogen in metals where hydrogen diffusion is relatively fast and, moreover, due to hydrogen embrittlement the samples are often in the form of a powder resulting in background gradients generally much larger than that of the magnet, Hahn's method cannot be relied upon to measure T_2. By using a multiple pulse sequence (90-τ-180°-2τ-180°...) Carr and Purcell (1954) showed that the effect of diffusion and background gradients is greatly reduced. This method was improved by Meiboom and Gill (1958) by phase

shifting all the 180° pulses by 90° relative to the first 90° pulse. This has the effect of eliminating the cumulative errors due to an inexact 180° pulse. In both methods a series of echoes is produced whose amplitude can then be expressed as

$$M(x,y) = M_o \exp\left(-\frac{2\tau}{T_2} - \frac{2D\gamma^2G^2\tau^3}{3n^2}\right) \qquad (3.5)$$

where n is the pulse number at time 2τ. This sequence known as the Carr-Purcell-Meiboom-Gill sequence (CPMG) was used for all T_2 measurements in the hydrides studied here. To be able to perform such a sequence two pulse programmer channel modules are required. The first is used to provide the 90° pulse and the second delayed by τ provides the series of 180° pulses with time separation 2τ. The measurements were always performed on resonance. Signal averaging was necessary and was performed using the Nicolet 1170 described in the previous section. The averager was again used in the external address advance mode and in order to record the full sequence of echoes giving a complete exponential decay for each sequence (i.e. 90°-τ-180°-2τ-180° ...) an address advance pulse was sent to the averager after each 180° pulse of the sequence. This was achieved using the time delayed trigger facility of the module producing the series of 180° pulses. Unfortunately in this case use of the integrator was only possible when relatively long spacings between 180° pulses could be used (i.e. $\tau \geq 0.25$ ms). This was inherent in the fact that a finite time had to be allowed for a reliable transfer of the data from the integrator to the averager and for the integrator to reset itself to zero. When the integrator was used the sampling gate was centred on the time for which the echo amplitude passed through a maximum by adjusting the time delay of the trigger pulse after each 180° pulse. The resulting dc signal, proportional to the

area of the echo, was fed to the averager together with an address advance pulse produced by the integrator so that the total magnetization decay described by equation (3.5) was measured for each sequence (i.e. 90°-τ-180°-2τ-180° ...). When τ < 0.25 ms the integrator could not be used and the signal was directly fed to the averager. As outlined previously the sampling window of the averager allowed only a very small portion of the echo to be sampled by a channel. In order to obtain the maximum signal to noise ratio possible the window was centred about the time for which the echo passed through a maximum, by setting the time delay of the trigger pulses provided by the channel producing the series of 180° pulses, to exactly t = τ. These trigger pulses were in this case used to address advance the sampling window to successive channels. In this method, only the amplitude of the echo at the maximum was sampled resulting in longer averaging time to achieve adequate signal-to-noise ratio. In both cases at the end of each CPMG sequence the averager was reset internally to the first channel automatically. The sequence was then repeated until the signal-to-noise ratio was adequate. The data were finally transferred to a Superbrain minicomputer for numerical analysis. The shortest T_2 measured using a CPMG sequence was T_2 = 70 μs. It was felt that although measurements of T_2 shorter than 70 μs could have been performed by fitting the F.I.D. to an exponential (when the line shape is purely Lorrentzian: $\Delta\omega\ \tau_D < 1$) or to a Gaussian ($\Delta\omega\ \tau_D > 1$) the resulting values of T_2 would have been too unreliable, for the reasons discussed above, to be adequately interpreted.

3.4.c. Diffusion coefficient measurements

Diffusion coefficients were measured using the best known and most widely used technique suggested by Stejskal and Tanner (1965). A magnetic field gradient of constant amplitude G is applied for a time δ between the 90° and 180° pulses and between the 180° pulse and the echo formation. The time interval between r.f. pulses is τ and the time interval between gradient pulses is Δ. The attenuation of the echo amplitude is then given by

$$A(2\tau) = A_o \exp\{-\frac{2\tau}{T_2} - \gamma^2 D^2 \{\delta^2 G^2 (\Delta - \delta/3) + {}^2/_3\, \tau^3 G_o^2 - \delta[(t_1^2 + t_2^2) + \delta(t_1 + t_2) + (2\delta^2)/3 - 2\tau^2]\vec{G}_o.\vec{G}\}\} \qquad (3.6)$$

where $t_2 = 2\tau - (t_1 + \Delta + \delta)$ and G_o is the background gradient. Fig. 3.13 illustrates the sequence used. Typically this technique was applied at constant spacing τ and for constant spacing Δ between magnetic field gradient pulses. The magnitude of the applied magnetic field gradient G was varied and the change in signal was monitored. Under these experimental conditions the attenuation of the echo caused by T_2 and G_o^2 background gradient processes becomes a constant and may be absorbed into the pre-exponential factor A_o. The accuracy of this method relies on the fact that the cross term $\vec{G}_o.\vec{G}$ can be neglected. Hence the inequality

$$|\vec{G}_o|/|\vec{G}| \ll {}^{\delta}/_{\tau} \qquad (3.7)$$

needs to be satisfied. Typically in the experiment performed to measure the diffusion coefficient of hydrogen in $YH_{1.98}$ δ = 2.028 ms and τ = 4 ms and the maximum value of G was 240 G/cm while for

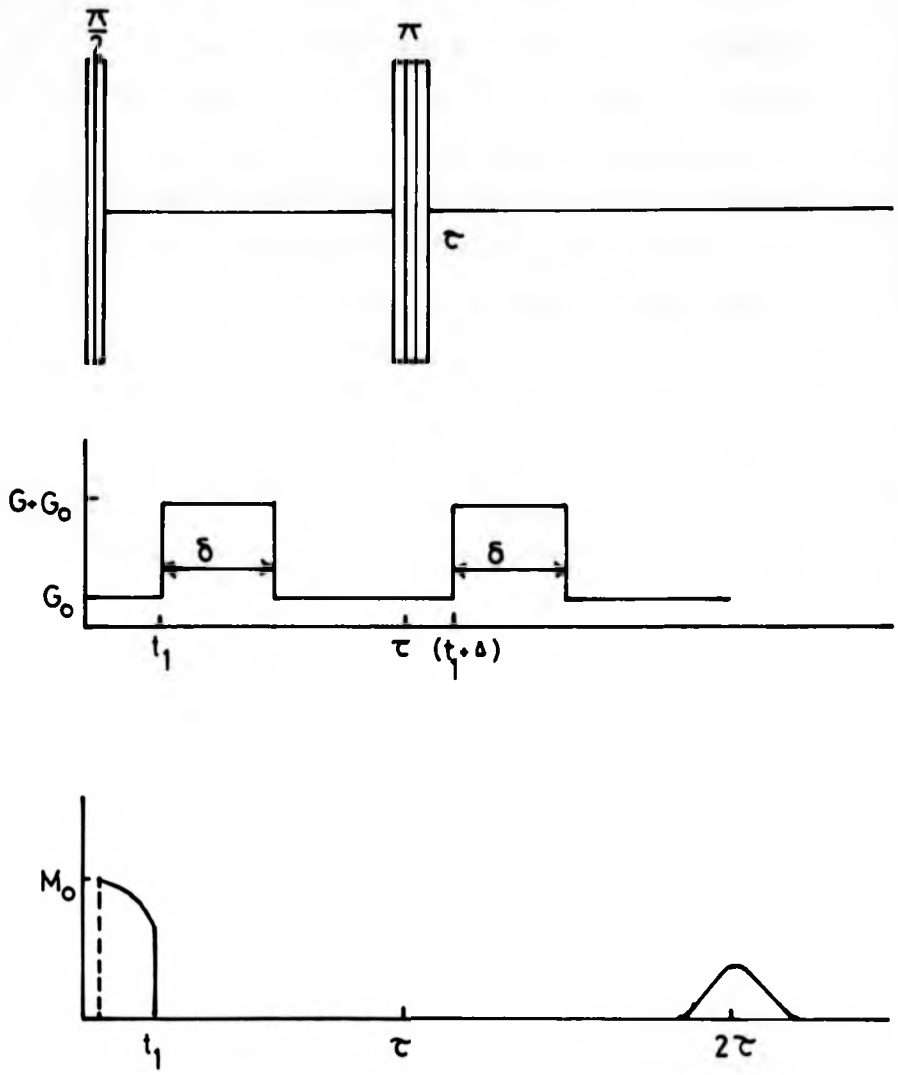

Fig. 3.13: The Stejskal and Tanner pulsed-gradient spin-echo sequence.

$Pd_{(1-y)}\ Y_{y=8\%}\ H_{0.51}$, δ = 3.5 ms, τ = 7 ms and G_{max} = 320 G/cm. To obtain a reasonably accurate value of D under these experimental conditions one requires G_o << 100 G/cm for $YH_{1.98}$ and G_o << 160 G/cm for $Pd_{(1-y)}\ Y_{y=8\%}\ H_{0.51}$. The background gradient arises since to overcome skin depth problems associated with metal hydrides and due to embrittlement of hydrogen polycristalline samples are used consisting of a random distribution of particles in which each particle experiences a local field due to the magnetization of nearby particles. If one considers that each particle has a magnetization $M \alpha \chi_V H_o R^3$ where χ_V is the volume susceptibility, H_o the applied field and R the radius of the particles. The magnetic field seen by other particles is $H \alpha M/r^3$ where r is the distance between particles hence the gradient G_o goes as M/r^4. Assuming a separation of particles equal to their radii, this gives a background magnetic field gradient $G_o \alpha \chi_V H_o/R$. The background gradient associated with the metallic powdered sample can be reduced by working at low magnetic field H_o. In our case the measurements were performed at 7 MHz, the lowest operating frequency available on the pulsed spectrometer corresponding to an operating field H_o = 1.644 kG. Murday and Cotts (1971) have applied a series expension of the $\vec{G}.\vec{G}_o$ term to the analysis of the Stejskal and Tanner pulsed gradient sequence. This analysis yielded the following approximate inequality for the diffusion coefficient.

$$D_{measured} < D < D_{measured} + \gamma^2 \bar{G}_o^{\,2} \tau^{*4} D^2_{measured}/(\Delta - \delta/3) \qquad (3.8)$$

Here $\tau^{*2} = [t_1^2 + t_2^2 + \delta(t_1 + t_2) + (2\delta^2)/3 - 2\tau^2]$

For measurements performed at constant τ

$$\bar{G}_o^{-2} = \int_{-G_1}^{G_1} \rho(G_o)\ G_o^2\ dG_o \qquad (3.9)$$

where $\rho(G_o)$ is a distribution of background gradients with maximum and minimum values G_1 and $-G_1$. In the derivation of the inequality it is assumed that the distribution $\rho(G_o)$ is continuous and symmetric about $|\vec{G}_o| = 0$ and that the magnitude of the background gradients experiences by a particle are independent of the particle's volume. These assumptions are justified by the fact that the sample $YH_{1.98}$ consists of a random packing of particles and that no observable-change in signal was observed when reversing the applied gradient. An estimation of G_o^{-2} can be obtained by performing a single echo experiment with no applied magnetic field gradient. Then

$$\mathrm{Ln}[A(2\tau)/A_o] = -\frac{2\tau}{T_2} + 2\tau^3 G_o^2 \gamma^2 D/3.$$

First T_2 is measured using a CPMG sequence then the echo amplitude is measured as a function of τ and finally an approximate value of D is obtained. From the slope of $\frac{1}{\tau}\mathrm{Ln}[A(2\tau)/A_o]$ as a function of τ^2, G_o^2 is obtained. This value which represents some distribution of $\vec{G}_o$ is used as an estimate for $\vec{G}_o^2$. For $YH_{1.98}$ at 832 K this experiment gave a value of G_o equal to 30 G/cm resulting in a correction factor, for a measured value of $D = 3.6\ 10^{-6}$ cm^2/sec, of $\Delta D = 1.6\ 10^{-6}$ cm^2/s so $3.6\ 10^{-6}$ $cm^2/s < D < 5.2\ 10^{-6}$ cm^2/s. D is uncertain by a factor of 1.5. The same experiment predicted a value of $G_o = 5$ G/cm at 341 K for $Pd_{(1-y)}\ Y_{y=8\%}\ H_{0.51}$. The measured diffusion coefficient was $D = 1.0\ 10^{-6}$ cm^2/sec and the correction factor $\Delta D = 2\ 10^{-8}$ cm^2/sec. The error of the values of D due to background gradient was in this case 2% which is less than the experimental error. The measurements were performed at constant τ and $\Delta = \tau$. The averaged amplitude of the echos was recorded as a function of the gradient strength. The diffusion coefficient was obtained from a linear least squares analysis of Ln $(A(2\tau))$ against G^2.

3.4.d. Field gradient coil calibration

The strength of the magnetic field gradient G has been shown to be related to the current I flowing in a quadrupolar coil by the linear relation.

$$G = CI \tag{3.10}$$

where C is the coil constant. In order to determine C, accurate values of I must be available. The measurement of the current was performed by digitally averaging the voltage across a known resistance connected in series with the quadrupolar coil. This method also allowed an accurate calibration of the pulse gradient width. To this effect the resistance of a piece of constantan wire, known for having a very weak temperature dependence of the resistivity, was accurately determined using a potentiometric method ($R = 0.0223 \pm 0.0001\ \Omega$). The value of the coil constant was then obtained from two different types of measurement performed on a water sample of known diffusion coefficient. In order to eliminate possible error due to geometrical differences in sample, the length and diameter of the water sample were made closely similar to those of the metal hydrides studied. Firstly the gradient strength was determined by analysis of the FID. For a cylindrical sample of radius r, Carr and Purcell (1954) have shown that the tail of the decay is modulated by a first-order Bessel function and has the form

$$My = 2M_o \cdot \frac{J_1(\gamma Grt)}{\gamma Grt} \tag{3.11}$$

where γ is the gyromagnetic ratio and t the time elapsed after application of the 90° rf pulse. The coil constant was deduced from the positions of the first three nodes of the first order Bessel function which occur when

$$G = \frac{3.83171}{\gamma r t} \qquad G = \frac{7.01559}{\gamma r t} \qquad G = \frac{10.17105}{\gamma r t} \ .$$

A least squares fit of the average value of the strength of the gradient for the 3 nodes against the intensity of the current was performed to extract the coil constant and background gradient due to the magnetic inhomogeneity. Fig. 3.1.4. shows a plot of G against I to illustrate the results of this method. The values of the coil constant obtained for the high and low temperature quadrupolar gradient coils were respectively

$$\begin{aligned} C_H &= 3.62 \pm 0.1 \ \text{G/cm.A} \\ C_L &= 15.7 \pm 0.8 \ \text{G/cm.A} \end{aligned} \qquad (3.12)$$

The gradient across the sample due to inhomogeneity of the static magnetic field when the sample was positioned in the best part of the magnet was estimated to be $G_o = 0.2$ G/cm from the intercept of G versus I. Secondly the coil constant was determined by measuring the attenuation of the height of the echo using the Stejskal and Tanner sequence (1965). The technique suffers from the need to assume a value for the diffusion coefficient of the sample used. The value of D was taken from the work of Gillen et al (1972). Ignoring the background gradient (this is justified in view of the value of G_o obtained using the first method), the echo amplitude at time 2τ after the 90° pulse is given by

$$A(2\tau) = A_o' \exp\{-\gamma^2 C^2 I^2 \delta^2 (\tau - \tfrac{1}{3}\delta)\} D \qquad (3.13)$$

where A_o' is a constant preexponential term involving G_o^2 and T_2. The coil constant was obtained from a linear least squares analysis of Ln $(A(2\tau))$ against I^2 as illustrated in fig. 3.15. The values obtained for the two different coils were

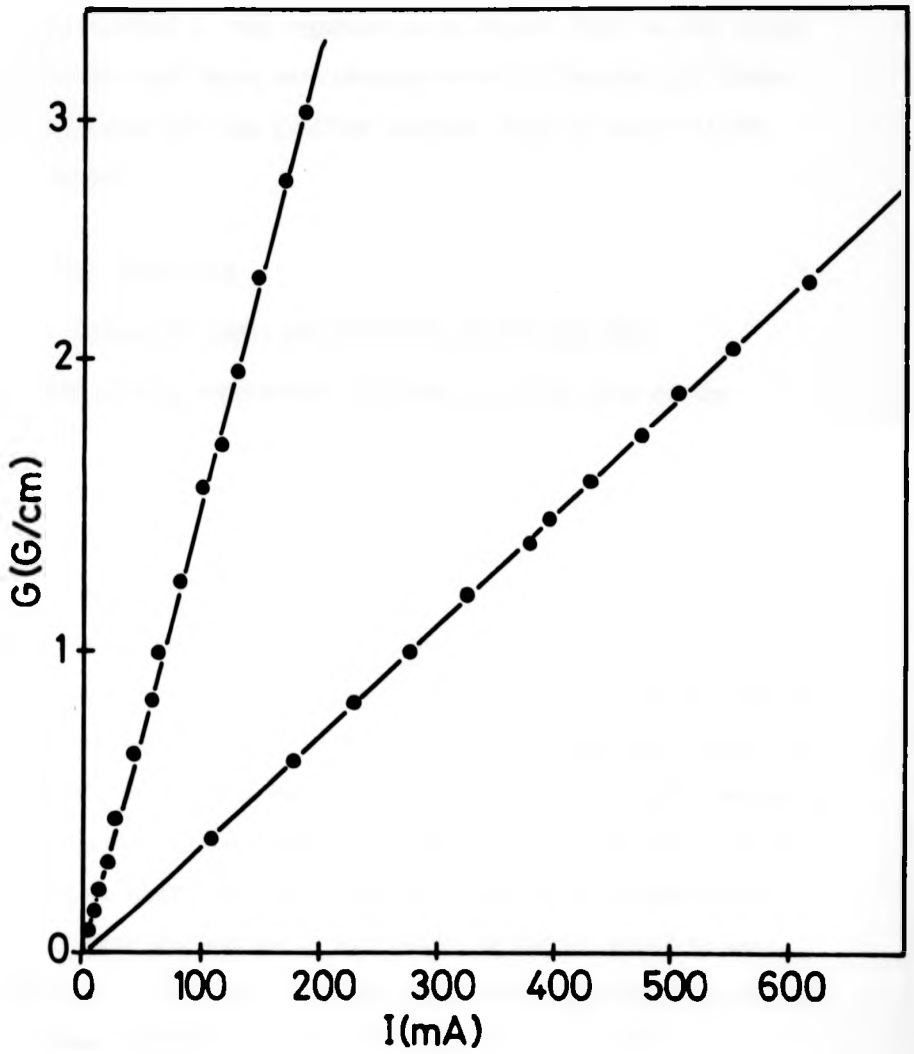

Fig. 3.14: Determination of C by analysis of the F.I.D. The upper curve and lower curve correspond to the low and high temperature gradient-coil respectively. The calculated slopes give

$C_L = 15.7 \pm 0.8\ G(cm.A)^{-1}$ and $C_H = 3.6 \pm 0.1\ G(cm.A)^{-1}$.

$$C_H = 3.70 \pm 0.10 \text{ G/cm A}$$
$$C_L = 16.5 \pm 0.5 \text{ G/cm A} \qquad (3.14)$$

The first method is only regarded as an elegant check on the values used in this work which were obtained with the Stejskal and Tanner sequence, since only low gradient currents could be used with the first method.

3.5. Data processing

3.5.a. Relaxation times and diffusion coefficient data

When fitting exponential functions as in the case of the magnetization expressions involving T_1 and T_2 and in the diffusion coefficient expressions two methods are suggested. A fit to a linear function can be performed by taking the logarithm of the appropriate variable or a non-linear fitting procedure can be used. In the first case if one considers that all the experimental points describing the exponential curve are subject to the same uncertainty, one can see that the error introduced by taking the logarithm of the appropriate variable increases as the value of the variable decreases. To make up for this overemphasis of the error for low values of the variable an appropriate weighting factor has to be introduced but there is some argument as to what weighting factor should be used. Furthermore in the case of T_1 measurements the expression giving rise to a linear function

$$\text{Ln } [M_o - M_z(\tau)] = C - \frac{\tau}{T_1}$$

is strongly dependent on the value of M_o. This can introduce cumulative errors resulting in inaccurate values of T_1. A nonlinear fitting

$$C_H = 3.70 \pm 0.10 \text{ G/cm A}$$
$$C_L = 16.5 \pm 0.5 \text{ G/cm A} \qquad (3.14)$$

The first method is only regarded as an elegant check on the values used in this work which were obtained with the Stejskal and Tanner sequence, since only low gradient currents could be used with the first method.

3.5. Data processing

3.5.a. Relaxation times and diffusion coefficient data

When fitting exponential functions as in the case of the magnetization expressions involving T_1 and T_2 and in the diffusion coefficient expressions two methods are suggested. A fit to a linear function can be performed by taking the logarithm of the appropriate variable or a non-linear fitting procedure can be used. In the first case if one considers that all the experimental points describing the exponential curve are subject to the same uncertainty, one can see that the error introduced by taking the logarithm of the appropriate variable increases as the value of the variable decreases. To make up for this overemphasis of the error for low values of the variable an appropriate weighting factor has to be introduced but there is some argument as to what weighting factor should be used. Furthermore in the case of T_1 measurements the expression giving rise to a linear function

$$\text{Ln } [M_o - M_z(\tau)] = C - \frac{\tau}{T_1}$$

is strongly dependent on the value of M_o. This can introduce cumulative errors resulting in inaccurate values of T_1. A nonlinear fitting

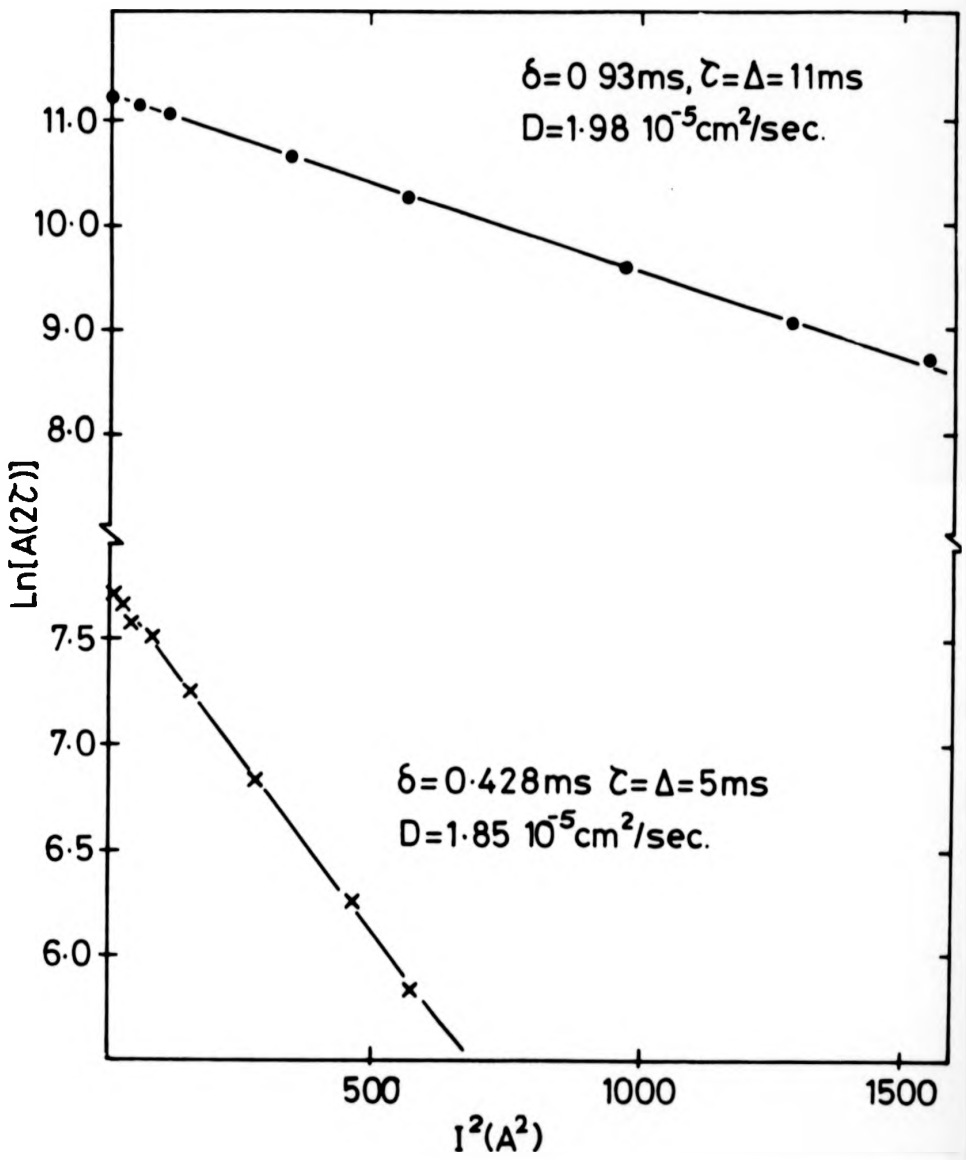

Fig. 3.15: Calibration of the gradient coil using the method of Stejskal and Tanner

$C_H = 3.7 \pm 0.1\ G(cm.A)^{-1}$ and $C_L = 16.5 \pm 0.5\ G(cm.A)^{-1}$

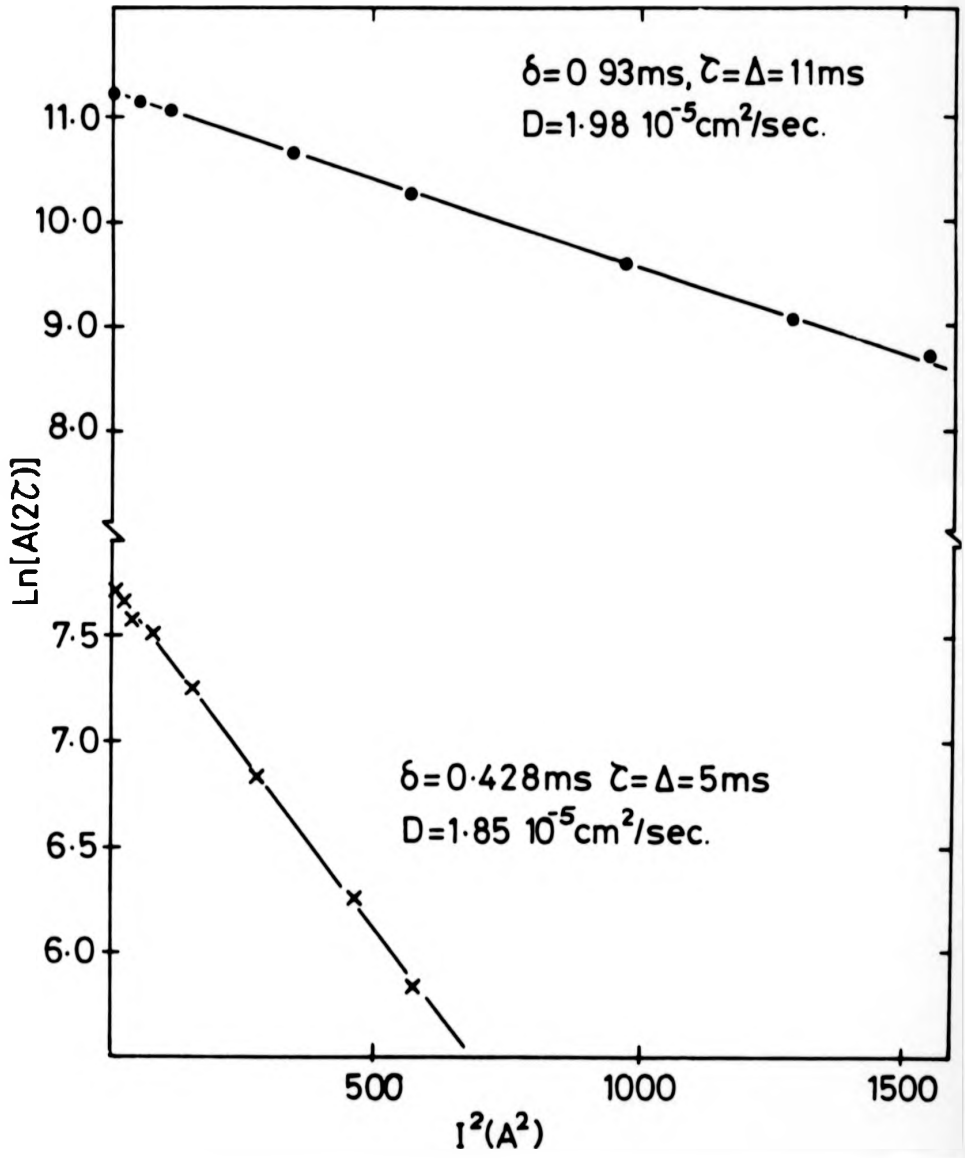

Fig. 3.15: Calibration of the gradient coil using the method of Stejskal and Tanner

$C_H = 3.7 \pm 0.1\ G(cm.A)^{-1}$ and $C_L = 16.5 \pm 0.5\ G(cm.A)^{-1}$

procedure on the other hand has the advantage not only of overcoming the problem related to the weighting factor and base line (M_o), but also of reducing the averaging time since normally one measures M_o several times in the course of a T_1 measurement. The only disadvantage is that the fitting procedure is more complex and an estimate of the starting parameters must be made. For the reasons outlined above the relaxation times T_1 and T_2 were fitted using an iterative nonlinear least-squares fit to the function

$$M(\tau) = A + B\ Exp(-\tau/T_{1,2})$$

where $A = M_o$ and $B = -2M_o$ in the case of T_1 measurements and A equals the base line offset and $B = M_o$ in the case of T_2 measurements. An example of the results achieved using this fitting method is given in fig. 3.16. The diffusion coefficient data were fitted using a linear least squares fit to the function

$$Ln[M(2\tau)] = A\text{-}BG^2$$

and the diffusion coefficient was calculated from the fitting parameter B using $D = \sqrt{B/\gamma^2\delta^2(\Delta-\delta/3)}$.

3.5.b. Fitting of results

The total relaxation rate is the result of several contributions and can be expressed as

$$\frac{1}{T_1} = \frac{1}{T_{1d}} + \frac{1}{T_{1p}} + \frac{1}{T_{1e}}$$

where T_{1d} is the dipole-dipole contribution, T_{1p} is the contribution due to paramagnetic impurities and T_{1e} is the result of interaction with the conduction electrons (only present in a metal). The same type of relation applies to T_2 and in the following although only

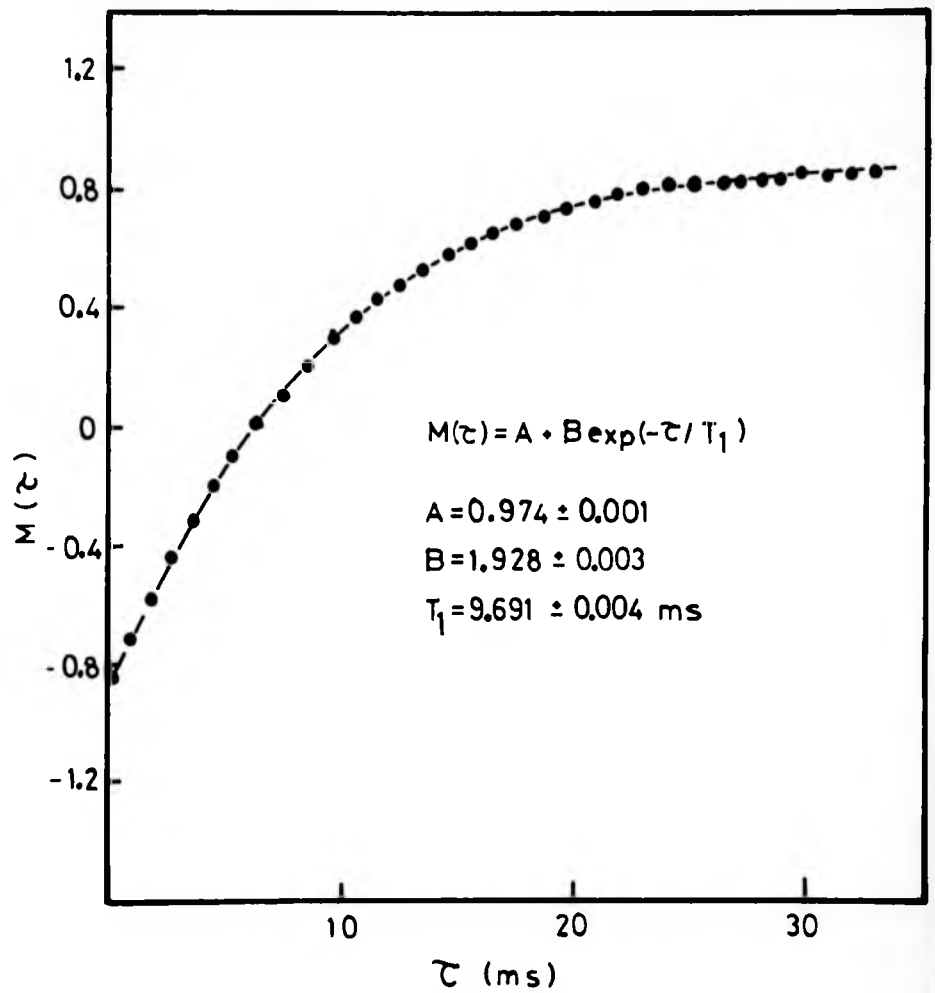

Fig. 3.16: Example of T_1 data fitted to an exponential decay

the T_1 fitting procedure is discussed, the same type of analysis has been applied to T_2. When the sample measured was thought to be free of paramagnetic impurities, the relaxation rate was fitted to

$$\frac{1}{T_1} = \frac{1}{T_{1d}} + \frac{1}{T_{1e}} .$$

In the previous chapter the different models giving analytical expressions or numerical solutions for T_{1d} and T_{1e} have been discussed. In the following two different models, the BPP formulation and the numerical values of Barton and Sholl (1980) have been used for the analysis of T_{1d}. The latter is a more rigorous treatment and therefore the values of the fitted parameters extracted are regarded as more reliable. T_{1e} has been fitted to the expression $T_{1e}T = K$ where T is the temperature and K the Korringa product. The fitting procedure used was an iterative non linear least-squares fit. This procedure linearises the adjustable parameters near the minimum of χ^2 which is a function describing the goodness of the fit, and uses a gradient search when away from χ^2min. In this method all the parameters are adjusted at the same time resulting in a more rapid convergence towards the true minimum of χ^2. The first derivative of the fitted function is required and this was calculated using a numerical method since an analytical form of the function was not always available. The adjustable parameters were: the value of the minimum in T_{1d}, the activation energy, the preexponential dwell time (i.e. τ_{Do}) and the value of the Korringa product.

An iterative Newton method to find the value of τ_D as a function of temperature was used as well as a check on the linearity of ln τ_D versus 1/T. Deviations from linearity are indicative of small residual concentration of impurities. When paramagnetic impurities

were present in the sample measured the term $1/T_{1p}$ was considered in the expression for the total relaxation time. There is indisputable evidence (as will be discussed in the next chapter) that for the case of YH_x + Gd, T_{1p} is the result of dipolar interactions. In this case T_{1p} was fitted to the analytical expression given by Richards (1978), discussed in the previous chapter. The fitting parameters used were the activation energy, the preexponential dwell time, the electronic spin lattice relaxation time τ_i and finally a scaling factor. A good description of the fitting methods used here can be found in Bevington (1969). Some of the programs used in these data fitting procedures are given in appendix 3.

3.6. Sample preparation

All the YH_x and $Y_{(1-y)}Gd_y H_x$ samples studied in this investigation were prepared in the Materials Science Division of the Ames Laboratory (USA), while the titanium manganese and palladium yttrium metal alloys were prepared at Birmingham University by R. Jordan and R. Harris respectively and hydrided at Warwick University.

Ti and $Ti_{(1-y)}Mn_{(y)}$ alloys were prepared from high purity titanium sheet, obtained from Goodfellow Metals, by arc melting the correct proportions of the constituents in an argon atmosphere. One of the resulting 5 gr alloy buttons was washed in a mild solution of HF in order to remove the oxide layer and other impurities that had formed at the surface. The button was rinsed in distilled water followed by a bath in methyl alcohol. After drying, the sample was placed in a vacuum of approximately 10^{-6} torr and annealed for 8 hours at 800°C. The sample was then exposed to one atmosphere of hydrogen and gradually cooled to room temperature over an eight hour period. The purity of the hydrogen gas used was ensured by first absorbing it into a titanium reservoir and then outgassing. A schematic diagram

of the hydriding system is shown in fig. 3.17. As the titanium button absorbed hydrogen it passed through a mixed phase region creating stresses in the Ti lattice which caused it to become brittle. The button was then crushed into a powder and sieved in a dry nitrogen atmosphere to the desired size d < 106 μm which was less than the skin depth at 45 MHz. During this procedure great care was taken to ensure that the sample was not exposed to air. The polycrystalline metal hydride was then reintroduced to the vacuum system and all the hydrogen outgassed at a temperature T = 800°C. At that stage the sample was sieved again to ensure that sintering occuring in the previous treatment had not affected the particle size of the powdered metal and finally weighed. The powder was then exposed to one atmosphere of hydrogen after evacuation at 600°C and maintained at this temperature until the pressure reached the equilibrium hydrogen pressure. The temperature was then decreased in stages, allowing equilibrium to be attained at each stage down to room temperature. This loading procedure, which takes about 8 to 9 hours, ensured that the concentration of hydrogen was homogeneous over the entire sample. The amount of hydrogen absorbed was calculated from the change in pressure and the known volume of the hydriding system. The ratio of hydrogen atoms to metal atoms was thus known to an accuracy of approximately 4%. This procedure was repeated for all the $Ti_{1-y}Mn_y$ samples. After completion of the hydriding, the metal hydrides were sealed in 9mm O/D quartz vials containing argon at a pressure of 0.3 atom.

The Pd and Pd-8%Y hydrides were each prepared from an alloy button made into a foil of thickness 25 μm. The foil was annealed at 700°C under vacuum for several hours before being rolled up with a hydrogen-free P.T.F.E. sheet in a dry nitrogen atmosphere. This

of the hydriding system is shown in fig. 3.17. As the titanium button absorbed hydrogen it passed through a mixed phase region creating stresses in the Ti lattice which caused it to become brittle. The button was then crushed into a powder and sieved in a dry nitrogen atmosphere to the desired size d < 106 μm which was less than the skin depth at 45 MHz. During this procedure great care was taken to ensure that the sample was not exposed to air. The polycrystalline metal hydride was then reintroduced to the vacuum system and all the hydrogen outgassed at a temperature T = 800°C. At that stage the sample was sieved again to ensure that sintering occuring in the previous treatment had not affected the particle size of the powdered metal and finally weighed. The powder was then exposed to one atmosphere of hydrogen after evacuation at 600°C and maintained at this temperature until the pressure reached the equilibrium hydrogen pressure. The temperature was then decreased in stages, allowing equilibrium to be attained at each stage down to room temperature. This loading procedure, which takes about 8 to 9 hours, ensured that the concentration of hydrogen was homogeneous over the entire sample. The amount of hydrogen absorbed was calculated from the change in pressure and the known volume of the hydriding system. The ratio of hydrogen atoms to metal atoms was thus known to an accuracy of approximately 4%. This procedure was repeated for all the $Ti_{1-y}Mn_y$ samples. After completion of the hydriding, the metal hydrides were sealed in 9mm O/D quartz vials containing argon at a pressure of 0.3 atom.

The Pd and Pd-8%Y hydrides were each prepared from an alloy button made into a foil of thickness 25 μm. The foil was annealed at 700°C under vacuum for several hours before being rolled up with a hydrogen-free P.T.F.E. sheet in a dry nitrogen atmosphere. This

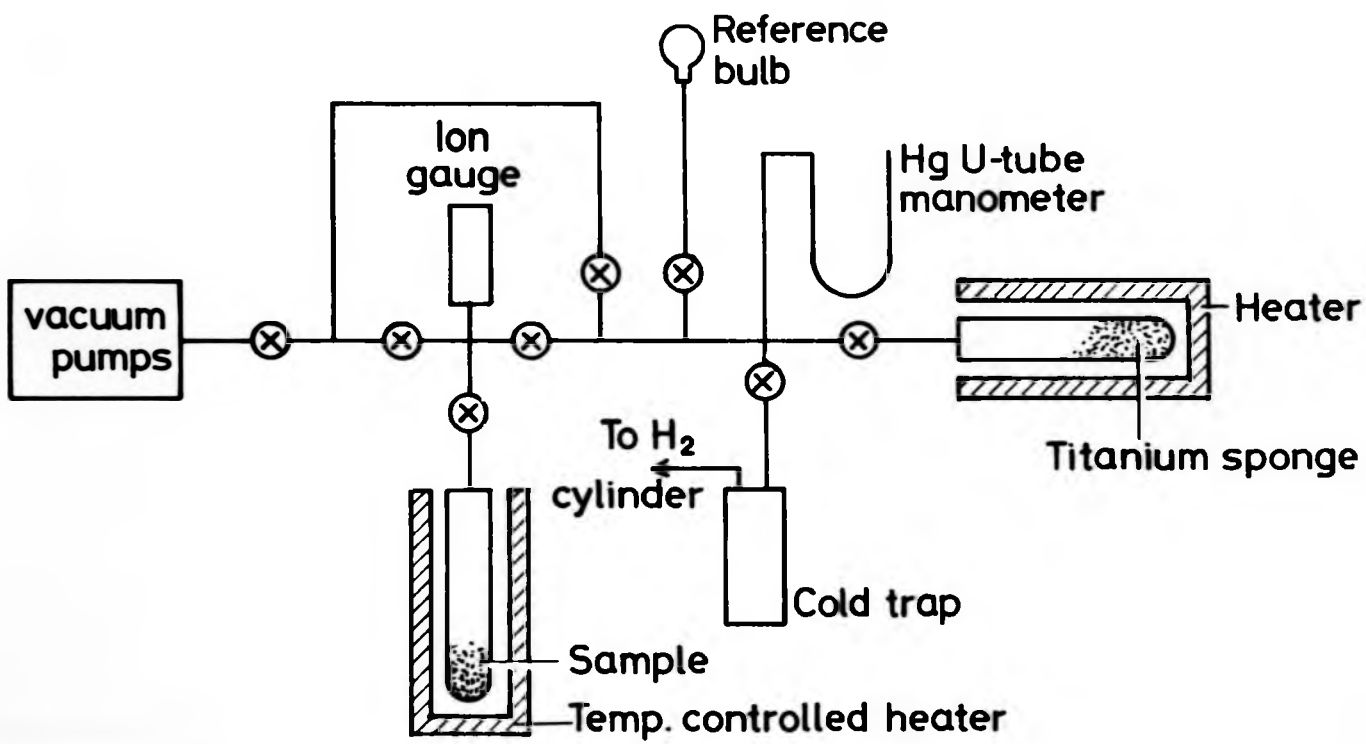

Fig. 3.17: Schematic diagram of the hydriding system

procedure ensured electrical insulation between the successive layers of metal. The sample was then exposed to hydrogen at a pressure of one atmosphere and at a temperature T = 200°C and very slowly cooled to room temperature. The hydrogen concentration was calculated following the procedure described earlier. The weight after absorption was also measured as a check of the previous method. The samples were sealed under vacuum. In order to avoid losing hydrogen during the sealing procedure the sample tubes were immersed in liquid nitrogen.

The yttrium and yttrium gadolinium hydrides were prepared by B. J. Beaudry and D. T. Peterson at Ames University from high purity Ames Laboratories metals. The starting pure metals were analysed by spark source mass spectrometry. An example of the analysis is listed in Appendix 2 . The metal was exposed to hydrogen, obtained from uranium hydride decomposition, at 1.34 atmosphere and 850°C. The sample was held at that temperature for about 24 hours. After hydriding was completed the sample was cooled down rapidly to prevent the formation of the yttrium trihydride phase. The exact hydrogen concentration was determined by hot vacuum extraction into a known volume. This resulted in a 2% uncertainty in the concentration. The yttrium dihydride was then ground into a fine powder before being sealed in a quartz tube.

When measuring the diffusion coefficients of $YH_{1.98}$ the particle size of the powdered sample must be large enough to prevent the observation of boundary effects on the diffusion which would add to the error on the measured diffusion coefficients. An approximate diffusion length of 4 μm was deduced from the interval of time τ = 8 ms during which the largest diffusion coefficient D = 5.010^{-6} cm^2/s was measured. A scanning electron microscope study of the

surface of the metal hydride particle showed that the particle size was an average greater than 30 μm and that most particle regions had a characteristic length of 10 to 15 μm in which no cracks were apparent. These values are larger than the 4 μm diffusion length. Therefore bounded diffusion effects should not be apparent in the diffusion measurements.

References

Adduci, D., P. Hornung, D. R. Torgeson: Rev. Sci. Instrum., 43, 661, (1977).

Barton, W. A., C. A. Sholl: J. Phys. C: Solid State Phys., 13, 2579 (1980).

Bevington, P. R.: Data Reduction and Error Analysis for the Physical Sciences, McGraw-Hill (1969).

Bloch, F: Phys. Rev., 70, 460 (1946).

Carr, H. Y., E. M. Purcell: Phys. Rev., 94, 688 (1954).

Conway, J. L : MSc Thesis, Cornell University (1974).

Gillen, K. T., D. C. Douglass, M. J. R. Hoch: J. Chem. Phys., 57, 5117 (1972).

Hahn, E. L: Phys. Rev., 80, 580 (1950).

Meiboom, S., D. Gill: Rev. Sci. Instrum., 29, 688 (1958).

Murday, J. S., R. M. Cotts: Z. Naturforsch, 26a, 85 (1971).

Richards, P. M: Phys. Rev., B18, 6358 (1978).

Stejskal, E. O., J. E. Tanner: J. Chem. Phys., 42, 288 (1965).

Webster, D. S., K. H. Marsden : Rev. Sci. Instrum., 45, 1232 (1974).

CHAPTER IV: YTTRIUM HYDRIDES - RESULTS AND DISCUSSION

As will become evident in this chapter very small amounts of paramagnetic impurities can have a large effect on the proton relaxation times in yttrium hydrides, consequently any parameters deduced from relaxation measurements, which yield information on the hydrogen diffusion and the metal hydride electronic structure, may lead to erroneous interpretations if the paramagnetic contribution to the total relaxation time is ignored as has generally been the case in the past. It has been found in this investigation that very small residual concentrations of Gd ($\sim$ 5 ppm) can have a large effect on T_1 and in order to quantify these effects an investigation of the relaxation times T_1 and T_2 has been conducted for various concentrations of Gd. The results of this investigation together with their discussion are presented first, while the results and discussion concerning the effects of changing the hydrogen concentration having taken account of paramagnetic impurity relaxation, are presented in the second part of this chapter.

4.1. The $Y_{1-y}Gd_yH_{1.98}$ systems

4.1.a. Results

The spin lattice and spin-spin relaxation times have been measured as a function of temperature for a series of yttrium dihydride samples doped with controlled amounts of gadolinium. The Gd was added to a nominally very pure batch of yttrium metal which contained about 2 ppm of Gd together with comparable amounts of Tb, Ce and Pr. This series of $YH_{1.98}$ samples containing 20, 50, 100, 200 and 915 ppm Gd was compared to a $YH_{1.98}$ sample obtained from the pure yttrium starting

metal. Fig. 4.1 shows a composite plot of T_1 versus 1000/T for the series of $YH_{1.98}$ + Gd samples measured at a frequency ν_o = 7 MHz in the temperature range T ∿ 280 K to T ∿ 1300 K. The value of T_1 for the purest sample goes through a minimum with $(T_1)_{min}$ = 6.8 ms at T = 525 K. It can be seen that as the gadolinium content increases the value of T_1 for a given temperature generally decreases. The most striking feature is the appearance of a subsidiary minimum at a lower temperature (T ∿ 450 K) than that of the main minimum which broadens but can still be clearly resolved for the highest concentrations of Gd. The subsidiary minimum is clearly resolved for the most heavily doped samples and its depth increases with increasing Gd content. At high temperature, T > 800 K, the value of T_1 increases before going through a maximum for T ∿ 1000 K and then starts decreasing. This cannot be accounted for by the decrease with temperature of T_{1e} and the effect does not seem to be correlated to the presence of Gd since it is clear that there is no apparent change with increasing Gd concentration. A discussion of this effect which is thought to have a different origin will therefore be deferred until the second part of the chapter. As the temperature decreases the spin-spin relaxation time decreases and the low temperature measurements at 7 MHz were therefore, limited by the recovery time of the apparatus. In order to investigate the effect of paramagnetic impurities at low temperature, the range of temperatures was extended down to T ∿ 150 K by going to a higher frequency, ν_o = 45 MHz, where the recovery time is much shorter. Fig. 4.2 shows a composite plot of T_1 versus 1000/T at 45 MHz. Here again the value of T_1 for a given temperature decreases with increasing Gd content. For the higher concentrations of Gd (y > 50 ppm) the value of T_1 increases as the temperature is decreased, goes through a maximum and starts decreasing as the temperature is further decreased. This indicates that the paramagnetic contribution, T_{1p}, to T_1 is certainly temperature dependent in this region. This is to be contrasted to the

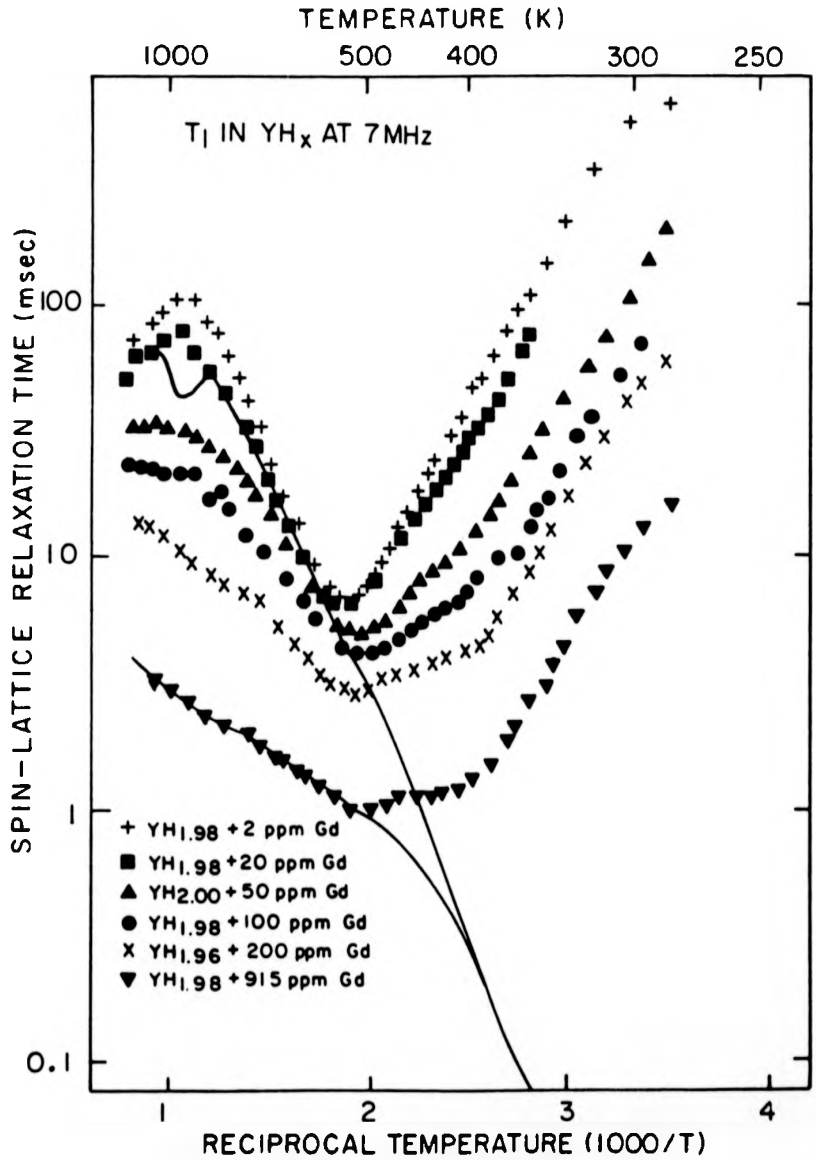

Fig. 4.1: Composite plot of T_1 versus 1000/T for the series of $YH_{1.98}$ doped with Gd at 7 MHz. For comparison the full curves indicate the T_2 behaviour for the corresponding concentrations of Gd.

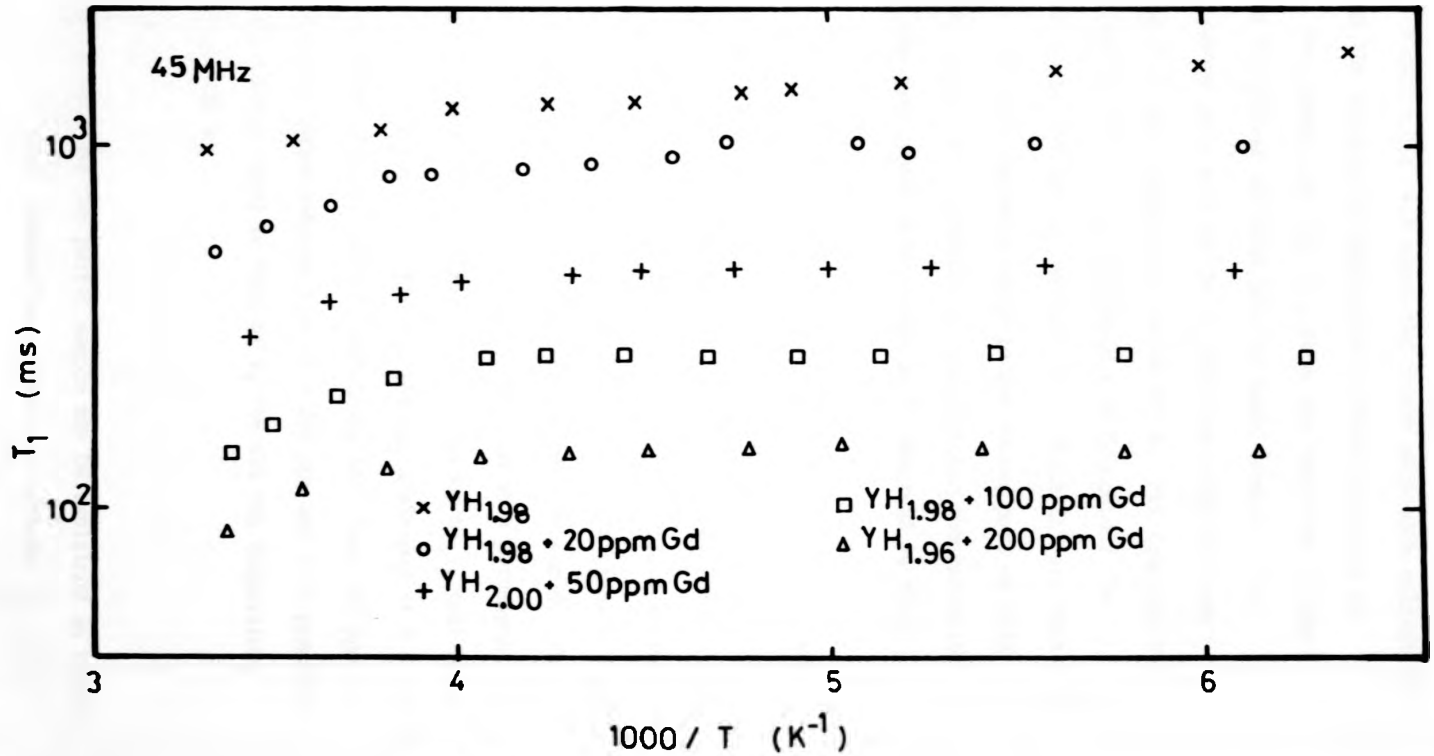

Fig. 4.2: Composite plot of T_1 versus 1000/T for $YH_{1.98}$ doped with Gd at 45 MHz.

general assumption that at low temperature $T_{1\rho}$ is temperature independent. Finally fig. 4.3 shows the proton spin-spin relaxation time T_2 versus the reciprocal temperature (1000/T) measured at ν_o = 7 MHz. For comparison fig. 4.3 shows the behaviour of the proton T_1 for the purest and most heavily doped samples. For the sake of clarity only part of the T_2 data available has been plotted in fig. 4.3. for temperatures below 500 K. For temperatures up to approximately 400 K T_2 is independent of Gd content for concentrations up to 200 ppm, in contrast to T_1 which is very sensitive to Gd content. As will become evident in the second part of this chapter T_1 and T_2 are very dependent on the hydrogen concentration and it is thought that small differences in T_2 observed in this temperature range are due to slight variations in hydrogen concentration from sample to sample, resulting in a shift of T_2 to lower or higher temperature. As the temperature is increased and reaches the value for which the main T_1 minimum occurs, it can be seen that the proton T_2 values are affected by the presence of Gd and this effect increases with increasing Gd concentration. At higher temperature (i.e. T $\sim$ 550 to 700 K) T_2 becomes equal to T_1 for all the samples measured. This is suggestive that $T_{1\rho} = T_{2\rho}$ where $T_{2\rho}$ is the spin-spin paramagnetic relaxation time. Above these temperatures the values of T_2 fall below those of T_1 before decreasing and passing through a minimum at T $\sim$ 1000 K This is only observed for the samples containing less than 200 ppm Gd. For the more heavily doped samples (i.e. y = 200 ppm and 9.15 ppm Gd) the value of T_2 remains equal to that of T_1 for all the temperature range T $\sim$ 550 to 1000 K.

4.1.b. Pure YH_2

The 7 MHz T_1 data for the purest sample may be explained in terms of the proton dipole-dipole interaction. This is confirmed by the excellent agreement obtained between the experimental value of T_1 at

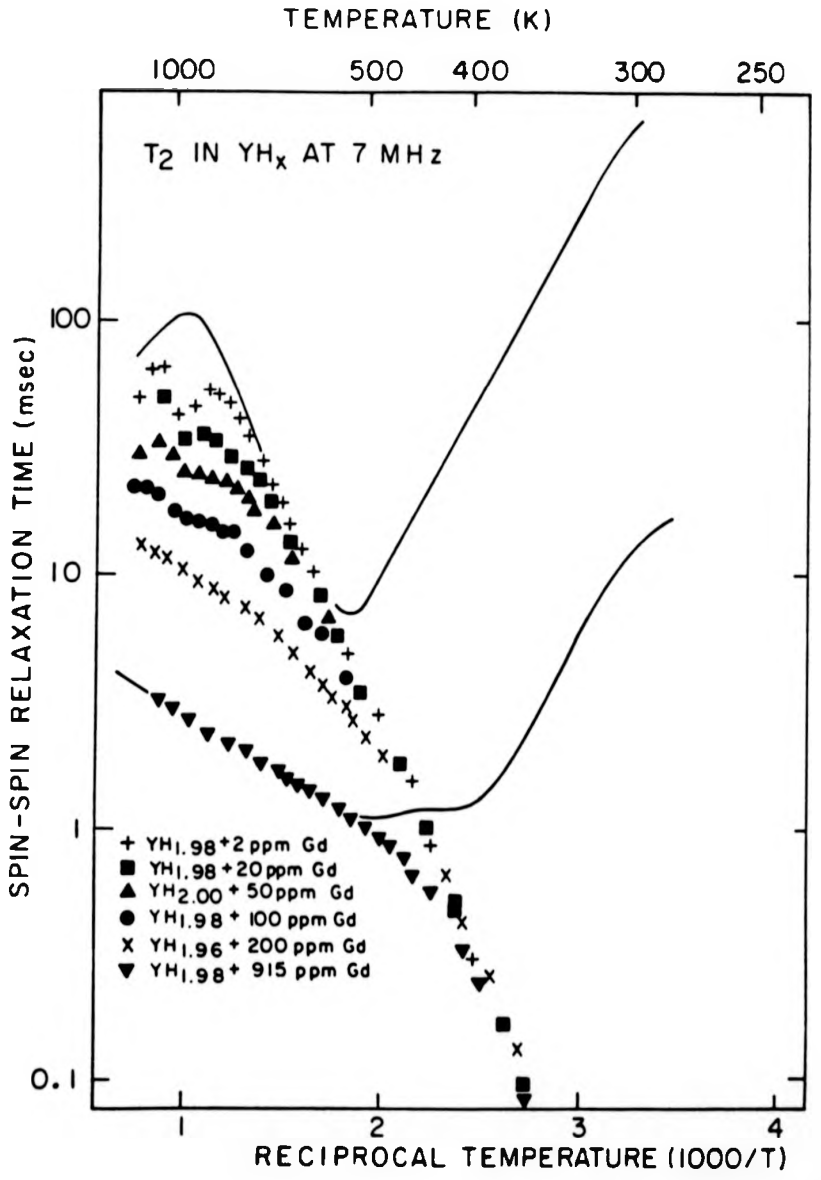

Fig. 4.3: Composite plot of T_2 versus 1000/T for the series of $YH_{1.98}$ doped with Gd, at 7 MHz. For comparison T_1 is indicated by the full curves.

the minimum, taking into account as discussed later, the electronic contribution to T_1, and those deduced from the BPP formulation and mean field theory assuming that the hydrogen atoms occupy the tetrahedral sites only. Table 4.1 gives these values together with those calculated assuming octahedral occupation. The excellent agreement is undoubtedly somewhat fortuitous (3% difference) particularly for the BPP model which is known to give values of T_1 at the minimum smaller than those given by the experiment. As already discussed, the dihydride phase of yttrium is characterised by a substantial occupation of octahedral sites which increases with hydrogen concentration resulting in an increase in the second moment of the proton resonance (Anderson et al 1980). Furthermore, in this treatment the paramagnetic contribution to T_1 has been neglected although some residual impurities are present in the sample. Either effect would give apparent better agreement with the value deduced from BPP. It should be stressed however, that even when it is assumed that the hydrogen atoms occupy the tetrahedral sites only and move on a sc lattice the good agreement between the experimental and theoretical values implies that diffusion parameters deduced from such an analysis should be reliable. In the remainder of this section the proton dipole-dipole relaxation times T_{1d} and T_{2d} will be expressed in terms of the BPP formulation which is consistent with the use of an exponential correlation function in the existing theory of T_{1p}. Furthermore within the BPP approximation which is insensitive to the details of the jump processes, in so far T_{1d} and T_{2d} can be expressed by a single correlation function, the small partial occupation of octahedral sites become irrelevant. Within this approximation the resulting accuracy of the preexponential correlation time (i.e. $\tau_c = \tau_{co} \exp E_a/kT$) cannot be assessed with certainty but the activation energy deduced should be very close (i.e. < 10%) to the exact value. To a first

Table 4.1: Values of $(T_{1d})_{min}$ deduced from theory

	BPP		Mean Field		Experimental
	Tetrahedral	Octahedral	Tetrahedral	Octahedral	
$(T_{1d})_{min}$ (ms)	6.75	31.44	7.37	33.98	6.89

approximation the paramagnetic contribution T_{1p} can be neglected in the expression for T_1 for the purest sample and thus

$$\frac{1}{T_1} = \frac{1}{T_{1d}} + \frac{1}{T_{1e}}$$

The value of T_{1e} is deduced from the low temperature 45 MHz T_1 data where the proton-proton dipole contribution becomes negligible Cotts (1978), (1982), Seymour (1982) . It is found that $T_{1e}T$ follows a Korringa relation with $T_{1e}T$ = 302 K.s. The 7 MHz T_1 data have then be fitted to the expression given above taking this value for $T_{1e}T$ and assuming a BPP expression for T_{1d}. This was achieved by using an iterative Newton method to obtain the value of τ_c as a function of temperature as illustrated in fig. 4.4 where Ln τ_c is plotted against 1000/T. The most striking feature of this graph is the break from linearity occuring at T = 428 K and the curve may be characterised by two linear portions resulting in (i.e. $\tau_c = \tau_D/2$)

$$\tau_D = 3.2 \times 10^{-12} \exp(0.425 eV/kT) \text{s} \quad 428 \text{ K} < T < 800 \text{ K}$$

$$\tau_D = 0.2 \times 10^{-10} \exp(0.260 eV/kT) \text{s} \quad 330 \text{ K} < T < 428 \text{ K}$$

Although, as will become apparent later in this section, the value of $T_{1e}T$ extracted from the 45 MHz data neglecting the paramagnetic contribution is not entirely reliable the uncertainty is not likely to exceed 10% and cannot account for the deviation from linearity of Ln τ_c versus 1000/T. Similar breaks in such plots have been reported and interpreted in the past, as due to multi-diffusion processes occuring at the same time (Weaver (1972), (1972)). In view of the partial octahedral site occupation in yttrium dihydride, it might be argued that two or more diffusion processes can take place. This type of misinterpretation for the present system will be discussed

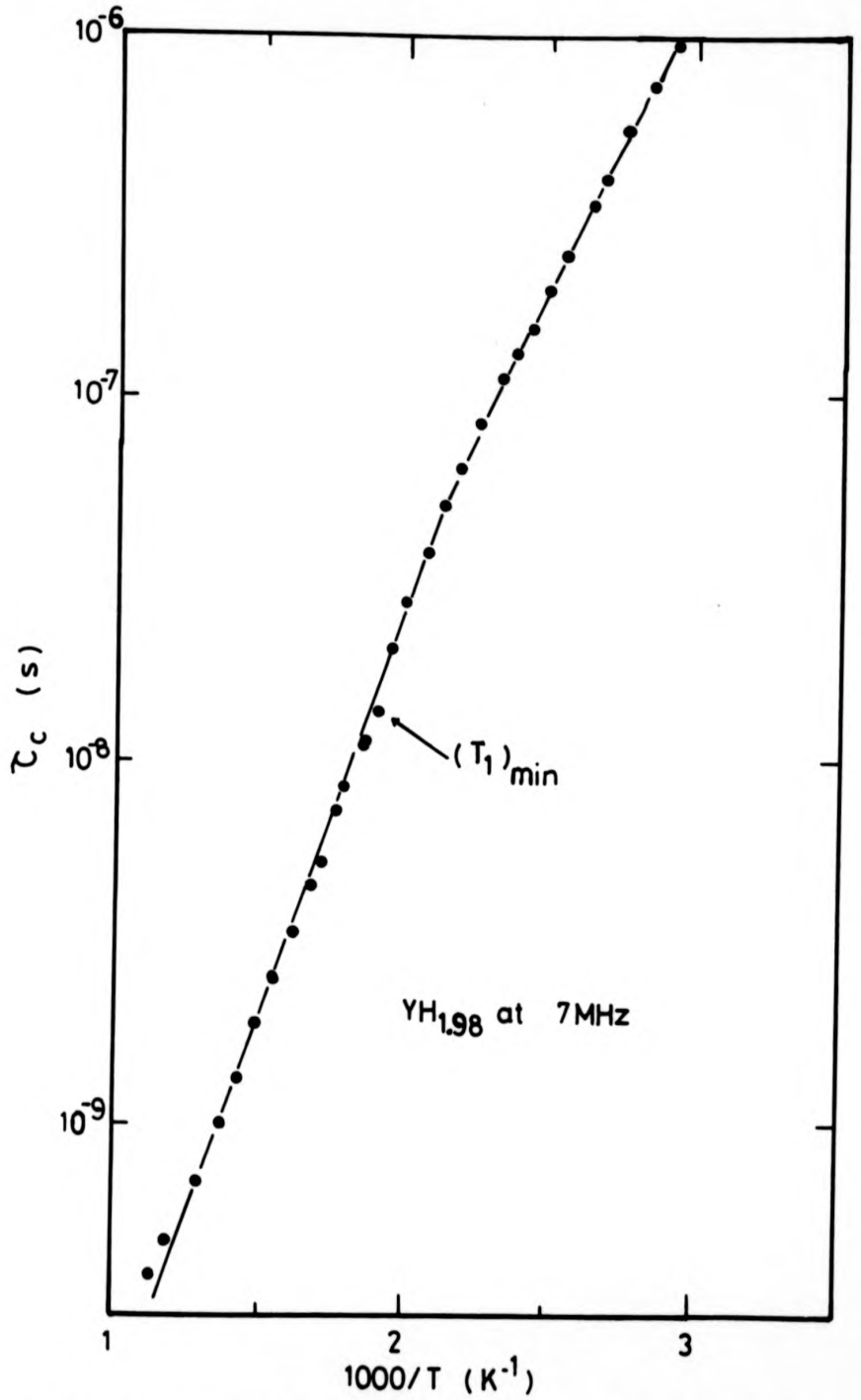

Fig. 4.4: τ_c as a function of the reciprocal temperature for $YH_{1.98}$. τ_c is obtained from T_1 data, using an exponential correlation function.

in section 4.1.f. Using the high temperature value of τ_D the proton dipolar relaxation time has been calculated over the temperature range of the measured T_1. This value of $\frac{1}{T_{1d}}$ has then been subtracted from $\frac{1}{T_1}$ in order to extract the extra contribution to T_1 which for reasons which will become evident later has been labelled T_{1p} in fig. 4.5 which illustrates the result of such a calculation. It can be seen that the resulting relaxation time T_{1p} goes through an asymmetric minimum at $T \sim 450$ K which is the temperature at which the subsidiary minimum occurs in the most heavily doped sample (i.e. $YH_{1.98}$ + 915 ppm Gd). It should be noted that the above calculation is not exact since in using the value of τ_D obtained from the high temperature T_1 values one assumes that T_1, for this range of temperature, is entirely governed by T_{1d} which is obviously not true (see Fig. 4.1). However, this error is not likely to lead to a large shift in temperature of the T_{1p} minimum. Thus the asymmetric behaviour of T_1 about the minimum resulting in a non-linear plot of Ln τ_c against 1000/T can confidently be attributed to the contribution of the residual concentration of Gd ($\sim$ 2 ppm) to the total relaxation time T_1. On the other hand the T_2 data can be adequately fitted to a theoretical BPP expression as can be seen in fig. 4.5 and yields the result

$$\tau_D = 2.30 \times 10^{-12} \exp(0.437/kT) \text{ s}$$

in good agreement with the high temperature value obtained from the T_1 data. This together with the observation made earlier on the insensitivity of T_2 to Gd content, reinforces the conclusion drawn above as regard T_{1p}. We turn now to a discussion of the controlled effects of Gd paramagnetic impurities on the relaxation times. We will first be concerned with the T_1 data.

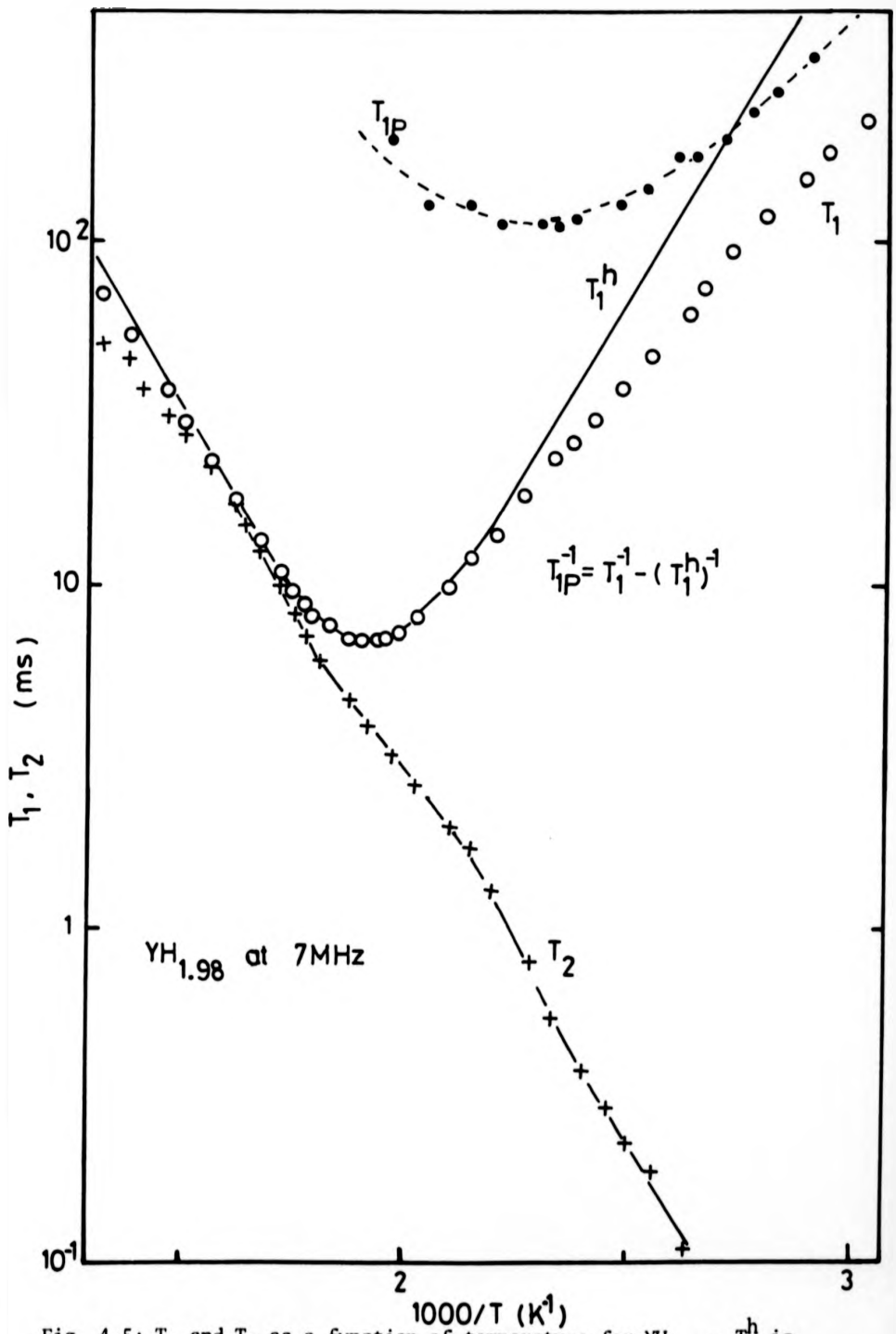

Fig. 4.5: T_1 and T_2 as a function of temperature for $YH_{1.98}$. T_1^h is calculated taking the high temperature values of τ_D and using BPP. T_2 has been fitted using BPP (full curve).

4.1.c. Spin lattice relaxation time data for Gd-doped YH_2

Assuming that the different contributions to the observed spin lattice relaxation rate are additive and that the different parameters characterising the motion of the hydrogen atoms and the electronic structure of the hydride are not affected by the presence of Gd, the paramagnetic relaxation rate can be obtained using

$$R_{1p} = R_1 - (R_1)_{pure}$$

where R_{1p} is the paramagnetic relaxation rate, R_1 the observed relaxation rate for a sample containing a given amount of Gd and $(R_1)_{pure}$ is the relaxation rate of the purest sample available (i.e. $(R_1)_{pure} \sim R_{1d} + R_{1e}$). As discussed by Richards (1978) the first assumption is justified in the high temperature limit of interest where there is negligible spin polarisation and the second assumption is, we think, justified because of the low levels of Gd present in the samples.

Fig. 4.6 and 4.7 show the resulting R_{1p} paramagnetic relaxation rates for various concentrations of Gd, as a function of the reciprocal temperature (1000/T). The main features of the graphs are that the low temperature R_{1p} at 45 MHz are characterised by a very weak temperature dependence while at 7 MHz for the higher range of temperatures R_{1p} shows a very strong temperature dependence for temperature up to $\sim$ 400 K and above 400 K a weaker but still pronounced temperature dependence. If we assume that the increase in the relaxation rate for temperatures below 400 K is due to a thermally activated process a characteristic activation energy $E_a' = 0.29$ eV can be derived which is, within experimental error, the same for the different concentration of Gd. As discussed in section 2.2.c of Chapter II, the paramagnetic relaxation rate in the case of dilute impurities is proportional to the

4.1.c. Spin lattice relaxation time data for Gd-doped YH_2

Assuming that the different contributions to the observed spin lattice relaxation rate are additive and that the different parameters characterising the motion of the hydrogen atoms and the electronic structure of the hydride are not affected by the presence of Gd, the paramagnetic relaxation rate can be obtained using

$$R_{1p} = R_1 - (R_1)_{pure}$$

where R_{1p} is the paramagnetic relaxation rate, R_1 the observed relaxation rate for a sample containing a given amount of Gd and $(R_1)_{pure}$ is the relaxation rate of the purest sample available (i.e. $(R_1)_{pure} \sim R_{1d} + R_{1e}$). As discussed by Richards (1978) the first assumption is justified in the high temperature limit of interest where there is negligible spin polarisation and the second assumption is, we think, justified because of the low levels of Gd present in the samples.

Fig. 4.6 and 4.7 show the resulting R_{1p} paramagnetic relaxation rates for various concentrations of Gd, as a function of the reciprocal temperature (1000/T). The main features of the graphs are that the low temperature R_{1p} at 45 MHz are characterised by a very weak temperature dependence while at 7 MHz for the higher range of temperatures R_{1p} shows a very strong temperature dependence for temperature up to $\sim$ 400 K and above 400 K a weaker but still pronounced temperature dependence. If we assume that the increase in the relaxation rate for temperatures below 400 K is due to a thermally activated process a characteristic activation energy E_a = 0.29 eV can be derived which is, within experimental error, the same for the different concentration of Gd. As discussed in section 2.2.c of Chapter II, the paramagnetic relaxation rate in the case of dilute impurities is proportional to the

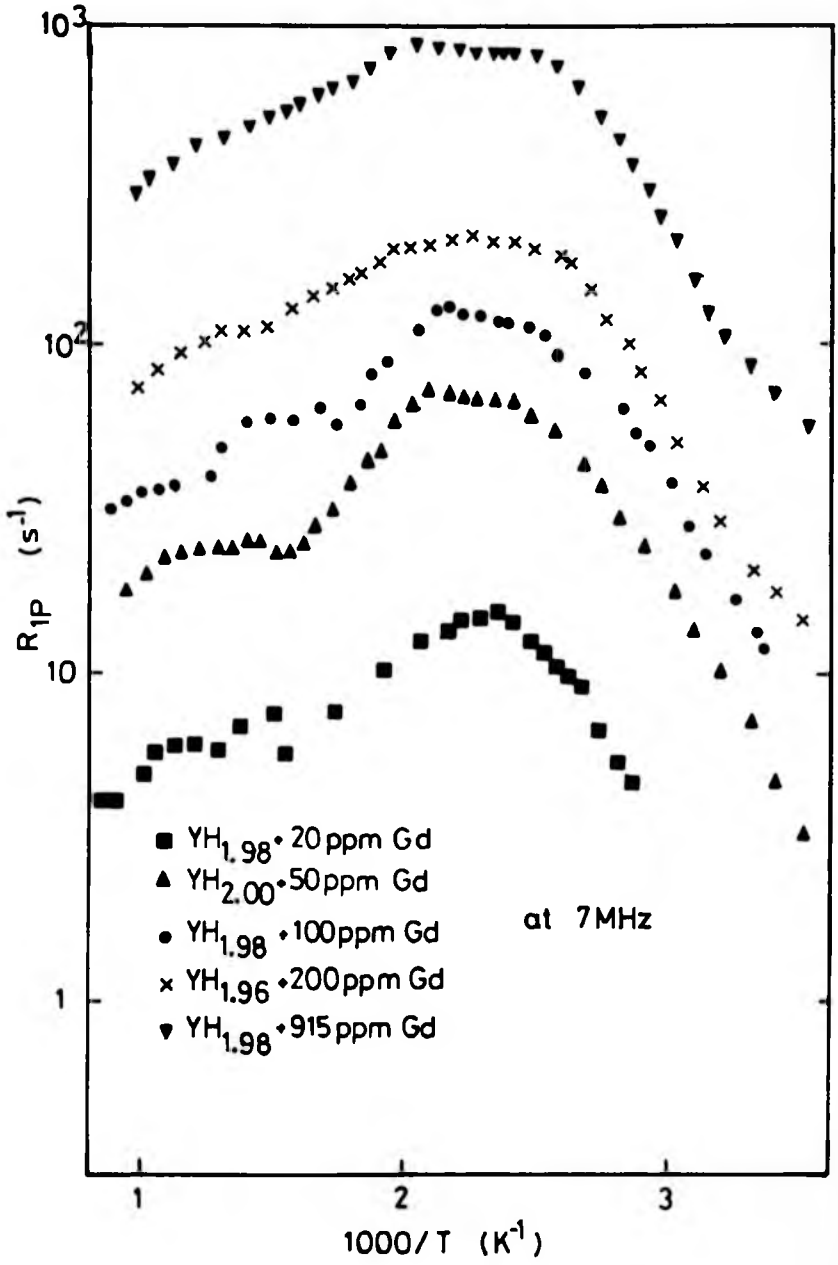

Fig. 4.6: Paramagnetic relaxation rate R_{1p} as a function of reciprocal temperature at 7 MHz.

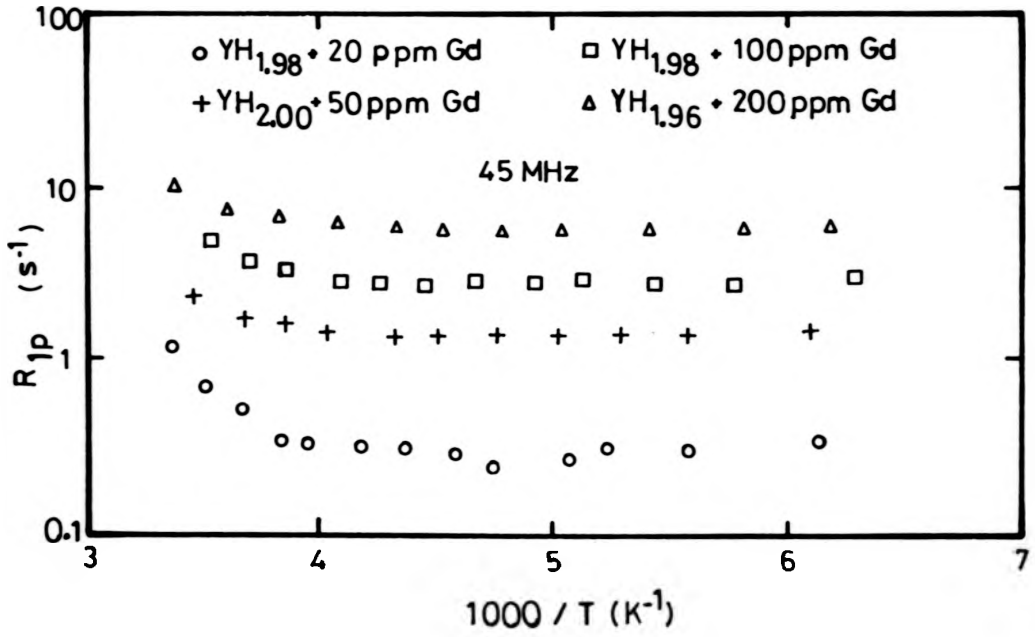

Fig. 4.7: Paramagnetic relaxation rate, R_{1p}, as a function of the reciprocal temperature at 45 MHz

concentration of impurities. Such behaviour can be seen in fig. 4.8 which shows clearly that the proportionality factor between R_{1p} and the concentration of Gd is temperature dependent.

Since R_{1p} is proportional to the Gd concentration allowance for the residual impurity present in the purest sample can be made in order to deduce the electronic contribution to T_1 and to compare the value of E_a and τ_{Do} obtained from the T_2 data. This was achieved by first subtracting from the observed R_1 at 45 MHz at low temperature a sufficient fraction of the known R_{1p} for the 200 ppm Gd specimen to obtain the best fit to a Korringa product. The latter was then also subtracted from the data over the entire temperature range of the remaining relaxation contribution fitted to a single BPP function at 7 MHz. The best fit for $YH_{1.98}$ was obtained for a residual concentration of 2.2 ppm Gd. This value is consistent with the known impurity content of this specimen (i.e. $\sim$ 2 ppm) confirming that the assumptions made at the beginning of this section are justified. The resulting parameters are $\tau_{Do} = (1.85 \pm 0.10) \times 10^{-12}$ s, $E_a = 0.432 \pm 0.006$ eV/atom and $\mathcal{J} = 349 \pm 10$ s.K. It should be noted that these values are in excellent agreement with those deduced from T_2 data without correcting for the residual concentration of impurities. This is clearly indicative of the fact that both T_1 and T_2 would be described by a single correlation function in an impurity free sample.

4.1.c.1. On the coupling between paramagnetic ions and protons

It is thought that the protons, in metal hydrides, are coupled to the paramagnetic ions both via direct dipolar interactions and indirectly via the conduction electrons (RKKY interaction). A direct contact interaction resulting from non zero spin density of localised f or d wavefunctionsat the hydrogen sites is ruled out for reasons given in Appendix 1 . Transition metals are characterised by a

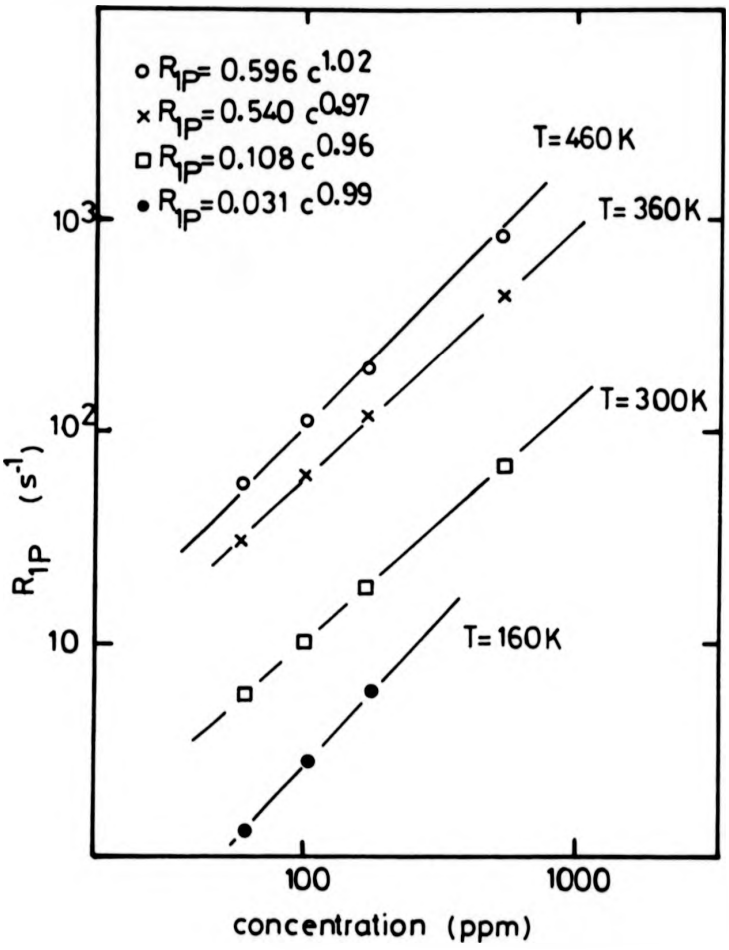

Fig. 4.8: Concentration dependence of the paramagnetic relaxation rate for various temperatures.

relatively narrow d band around the Fermi energy implying that the d-character spin density at the hydrogen sites (octahedral or tetrahedral) is much smaller than that at the metal sites. On adding hydrogen, hybridised states appear having a large s character at the hydrogen sites (Swintendick 1980) but since they lie below the Fermi energy they can only contribute indirectly via interaction with d-conduction electrons (i.e. core polarisation) to the hyperfine fields. Therefore although the RKKY interaction between the ions themselves is important in determining their cooperative magnetic properties (section 2.2.b), it is much less effective between ions and protons due to the small hyperfine interactions between protons and conduction electrons which involve the electronic spin density at the Fermi level at the hydrogen sites. For instance a proton hyperfine field of 2 kG is observed by Bohn and Arons (1982) for the ferromagnetic phase of NdH_2. From that result an RKKY hyperfine field of approximately 500 G from each of the four nearest neighbour Nd^{3+} ions can be deduced (NdH_2 has the CaF_2 structure) which is much smaller than the local dipolar field $H_d \sim \mu/r^3$ due to the Nd^{3+} moment of $\mu = 3.52\ \mu_B$ resulting in $H_d \sim 2.9$ kG. As discussed in section (2.2.c.2), the correlation times involved in both the RKKY and dipolar interactions are the same. Therefore the time correlation of the interactions cannot give rise to differences in their effectiveness. Furthermore only the anisotropic part of the hyperfine interaction includes $S_z I_\pm$ terms giving $R_{1p} \propto \frac{\tau_c}{1+\omega_e^2\tau_c^2}$ compared with $R_{1p} \propto \frac{\tau_c}{1+\omega_e^2\tau_c^2}$ for the isotropic part. The former expression is much more important in determining the effectiveness of the relaxation than the latter and if we consider that $\omega_o\tau_c \sim 1$ we obtain a ratio of $\frac{R_{1p}(\text{Anisotropic})}{R_{1p}(\text{Isotropic})} \sim \frac{\omega_e^2}{\omega_o^2} = \left(\frac{\gamma_e}{\gamma_n}\right)^2 \simeq 4\times10^5$. The anisotropy of the RKKY

interaction would be associated with the dipolar part of the hyperfine interaction which in transition metals is known to be small (Winter 1971) and furthermore due to the cubic symmetry of our compounds is likely to be negligibly small compared to the isotropic part of the hyperfine interaction. It is therefore considered that the direct dipolar coupling will dominate the paramagnetic impurities relaxation rates (Belhoul et al 1982).

4.1.c.2. Characterisation of the different regimes

The dipolar interaction has been extensively discussed in section (2.2.c.2) and we can now identify the different regimes described there as the spin-diffusion, slow atomic diffusion and fast atomic diffusion regions which are well defined in this system. Taking the value of R_{1p} for the 200 ppm Gd sample as a quantitative example the temperatures delimiting the different regimes can be deduced from theory using experimental parameters and compared to those deduced from the R_{1p} experimental data. In what follows the value of τ_D used is $\tau_D = 2.0\ 10^{-12} \exp(0.435/kT)$s (average of τ_D deduced from T_2 and T_1). The spin diffusion region gives way to the atomic diffusion region at temperatures for which $D_a = D_s$ or $\tau_D \sim T_{2RL}$. From NMR linewidth measurements performed at low temperature it has been deduced that $T_{2RL} = 12$ µsec giving rise to a changeover temperature of $T \sim 300$ K. This value is in very good agreement with the temperature of the observed change of slope in fig. 4.6. The upper limit of the slow atomic diffusion region occurs at the temperature for which $\tau_D = {}^1/_{n_1}(a_o)$ or $\beta \simeq a_o$ where $n_1(a_o) = \frac{C_i}{a_o^6}$ and C_1 is defined by equation (2.43). It should be noted that this limit gives the temperature for which the relaxation rate goes through a maximum. In order to calculate this temperature, values of τ_i as a function of temperature are required.

ESR observations of the Gd^{3+} resonance in $YH_{1.98}$ + 100 ppm Gd at 9.3 GHz have been reported by Phua et al (1983). From the measured linewidths at 245 K and 77K and assuming a Korringa relation it is found that $\tau_i T = 3.7 \times 10^{-8}$ s.K. It should be noted that the assumption that τ_i follows a Korringa relation is consistent with the fact that the measured widths for 3% Gd in $YH_{1.85}$ increase linearly with increasing temperature in the range T = 80 to 320 K (Drulis 1974). For comparison the Korringa product deduced from the latter measurements, assuming a life-time broadening of the line shape, is $\tau_i T = 1.0\ 10^{-7}$ s K. The two values differ by a factor of ~ 3 but this discrepancy is not regarded as serious since both the concentrations of hydrogen and Gd are different. At higher temperatures one might expect τ_i to have a phonon contribution which would result in a different temperature dependence of τ_i. Gd^{3+} is an s state ion (4f shell half filled and total spin s = $^7/2$) thus $\ell = 0$ and since the phonon contribution to the relaxation time τ_i is the result of changes in the interaction between the crystal field and orbital moment induced by lattice vibrations, this contribution may be neglected to first order. Using the value of $\tau_i T = 3.7\ 10^{-8}$ s.K, taking $J = S = \frac{7}{2}$ and g = 2.0 for Gd^{3+} and noting that for the change over temperature T = 300 K at the highest operating frequency ν_o = 45 MHz, $\omega_o^2 \tau_c^2 \sim 0.0012$, the expression for C_1 (equation (2.43)) may be reduced to

$$C_1 = 1.55\ 10^{-30} \left| \tau_i + \frac{7\tau_i}{3(1+\omega_e^2 \tau_i^2)} \right| \qquad (4.1)$$

using this result together with $a_o = \sqrt{3}\ a/4 = 2.253\ 10^{-8}$ cm a value of T = 445 K is obtained for the temperature of the change over from slow to fast atomic diffusion. This is in excellent agreement with the temperature T = 450 K at which the experimental R_{1p} goes through a

maximum. At this stage it is interesting to compare the theoretical values of R_{1p} to those obtained experimentally for $YH_{1.98}$ + 200 ppm Gd specifically, beginning with the spin diffusion regime.

4.1.c.3. Spin diffusion regime

In order to calculate the relaxation rate R_{1p}, a value of the spin diffusion coefficient is required (see equation 2.48). The spin diffusion coefficient is calculated from the expression given by Lowe and Gade (1967) for the case of isotropic diffusion on a simple cubic lattice (i.e. it is assumed that the hydrogen atoms occupy tetrahedral sites only). The value obtained is $D_s = 4.3\ 10^{-12}$ $cm^2 s^{-1}$. For the specific temperature T = 170 K at 45 MHz, $\omega_o^2\tau_i^2 = 0.0038$ and $\omega_e^2\tau_c^2 \sim 40$ and thus equation (4.1) can be reduced to $C_1 = 1.55\ 10^{-30}\ \tau_i$. Using this value it is found that the pseudo-potential radius is $\beta = 9.4$ Å at this temperature. The spin diffusion barrier radius b at the operating field $H_o = 10.545$ kG corresponding to the proton resonance frequency $\nu_o = 45$ MHz is deduced from equation (2.47) and (2.46). The value obtained using $T_{2RL} = 12$ μsec is b = 9.6 Å. These values of β and b satisfy the limiting conditions R > b, β specified by Rorschach (1964) in deriving equation (2.48) since here $R = \left(\frac{3V}{4\pi}\right)^{1/3} = \left(\frac{3a^3}{16\pi c}\right)^{1/3} = 35$ Å where c is the fractional impurity concentration (in fact these conditions are satisfied for all the samples studied because for the most heavily doped sample c = 915 ppm, R = 22 Å). At the temperature T = 170 K, making use of the different parameters discussed above the value of R_{1p} calculated from equation (2.48) is $R_{1p} = 7.5\ s^{-1}$ compared to the experimental value $R_{1p} = 6.6 s^{-1}$. Theory over-estimates the relaxation rate by about 12%. This is almost certainly the result of the approximation made in the derivation of some of the parameters used (mainly b and D_s). In deriving b it has

been assumed that there is a sharp transition from a region where the spin diffusion occurs to a region where spin diffusion can no longer occur. Horvitz (1971) has derived an expression for the spin diffusion within the barrier radius b. This may be interpreted as resulting in a smaller effective barrier radius which in turn would affect the value of R_{1p}. However the effect, would be to increase the value of $\delta = \frac{\beta^2}{2b^2}$ which through the factor $I_{3/4}(\delta)/I_{-3/4}(\delta)$ would increase R_{1p} if spin diffusion within b is taken into account and this adds to the discrepancy. In fact the spin diffusion coefficient within b, D_{sb}, may be calculated from

$$D_{sb} = \frac{\pi \gamma_n^6 \hbar^2 \tau_i \langle \mu_p \rangle^2}{20\, a_1^{10}} \left| \frac{1}{n_j^3} - \frac{1}{n_i^3} \right| I$$

where $I = \frac{1}{(\omega_{jo} - \omega_{io})^2}$ if $\gamma_n [H_j(0) - H_i(0)] \tau_i << 1$.

where a_1 is the distance between protons. n_i is the number of lattice spacings between the impurity and the i^{th} nucleus and $\omega_{jo} - \omega_{io} = \gamma_n [H_j(0) - H_i(0)]$ where $H_j(0)$ is the local average field due to the ion. Considering only the nearest and second nearest neighbours to the Gd^{3+} ions, which is consistent with the value of b deduced earlier.

$$\omega_{jo} - \omega_{io} \sim \gamma_n \left| \frac{\langle \mu_p \rangle}{r_j^3} - \frac{\langle \mu_p \rangle}{r_i^3} \right| \sim \frac{\gamma_n \mu_p^2 H_o}{kT} \left| \left(\frac{2}{\sqrt{3} a_1} \right)^3 - \left(\frac{2}{\sqrt{11} a_1} \right)^3 \right| \sim 3\ 10^{-7}\ s^{-1}$$

resulting in $D_{sb} = 0.0\ 10\ 10^{-12}\ cm^2\ s^{-1}$ which is much smaller than $D_s = 4.3\ 10^{-12}\ cm^2\ s^{-1}$. Thus the effect is negligible and could not explain the discrepancy even if it was in the right direction. From the values of b and β calculated for T = 170 K the value of $\delta = 0.474$ is deduced. This indicates that we are in an intermediate region

between the fast spin diffusion regime (equation (2.50): $\delta \ll 1$) and the slow spin diffusion regime (equation (2.49): $\delta \gg 1$). This regime can only be described correctly by equation (2.48) resulting in a temperature dependent relaxation rate (this is seen in fig. 4.7) and a frequency dependence arising from the dependence of the barrier radius on magnetic field which will be discussed later. The temperature dependence of the relaxation rate R_{1p} is the result of the variation of β and δ with temperature, the former through the quantity C_1 which depends on the variable τ_i and the latter through the quantities β and b which depend on both the variables τ_i and B(x) [equations (2.46) and (2.47)]. Again taking the 200 ppm Gd sample as representative and using the parameters discussed earlier, the calculated relaxation rate can be fitted to $R_{1p} = AT^{-n}$. The theory yields a value of n = 0.28 compared to the experimental value n = 0.176 and if from fig. 4.9 which gives the best fit to the equation quoted above the average value of n = 0.16 for the series of $YH_{1.98}$ + Gd samples at 45 MHz is taken the disagreement is worse. But one should remember that up to now no adjustable parameters have been used.

4.1.c.4. Slow atomic diffusion regime

At $T \sim 300$ K the transition from the spin diffusion regimes to the slow atomic diffusion regime occurs. In the latter the atomic diffusion becomes more effective than spin diffusion in transporting the nuclear magnetisation to a region of the sample where the impurity is active. Therefore the relaxation rate R_{1p} should reflect a temperature dependence related to the activation energy of the thermally activated hydrogen diffusion. In this case the barrier radius, which becomes irrelevant, is replaced by the closest distance of approach to

between the fast spin diffusion regime (equation (2.50): $\delta \ll 1$) and the slow spin diffusion regime (equation (2.49): $\delta \gg 1$). This regime can only be described correctly by equation (2.48) resulting in a temperature dependent relaxation rate (this is seen in fig. 4.7) and a frequency dependence arising from the dependence of the barrier radius on magnetic field which will be discussed later. The temperature dependence of the relaxation rate R_{1p} is the result of the variation of β and δ with temperature, the former through the quantity C_1 which depends on the variable τ_i and the latter through the quantities β and b which depend on both the variables τ_i and B(x) [equations (2.46) and (2.47)]. Again taking the 200 ppm Gd sample as representative and using the parameters discussed earlier, the calculated relaxation rate can be fitted to $R_{1p} = AT^{-n}$. The theory yields a value of n = 0.28 compared to the experimental value n = 0.176 and if from fig. 4.9 which gives the best fit to the equation quoted above the average value of n = 0.16 for the series of $YH_{1.98}$ + Gd samples at 45 MHz is taken the disagreement is worse. But one should remember that up to now no adjustable parameters have been used.

4.1.c.4. Slow atomic diffusion regime

At T $\sim$ 300 K the transition from the spin diffusion regimes to the slow atomic diffusion regime occurs. In the latter the atomic diffusion becomes more effective than spin diffusion in transporting the nuclear magnetisation to a region of the sample where the impurity is active. Therefore the relaxation rate R_{1p} should reflect a temperature dependence related to the activation energy of the thermally activated hydrogen diffusion. In this case the barrier radius, which becomes irrelevant, is replaced by the closest distance of approach to

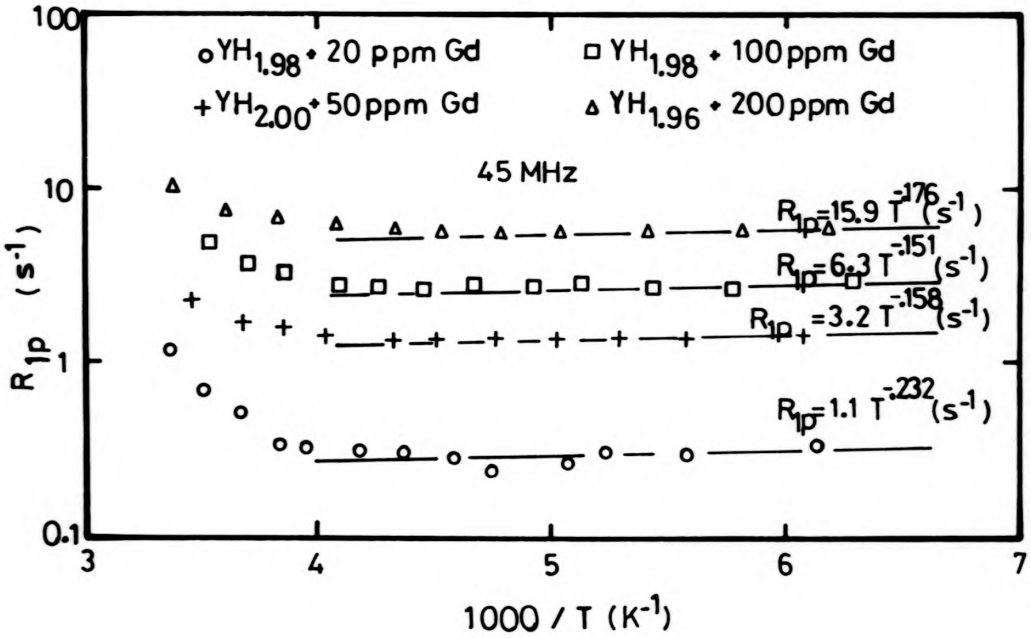

Fig. 4.9: $\bar{R}_{1p}$ as a function of 1000/T at 45 MHz. The full curves are the best fit to equation $R_{1p} = AT^{-n}$.

a magnetic centre and the relaxation rate R_{1p} is expressed by equation (2.51). If the temperature dependence arising from the Bessel functions through the variable δ is ignored, the temperature dependent terms are $C_1^{1/4}$ and $D_a^{3/4}$ and the relaxation rate can be approximated by $R_{1p} \alpha C^{1/4} D_a^{3/4}$. The temperature dependence of this expression is dominated by that of D_a and should display an apparent activation energy $E_a'' = {}^3/4\ Ea$. This value (i.e. $\frac{3 \times 0.435\ eV}{4}$) $E_a'' = 0.32$ eV is satisfactorily close to the value $E_a' = 0.29$ eV observed experimentally. The discrepancy can be completely removed when taking into account the temperature dependence of the Bessel functions. The ratio $\frac{I_{3/4}(\delta)}{I_{-3/4}(\delta)}$ decreases with increasing temperature giving rise to a smaller slope and resulting in an apparent activation energy lower than expected if the temperature dependence of $I_{3/4}(\delta)$ and $I_{-3/4}(\delta)$ is ignored. In this region, therefore, the quantitative agreement with theory is excellent.

4.1.c.5. Fast atomic diffusion regime

The transition from slow to fast atomic diffusion regimes is characterised by $\beta' = a_o$ or $\tau_D = {}^1/n_1(a_o)$. This occurs for T = 445 K. At this temperature the transition from strong to weak collisions occurs and the relaxation rate R_{1p} goes through a maximum. Above this temperature $\beta' < a_o$ and equation (2.51) reduces to equation (2.52). For $YH_{1.98}$ + 200 ppm Gd, using the parameters discussed earlier this equation can be written as

$$R_{1p} = 3.24\ 10^{12}\ [\tau_i^* + \frac{7\tau_i^*}{3(1+\omega_e^2\tau_i^{*2})}]\ s^{-1} \qquad (4.2)$$

here $(\tau_i^*)^{-1} = (\tau_i)^{-1} + (\tau_D)^{-1}$, but since $\tau_i \ll \tau_D$ in the range of temperature investigated $\tau_i^* = \tau_i$. Furthermore for the range of

a magnetic centre and the relaxation rate R_{1p} is expressed by equation (2.51). If the temperature dependence arising from the Bessel functions through the variable δ is ignored, the temperature dependent terms are $C_1^{1/4}$ and $D_a^{3/4}$ and the relaxation rate can be approximated by $R_{1p} \propto C^{1/4} D_a^{3/4}$. The temperature dependence of this expression is dominated by that of D_a and should display an apparent activation energy $E_a'' = {}^3/4\ Ea$. This value (i.e. $\frac{3 \times 0.435\ eV}{4}$) $E_a'' = 0.32$ eV is satisfactorily close to the value $E_a' = 0.29$ eV observed experimentally. The discrepancy can be completely removed when taking into account the temperature dependence of the Bessel functions. The ratio $\frac{I_{3/4}(\delta)}{I_{-3/4}(\delta)}$ decreases with increasing temperature giving rise to a smaller slope and resulting in an apparent activation energy lower than expected if the temperature dependence of $I_{3/4}(\delta)$ and $I_{-3/4}(\delta)$ is ignored. In this region, therefore, the quantitative agreement with theory is excellent.

4.1.c.5. Fast atomic diffusion regime

The transition from slow to fast atomic diffusion regimes is characterised by $\beta' = a_o$ or $\tau_D = {}^1/n_1(a_o)$. This occurs for T = 445 K. At this temperature the transition from strong to weak collisions occurs and the relaxation rate R_{1p} goes through a maximum. Above this temperature $\beta' < a_o$ and equation (2.51) reduces to equation (2.52). For $YH_{1.98}$ + 200 ppm Gd, using the parameters discussed earlier this equation can be written as

$$R_{1p} = 3.24\ 10^{12}\ [\tau_i^* + \frac{7\tau_i^*}{3(1+\omega_e^2\tau_i^{*2})}]\ s^{-1} \qquad (4.2)$$

here $(\tau_i^*)^{-1} = (\tau_i)^{-1} + (\tau_D)^{-1}$, but since $\tau_i \ll \tau_D$ in the range of temperature investigated $\tau_i^* = \tau_i$. Furthermore for the range of

a magnetic centre and the relaxation rate R_{1p} is expressed by equation (2.51). If the temperature dependence arising from the Bessel functions through the variable δ is ignored, the temperature dependent terms are $C_1^{1/4}$ and $D_a^{3/4}$ and the relaxation rate can be approximated by $R_{1p} \propto C^{1/4} D_a^{3/4}$. The temperature dependence of this expression is dominated by that of D_a and should display an apparent activation energy $E_a'' = {}^3/4\ Ea$. This value (i.e. $\frac{3 \times 0.435\ eV}{4}$) $E_a'' = 0.32$ eV is satisfactorily close to the value $E_a' = 0.29$ eV observed experimentally. The discrepancy can be completely removed when taking into account the temperature dependence of the Bessel functions. The ratio $\frac{I_{3/4}(\delta)}{I_{-3/4}(\delta)}$ decreases with increasing temperature giving rise to a smaller slope and resulting in an apparent activation energy lower than expected if the temperature dependence of $I_{3/4}(\delta)$ and $I_{-3/4}(\delta)$ is ignored. In this region, therefore, the quantitative agreement with theory is excellent.

4.1.c.5. Fast atomic diffusion regime

The transition from slow to fast atomic diffusion regimes is characterised by $\beta' = a_o$ or $\tau_D = {}^1/n_1(a_o)$. This occurs for T = 445 K. At this temperature the transition from strong to weak collisions occurs and the relaxation rate R_{1p} goes through a maximum. Above this temperature $\beta' < a_o$ and equation (2.51) reduces to equation (2.52). For $YH_{1.98}$ + 200 ppm Gd, using the parameters discussed earlier this equation can be written as

$$R_{1p} = 3.24\ 10^{12}\ [\tau_i^* + \frac{7\tau_i^*}{3(1+\omega_e^2\tau_i^{*2})}]\ s^{-1} \qquad (4.2)$$

here $(\tau_i^*)^{-1} = (\tau_i)^{-1} + (\tau_D)^{-1}$, but since $\tau_i \ll \tau_D$ in the range of temperature investigated $\tau_i^* = \tau_i$. Furthermore for the range of

temperatures 170 K - 450 K there is no evidence of a phonon contribution to τ_i, but for an s state ion, this is only a second-order process there might be a contribution giving rise to a τ_i which is both field and temperature dependent (i.e. $\tau_i(\text{phonon}) \propto \frac{c}{H_o^4 T^2}$ for $T > \theta_D \cong 200$ K). Thus the high temperature data should give us information on the nature of the interaction involved in τ_i. At the operating frequency ν_o = 7 MHz, $\omega_e = 28950.310^6$ rad/s and for T = 445 K assuming $\tau_i T = 3.8\ 10^{-8}$ s K, we obtain $\omega_e \tau_i = 2.4$. Any significant phonon contribution would reduce τ_i and yield a value $\omega_e \tau_i << 2.4$. Now, assuming that above T = 450 K $\omega_e \tau_i << 1$ equation 4.2 reduces to

$$R_{1p} = 10.8\ 10^{+12}\ \tau_i \quad s^{-1} \qquad (4.3)$$

which will reflect the temperature dependence of τ_i. In fig 4.10 the relaxation time T_{1p} is plotted against T. It can be seen that the experimental data follow a relatively good linear relation. The slight curvature may be explained by the fact that with $\tau_i T = 3.7\ 10^{-8}$ s.K, the relaxation rate T_{1p} is a more complex function of τ_i than that described by equation (4.3). Thus there is no indication of a significant phonon contribution to the electronic relaxation time τ_i. At this point it is interesting to extract values for τ_i from the experimental data for the two limiting cases $\omega_e \tau_i << 1$ characterised by equation (4.3) and $\omega_e \tau_i >> 1$ for which equation (4.2) can be reduced to

$$R_{1p} = 3.24\ 10^{12}\ \tau_i\ s^{-1} \qquad (4.4)$$

with the assumption that $\tau_i T$ = constant based on the evidence discussed above. The former should give a lower limit on the value of $\tau_i T$ while the latter is the upper limit. Under these conditions

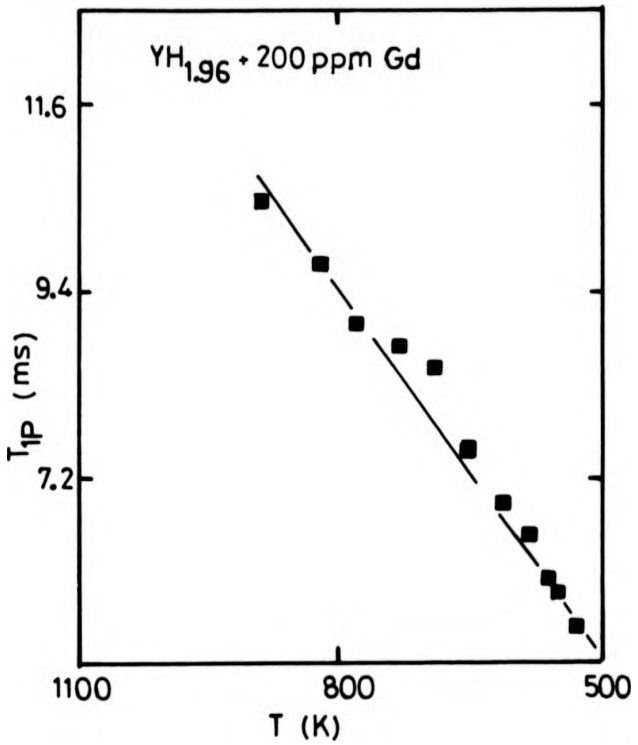

Fig. 4.10: Paramagnetic relaxation time T_{1p} for temperatures above 500 K. The full curve is a guide to the eye.

for $\omega_e\tau_i$ << 1 the 7 MHz data for T > 600 K may be fitted using $\tau_i T = 1.1\ 10^{-8}$ s.K and at the other extreme, $\omega_e\tau_i$ >> 1, the value of $\tau_i T$ deduced from the slope of the experimental data is $\tau_i T = 3.7\ 10^{-8}$ s.K. Regarding the value of $\omega_e\tau_i$ for T = 600 K ($\omega_e\tau_i$ = 1.8 using $\tau_i T$ deduced from ESR) we are in a region intermediate between these two limiting conditions and the value of $\tau_i T$ should lie between $1.1\ 10^{-8}$ and $3.7\ 10^{-8}$ s.K. The value derived under the condition $\omega_e\tau_i$ >> 1 is in excellent agreement with the value deduced from ESR measurement, however the magnitude of the calculated R_{1p} values does not agree with experiment and taking this value of $\tau_i T$ the condition $\omega_e\tau_i$ >> 1 is not strictly fulfilled (i.e. for T = 600 K, $\omega_e\tau_i$ = 1.8).

In summary we may say that although quantitative agreement with theory is not always obtained, very good qualitative agreement is obtained in the three characteristic regimes. The discrepancies are almost certainly due to the various assumptions made in the derivation of the relevant parameters when experimental values were not available. Fig. 4.11 shows the results of the calculation made using no adjustable parameters together with the experimental R_{1p} as a function of the reciprocal temperature.

4.1.c.6. Frequency dependence of R_{1p}

The dependence of R_{1p} upon the frequency (i.e. magnetic field) is different in the spin diffusion and atomic diffusion regimes and will therefore be discussed separately.

(i) Spin diffusion regime

From the value deduced earlier, δ = 4.8, we have deduced that the relaxation rate R_{1p} follows equation (2.48) which exhibits a frequency dependence through the parameters β and δ. β depends on

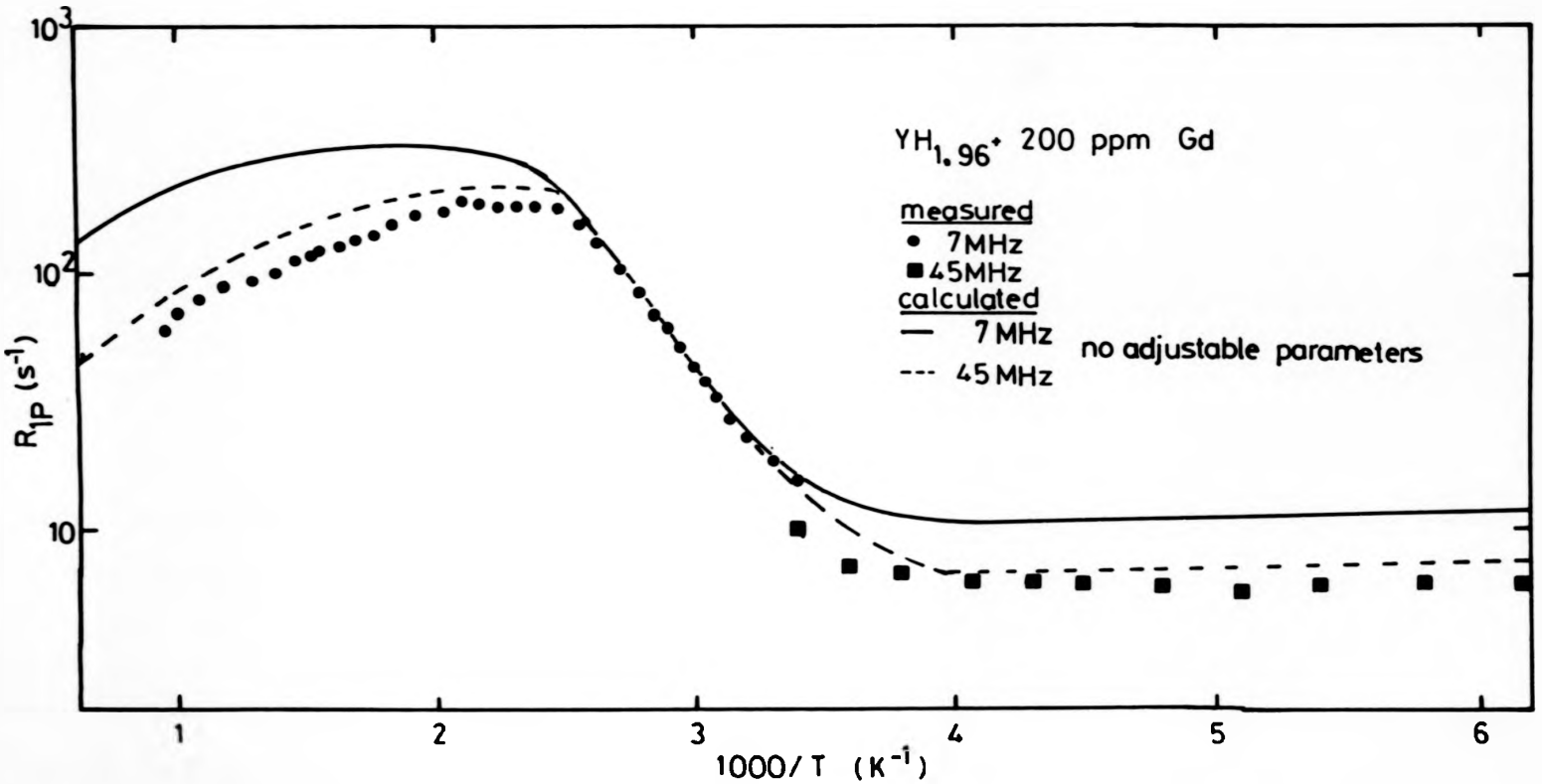

Fig. 4.11: Theoretical prediction of the temperature variations of R_{1p} in yttrium dihydride containing 200 ppm Gd, using the nonadjustable parameters discussed in the text. The variations deduced from experiment are shown for comparison.

the frequency through C_1 which is a function of both ω_o and ω_e and δ shows a frequency dependence through C_1 and the barrier radius b which depends on the Brillouin functions B(x) where $x = \frac{\mu_p . H_o}{kT}$. In this region the rate R_{1p} is only available at 45 MHz and in order to investigate its frequency dependence it is compared to that obtained at 40 MHz as a function of temperature by Phua (1982) and at 60, 24, 12.2 MHz for T = 200 K by Phua et al (1983). For this range of frequencies and assuming $\tau_i T = 3.7\ 10^{-8}$ s. K, the conditions $\omega_o^2 \tau_c^2 << 1$ and $\omega_e^2 \tau_i^2 >> 1$ are always satisfied. Furthermore in view of the linearity of τ_i versus 1000/T in this range of temperature (Drulis 1974) we may rule out any field dependence of τ_i. Thus the frequency dependence of R_{1p} arises only from the field dependence of δ. We first consider the frequency dependence of R_{1p} at 40 MHz and 45 MHz as a function of temperature. As discussed earlier, the rate R_{1p} can be fitted to a good approximation by $R_{1p} = AT^{-n}$. The calculated values of R_{1p} yield $R_{1p} = 32.4\ T^{-0.28}\ s^{-1}$ and $R_{1p} = 36.0\ T^{-0.29} s^{-1}$ for ν_o = 45 and 40 MHz respectively compared to the experimental expressions $R_{1p} = 13.8\ T^{-0.16}$ and $R_{1p} = 15.1\ T^{-0.16}$. In the case of the experimental data the temperature exponent and prefactor are the averaged values, scaled to 200 ppm Gd, of those obtained for the series of samples. Here we are not interested in absolute agreement between experiment and theory but in accounting for the relative change of the fitted parameters with decreasing frequency. The very small relative change of the calculated temperature exponent with frequency can be said to be consistent with that deduced from experiment within experimental error, and it is interesting to note that the ratio of the prefactors deduced from the theoretical expressions for R_{1p} is 0.90 in excellent agreement with the experimental value of 0.91.

We may conclude therefore that while the actual magnitude of the fitted parameters deduced from experiment and theory do not agree very well, their relative changes with frequency can be understood in terms of the frequency dependence of the barrier radius b. It should be stressed however, that the relative frequency difference between 40 and 45 MHz is only 10% and only a very strong frequency dependence would give a reliable indication of the agreement between theory and experiment. In order to draw firmer conclusions the 45 MHz R_{1p} for $YH_{1.98}$ + 200 ppm Gd scaled up to 475 ppm are compared to those obtained at 60 MHz, 40 MHz, 24 and 12.2 MHz at T = 200 K. Fig. 4.12 shows a plot of the relaxation rates R_{1p} versus frequency normalised to that obtained at 40 MHz together with the theoretical predictions. The experimental results shows a stronger frequency dependence than that predicted by the theory using the parameters discussed earlier. It is interesting to consider the two limiting cases for fast spin diffusion $\delta << 1$ and slow spin diffusion $\delta >> 1$, in order to see if better agreement may be obtained. In the former limit the relaxation is described by equation (2.50) (i.e. $R_{1p} = \frac{4\pi}{3} \frac{NC}{b^3} I$). At T = 200 K and for all the frequencies $x = \frac{\mu_p H_o}{kT} << 1$ and $\langle \mu_p \rangle = [g^2 \mu_o^2 s^2 \{\frac{9}{49} x^2 + \frac{6}{2\pi} \tan^{-1} \frac{2\pi\tau_i}{T_{2RL}}\}]^{\frac{1}{2}}$, resulting in $(R_{1p})^{-8/3} = a\,\nu_o^2 + b$. Fitting the experimental results to this expression we deduce that $\tau_i T = 1.5\ 10^{-9}$ s.K. On the other hand in the slow diffusion limit R_{1p} is independent of frequency. This can be achieved theoretically by putting $\tau_i T \simeq 1.0\ 10^{-5}$ s.K. The value of $\tau_i T$ obtained for both limiting regimes when compared to the experimental value $\tau_i T = 3.7\ 10^{-8}$ s.K confirm that at 200 K we are in a regime intermediate between fast and slow spin diffusion, but we are not able to account for the difference between theoretical

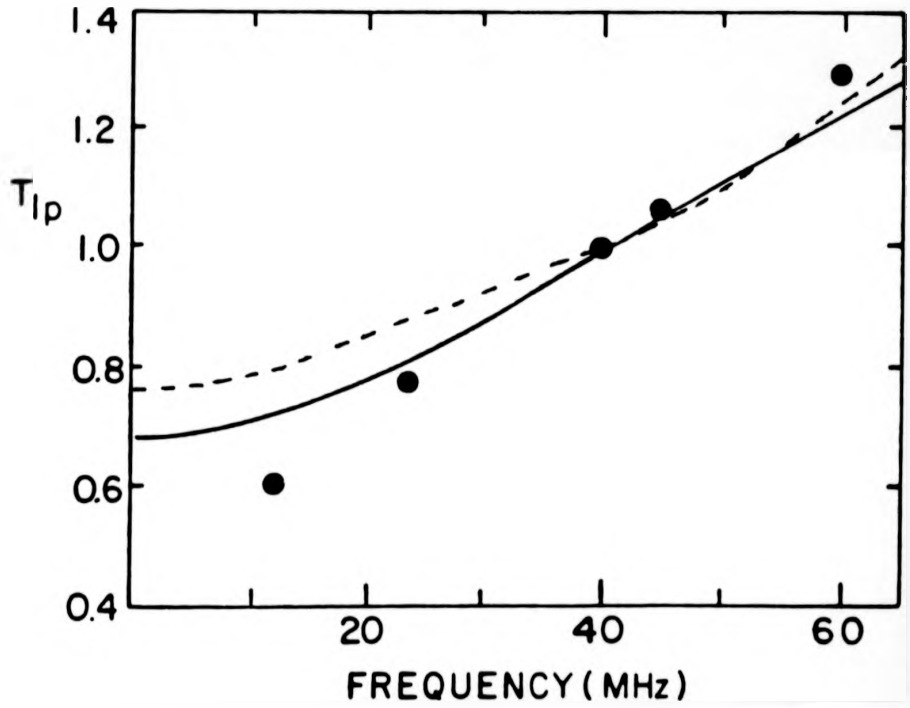

Fig. 4.12: Proton spin-lattice relaxation time due to Gd^{3+} in $YH_{1.98}$ + 475 ppm Gd at 200 K, measured as a function of frequency. The ordinate is T_{1p} normalized to the value of 40 MHz. The full curve is the theoretical prediction using the non-adjustable parameters described in the text. The broken curve is the theoretical prediction using the fitted parameters (see text).

and experimental frequency dependence in this region.

(ii) Atomic diffusion regime

The frequency dependence expected, comes from the term β' involving C_1. Therefore a frequency dependence is expected only for the range of temperature for which $\omega_e\tau_i \sim 1$ with the assumption that τ_i is field independent. Fig. 4.13 which shows R_{1p} versus 1000/T at 40 and 45 MHz indicates that for temperatures greater than 600 K the experimental data show no frequency dependence. This suggests that either $\omega_e\tau_i \gg 1$ or $\omega_e\tau_i \ll 1$, and that τ_i is field independent but in view of the fact that the frequency dependence in the spin diffusion region, cannot be fully accounted for by the existing theory, assuming a field independent parameter τ_i, let us first analyse the high temperature data in term of a τ_i field dependence.

In fig. 4.13 it can be seen that the maximum in R_{1p} which occurs at T = 454 K for the 7 MHz data is shifted to T = 525 K at 40 MHz. Attributing the shift in temperature to a field dependence of τ_i and since the maximum occurs for $\tau_D = a_o^6/C_1$ where C_1 is approximated by $C_1 = 1.55\ 10^{-30}\ \tau_i$ (this approximation does not affect this interpretation) the values τ_i (40 MHz) = $2.8\ 10^{-9}$ s at T = 525 K and τ_i (7 MHz) = $5.5\ 10^{-10}$ s at T = 454 K are obtained. Those values have a ratio of 5 which should result in a similar ratio for the values of $(R_{1p})_{max}$ at 40 MHz and 7 MHz ($(R_{1p})_{max}$ (40 MHz) $\sim$ 745 s^{-1} and $(R_{1p})_{max}$ (7 MHz) $\sim$ 149 s^{-1}). The experimental change is however in the opposite direction to that predicted. It should be noted that the approximation made above, $\omega_e\tau_i \gg 1$, does not in fact affect the discussion since it can be seen that if this condition were not satisfied a smaller value of τ_i (7 MHz) would be deduced

adding to the discrepancy. A field dependence of τ_i can therefore be ruled out and we may now consider the first suggestion. If the condition $\omega_e\tau_i >> 1$ were satisfied we would deduce a value of $\tau_i T = 3.7\ 10^{-8}$ sK (see section 4.1.c.5.) in excellent agreement with the value deduced from ESR. However, in this case, no frequency dependence would be predicted at lower temperatures. If the alternative condition $\omega_e\tau_i << 1$ were satisfied at high temperatures then the observed frequency dependence at lower temperatures (300 K<T< 600 K) might be due to the $\omega_e\tau_i$ term which increases with decreasing temperature. Furthermore as the temperature is decreased below T $\sim$ 450 K the frequency dependence should become less apparent, because in this range of temperature (i.e. slow atomic diffusion) the relaxation rate is described by equation (2.51) and is proportional to $\beta' = \left(\frac{C_1}{Da}\right)^{1/4}$ whereas above 450 K, R_{1p} can be expressed by equation (4.2) and is now directly proportional to C_1. Finally the value of R_{1p} should decrease with increasing frequency since any contribution of the term containing $\omega_e\tau_i$ at 7 MHz (i.e. $\omega_e\tau_i \sim 1$) would be reduced at higher frequency making C_1 decrease with frequency and since $R_{1p} \propto C_\varphi^n$ where n is either 1 or $^1/_4$, R_{1p} is expected to decrease with increasing frequency. These qualitative arguments seem to fit the trend followed by the experimental observation. However the value $\tau_i T = 1.1\ 10^{-8}$ s.K deduced earlier in this limit yields values of R_{1p} at low temperatures in poor agreement with experiment. For example for T = 150 K, R_{1p} (4 5 MHz) = 2.2 s^{-1} compared with the experimental value of 6.6 s^{-1}. Moreover the shift of the temperature (R_{1p}) with frequency would be in the opposite direction to that observed experimentally.

To summarize the foregoing discussion it may be said that the existing theory of the dipolar interaction between proton and paramagnetic ions gives very good qualitative and in some respects

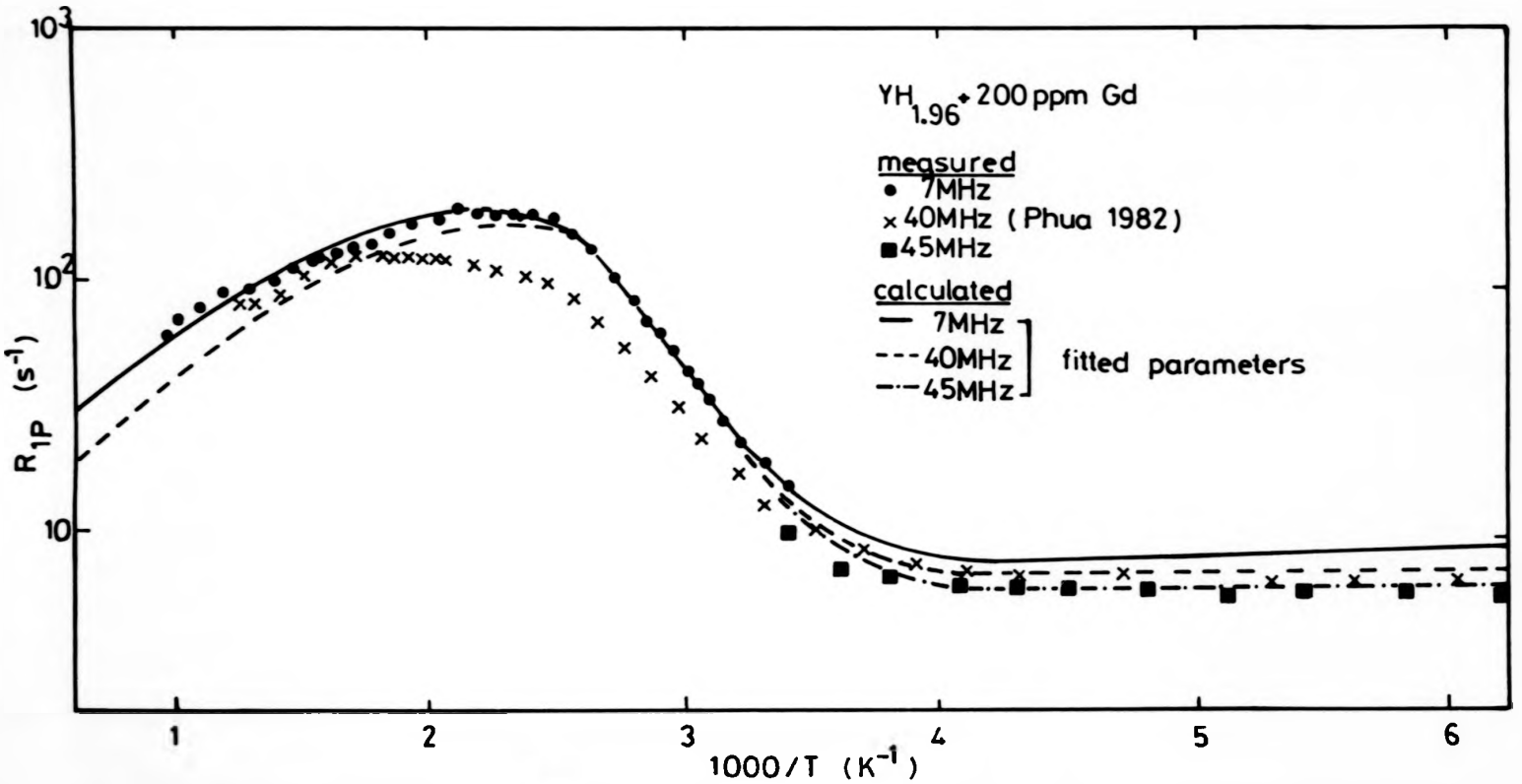

Fig. 4.13: Theoretical prediction of R_{1p} as a function of temperature using the fitted parameters deduced from the analysis of the 7 MHz R_{1p} data (see text). For comparison the experimental results obtained at 7, 45 MHz (this work) and 40 MHz (Phua 1982) are shown.

quantitative agreement with experiment. The agreement in the spin diffusion and slow atomic diffusion regimes at 7 MHz is very good while only qualitative agreement is obtained in the fast atomic diffusion regime. The frequency dependence expected from the theory cannot be fully understood using fixed parameters derived either from experiment or existing theories. This is particularly the case for the high temperature (T > 300 K) frequency dependence observed. In order to investigate if a better agreement with theory may be obtained, the data have been fitted using adjustable parameters.

4.1.c.7. Adjustable parameters

In order to obtain reliable fitted parameters their numbers have been kept to a minimum. The adjustable parameters are the activation energy, the pre-exponential dwell time, the Korringa product $\tau_i T = K$, the spin diffusion coefficient and finally a constant factor f_T introduced in the atomic diffusion regime only. The adjustment of these parameters may be justified by the following considerations:

(a) The activation energy obtained from T_1 and T_2 may be subject to some uncertainties owing to the effect of other paramagnetic impurities present in the samples.

(b) The preexponential dwell time τ_{Do} may be in error by as much as 100% using BPP theory.

(c) The value of $\tau_i T$ was deduced from ESR measurements at only two temperatures and may be subject to error. It should be noted that the assumption that $\tau_i T = K$ is the result of fitting procedure using $(\tau_i)^{-1} = aT + bT^n$ which always gave a negligible contribution from the second term.

(d) The value of D_s used earlier was derived from the expression given by Lowe and Gade (1972) assuming that the hydrogen atoms occupy the tetrahedral sites only, although it is known (Venturini et al 1980) that a fraction of the octahedral sites are also occupied.

(e) The atomic diffusion coefficient used has been defined by $D_a = \frac{a_1^2}{6\tau_D}$ which does not take into account the tracer correlation factor f_T (i.e. $D_a = f_T \frac{a_1^2}{6\tau_D}$), where f_T is 1 for an uncorrelated random walk jump process and decreases with decreasing vacancy concentration.

The 7 MHz data were fitted first, to equation (2.51) in order to simplify the function used, since the lowest temperature R_{1p} data indicates that we are already in the atomic diffusion regime. The various parameters obtained are then used without adjustment when fitting the 45 MHz data in order to obtain D_s. Example of this fitting method are given in fig. 4.14 for the two samples of $YH_{1.98}$ containing 200 and 915 ppm Gd respectively while the resulting fitted parameters are listed in table 4.2 . The activation energy obtained which is the same for the two samples is in excellent agreement with that obtained from T_1 and T_2 measurements giving credibility to the method. The value of $\tau_i T$ is again nearly the same for the different samples and in excellent agreement with the value derived from the experimental data of Drulis (1974) confirming that there is no appreciable phonon contribution to τ_i. The preexponential dwell times obtained differ from one sample to the other and are not in good agreement with that obtained in the first section (i.e. $\tau_{Do} = 2.0\ 10^{-12}$ s), but knowing that a τ_{Do} derived using BPP is prone to large error, this disagreement should not be regarded as too serious. The values of f_T obtained are more difficult to explain since the minimum value

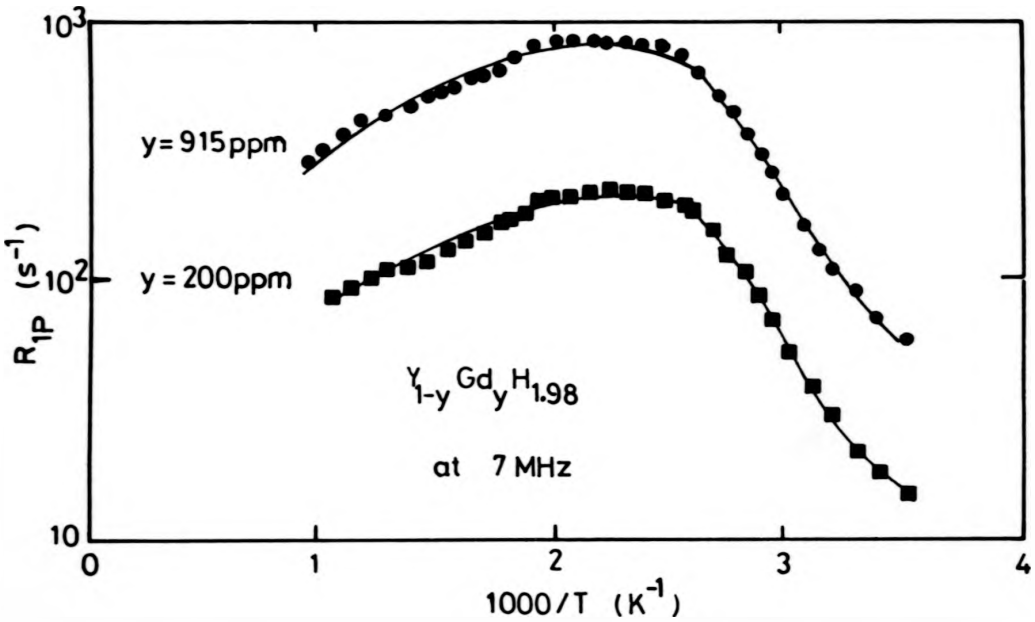

Fig. 4.14: R_{1p} versus the reciprocal temperature (1000/T) for $YH_{1.98}$ containing 200 and 915 ppm Gd repectively. The solid line is the result of the fit to equation (2.51). The fitted parameters are listed in table 4.2.

Table 4.2: Results of the fitting procedure

Samples	τ_{DO}(s)	E_a(eV)	$\tau_i T$(s.k)	f_T	D_s($cm^2 s^{-1}$)
$YH_{1.98}$ + 200 ppm Gd	0.392×10^{-12}	0.439	1.0×10^{-7}	0.197	52.4×10^{-13}
$YH_{1.98}$ + 915 ppm Gd	0.426×10^{-12}	0.431	1.04×10^{-7}	0.186	-

of f_T obtainable, in the monovacancy limit, is $f_T = 0.67$ (Sankey and Fedders 1977) which is about 3.4 times larger than the fitted parameters. But if we concentrate on the value of $D_o = f_T \frac{a_1^2}{6 \tau_{Do}}$ where $a_1 = a/2$ we find $D_o = 4.9\ 10^{-5}$ cm^2/s and $D_o = 5.9\ 10^{-5}$ cm^2/s for the 915 and 200 ppm Gd samples respectively. These values compare very well to that calculated with $\tau_{Do} = 2.0\ 10^{-12}$ s and $f_T = 1$, giving $D_o = 5.6\ 10^{-5}$ cm^2/s. And therefore the small values of f_T and τ_{Do} obtained here should not be regarded as resulting from a failure of the method. At low temperature the fitted value of the spin diffusion coefficient $D_S = 52.4\ 10^{-13}$ cm^2/s is larger than that used previously $D_S = 43.5\ 10^{-13}$ cm^2/s. This can be understood in terms of partial octahedral occupation which due to the smaller O-T distance gives rise to an increase in the second moment M_2 and since $T_{2RL} \propto M_2^{-\frac{1}{2}}$ and $D_S \sim \frac{a_1}{50 T_{2RL}^2}$ (Bloembergen 1949), a larger spin diffusion coefficient is expected, than that deduced assuming T-site occupation only.

We may summarize by saying that the theory gives a quantitative description of the experimental observations and that the changes in the values of the derived parameters compared with those used earlier may be understood in terms of partial occupation of octahedral sites. In view of this very good agreement it is worth investigating again the frequency dependence of R_{1p} using the fitted parameters.

The broken curve in fig. 4.12 shows the calculated values of R_{1p} at T = 200 K for the frequencies 60, 45, 40, 24 and 12.2 MHz. It can be seen that the frequency dependence is even less strong than that predicted using the non adjustable parameters (full curve) and agreement with experiment is poor. The frequency dependence in the atomic diffusion regime can be seen in fig. 4.13 where the 7 and 40 MHz experimental data have been plotted together with the theoretical calculations using the adjustable parameters. Quantitative agreement with the 40 MHz data is now much better but the overall frequency dependence exhibited

by the experimental data cannot yet be understood in terms of the existing theory unless τ_i is field dependent which from the experimental evidences discussed above is surely not the case.

4.1.d. Discussion of the T_2 data

As mentioned earlier the T_2 data are very little affected by the presence of Gd for temperatures below 400 K and give consistent results when fitted to theories describing the proton dipole-dipole interaction . Fig.4.15 shows examples of these fitted curves. For temperatures between 550 K and 700 K T_1 and T_2 are equal for all specimens and since in this range of temperature $T_{1d} = T_{2d}$, T_{1p} and T_{2p} are also equal. For temperatures above $\sim$ 700 K T_2 falls below T_1 for the purer samples and, this will be discussed in the second part of this chapter. The main theoretical difference between T_{1p} and T_{2p} lies in the expression for C_α due to the different components of the fluctuating magnetic field produced by the electronic spin flip of the magnetic ion at the hydrogen site which are involved in the T_{1p} and T_{2p} processes. We have pointed out earlier that for $T < 600$ K, $\omega_e\tau_i >> 1$ and $\omega_o\tau_i << 1$ for all temperatures. With these conditions the expression for C_2 used in the derivation of T_{2p} is

$$C_2 = \frac{2}{5}\gamma_p^2\gamma_n^2\hbar^2 J(J+1)\left[\frac{2}{3}\tau_i + \frac{\tau_i}{2(1+\omega_o^2\tau_i^2)} + \frac{13}{6}\frac{\tau_i}{(1+\omega_e^2\tau_i^2)}\right]$$

which reduces to

$$C_2 = \frac{2}{5}\gamma_p^2\gamma_n^2\hbar^2 J(J+1)\left[\frac{7}{6}\tau_i\right] = 1.82\ 10^{-30}\ \tau_i$$

In the spin diffusion and slow atomic diffusion regimes below 450 K, $R_{2p} \propto C_2^{1/4}$ resulting in the ratio $\frac{R_{2p}}{R_{1p}} = 1.04 \sim 1$. Therefore in this regime $R_{1p} \sim R_{2p}$, in agreement with experiment. In the fast atomic

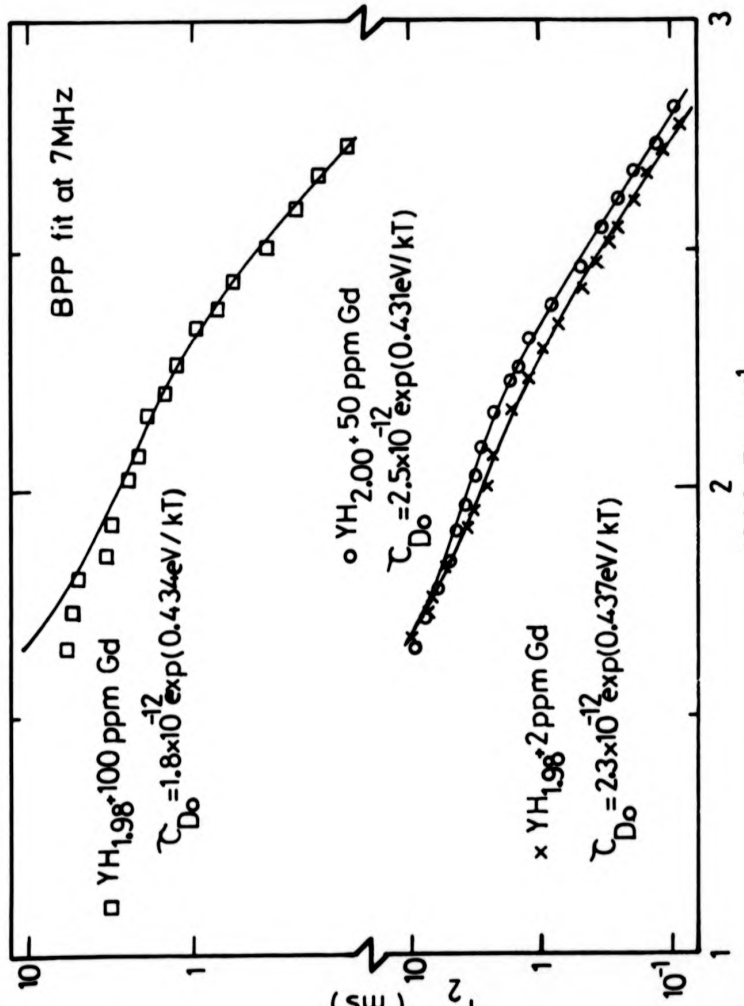

Fig. 4.15: Examples of T_2 data fitted to BPP for various concentrations of Gd. Note the change of scale for clarity purpose.

diffusion regime, above 450 K, R_{2p} is characterised by equation (2.52) which can be simplified to $R_{2p} \propto C_2$ leading to the ratio $\frac{R_{2p}}{R_{1p}} = 1.17$. The data are entirely consistent with the near equality of T_{1p} and T_{2p} throughout the range of temperature discussed here. The absence of a detectable minimum in T_2 for $\tau_D = {}^1/\eta_2(a_o)$ which in view of the very small difference between $\eta_2(a_o)$ and $\eta_1(a_o)$ is expected to occur at T = 445 K (the same temperature as for T_{1p}), results from the relative magnitudes of the nuclear-nuclear and nuclear-impurity dipole contributions to the observed relaxation time. Such minima in T_2 have been observed, for example in PbF_2 doped with Mn (Vernon et al 1981).

These considerations may be compared to those involved in $(T_{1\rho})_p$ In YH_2 no subsidiary minimum is observed in $T_{1\rho}$ (Anderson et al 1980). Around and below the temperature for which $T_{1\rho}$ goes through a minimum associated with the familiar condition $\omega_1\tau_c \sim 1$, the values of the proton-proton dipole relaxation time are intermediate between those of T_{1d} and T_{2d}. Since it can be shown for $(T_{1\rho})_p$, that for the range of temperaturesbelow 600 K $T_{1p} \sim T_{2p} = (T_{1\rho})_p$, in view of the magnitude of $(T_{1\rho})_d$, only a minor effect should be expected on the observed $T_{1\rho}$ values for our range of Gd concentrations.

The small effect of Gd on the observed spin-spin relaxation time particularly at low temperature (T < 500 K) where the proton-proton dipole contribution dominates the relaxation time means that a comparison of T_2 and T_1 measurements should give unambiguous evidence of the presence of paramagnetic impurities. T_2 measurements although subject to larger experimental errors (i.e. particularly in powdered metal-hydrides), may be preferred to T_1 measurements, in those samples where the presence of paramagnetic impurities is suspected, for the accurate determination of the activation energy and preexponential time τ_{DO}. Similarly $T_{1\rho}$ which is less affected than T_1 by the presence

of impurities may be a preferable type of measurements.

4.1.e. Determination of the Korringa product

The effect of paramagnetic impurities has been shown to be important for very low concentration (i.e 2ppm) at low temperature (spin diffusion regime) contributing strongly to the total relaxation time measured. It has been usual to determine the conduction electron contribution in this range of temperature where it dominates T_1. However, if paramagnetic ions are present the Korringa product derived from the low temperature T_1 may be subject to large error if T_{1p} is not taken into account. This effect was suspected for instance in LaH_x by Cotts and Schreiber (1963), but for low concentrations of impurities it has always been assumed to be insignificant. For high impurity concentrations the measured T_1 in the rigid-lattice regime is reported to decrease with decreasing temperature (Phua et al (1983), Kashaev (1980)). In such cases the presence of impurities even if unsuspected may clearly be detected. The separation of R_{1e} and R_{1p} may not be easily made but at least care may be taken regarding the reliability of the extracted Korringa product. The effect of paramagnetic impurities is not as easily resolved for lower concentrations of ions (i.e. < 200 ppm Gd in this study) and for instance the low temperature 45 MHz data may be reasonably well fitted to a Korringa relation for the purest (i.e. $\sim$ 2 ppm Gd) and less pure ($\sim$ 20 ppm Gd) samples. In this situation the effect of paramagnetic impurities is not evident leading to values of the Korringa product derived from the observed data which are subject to large errors. Some methods which allow a better estimate of the Korringa product are currently under investigation.

An obvious and very good method is to investigate the concentration dependence of the paramagnetic contribution to the observed rate and

to subtract from the observed R_1 a sufficient fraction of the known R_{1p}, for a given concentration, to give the best fit to a Korringa relation. This method which does not require a knowledge of the parameters discussed earlier has been applied here and the deduced Korringa product is $T_{1e}T$ = 349 s.k instead of $T_{1e}T$ = 302 s.k obtained from the purest sample neglecting R_{1p}. The relative uncertainty which is $\sim$ 15% for a concentration of only 2 ppm Gd, is much larger when dealing with concentrations of 20 ppm or 50 ppm Gd. Unfortunately this method suffers from the need to investigate a large number of samples. Alternatively, one may apply the method often used when the presence of impurities is suspected in the samples (Goring et al (1981), Zogal and Idriak (1981)). The observed rate is fitted to $R_1 = R_{1e} + B$ with the assumption that B is temperature independent. A linear plot of this relation against temperature yields a straight line whose reciprocal slope gives the Korringa product and whose intercept gives the value of the impurity rate. In view of the previous observations it should be stressed that this method can only be applied to those cases where the paramagnetic impurity concentration is sufficiently low that its contribution to the total observed rate may be taken as temperature independent. This method of analysis has been applied to the 45 MHz T_1 data for the three samples containing 2, 20 and 50 ppm Gd respectively. The results of such an analysis are shown in fig. 4.16 where the solid lines are the results of the least squares fit to the relation mentioned above. The value obtained for the 2 ppm Gd sample $T_{1e}T$= 352 s.k is in excellent agreement with that deduced above (349 s.K) but as the concentration of Gd increases the agreement becomes less good. This emphasizes that, this method is only applicable in cases where the impurity induced rate R_{1p} is sufficiently small, but whenever applicable has the great advantage of giving to good accuracy, the value of $T_{1e}T$ directly. Other methods

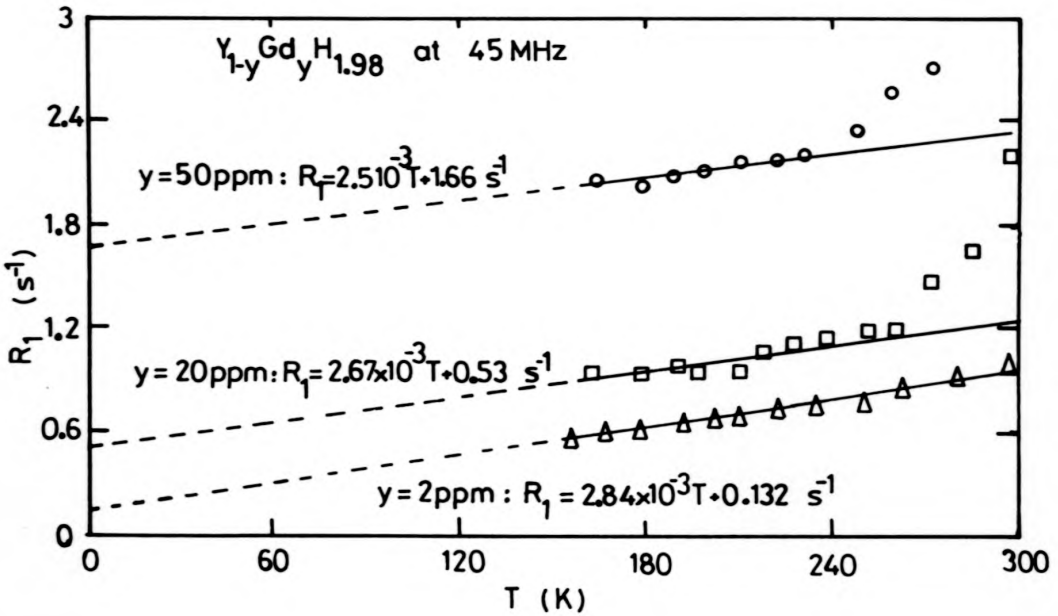

Fig. 4.16: Relaxation rate R_1 as a function of temperature for various Gd concentrations, at 45 MHz. The solid lines are the results of the least squares fit to $R_1 = AT + B$.

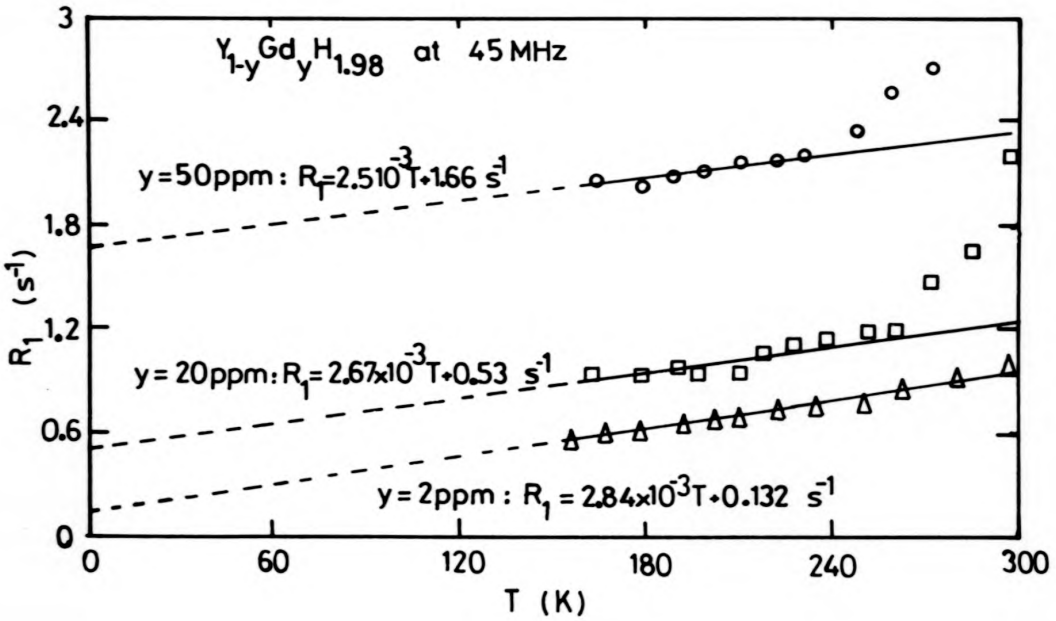

Fig. 4.16: Relaxation rate R_1 as a function of temperature for various Gd concentrations, at 45 MHz. The solid lines are the results of the least squares fit to $R_1 = AT + B$.

may also be mentioned. For instance it has been clearly shown that the relaxation rate R_{1p}, in the spin diffusion regime, is frequency dependent. The frequency dependence, in this region may to a good approximation be expressed as $R_{1p} = A\ \nu_o^{-b}$ where ν_o is the frequency in MHz. Therefore an alternative way of deducing $T_{1e}T$ is to measure R_1 at the highest possible operating frequency. Alternatively as discussed by Tse and Lowe (1968), in the spin diffusion regime, $(R_{1\rho})_p \propto C_\rho^{1/4} D_s^{\rho 3/4}$ while $(R_{1p}) \propto C_1^{1/4} D_s^{3/4}$. We have seen that for $\omega_1\tau_i \ll 1$, $\omega_o\tau_i \ll 1$ and $\omega_e\tau_i \gg 1$, $C_\rho = \frac{7}{6} C_1$. Tse and Lowe have shown that $D_s^\rho = \frac{1}{2} D_s$ resulting in a ratio $\frac{(R_{1\rho})_p}{R_{1p}} = 0.617$ or $(T_{1\rho})_p = 1.62\ T_{1p}$. Therefore the Korringa product deduced from $T_{1\rho}$ measurements are less liable to be affected by the presence of impurities. Finally a method which gives a considerable reduction of the value of the spin diffusion coefficient and hence of R_{1p}, in the spin diffusion regime, without altering other parameters, is to substitute part of the hydrogen atoms by deuterons. This method has been applied to the case of La doped with Gd (Seymour, Phua et al 1983). The resulting Korringa product was found to be larger than that found in the purest hydride available.

Among all the methods presented here the most unambiguous is the first because all the others rely on the fact that the range of temperatures in which one deduces the Korringa product is also the spin-diffusion regime for the paramagnetic relaxation. However in the case where measurements are extended to low enough temperature, ensuring that $\tau_D \gg T_{2RL}$, partial deuteration of the hydrides is certainly the most attractive method since it does not require a knowledge of the concentration of impurities, although it may be argued that the electronic properties of the hydride may be different from that of the partially deuterated sample.

Having understood the effects that small amounts of paramagnetic

impurities can have on the apparent relaxation time in metal hydrides it is interesting to consider a possible misinterpretation of the data for the purer samples (2 α 20 ppm Gd) since such low concentrations may accidentally be present in hydrides generally. This alternative interpretation is discussed in 4.1.f since in several published papers a similar interpretation has been placed upon subsidiary minima observed on the low temperature side of the main dipole-dipole minima.

4.1.f. Misinterpretation of T_1 minima

The appearance of a discontinuity in the linearity of $Ln\tau_D$ versus 1000/T (plots derived from NMR T_1 measurements) has been reported for a number of hydrides. These include YH_x (Kashaev 1980), LaH_x (Kashaev 1980), ScH_x (Weaver 1972) and VH_x (Fukai and Kazama 1977) among others. These departures from normal behaviour have sometimes been explained in terms of hydrogen motion on two sublattices formed by different interstitial sites. This misinterpretation is understandable in view of the partial octahedral sites occupation found in most of these compounds (Venturini and Richards 1980). Both NMR (Anderson et al 1980) and neutron scattering experiments (Khatamian et al 1980) have unambiguously shown partial O site occupation in YH_2. Two cases may be considered, in the analysis of the T_1 data, as follows. Firstly the O-site and T-site hydrogens are differentiated by the fact that they cannot be characterised by a common spin temperature resulting in the observation of two different spin-lattice relaxation times which assuming an exponential correlation function, may be described by the two following equations

$$\frac{1}{T_1(T)} = K\left\{537.7\ \beta\left[\frac{\omega_o\tau_{CTT}}{1+\omega_o^2\tau_{CTT}^2}+\frac{4\omega_o\tau_{CTT}}{1+4\omega_o^2\tau_{CTT}^2}\right]+660.6\ \alpha\left[\frac{\omega_o\tau_{CTO}}{1+\omega_o^2\tau_{CTO}^2}+\frac{4\omega_o\tau_{CTO}}{1+4\omega_o^2\tau_{CTO}^2}\right]\right\} \qquad (4.4)$$

$$\frac{1}{T_1(0)} = K\left\{115.6\ \alpha\left[\frac{\omega_o\tau_{COO}}{1+\omega_o^2\tau_{COO}^2}+\frac{4\omega_o\tau_{COO}}{1+4\omega_o^2\tau_{COO}^2}\right]+1321\ \beta\left[\frac{\omega_o\tau_{COT}}{1+\omega_o^2\tau_{COT}^2}+\frac{4\omega_o\tau_{COT}}{1+4\omega_o^2\tau_{COT}^2}\right]\right\}$$

(4.5)

where

$$\frac{1}{\tau_{CTT}}=\frac{1}{\tau_{DTT}}+\frac{1}{\tau_{DTT}},\quad \frac{1}{\tau_{COO}}=\frac{1}{\tau_{DOO}}+\frac{1}{\tau_{DOO}},\quad \frac{1}{\tau_{CTO}}=\frac{1}{\tau_{COT}}=\frac{1}{\tau_{DTT}}+\frac{1}{\tau_{DOO}},$$

where τ_{DTT} and τ_{DOO} are the dwell times associated with T-T and 0-0 jumps respectively, $K=\frac{2}{5}\frac{\gamma_I^4\hbar^2 I(I+1)}{\omega_o a^6}$ and $2\beta+\alpha = x$ where x is the hydrogen to metal atom ratio. For all the T_1 measurements the magnetization recoveries followed a single exponential and only a single T_1 was observed leading to the conclusion that the 0 and T sublattices are characterised by a common spin temperature. This is to be expected since the two sublattices are interpenetrating and the shift of the resonance frequencies for hydrogens on 0 and T sites is expected to be much smaller than the line width so that mutual spin flips between nearest neighbour 0 and T sites can occur. In this case if the jumps between 0 and T sites are not too frequent compared to $^1/\tau_{DOO}$ and $^1/\tau_{DTT}$ the resulting T_1 may be expressed as the weighted sum of equations (4.4) and (4.5), that is

$$\frac{1}{T_i}=\frac{\alpha}{\alpha+2\beta}\frac{1}{T_i(0)}+\frac{2\beta}{\alpha+2\beta}\frac{1}{T_1(T)}\quad \text{resulting in}$$

$$\frac{1}{T_i}=\frac{K}{\alpha+2\beta}\left|115.6\ \alpha^2\left[\frac{\omega_o\tau_{COO}}{1+\omega_o^2\tau_{COO}^2}+\frac{4\omega_o\tau_{COO}}{1+4\omega_o^2\tau_{COO}^2}\right]+2643\ \alpha\beta\left[\frac{\omega_o\tau_{CTO}}{1+\omega_o^2\tau_{CTO}^2}+\frac{4\omega_o\tau_{CTO}}{1+4\omega_o^2\tau_{CTO}^2}\right]\right.$$

$$\left.+\ 1076.4\ \beta^2\left[\frac{\omega_o\tau_{CTT}}{1+\omega_o^2\tau_{CTT}^2}+\frac{4\omega_o\tau_{CTT}}{1+4\omega_o^2\tau_{CTT}^2}\right]\right| \qquad (4.6)$$

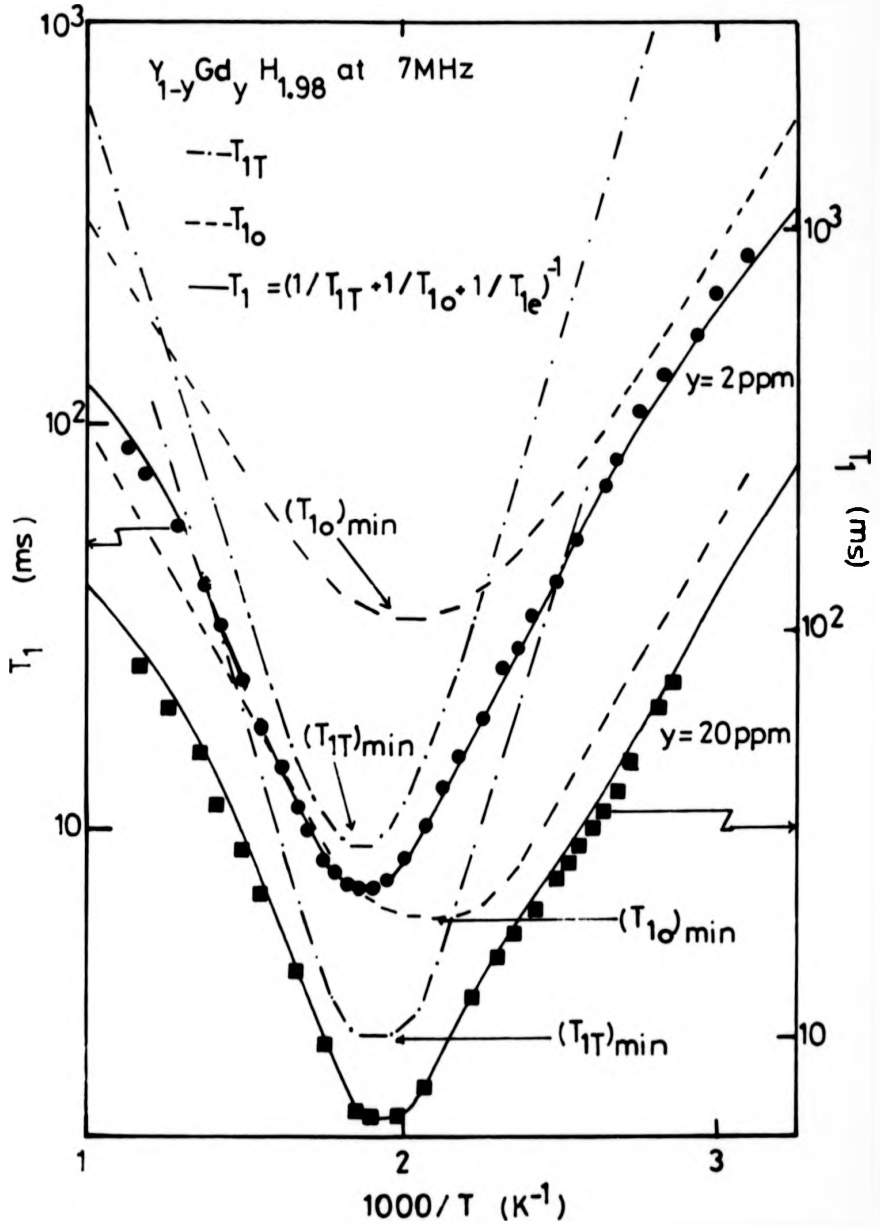

Fig. 4.17: Examples of T_1 data fitted to equation (4.6)

According to this expression three minima in T_1 are expected, for $\omega_o\tau_{COO} \sim 1$, $\omega_o\tau_{CTO} \sim 1$ and $\omega_o\tau_{CTT} \sim 1$ respectively. However, the weighting factors for the different expressions in brackets are very different and since $\beta >> \alpha$ the first term of equation (4.6) can be neglected, resulting in the observation of only two minima. Finally the case where the jumps between O and T sites are frequent compared with $^1/_{\tau_{DTT}}$ and $^1/_{\tau_{DOO}}$, would certainly result in a spectral density which could not be expressed as the weighted sum of O and T spectral densities. This is because the distinction between O and T sites is blurred by the fast jump frequency between these sites. Fig. 4.17 shows examples of T_1 fitted to equation (4.6) for $YH_{1.98}$ + 2 ppm Gd and $YH_{1.98}$ + 20 ppm Gd at 7 MHz. The fits are very good over the entire temperature range. From the ratio of $(T_{1O})_{min}$ and $(T_{1T})_{min}$ we may deduce, following this interpretation, the fractional occupancies α and β of O and T sites respectively. Phua (1982) reports values of α = 11% for $YH_{1.98}$ + 20 ppm Gd at T = 420 K and 40 MHz while this analysis yields α = 10.3% for $YH_{1.98}$ + 2 ppm at T = 420 K. These values are compared to those obtained from the temperature dependence of O site occupation given by Venturini and Richards (1980) who have assumed a simple gas lattice model then

$$\alpha = x-4x/\{2+x+B(1-x)+\sqrt{8B+2[2-x-B(1-x)]^2}\} \qquad (4.7)$$

where B = exp - 0.070 (eV)/KT. It should be stressed however, that using values of α and β predicted by equation (4.7), the linewidth of the proton resonance ΔH, deduced from the second moment M_2, as follows

$$M_2 = \frac{Ca^{-6}}{2\beta+\alpha}\,(115.6\,\alpha^2 + 2643\,\alpha\beta + 1075.4\,\beta^2 + 1.42\,\beta + 0.46\,\alpha)$$

where $c = 3.57\ 10^{-46}$ G^2 cm^2, a = 5.204 Å and $\frac{M_2}{\Delta H^2} = (\frac{n}{n-1})^{2/n}\,\frac{\Gamma(3/n)}{4\Gamma(1/n)}$

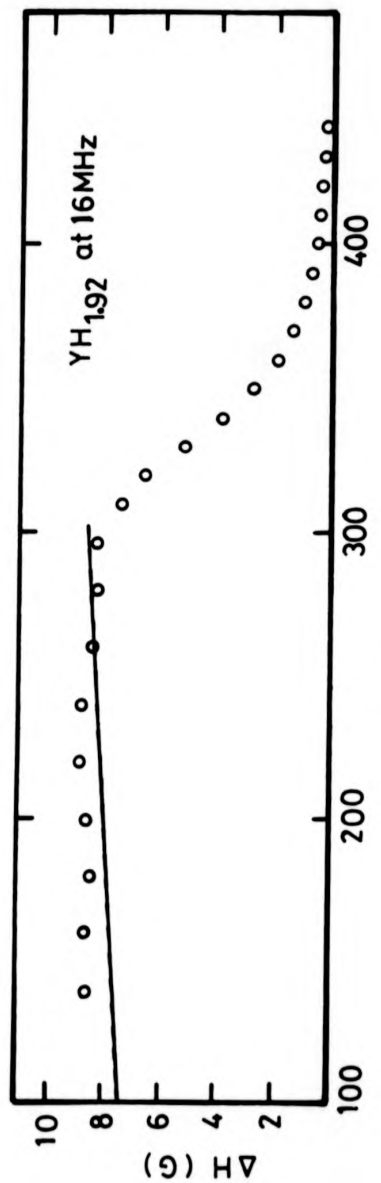

Fig. 4.18: Temperature dependence of the line width of $YH_{1.92}$. The full curve is the calculated line width using the values of α and β deduced from equation (4.7).

where n = 2.4 is the Harper-Barnes parameters, shows a stronger temperature dependence than that obtained from the experimental line-widths as a function of temperature (Anderson 1979). This is illustrated in fig. 4.18 which shows the calculated line-width (full curve) together with the experimental data. Therefore the values of α deduced from this model should be regarded as an upper limit. Thus α values derived from experiment should lie between the two limiting values obtained from low temperature NMR data (Anderson et al 1980) and that obtained using equation (4.7) which are 11.5% and 28% respectively. The agreement may be regarded as good if the experimental results are interpreted independently and may give support to this type of interpretation. However, from equation (4.6) the temperature of both minimum ($T_{1(O)}$ and $T_{1(T)}$) should decrease with frequency. This is not the case here since although the main minimum is shifted to lower temperature as expected for dipole-dipole relaxation, $T_{1(O)}$ goes through a minimum for the same temperature, for both 7 MHz and 40 MHz frequencies. To summarize, we do not believe that the appearance of the subsidiary minimum can be explained in term of the weighted sum of two correlation functions. This type of analysis which finds grounds in the fact that the experimental data can be fitted very well using such a model, may be very misleading, but the frequency dependence of T_1 measurements coupled with T_2 or $T_{1\rho}$ data should remove any doubts as to whether the data may be interpreted using this model. Above all the model does not seem physically viable.

4.2. The YH_x system

4.2.a. Experimental results

The series of yttrium hydrides, YH_x where x = 1.72, 1.81, 1.92, and 1.98, studied here was not prepared from the same yttrium metal

where n = 2.4 is the Harper-Barnes parameters, shows a stronger temperature dependence than that obtained from the experimental line-widths as a function of temperature (Anderson 1979). This is illustrated in fig. 4.18 which shows the calculated line-width (full curve) together with the experimental data. Therefore the values of α deduced from this model should be regarded as an upper limit. Thus α values derived from experiment should lie between the two limiting values obtained from low temperature NMR data (Anderson et al 1980) and that obtained using equation (4.7) which are 11.5% and 28% respectively. The agreement may be regarded as good if the experimental results are interpreted independently and may give support to this type of interpretation. However, from equation (4.6) the temperature of both minimum ($T_{1(0)}$ and $T_{1(T)}$) should decrease with frequency. This is not the case here since although the main minimum is shifted to lower temperature as expected for dipole-dipole relaxation, $T_{1(0)}$ goes through a minimum for the same temperature, for both 7 MHz and 40 MHz frequencies. To summarize, we do not believe that the appearance of the subsidiary minimum can be explained in term of the weighted sum of two correlation functions. This type of analysis which finds grounds in the fact that the experimental data can be fitted very well using such a model, may be very misleading, but the frequency dependence of T_1 measurements coupled with T_2 or $T_{1\rho}$ data should remove any doubts as to whether the data may be interpreted using this model. Above all the model does not seem physically viable.

4.2. The YH_x system

4.2.a. Experimental results

The series of yttrium hydrides, YH_x where x = 1.72, 1.81, 1.92, and 1.98, studied here was not prepared from the same yttrium metal

and the concentration of paramagnetic impurities may vary from one hydride to the next. The amount of impurity is only known for $YH_{1.81}$ which contains 20 ppm Gd and for $YH_{1.98}$ which contains 2 ppm Gd. The suspected amount of Gd in $YH_{1.72}$ is about 2 to 5 ppm and about 15 ppm in $YH_{1.92}$. The spin lattice relaxation time T_1 and the spin-spin relaxation times T_2 have been measured for this series of samples. T_1 and T_2 have been measured at 7 MHz for the range of temperature 300 to 1200 K and T_1 has also been measured at 45 MHz for the range of temperature below 300 K. A composite plot of T_1 and T_2 at 7 MHz against the reciprocal temperature is shown in fig. 4.19 while T_1 data at 45 MHz are shown in fig. 4.20. The T_1 data at 45 MHz which shows nearly identical T_1 behaviours for $YH_{1.98}$ and $YH_{1.72}$ containing $\sim$ 2 ppm Gd and for $YH_{1.92}$ and $YH_{1.81}$ which contain $\sim$ 20 ppm Gd seem to indicate that the Korringa product is at least,comparable for each pair of samples. At higher temperature the 7 MHz spin-lattice and spin-spin relaxation times follow the behaviour expected in the case of a proton dipole-dipole interaction. No clear subsidiary minimum can be detected on the low temperature side of $(T_1)_{min}$ and the situation is similar to that discussed earlier for the low-impurity content $YH_{1.98}$ samples (i.e. less than 20 ppm Gd). The most striking feature is the decrease of the temperature of the $(T_1)_{min}$ with increasing hydrogen concentration. From fig. 4.19 we can see also that the slope, on both sides of the $(T_1)_{min}$, decreases with increasing hydrogen concentration. This suggests that the activation energy for hydrogen diffusion decreases with increasing H/M ratio. Similar behaviour was noted by Schreiber and Cotts (1963) and Phua (1982) in the case of lanthanum dihydride. Finally having allowed for the difference in frequencies between the measurements, the values of T_1 here are much longer throughout the temperature range than those reported by Kashaev et al (1980) suggesting

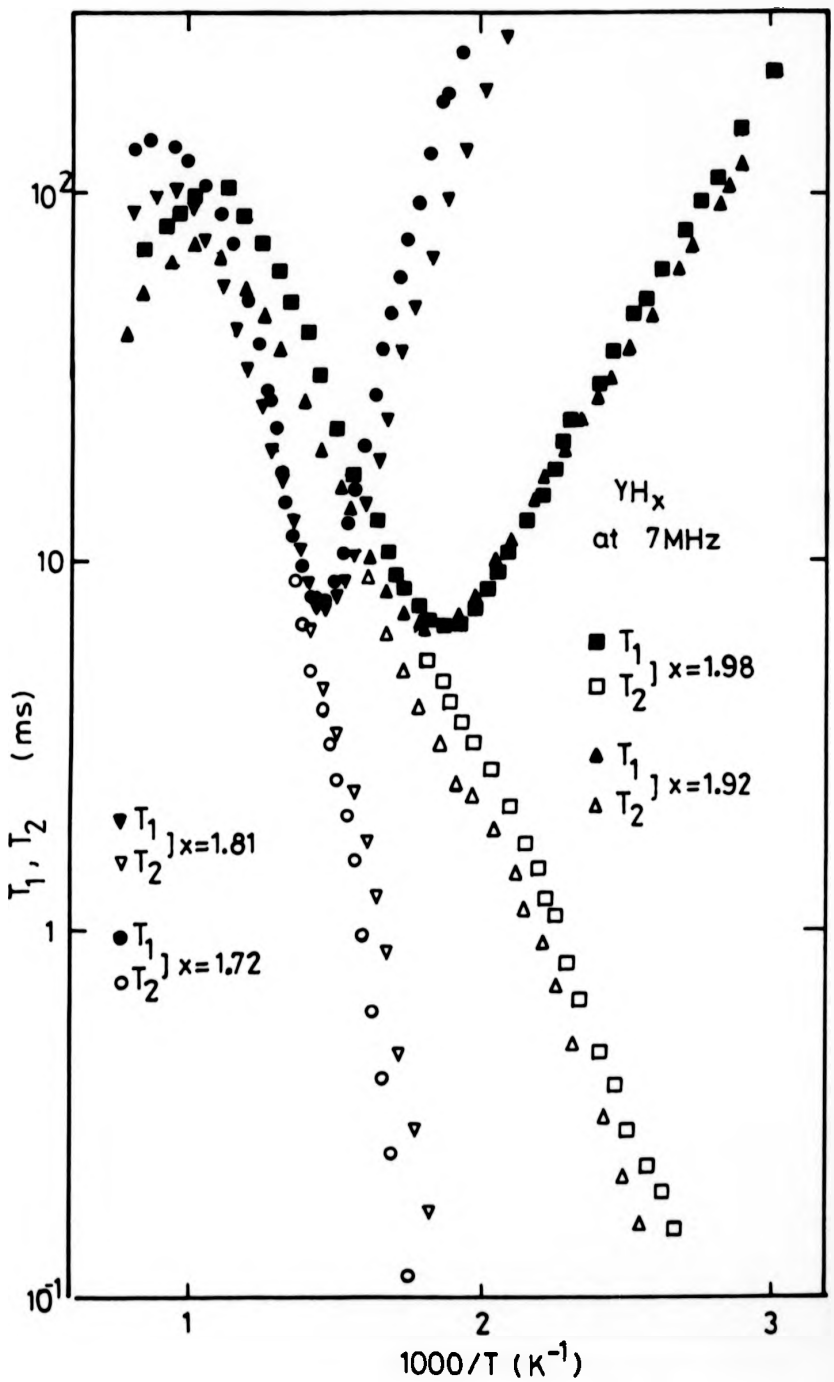

Fig. 4.19: Proton spin-lattice and spin-spin relaxation times as a function of the reciprocal temperature in YH_x. For the sake of clarity the low temperature T_2 data only, are shown.

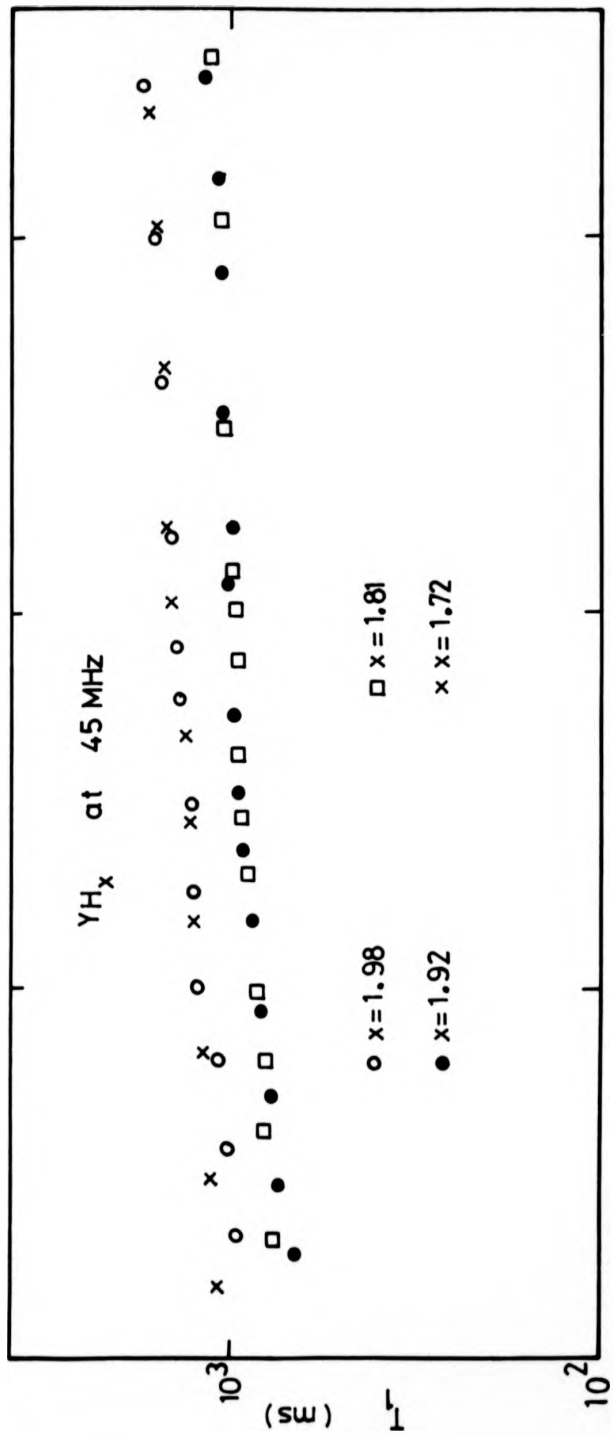

Fig. 4.20: Proton spin-lattice relaxation time in YH_x at 45 MHz.

that their samples contained considerable levels of paramagnetic impurity. Above $\sim$ 1000 K, T_1 starts decreasing with increasing temperature in a manner which cannot be accounted for by a $T_{1e}T$ term independent of temperature. For temperatures above 700 K T_2 falls below T_1 then goes through a minimum at T $\sim$ 1000 K and cannot be understood in terms of a simple dipole-dipole interaction. Similar anomalous behaviour was observed by Boyce et al (1977), in the temperature dependence of the ^{19}F nuclear relaxation times T_1 and T_2, in pure PbF_2. The high temperature T_1 and T_2 data were at first thought to be the result of reactions between the yttrium metal and the silica vial but in view of the reproducibility of the T_1 and T_2 results with decreasing temperature, this behaviour is thought to be real.

4.2.b. Characterisation of the samples

The lower boundary of the dihydride β phase of yttrium cannot accurately be determined from the phase diagram reported by Mueller et al (1968). From NMR measurements Anderson et al (1979) deduced that the lower limiting composition of the dihydride phase was given for the atomic ratio H/Y = 1.80 ± 0.1 at room temperature. Our wide-line NMR measurements are not as conclusive. The α phase resonance was only observed in $YH_{1.72}$ at liquid nitrogen temperature and no α phase resonance was detected for $YH_{1.81}$ either at room temperature or liquid nitrogen temperature as shown in fig. 4.21. This seems to agree with the T_1 data which will be discussed later. Furthermore Dantzer and Kleppa (1980) reported that the dihydride phase of yttrium extends from $YH_{1.1}$ to YH_2 at 900 K, and since T_1 and T_2 were measured at 7 MHz in the range of temperature above room temperature we conclude that our samples are single β phase hydrides.

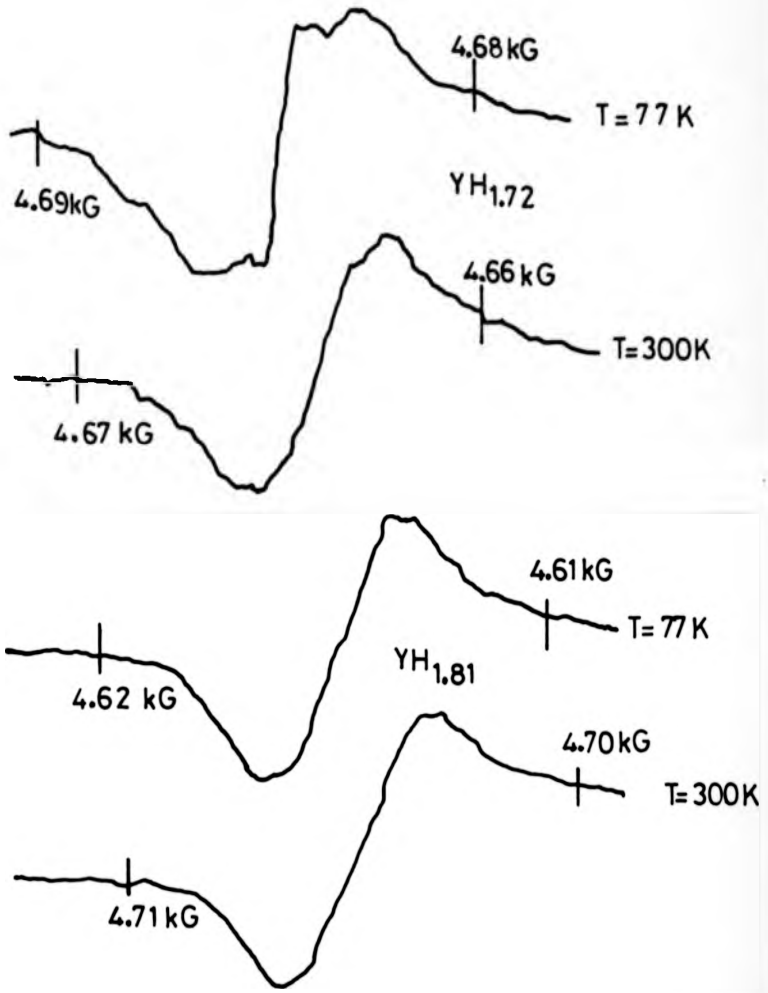

Fig. 4.21: Proton line width at T = 77 and 300 K for $YH_{1.72}$ and $YH_{1.81}$. The modulation amplitude was kept to 0.1 G for all the measurements.

4.2.c. Discussion of the low temperature results at 45 MHz

Low temperature T_1 observations, are usually accounted for by assuming that the hydrogen nuclei interact with the conduction electrons (Cotts 1978) but in our case this picture is complicated by the presence of paramagnetic Gd^{3+}. We have discussed in section (4.1.e.), some methods which permit a reliable value of the Korringa product to be obtained. Here the maximum amount of Gd present in the specimens is 20 ppm. We have shown that for 20 ppm Gd we can extract a value of $T_{1e}T$ within 10% of its real value by assuming that $R_1 = R_{1e}+B$. The values of the Korringa product shown in table 4.3 for the different samples have been obtained using this method. These values are equal within experimental error including the added uncertainty due to the method of extraction of $T_{1e}T$. Similar behaviour is reported in LaH_x where the value of $T_{1e}T$ increases only slightly (< 10%) as x varies from 1.8 to 2.27 (Phua 1982) and since YH_2 and LaH_2 should present some similarities due to their similar electronic structure (d^1s^2 outer electron) and similar dihydride phase structure, our values of $T_{1e}T$ are regarded as satisfactory. This is to be contrasted to the results obtained by Korn (1978) for TiH_x where $T_{1e}T$ varied between 190 and 62 s.K as x varied from 1.55 to 1.90. Korn used a semi rigid-band model to explain the deereases of the density of state at the Fermi level. This was based on the rigid band model developed by Schrieber and Cotts (1963) to explain the metal to semi-conductor transition as the hydrogen to metal atom ratio reaches 3. A protonic model was used based on the fact that no hydrogen Knight shift was observed (no electronic charge around the hydrogen atom). In fact as discussed earlier, band calculations consistent with experimental work indicate not only that the rigid band concept is invalid but that a relatively

large amount of negative charge resides at the proton sites. The relaxation time due to the conduction electrons as seen in Chapter II is directly related to the density of state at the Fermi energy. There are three contributions to the relaxation time from the orbital, the core polarisation and the s contact interactions. The last is proportional to the s-like density of states at the Fermi level. Band calculations performed by Swintendick (1980) for non-stochiometric YH_x for $x \geq 2$ indicate that very little s state density is present at the tetrahedral sites but that occupation of octahedral sites is accompanied by a large increase of s density of states at the Fermi level at the octahedral sites. Similar calculations in LaH_2 (Kulikov 1982) indicate the same trend. If the s contact term was dominant a large decrease in $T_{1e}T$ would be expected in LaH_x as the concentration of hydrogen exceeds $x = 2$. This is not the case experimentally and we conclude that the contact term is negligible. Similarly in YH_x as x varies from 1.72 to 1.98 a substantial increase in 0-site occupation is expected (Venturini et al 1980) and one would expect $T_{1e}T$ to decrease if the contact term was significant. Furthermore Weaver and Peterson (1980) measured the photo electron emission intensity for $YH_{1.73}$ and $YH_{1.98}$ and found that the derived conduction electron emission d band shows no difference near the Fermi level, the only additional feature in the case of $YH_{1.98}$ compared to $YH_{1.73}$ being the increase in emission intensity approximately 1.5 eV below the Fermi level. Thus we conclude that the s contact term is not significant. Further evidence for this comes from the sudden increase in the Korringa product for $LaH_{2.4}$. This cannot be explained by the growing s-like density of states at the Fermi level at the octahedral sites but is understood in term of the decrease of the d-density of states at the Fermi level which was experimentally verified by Weaver et al (1983) in agreement with band calculations. Recent NMR

studies of several Ti based hydrides (Bowman et al (1982), Güring et al (1981)) and Zr hydrides (Korn 1983) have indicated that the orbital hyperfine interaction does not give significant contributions to the proton Knight shift and T_{1e} parameter. Similarly, the orbital contribution may be assumed to be unimportant for the proton parameters in YH_x, leaving only the core polarisation contribution which may be considered to be due to hydrogen-centred orbitals arising from a combination of metal d-electrons at the Fermi level interacting with hydrogen centred inner valence s-electrons. This picture is consistent with band calculations which indicate a large DOS having s character below the Fermi level, at the tetrahedral sites. A Korringa type relation exists for core polarization (Yafet and Jaccarino 1964) which may be expressed as

$$K^2 T_{1e} T = \left[\frac{4\pi}{\hbar} \frac{\gamma_p^2}{\gamma_e^2} kq \right]^{-1}$$

where γ_e and γ_p are the gyromagnetic ratio of an electron and proton, q is the reduction factor which has been defined in section 2.2.b. and K is the Knight shift of the proton resonance. Using the value of q calculated for the γ phase of TiH_x (Nowak et al 1979) which for the cubic symmetry of the fcc structure of the hydride ranges from a maximum value of 0.5 to a minimum value of 0.2 (Yafet and Jaccarino 1964), it is possible to estimate a maximum and a minimum values for the Knight shift $K_{min} = 38 \times 10^{-6}$ and $K_{max} = 61 \times 10^{-6}$. These values are very small and the fact that Schreiber and Cotts (1963) and Schreiber (1965) did not detect any proton Knight shift may be understood by the fact that the shift is a very small fraction of the linewidth (i.e. ΔH = 1832 ppm at 7 MHz and $\Delta H \sim$ 320 ppm at 45 MHz) which may be greatly broadened by the large demagnetisating field resulting from the use of a powdered metallic sample. Although the absence of

Table 4.3: Fitted values of $T_{1e}T$ using $R_1 = R_{1e} + B$

Samples	$YH_{1.72}$	$YH_{1.81}$	$YH_{1.92}$	$YH_{1.98}$
$T_{1e}T$ (S.K)	345 ± 35	363 ± 36	358 ± 36	349 ± 35

Table 4.4: Values of the fitted parameters deduced from the analysis of T_2 using two different theoretical models.

Samples	BPP		Mean Field	
	E_a (eV)	$\nu_o = \frac{1}{\tau_{DO}}$ (s^{-1})	E_a (eV)	$\nu_o = \frac{1}{\tau_{DO}}$ (s^{-1})
$YH_{1.72}$	0.977	$1.03\ 10^{15}$	0.988	2.26×10^{15}
$YH_{1.81}$	0.873	3.69×10^{13}	0.873	7.75×10^{13}
$YH_{1.92}$	0.475	7.75×10^{11}	0.476	1.63×10^{12}
$YH_{1.98}$	0.437	4.35×10^{11}	0.435	4.85×10^{11}

proton Knight shift reported by Schreiber might be the result of both positive orbital and negative core-polarisation contributions, in view of the very small values of the Knight shift calculated here assuming core polarisation contributions only and the results of both band calculations and experimental work in other related systems we may conclude that the main contribution to the electronic relaxation time is the core-polarisation term and that the d-density of states at the Fermi level remains constant across the dihydride phase of yttrium.

4.2.d. T_1 and T_2 results at 7 MHz up to 700 K

In this section it is proposed to analyse the 7 MHz data without considering the data above T ∿ 700 K which will be discussed later. As already mentioned the purity of some samples is not accurately known but, the value of $(T_1)_{min}$ at 7 MHz is not greatly affected by the presence of paramagnetic impurities if their concentration is less than 20 ppm so the effect of hydrogen concentration on the value of $(T_1)_{min}$ can be investigated. We have seen that for $YH_{1.98}$ the value of T_1 at the minimum is consistent with those obtained from both the mean-field theory and BPP model assuming dipole-dipole interactions. If we assume that the hydrogen atoms are located at the tetrahedral sites the value of $(T_{1d})^{-1}_{min}$ should be directly proportional to the probability of occupation of a T-site: $\beta = \frac{x}{2}$ where x is the hydrogen to metal ratio. Fig. 4.22 shows a plot of $(T_{1d})^{-1}_{min}$ as a function of β together with the theoretical predictions using mean-field theory and a simple exponential correlation function (BPP). The deviation of the experimental point, for $YH_{1.92}$, from the straight line is due to the paramagnetic impurity contribution to T_1 which has

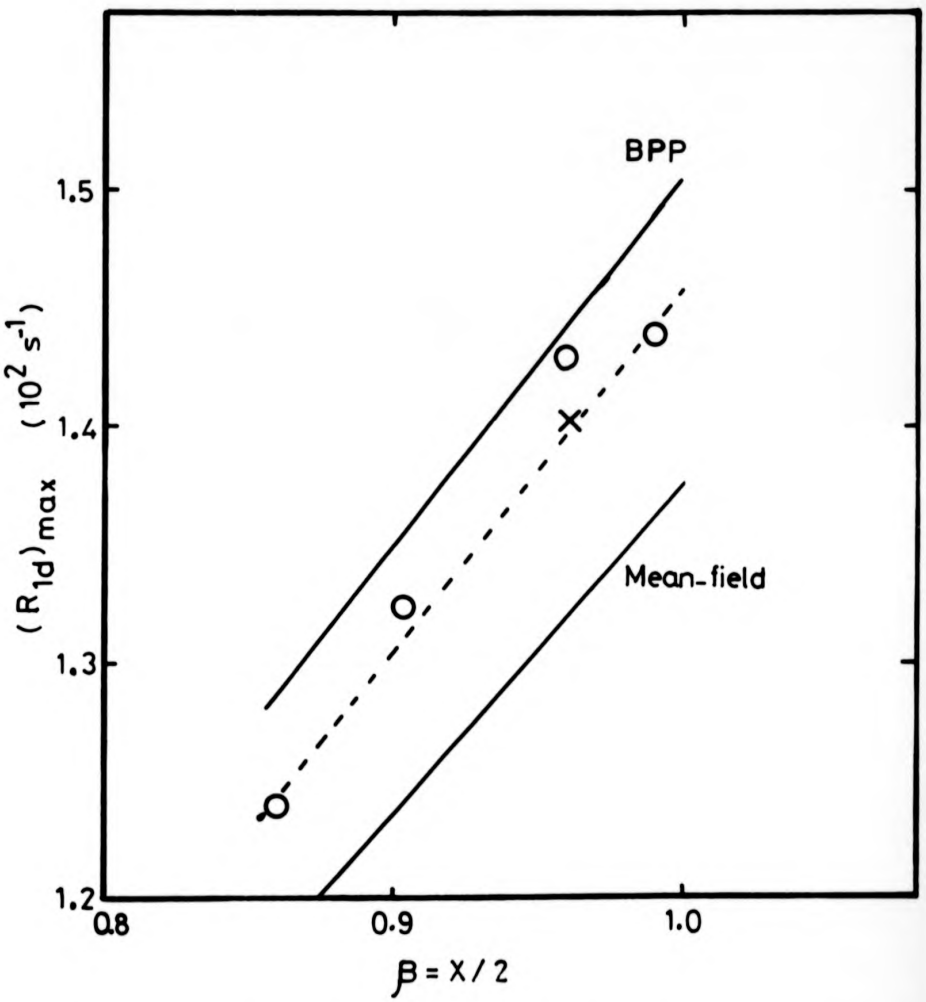

Fig. 4.22: Variation of the relaxation rate at the maximum with concentration of hydrogen. The full curve are the theoretical predictions. The 'X' is the value of $(R_{1d})_{max}$ obtained when allowing for a residual concentration of 17 ppm Gd in $YH_{1.92}$.

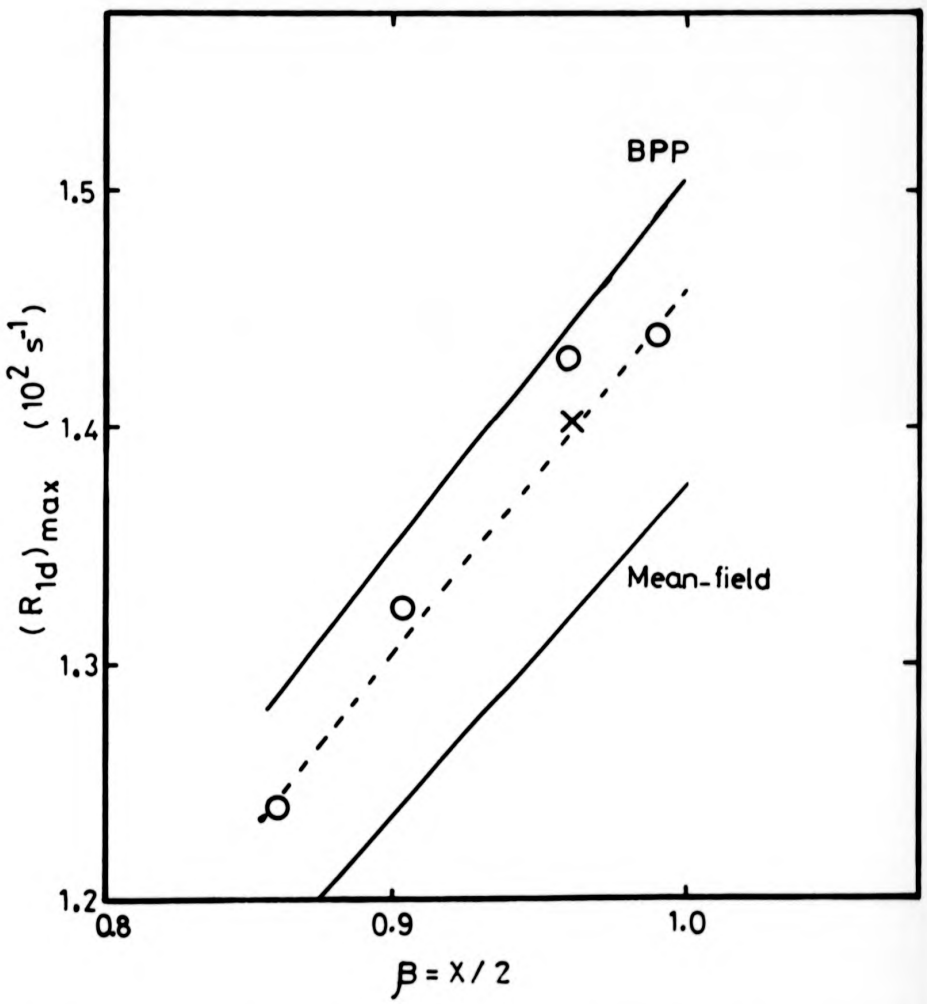

Fig. 4.22: Variation of the relaxation rate at the maximum with concentration of hydrogen. The full curve are the theoretical predictions. The 'X' is the value of $(R_{1d})_{max}$ obtained when allowing for a residual concentration of 17 ppm Gd in $YH_{1.92}$.

not been removed. But if we allow for the presence of 17 ppm Gd the agreement is much better. The fact that no obvious deviation for $YH_{1.81}$ + 20 ppm Gd is due to the smaller T_{1p} contribution at high temperatures. The BPP model over-estimates the value of R_1 at the maximum and mean field theory should give better agreement with experiment. In this case it seems that BPP is in better agreement with the experimental data. However, one should bear in mind that any paramagnetic impurity contribution to the rate would lead to a larger observed value $(T_1)^{-1}_{min}$ which in turn would be in better agreement with that deduced from BPP and we conclude that the data are in good agreement with theory. The value of $(T_{1d})^{-1}_{min}$ deduced for $YH_{1.72}$ indicates clearly that this sample is entirely in the β phase for that temperature, in agreement with the wide-line measurement at room temperature. If the sample had been composed of a mixture of β and α phases a value of $(T_{1d})^{-1}_{min}$ close to that obtained for $YH_{1.81}$ would have been deduced. In this analysis no allowance for 0-site occupation which increases at low temperature with increasing hydrogen concentration, has been made and in view of the relatively good agreement between theory and experiment (i.e. the difference is always less than 5%) and the proportionality between $(T_{1d})^{-1}_{min}$ and β, we conclude that the 0-site occupation, at least at the temperatures of the different maxima, is very small i.e. a substantial 0-site occupation would increase the second moment because of the smaller 0-T distance, resulting in larger values of T_1^{-1}. This is in agreement with the theory elaborated by Richards (1982) and Goldstone et al (1983) which predicts a decrease of 0-site occupation with increasing temperature as opposed to the increase in 0 sites with increasing temperature predicted by the very simple gas lattice model developed by Venturini et al (1980). This is in agreement with the comment made earlier about the temperature dependence of the line width in the rigid lattice.

One of the main concluding remarks drawn from the investigation of the paramagnetic impurity contribution to the relaxation times is that T_2 is less sensitive to the presence of impurities than T_1. Therefore, although the T_1 data are analysed they are used only as a means of comparing the different values of the various parameters which are extracted from the T_2 data assuming that their behaviour can be assigned to proton dipole-dipole interaction . The T_2 data is analysed using two different theoretical models. Firstly using an exponential correlation function and secondly using the computed values given by Barton and Sholl (1980) for the case of first nearest neighbour jumps on a s.c. lattice. The data were fitted to the expression

$$\frac{1}{T_{2,1}} = \frac{1}{(T_{2,1})_d} + \frac{1}{T_{1e}} \ .$$

The conduction electron contribution to $\frac{1}{T_1}$ and $\frac{1}{T_2}$ is the same because of the very fast correlation times involved in the hyperfine interaction compared to the characteristic frequencies ω_o and ω_e. We have seen that within the analytical error introduced by the presence of residual impurities, the value of $T_{1e}T$ is independent of hydrogen concentration. The value $T_{1e}T$ = 349 s.K, which is thought to be the most accurate, is used here. The results of the analysis of T_2 data are given in table 4.4. The most striking feature is the large decrease of the activation energy and of the jump attempt frequency ν_o with increasing concentration of hydrogen. This situation is similar to that found in LaH_2 (Phua 1982) as opposed to that of TiH_x (Korn 1978) or PdH_x (Davis et al 1976). It is well established that hydrogen is located at the tetrahedral sites (this is supported by the analysis of $(T_1)_{min}$ discussed above) and that the hydrogen atoms diffuse on the s.c. lattice formed by the T sites. The binary hydrides with b.c.c. structures (group VB) generally have lower activation

energies than the hydrides having f.c.c. structures. The b.c.c. structure is less dense than that of the close packed f.c.c. structure, suggesting that the strain energy involved in the distortion of the lattice during the diffusion jump is related to the density of the compounds. Intuitively a decrease in activation energy may be related to a large lattice expansion on adding hydrogen. In rare-earth hydrides although the lattice expands upon adding hydrogen to T-sites it contracts when hydrogen goes into O-sites. This has been confirmed for the light rare earths e.g. LaH_2 (Mueller et al 1979) and recently for YH_2 (Morosin 1983). X-ray data show that the lattice constant for LaH_x is nearly independent of x for $1.9 < x < 2.0$ and decreases linearly with x for $2.0 < x < 2.4$. This implies that the increase in lattice constant due to increasing T-site occupation ($1.9 < x < 2.0$) is compensated by the contraction of the lattice due to fractional occupation of O-sites. In view of the similarities presented by both LaH_2 and YH_2 it may be assumed that the lattice parameter remains constant for $1.72 < x < 2.0$ (the β phase of yttrium exists over a wider range of hydrogen concentration than that of La). Thus it is difficult to ascribe this change in activation energy to lattice expansion. As the concentration of hydrogen is increased towards the limit $\beta \sim 1$ (vacancy diffusion regime) one would expect the activation energy to increase as is the case of ZrH_2 (Bowman) i.e. the total activation energy would be that required to create the vacancy which can be created by a thermally activated process plus that which characterises the hydrogen motion ($E_{a\ TOT} \approx 2E_a$). Evidence obtained from measurements made in YH_2 (Phua et al 1983) where E_a is even lower than that for $YH_{1.98}$ indicates that the O-site availability in YH_2 plays an important role in the diffusion process. It has been shown that O-site occupation increases with hydrogen concentration

energies than the hydrides having f.c.c. structures. The b.c.c. structure is less dense than that of the close packed f.c.c. structure, suggesting that the strain energy involved in the distortion of the lattice during the diffusion jump is related to the density of the compounds. Intuitively a decrease in activation energy may be related to a large lattice expansion on adding hydrogen. In rare-earth hydrides although the lattice expands upon adding hydrogen to T-sites it contracts when hydrogen goes into O-sites. This has been confirmed for the light rare earths e.g. LaH_2 (Mueller et al 1979) and recently for YH_2 (Morosin 1983). X-ray data show that the lattice constant for LaH_x is nearly independent of x for $1.9 < x < 2.0$ and decreases linearly with x for $2.0 < x < 2.4$. This implies that the increase in lattice constant due to increasing T-site occupation ($1.9 < x < 2.0$) is compensated by the contraction of the lattice due to fractional occupation of O-sites. In view of the similarities presented by both LaH_2 and YH_2 it may be assumed that the lattice parameter remains constant for $1.72 < x < 2.0$ (the β phase of yttrium exists over a wider range of hydrogen concentration than that of La). Thus it is difficult to ascribe this change in activation energy to lattice expansion. As the concentration of hydrogen is increased towards the limit $\beta \sim 1$ (vacancy diffusion regime) one would expect the activation energy to increase as is the case of ZrH_2 (Bowman) i.e. the total activation energy would be that required to create the vacancy which can be created by a thermally activated process plus that which characterises the hydrogen motion ($E_{a\ TOT} \approx 2E_a$). Evidence obtained from measurements made in YH_2 (Phua et al 1983) where E_a is even lower than that for $YH_{1.98}$ indicates that the O-site availability in YH_2 plays an important role in the diffusion process. It has been shown that O-site occupation increases with hydrogen concentration

(Venturini et al 1980) and it is very tempting to ascribe the decrease in activation energy to the increase in 0-site occupation. Band calculations show clearly that a large charge transfer towards the proton occurs within the yttrium dihydride phase (Switendick (1980), Weaver et al (1983)), screening it from its environment. These electrons having a large s character at the T-sites (better screening), weaken the interactions between the hydrogen and metal atoms making the occupation of 0-sites more likely. Furthermore the H-H short range repulsion interactions have been shown to be important in YH_2 (Goldstone et al 1983) and are expected to increase with increasing hydrogen concentration. These two effects coupled together would produce a large decrease in activation energy with increasing hydrogen concentration. The smaller change in activation energy with increasing hydrogen concentration in LaH_2 may be understood in terms of weaker H-H repulsive interactions due to the larger lattice parameter.

The preexponential factor ν_o should be proportional to the number of vacancies and with the assumption that E_a is independent of x could be written as $(1-\beta)\nu_{oo}$. The parameter ν_o which is obtained by extrapolating the attempt frequency ν to infinite temperature, is very sensitive to the value of E_a. If the diffusion mechanism dependents on the temperature the value of ν_o deduced from a limited range of temperature is questionable. The fact that the factor decreases by about 3 orders of magnitude when x is varied from 1.72 to 1.98 is certainly due to the fact that the activation energy decreases by a factor $\sim$ 2.3. A decrease of ν_o by 3 orders of magnitude is reported by Schreiber and Cotts (1963) as the activation energy E_a decreases by a factor of 2.5 in LaH_2. Similar variations in ν_o are also reported by Bowman et al (1982). If we compare the vibrational frequency determined from inelastic neutron scattering for YH_2,

Goldstone et al (1983) $\nu_{oo} = 2.9 \times 10^{+13}\ s^{-1}$, to the value obtained for $YH_{1.98}$ from our measurements $\nu_{oo} = \frac{\nu_o}{1-\beta} = 4.85 \times 10^{13}\ s^{-1}$, the agreement is not very good. But more detailed comparison does not seem to be warranted in view of the arguments discussed above and the dependence of the vacancy factor on interactions between diffusing atoms as has been discussed for the case of Fe ion diffusion in FeS (Murch et al 1974).

4.2.e. Discussion of the hydrogen diffusion coefficient results

The diffusion coefficient of hydrogen in $YH_{1.98}$ has been measured at 7 MHz for the range of temperatures 662 K - 874 K. Measurements were restricted at low temperatures by the short value of $T_2 \sim 10$ ms and at high temperatures by a poor signal to noise ratio. Values of the hydrogen diffusion coefficient in YH_x have been reported by Frisius et al (1976). The diffusion coefficient is deduced from the time dependence of the hydrogen concentration gradient across a sample which was originally partially loaded with a concentration of hydrogen ranging between 1000 and 2000 ppm and it is found that D(673 K) $= 1.05 \times 10^{-6}\ cm^2\ s^{-1}$ and D(773 K) $= 3.69 \times 10^{-6}\ cm^2\ s^{-1}$. From these values they deduced $D = 0.103 \exp - \frac{0.668\ (eV)}{kT}\ cm^2\ s^{-1}$. Although, due to the low hydrogen concentration, this is not representative of the dihydride phase, it is interesting to note that these values compare well with ours which are listed in table 4.5. The diffusion coefficient is related to the jump path $\langle \ell \rangle$ and jump frequency ν through the relation $D = f_T \frac{\langle \ell \rangle^2 \nu}{6}$. Thus when both values of D and ν obtained from T_1 or T_2 measurements are available the average jump length can, in principle, be deduced. The large error (much larger than the experimental) resulting from the large background magnetic field gradient has been discussed in section 3.4.c. and is estimated to be 75%. It is thought that the value of the activation energy $E_a = 0.22$ eV

Table 4.5: Experimental and calculated values of the diffusion coefficient

T(K)	662	759	832	851	865	874
D_{exp} ($cm^2\ s^{-1}$)	2.3×10^{6}	2.6×10^{-6}	3.6×10^{-6}	2.5×10^{-6}	3.5×10^{-6}	3.9×10^{-6}
D_{cal} ($cm^2\ s^{-1}$) 1 NN	1.8×10^{-8}	4.7×10^{-8}	8.4×10^{-8}	9.7×10^{-8}	1.1×10^{-7}	1.1×10^{-7}
D_{cal} ($cm^2\ s^{-1}$) 3NN	4.0×10^{-8}	1.1×10^{-7}	1.9×10^{-7}	2.2×10^{-7}	2.5×10^{-7}	2.6×10^{-7}

deduced from the temperature dependence of D , compared to E_a = 0.435 eV obtained from T_2 measurements is the result of the large error in D . For this reason the data are not analysed in detail and the experimental data are compared to the calculated diffusion coefficient using the values of ν obtained from T_2 data (mean field theory) for two different possible jump paths. Firstly the case of nearest neighbour jumps on the s.c. lattice formed by the tetrahedral sites is considered. The tracer correlation factor f_T used is that deduced from the expression

$$f_T = 1-A\beta/(2-\beta) + Bx(3\beta-2)/(2-\beta)^2$$

given by Sankey and Fedders (1977) where for a simple cubic lattice A = 0.419 and B = 0.088. This gives f_T = 0.67 for 1% vacancy concentrations. Secondly the case of third nearest neighbour jumps on the tetrahedral sites which correspond to hopping on a diamond lattice, is considered. At monovacancies it is well known that f_T = 0.50 for a diamond lattice. Bustard (1979) indicates that to a first approximation f may be considered to have straight line behaviour between its two limiting values for monovacancies and random walk (f_T = 1). This yields f_T = 0.51 for 1% vacancy concentrations. It should be noted that the values of ν are obtained assuming first nearest neighbour jumps (1NN) on the s.c.lattice formed by the T-sites and that in order to calculate D in the case of third nearest neighbour jumps (3NN) on T sites, T_2 should be reanalysed assuming third nearest neighbour hops. The analysis of T_1 data for $TiH_{1.70}$ performed by Bustard (1979) indicates that the values of ν deduced from 1 NN and 3NN analysis are different by only about 10-20% and in view of the large uncertainty in D the values of ν deduced from an analysis of 1NN jumps are used. The results of this calculation are shown in table 4.5. The large discrepancy between the calculated and measured diffusion coefficients prevents any reliable conclusions about the

jump mechanism involved in the hydrogen diffusion. A similar discrepancy is obtained between the measured D in the α phase and those deduced from line narrowing NMR experiments assuming that the hydrogens hop on the sublattice formed by the 0-sites (Anderson et al 1979).

4.2.f. Anomalous behaviour above 700 K

Above 700 K, T_2 is observed to fall below T_1 and to go through a minimum for T ∿ 1000 K while T_1 departs from the behaviour expected and goes through a maximum at T ∿ 1000 K before decreasing. Similar behaviour is reported by Boyce et al (1977) for the ^{19}F resonance in PbF_2 which forms the fluorite structure. The T_2 anomaly observed was interpreted as due to the contribution, at high temperatures, from the motion due to jumps into interstitial positions (0 sites of the fcc Pb lattice) which is slower than that of the vacancy motion (Frenkel disorder of the F-lattice) which dominates at low temperatures. The additional contribution to $\frac{1}{T_2}$ is proportional to $n_i/\tau e$; where n_i is the fraction of interstitial ions and τ_e is the exchange time. This interpretation was questioned by Vernon et al (1981), who argued that such behaviour could be explained by the contamination of the sample with ∿ 1 ppm of slowly relaxing paramagnetic impurities. The decrease of T_1 with temperature for T greater than 720 K, which corresponds to the range of temperatures in which the specific heat anomaly was observed (Derrington 1974), was interpreted as due to highly correlated motion as the fraction of F^- ions in motion approaches unity. This results in an enhancement of the low frequency $J(\omega)$ due to these low frequency modes which can account for the observed decrease in T_1. This behaviour could not be explained in terms of a paramagnetic impurity contribution to T_1. As mentioned earlier the anomaly observed here

cannot be attributed to the presence of Gd in the sample (see section 4.1.a.). Furthermore this effect if attributed to paramagnetic impurities would require a very slowly relaxing impurity. This is very unlikely in a metal where the conduction electrons couple the impurity to the reservoir (lattice) very effectively, especially in view of the fact that the other impurities present in the purest sample, namely Tb, Ce, Pr, are fast relaxers (Phua 1982). Therefore it seems unlikely that this anomalous behaviour is due to an extra paramagnetic contribution to T_1 and T_2.

Markin et al (1979) report λ-shaped anomalies in the resistivity, thermal e.m.f. and magnetic susceptibility at T = 785 K. They indicate that these anomalies are almost independent of hydrogen concentration for $YH_{1.92}$ to $YH_{1.98}$. The resistivity anomaly in YH_2 was also reported by Savin et al (1967) where it was tentatively associated with the possible redistribution of hydrogen atoms in the metal sublattice.

Fig. 4.23, which shows the high temperature T_1 and T_2 data plotted against 1000/T (enlarged scale), indicates that the sudden change in T_2 which occurs at $T \sim 800$ K, nearly independently of hydrogen concentration, may be related to the anomalies observed by Savin et al (1967). Furthermore fig. 4.24 which shows τ_c versus 1000/T for both $YH_{1.98}$ and $YH_{1.72}$ shows a departure from linearity at $T \sim 800$ K. Here only τ_c for these samples has been plotted because $YH_{1.81}$ and $YH_{1.92}$ contain substantial amounts of Gd which masks the effect observed in the purest sample.

Richards (1982) included the possibility of multilevels energy structure for the hydrogens at each site in the simple gas lattice model (Venturini and Richards 1980) to account for the decrease of disorder (0 occupation) with increasing temperatures. At high temperature where the occupation of higher energy levels is likely

cannot be attributed to the presence of Gd in the sample (see section 4.1.a.). Furthermore this effect if attributed to paramagnetic impurities would require a very slowly relaxing impurity. This is very unlikely in a metal where the conduction electrons couple the impurity to the reservoir (lattice) very effectively, especially in view of the fact that the other impurities present in the purest sample, namely Tb, Ce, Pr, are fast relaxers (Phua 1982). Therefore it seems unlikely that this anomalous behaviour is due to an extra paramagnetic contribution to T_1 and T_2.

Markin et al (1979) report λ-shaped anomalies in the resistivity, thermal e.m.f. and magnetic susceptibility at T = 785 K. They indicate that these anomalies are almost independent of hydrogen concentration for $YH_{1.92}$ to $YH_{1.98}$. The resistivity anomaly in YH_2 was also reported by Savin et al (1967) where it was tentatively associated with the possible redistribution of hydrogen atoms in the metal sublattice.

Fig. 4.23, which shows the high temperature T_1 and T_2 data plotted against 1000/T (enlarged scale), indicates that the sudden change in T_2 which occurs at $T \sim 800$ K, nearly independently of hydrogen concentration, may be related to the anomalies observed by Savin et al (1967). Furthermore fig. 4.24 which shows τ_c versus 1000/T for both $YH_{1.98}$ and $YH_{1.72}$ shows a departure from linearity at $T \sim 800$ K. Here only τ_c for these samples has been plotted because $YH_{1.81}$ and $YH_{1.92}$ contain substantial amounts of Gd which masks the effect observed in the purest sample.

Richards (1982) included the possibility of multilevels energy structure for the hydrogens at each site in the simple gas lattice model (Venturini and Richards 1980) to account for the decrease of disorder (0 occupation) with increasing temperatures. At high temperature where the occupation of higher energy levels is likely

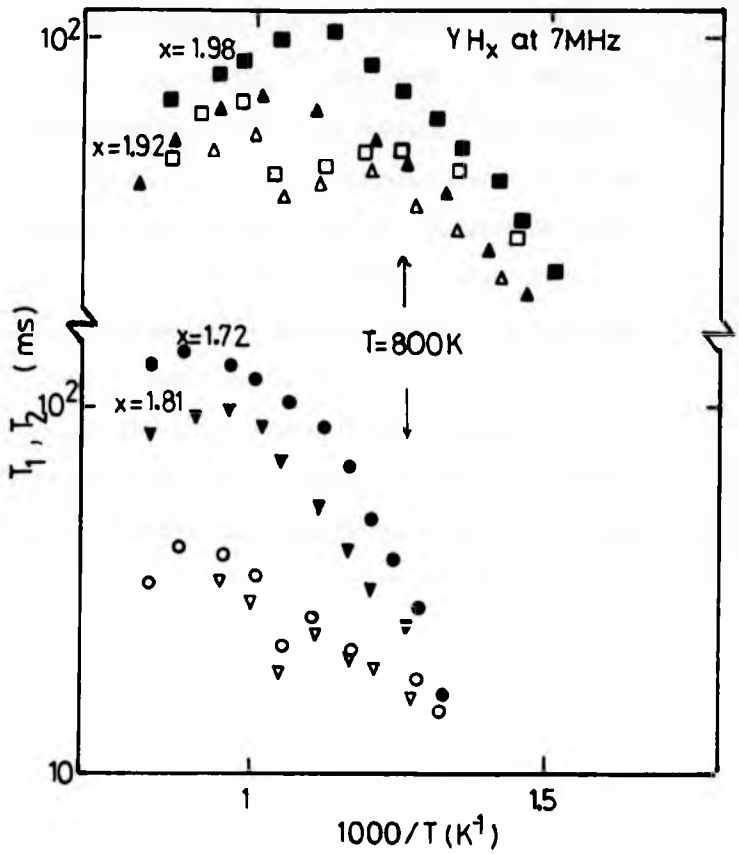

Fig. 4.23: High temperature behaviour of T_1 and T_2 in YH_x. The filled and open symbols represent T_1 and T_2 respectively.

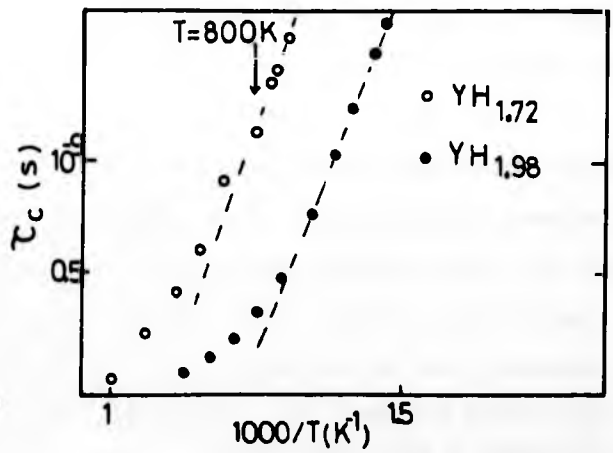

Fig. 4.24: High temperature values of τ_c versus 1000/T.

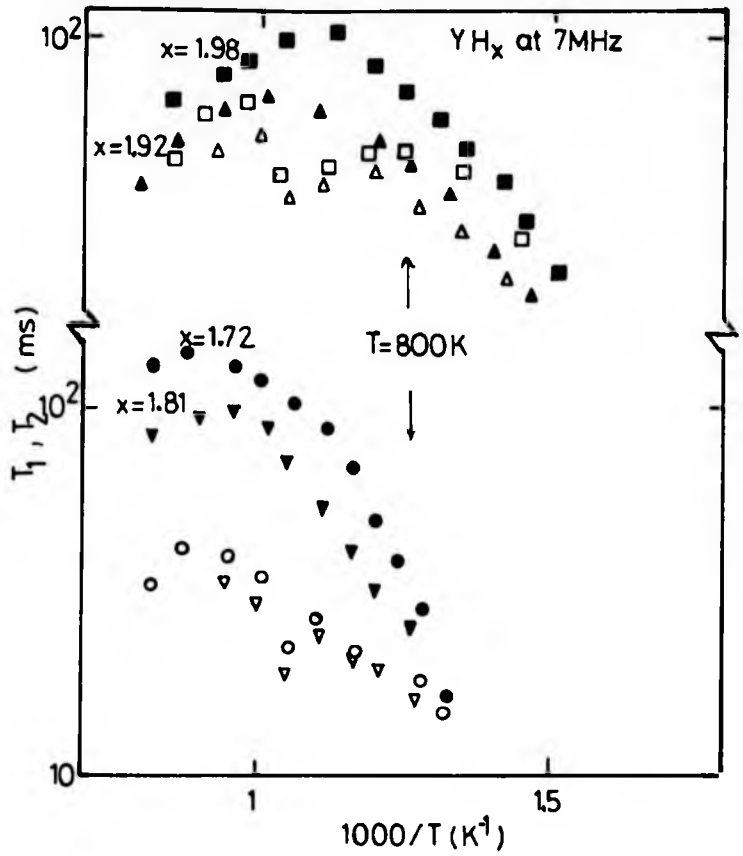

Fig. 4.23: High temperature behaviour of T_1 and T_2 in YH_x. The filled and open symbols represent T_1 and T_2 respectively.

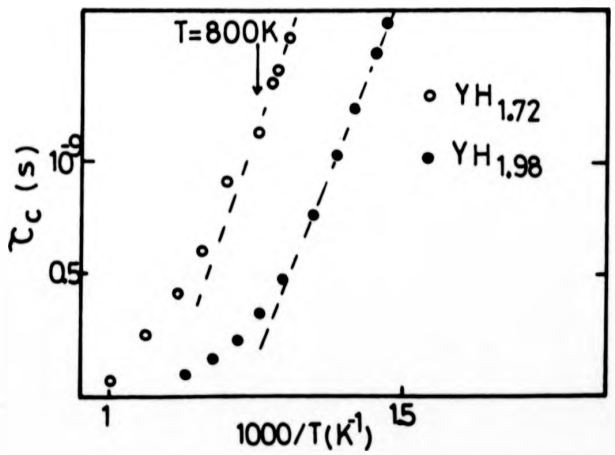

Fig. 4.24: High temperature values of τ_c versus 1000/T.

to be important (vibration energies are $\sim$ 110 meV ($\sim$ 1300 K) and $\sim$ 75meV ($\sim$ 850 K) for T and 0-sites, respectively), the motion is assumed to be described by site to site hopping. The proton-proton repulsion at short range forbids large-amplitude vibrations towards a site which is occupied and the metal ions prevent vibrations between T-sites (consistent with diffusion taking place along T-0-T), thus the site occupation is determined by T-0 interactions. Consequently high energy states may be occupied at x=2 only if hydrogens are confined to T-sites, making 0-site occupation less favourable. Thus one may anticipate, at high temperature where 0-site occupation is unfavourable if neighbouring T sites are occupied, that the site to site hopping along T-0-T paths becomes highly correlated. The resulting modes of motion are characterised by a correlation time $(\tau_c)^{-1} = (1-\rho_c)(\tau_D/2)^{-1} + \rho_c(\tau_c')^{-1}$ where $\tau_D/2$ is the correlation time of the uncorrelated motion and τ_c' is the correlation time characterising the correlated motion and ρ_c is the degree of correlation ($\rho_c = 1$ for highly correlated motion and $\rho_c = 0$ for random walk). The degree of correlation depends on the vacancy concentration (therefore on the hydrogen concentration) and on the temperature. Wolf (1971) and Cavelius (1974) show that τ_c is larger than $\tau_D/2$ by a factor that depends on the degree of correlation that exists. Therefore in the limit $\omega_o \frac{\tau_D}{2} < \omega_o\tau_c << 1$ where $(T_1)^{-1} \alpha \tau_c$ the relaxation time is expected to decrease with temperature. Furthermore the value of ρ_c will approach unity for low vacancy concentrations at lower temperature than for high vacancy concentrations. This would explain qualitatively the decrease in the T_1 and T_2 values at high temperature and the increase in the temperature of the T_1 turnover with decreasing hydrogen concentration. The correlated motion might also explain the λ shaped anomalies discussed above which is suggestive of a second-order phase transformation i.e. decrease in the vibrational degrees of freedom.

4.3. Discussion of the $YD_{1.88}$ T_1 data

The spin-lattice relaxation time of the ^2D nucleus in $YD_{1.88}$ has been measured at 7 MHz in the temperature range 269 to 670 K. The results are shown in Fig. 4.25, where it can be seen that T_1 goes through a minimum of T_1 = 446 ms at T = 411 K. In this system it is clear that the nuclear magnetic dipolar relaxation mechanism is not sufficiently strong to account for the results observed. In fact if the T_1 minimum for $YH_{1.92}$ (nearest hydrogen concentration available) is scaled to allow for the difference between the magnetic moments of ^1H and ^2D, then the value of T_1 predicted at the minimum for ^2D is approximately 10 times the experimental value. Similarly, we expect the contribution to the rate from the conduction electrons, T_{1e}, to be very much smaller than for the corresponding hydride. The values for T_{1e} obtained by scaling the T_{1e} values for $YH_{1.92}$ by the ratio $\gamma^2(^2D)/\gamma^2(^1H)$ are shown in fig. 4.25 for information (broken line). Generally in metal deuteride systems the dominant contribution to the relaxation rate is due to the interaction between the electric quadrupole moment of the ^2D nucleus with randomly fluctuating electric field gradients resulting from the diffusion of the deuterium atoms (Cotts (1978), Weaver (1974)). As discussed in section 2.2.a.2 for the dilute limit ($\beta \to 0$) and assuming an unscreened central potential (i.e. $v(r) \propto r^{-1} \to \frac{d^2V(r)}{dr^2} \propto r^{-3}$), the spectral density is $J(\omega) = \beta\ J_1(\omega)$ where $J_1(\omega)$ describes the spectral density characterising the two particle function and, with these assumptions, is identical to that resulting from dipole-dipole interactions. Therefore the quadrupolar relaxation can be derived from existing calculations of $J_1(\omega)$ (e.g. BPP, Barton and Sholl (1980)). In this limit taking the results of Barton and Sholl a minimum in the relaxation time is expected when $\omega_o\tau_D = 0.766$ however, here $\beta = 0.94$ and the three particle term has to be taken into account.

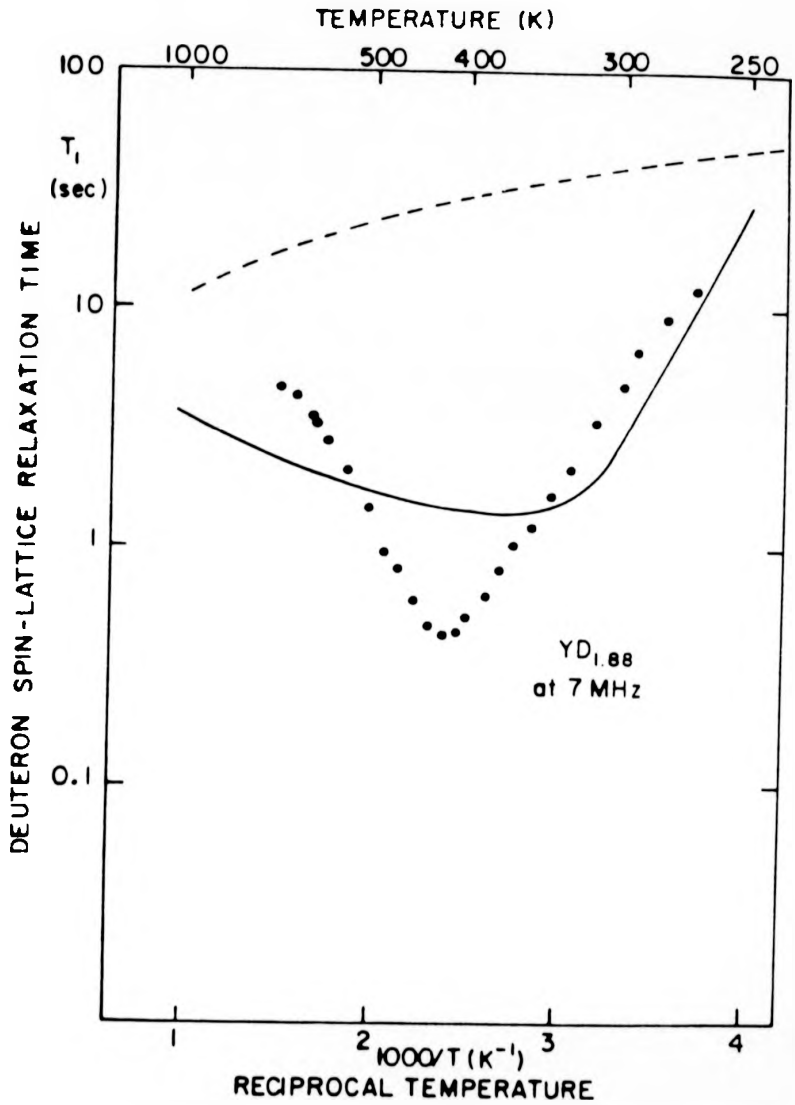

Fig. 4.25: The temperature dependence of the deuterium T_1 at 7 MHz in $YD_{1.88}$. For comparison the full line shows the theoretical paramagnetic contribution calculated as indicated in the text and the broken line shows T_{1e} as deduced from that in $YH_{1.92}$ allowing for the difference in the ^2D and ^1H gyromagnetic ratios.

In this case the spectral density is $J(\omega) = \beta(1-\beta)\ J_1(\omega) + \beta^2 \Delta J_2(\omega)$ (equation 2.31). This yields values of $\omega\tau$ at $(T_1)_{min}$: $\omega_o\tau_D = 2.14$ and $\omega_o\tau_D = 3.0$ respectively for an unscreened central potential and for a Thomas-Fermi screened central potential of the form $V(r) \propto r^{-1}$ exp(-Kr) where K is the screening factor, respectively (Barton, Belhoul and Barton (1981)). According to the classical picture, in $YD_{1.88}$, τ_D will be given by

$$\tau_D = \sqrt{2}\ \tau_o \exp[E_a/kT]$$

and is thus increased by the factor $\sqrt{2}$ (the ratio of the square roots of the isotopic masses for ^2D and ^1H) over that for hydrogen but exhibits the same activation energy. The assumption that the diffusion process is described by classical rate theory is to some extent justified by heat capacity measurements reported by Flotow et al (1962). Assuming that the difference in heat capacity of YH_2 and YD_2 is due to the contribution from optical phonons, they were able to extract the vibration frequencies $\nu_H = 3.1\ 10^{13}\ s^{-1}$ and $\nu_D = 2.18\ 10^{13}\ s^{-1}$, which gives a classical isotope effect $\nu_D = \nu_H/\sqrt{2}$. This was confirmed later by Rush et al (1966) from neutron inelastic scattering measurement ($\nu_H = 3.07\ 10^{13}\ s^{-1}$ and $\nu_D = 2.17\ 10^{13}\ s^{-1}$). As a result of both the isotope effect and inclusion of three particle effects (screened potential), the minimum in the quadrupolar relaxation should be shifted by approximately 45 K to lower temperature relative to the position of the dipolar minimum in $YH_{1.92}$ (here the effect of the three particle effect is readily seen since a shift of about 20 K to higher temperature would be predicted if only the two particle spectral density was considered). As can be seen in fig. 4.25, however the minimum in $YD_{1.88}$ occurs at 411 K compared with 524 K for the dipolar minimum in $YH_{1.92}$ which is a much greater shift (e.g. ΔT = 113 K) than predicted. Furthermore it has been seen in earlier sections

that the activation energy decreases with increasing hydrogen concentration and as a consequence the corresponding hydride $YH_{1.88}$ is expected to produce a minimum in the relaxation time T_1 at a higher temperature than that observed for $YH_{1.92}$, adding to the discrepancy. If the minimum in $YD_{1.88}$ is entirely due to quadrupole effects, the large temperature shift observed can only be explained in terms of a much lower activation energy for $YD_{1.88}$ than that for the corresponding hydride. In fact the apparent activation energy deduced from the slope of T_1 versus $^1/T$ on both sides of the minimum (assuming $T_1 \propto \omega_o^2\tau_D$ when $\omega_o\tau_D >> 1$ and $T_1 \propto 1/\tau_D$ when $\omega_o\tau_D << 1$), is only 0.29 eV for $YD_{1.88}$ compared to 0.475 eV for $YH_{1.92}$. This value is a lower limit and a more reliable,although still somewhat doubtful activation energy E_a = 0.32 eV is obtained using mean field theory. This may suggest that the classical theory does not adequately describe the diffusion process, but the more appropriate quantum treatment predicts only a decrease of $\sim$ 6% in activation energy ($E_{aD} < E_{aH}$) (Weiner (1976), Matthew (1970)). These theories deal mainly with influence of the different mass of the isotope without including electronic effects which may be different for ^1H or ^2D. Kathamian et al (1980) have reported that the 0-site occupation factor together with the lattice parameter of $YD_{1.88}$ are smaller than those for $YH_{1.92}$. This suggests that the metal-deuteron force constant is larger than that for metal-hydrogen and an increase of activation energy is expected. This is consistent with the qualitative model presented by Hauck (1979) which predicts a larger activation energy for ^2D diffusion than for ^1H. It therefore seems unlikely that the minimum in $YD_{1.88}$ is entirely due to quadrupole effects, and knowing that residual concentrations of Gd in excess of 20 ppm are accidentally present in some samples, it seems probable that the presence of small amounts of Gd might be

partly responsible for the results observed. In the temperature range for which results have been obtained atomic diffusion dominates since at the lowest temperature, T = 269 K, $D_a = 4.6\ 10^{-11}\ cm^2 s^{-1}$ compared with $D_s = 1.03\ 10^{-13}\ cm^2\ s^{-1}$ obtained using the Lowe and Gade results. Thus the paramagnetic contribution to the ^2D relaxation rate has been calculated using equation (2.51). In the calculation the values used for τ_D, E_a are those for $YH_{1.92}$ except that τ_D is increased by the $\sqrt{2}$ factor described above and τ_i takes the value used in earlier calculations. It is assumed that the Gd concentration is 20 ppm which is consistent with the known concentration of some yttrium dihydrides studied here and considered as pure. The results of the calculation are shown in fig. 4.25 (full curve) where it should be noted that, as discussed above, the activation energy of the corresponding hydride (e.g. $YH_{1.88}$) should be higher than that used in the calculation resulting, for a given temperature, in a larger value of τ_D than that for $YH_{1.92}$. Thus the minimum in T_{1p} which occurs when $\tau_D = 1/n_1(a_o)$ should be shifted to higher temperature. This shows that even for the ^2D resonance paramagnetic impurities can play an important role in relaxation and indeed in this case, it appears that the impurity and quadrupole rates are quite comparable. It has also been shown that the three particle effect must be considered.

REFERENCES

Anderson, D.L: MSc Thesis, Iowa State University (1979).

Anderson, D. L., R. G. Barnes, D. T. Peterson, D. R. Torgeson: Phys. Rev., B21, 2625 (1980): Phys. Lett., 74A, 427 (1979).

Barton, W. A. (Private communication).

Belhoul, M., W. A. Barton: B.R.S.G. meeting Nottingham (1981).

Belhoul, M., G. A. Styles, E. F. W. Seymour, T-T. Phua, R. G. Barnes, D. R. Torgeson, D. T. Peterson: J. Phys. F: Met. Phys. 12, 2455 (1982).

Bohn, H. G., R. R. Arons: J. Appl. Phys., 53, 2072 (1982).

Boyce, J. B., J. C. Mikkelson, M. O'Keefe: Solid State Commun. 21, 955 (1977).

Bowman, R. C. (Private communication).

Bowman, R. C. Jr., A. J. Moeland, W. K. Rhim: Phys. Rev., B26, 6362 (1982).

Bustard, L. D : Ph.D. Cornell University (1979).
Cavelius, E: Phys. Stat. Sol., b65, 181 (1974).
Cotts, R. M : in Hydrogen in Metals I. Basic Properties, ed. by G. Alefeld and J. Völkl (Spring Verlag, Berlin, 1978).

Cotts, R. M : in Electronic Structure and Properties of Hydrogen in Metals, ed. by P. Jena and C. B. Satterthwaite (Plenum Press, New York and London, 1982).

Dantzer, P. G., D. J. Kleppa: J. Chem. Phys. 73, 5259 (1980).

Davis, P. P., E. F. W. Seymour, D. Zamir, W. David Williams, R. M. Cotts : J. Less-Common. Met., 49, 159 (1976).

Derrington, C. E., M. O'Keefe: Solid State Commun. 15, 1175 (1974).
Drulis, H: Arch. Sci., 27, 243 (1974).
Flotow, H. E., D. W. Osbourne, K. Otto: J. Chem. Phys., 36, 866 (1962).

Frisius, V. F., H. Hackparth, P. Wille: Atomkernenergie, 27, 287 (1976).

Goldstone, J. A., J. Eckert, P. M. Richards, E. L. Venturini: to be published in Phys. Rev. Lett., (1983).

Göring, R., R. Lukas, K. Bohmhammel : J. Phys. C. 14, 5675 (1981).

Hauck, J : Z. Phys. Chem. Neu, 114, 165 (1979).

Horvitz, E. P : Phys. Rev. B3, 2868 (1971).

Kashaev, R. S., E. F. Gubaidullin, A. N. Gilmanov, M. E. Kost: Sov. Phys. Solid State, 22, 530 (1980).

Khatamian, D., W. A. Kamitakahara, R. G. Barnes, D. T. Peterson: Phys. Rev. B21, 2622 (1980).

Korn, C: Phys. Rev., B17, 1707 (1978).

Kulikov, N. I : J. Less-Common. Met., 88, 307 (1982).

Lowe, I. J., S. Gade: Phys. Rev., 156, 817, (1967).

Markin, V. Y. A., V. I. Savin, A. S. Chernikov : Phys. Met. Metallo, 48, 893 (1979); Savin, V.I., R.A. Andriyevskiy: Ibid, 24, 636 (1967).

Matthew, J. A. D : Physica Status Solidi, 42, 841 (1970).

Morosin, B. (unpublished work 1983).

Mueller, W. M., J. P. Blackledge, G. G. Libowitz:in Metal Hydrides (Academic Press, New York and London 1968).

Mueller, W. M., P. Knappe, O. Greis: Z. Physik, Chem., 114, 47 (1979).

Murch, G. E., J. M. Rolls, H. J. De Bruin: Phil. Mag., 29, 337 (1974).

Nowak, B., O. J. Zogal, M. Minier: J. Phys. C., 12, 4591 (1979).

Phua, T-T: Ph.D. Thesis, Iowa State University (1982).

Phua, T-T, B. J. Beaudry, D. T. Peterson, D. R. Torgeson, R. G. Barnes, M. Belhoul, G. A. Styles, E. F. W. Seymour: To be published in Phys. Rev.,B (1983).

Richards, P. M: J. Solid State Chem. 43, 5 (1982): Phys. Rev., B18, 6358 (1978).

Rorschach, H. Jr : Physica, 30, 38 (1964).

Rush, J. J., H. E. Flotow, D. W. Connor, C. L. Tharper: J. Chem. Phys., 45, 3817 (1966).

Sankey, O. F., P. A. Fedders: Phys. Rev., B15, 3586 (1977).

Schreiber, D. S., R. M. Cotts: Phys. Rev., 131, 1118 (1963).

Schreiber, D. S : Phys. Rev., A137, 860 (1965).

Seymour, E. F. W: J. Less. Common. Met., 88, 323 (1982):(Private Communication).

Stoneham, A. M: Ber. Busenges. Physik. Chem., 76, 816 (1972).

Stoneham, A. M: J. Nucl. Mat., 69-70, 109 (1978).

Swintendick, A. C: Solid State Commun, 8, 1463 (1970).

Swintendick, A. C: Int. J. Quantum. Chem., 5, 459 (1971).

Swintendick, A. C: J. Less-Common. Metals, 74, 199 (1980).

Tse, D., I. J. Lowe: Phys. Rev., 166, 279 (1968).

Venturini, E. L., P. M. Richards: Phys. Let., 76A, 344 (1980).

Vernon, S, P. Thayamballi, R. Hogg, D. Hone, V. Jaccarino: Phys. Rev., B24, 3756 (1981).

Weaver, H. T: Phys. Rev., B5, 1663 (1972): J. Chem. Phys., 56, 3193 (1972).

Weaver, H. T: J. Magn. Res., 15, 84 (1974).

Weaver, J. H., D. T. Peterson: J. Less-Common Met., 74, 207 (1980).

Weaver, J. H., D. T. Peterson, R. L. Benbow: Phys. Rev., B20, 5301 (1979).

Weaver, J. H., D. J. Peterman, D. T. Peterson: in Electronic Structure and Properties of Hydrogen in Metals, ed. by P. Jena and C. B. Satterthwaite (Plenum Press, New York and London 1983).

Weiner, J. H: Phys. Rev., B14, 4741 (1976).

Winter, J: in Magnetic Resonance in Metals (Clarendon Press, Oxford, (1971).

Wolf, D. Z: Z. Naturf., 261, 1816 (1971).

Yafet, Y., V. Jaccarino: Phys. Rev., A133, 1630 (1964).

Zogal, O. J., S. Idriak: Physica, 104B, 365 (1981).

CHAPTER V: THE $Ti_{(1-y)}\ Mn_y\ H_{1.74}$ SYSTEM

This investigation was motivated, in the light of the evidence discussed in the previous chapter with regard to the paramagnetic impurities, by a number of anomalies in the NMR data reported in the literature for titanium dihydrides (Pope et al (1981), Bowman and Rhim (1981)). The impurity most likely to be found in Ti is iron (Beaudry 1982) but there is evidence that Fe does not retain a local magnetic moment in Titanium dihydride (Barnes (1983), Belhoul et al (1983)). However, Mn^{2+} is known to have a local magnetic moment in palladium hydride for instance (Alquie et al 1976). Therefore, as part of a comprehensive study of the effects of paramagnetic impurities in transition metal hydrides, we have studied NMR relaxation times in Ti $H_{1.74}$ containing small amounts of added Mn^{2+} ions.

5.1. Experimental results

In order to investigate the effects of Mn^{2+} impurities added to the γ phase of titanium dihydride, on the proton relaxation times a series of Ti $H_{1.74}$ samples doped with 150 ppm, 500 ppm and 1% Mn were prepared. All the samples were manufactured from the same batch of pure titanium metal to ensure identical effects from possible residual impurities. The proton spin-lattice and spin-spin relaxation times have been measured as a function of temperature at 7 MHz and 45 MHz. A pure Ti $H_{1.74}$ reference sample has also been measured. The T_1 measurements at 7 MHz do not extend to such low temperature as those at 45 MHz because of the longer recovery time of both the probe system and receiver at the lower operating frequency.

As can be seen in fig. 5.1, which shows the spin-lattice and spin-spin relaxation times at 45 MHz plotted as a function of the reciprocal temperature, T_1 for the pure sample goes through a minimum $(T_1)_{min}$ = 18 ms for T = 610 K. The appearance of a subsidiary minimum in T_1 can be detected at T ∿ 290 K for Ti $H_{1.74}$ + 150 ppm Mn^{2+}, but for temperatures below 220 K and above ∿ 450 K, T_1 is essentially equal to that for the pure sample. The slight difference in T_1's for the range of temperature extending above 450 K is thought to be due to a small difference in hydrogen concentration. The subsidiary minimum appears to be shifted to higher temperatures as the concentration of Mn present in the sample increases. For the highest concentration sample (containing 1% Mn) T_1 always fall below that of the pure sample, except for temperatures above 450 K. The T_2 data which are expected to be equal to T_1 for temperatures above that of the $(T_1)_{min}$ fall below T_1 for temperatures above ∿ 650 K. This, which can also be observed for the pure sample, is somewhat surprising and will be discussed in detail in the next section.

The T_1 and T_2 data at 7 MHz plotted against the reciprocal temperature are shown in fig. 5.2. For the pure sample, T_1 goes through a minimum $(T_1)_{min}$ = 3 ms at T = 530 K. At this frequency, it can be seen, that T_1 does not seem to be affected by the presence of Mn^{2+} in the sample. As discussed in the previous chapter, this is certainly due to the larger contribution to $T_1$of the proton dipole-dipole interaction at this lower frequency which masks the impurity effects. The spin-spin relaxation time, which becomes equal to T_1 for temperatures above ∿ 570 K, follows the behaviour expected in the case where the only contribution to T_2 comes from the proton dipole-dipole interaction. This is to be contrasted to the T_2 data at 45 MHz.

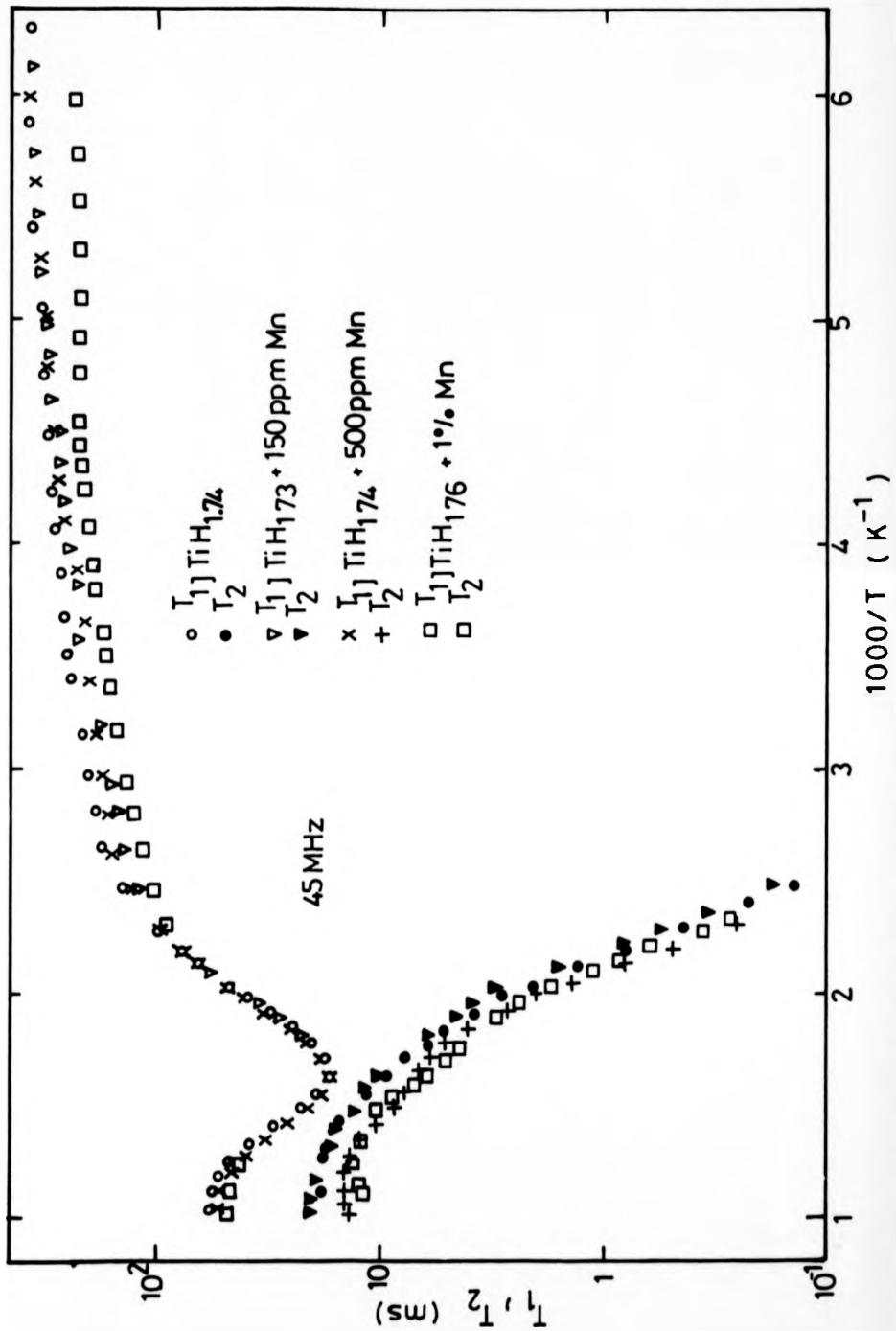

Fig. 5.1: Proton spin-lattice and spin-spin relaxation times as a function of temperature in $TiH_{1.74}$ doped with manganese.

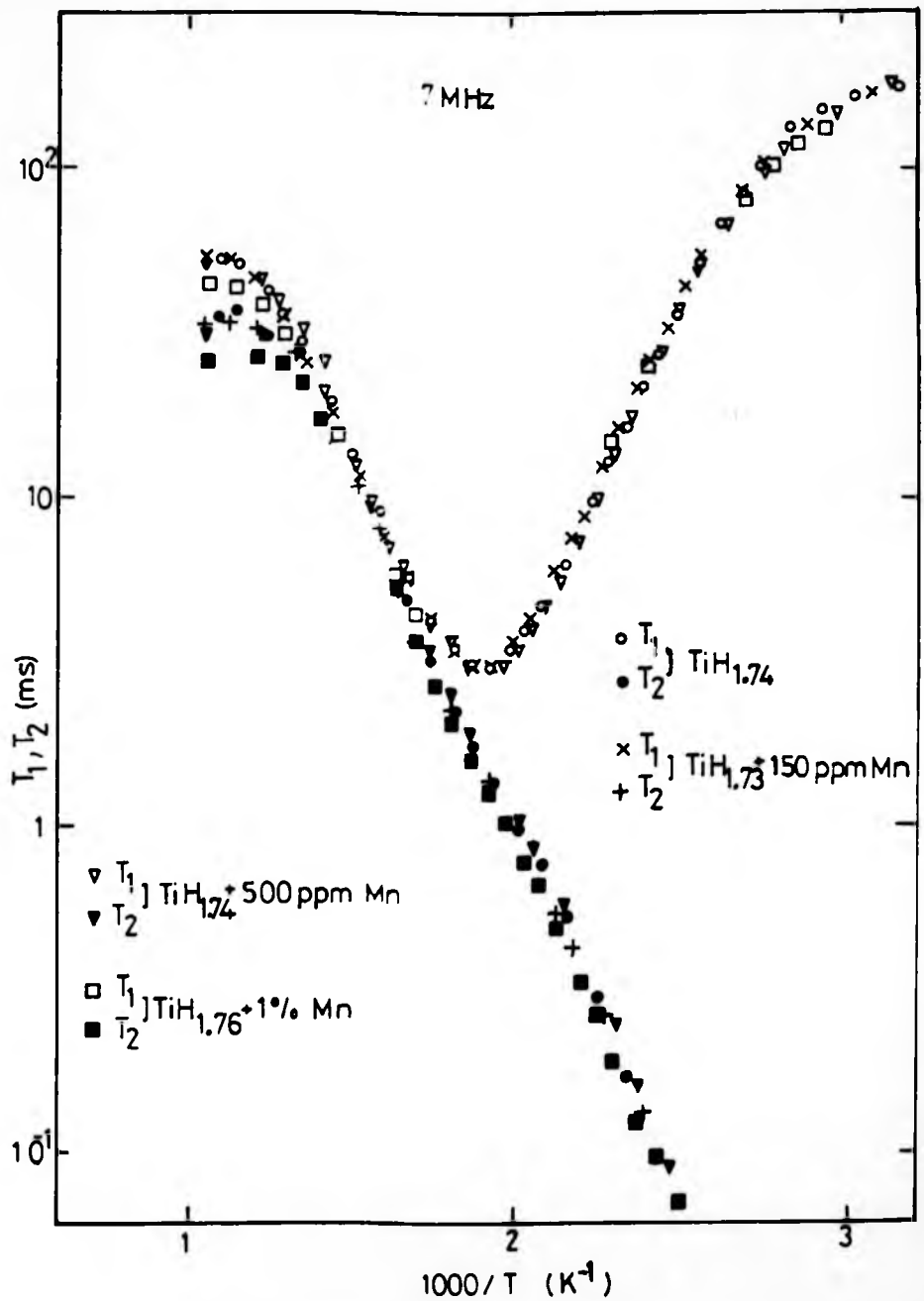

Fig. 5.2: Proton spin-lattice and spin-spin relaxation times at 7 MHz for $TiH_{1.74}$ for various concentrations of Mn.

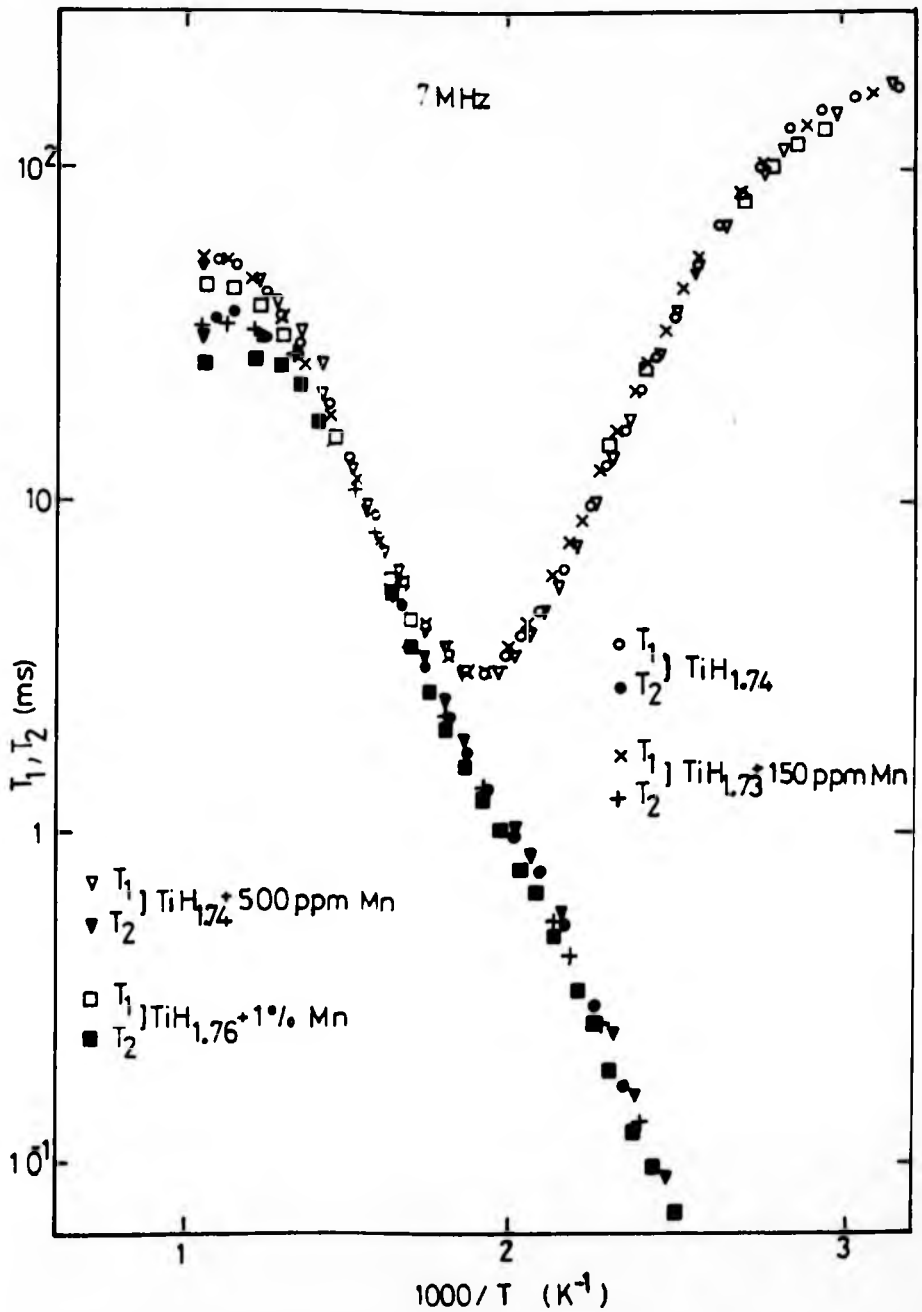

Fig. 5.2: Proton spin-lattice and spin-spin relaxation times at 7 MHz for $TiH_{1.74}$ for various concentrations of Mn.

5.2. Discussion of the relaxation times for the pure sample

The observed relaxation time is the result of several contributions due to the different types of interactions experienced by the protons. For the pure Ti $H_{1.74}$ sample we assume that the spin-lattice relaxation time is given by

$$\frac{1}{T_1} = \frac{1}{T_{1d}} + \frac{1}{T_{1e}} \qquad (5.1)$$

where T_{1d} is the relaxation time due to proton dipole-dipole interaction and T_{1e} is that due to interactions of the protons with the conduction electrons. A similar expression is assumed for the spin-spin relaxation time

$$\frac{1}{T_2} = \frac{1}{T_{2d}} + \frac{1}{T_{1e}} \qquad (5.2)$$

in this expression T_{2e} is replaced by T_{1e} since, as discussed earlier, the correlation times involved in the latter interaction are much faster than the reciprocal of the relevant frequencies i.e. ω_o and ω_e. The value of $(T_{1d})_{min}$ = 3.26 ms, calculated using mean field theory and assuming only dipole-dipole interactions agrees very well with the experimental value $(T_{1d})_{min}$ = 3.23 ms at 7 MHz justifying the assumption made above. Both the T_1 and T_2 data at 7 MHz have been fitted to equations (5.1) and (5.2) respectively while, in view of the anomalous behaviour of T_2, only the T_1 data has been analysed at 45 MHz. In order to be able to compare the results of such an analysis with existing data (Korn and Zamir 1970) two different correlation functions are used in the derivation of the analytical form of T_{1d}. These are firstly a simple exponential correlation function and secondly the results of the more rigorous calculations by Barton and Sholl (1980). T_{1e} is assumed to follow a Korringa

relation i.e. $T_{1e}T$ = constant although it should be noted that the derivation of this equation depends on the assumption of infinitly sharp Fermi distribution (i.e. step function) which is only obtained for T = 0 K. At finite temperatures this equation should be replaced by (Yafet and Jaccarino 1964).

$$(T_{1e}T)^{-1} = (T_{1e}T)^{-1}_{T=0} \left[1 + \frac{1}{3}\pi^2 k^2 \left(\frac{1}{N(E)}\frac{d^2N(E)}{dE^2}\right)_{E=E_F} T^2\right]$$

where $(T_{1e}T)_{T=0}$ = constant, k is Boltzmann constant and N(E) is the density of states. The temperature dependence of this effect is usually negligible since it involves the second derivative of N(E) with respect to E, but in the case where the Fermi energy is located at a rapidly changing density of states, this effect should be considered. This has been shown to be the case in zirconium hydride (Korn 1983) for instance. In our case however, this effect is of no consequence as will become evident later and a Korringa relation is assumed. Fig. 4.3 shows the results of such a fitting procedure and the parameters extracted are given in table 5.1. The values of the activation energy and the preexponential dwell time obtained for the measurements made at the two different frequencies agree very well within experimental error and are in excellent agreement with existing data extrapolated to this concentration of hydrogen (i.e. Ti $H_{1.74}$) (Korn and Zamir (1970), Bustard et al (1979)). The values of the Korringa product deduced from analysis at both 7 and 45 MHz, however, are smaller than the extrapolated values deduced from the results reported by Korn (1978). This suggests that the pure sample contains some residual paramagnetic impurities. However, in view of the very good agreement obtained between theory and experiment when taking the ratio of the relaxation times at the minimum obtained for the two frequencies i.e.

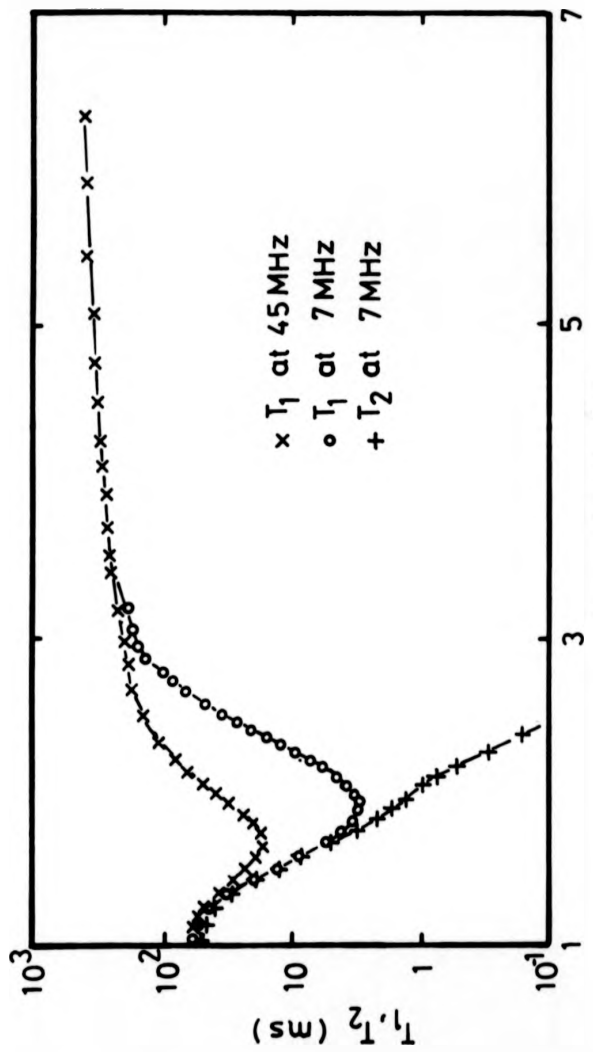

Fig. 5.3: Result of the fitting procedure using mean field theory

$$\text{ratio (theory)} = \frac{(T_{1d})_{min}\ (45\ \text{MHz})}{(T_{1d})_{min}\ (7\ \text{MHz})} = \frac{45}{7} = 6.43 \text{ and ratio (exp)} = \frac{20.6}{3.23}$$

$$= 6.38$$

and the good agreement between the values of E_a, τ_{DO} and $(T_{1d})_{min}$ reported here and those given in previous publications, it seems that the paramagnetic contribution is negligibly small for those temperatures where the dipole-dipole contribution to the relaxation time becomes dominant.

The effect of background magnetic field gradients, in powdered metallic samples, has been discussed in section 3.4.c., in connection with diffusion coefficient measurements. It has been found that approximately $G_o \propto \chi_v H_o/R$ where χ_v is the volume susceptibility, H_o the applied magnetic field and R the radius of the metal particle. Large background gradients may also result in smaller measured values of T_2 even when using a CPMG sequence which partly overcomes this problem. The effect of background gradients is more severe at high field (high operating frequency). Furthermore, in Ti $H_{1.69}$, Trzebiatowsky and Stalinski (1953) have reported that the magnetic susceptibility increases slightly with temperature. Hence we attribute the anomalous behaviour of T_2, at high temperatures at 45 MHz, to the inadequacy of the experimental technique used in the presence of large background gradients. This is confirmed both by a dependence of the measured T_2 on the pulse spacing τ (i.e. 90-τ-180°-2τ-180°...) and the normal behaviour shown by T_2 at lower field (7 MHz). The values of T_2 given in the figures were obtained using the minimum possible pulse spacing, τ, in the CPMG sequence.

5.3. Discussion of T_1 in the doped samples - Paramagnetic impurity effects

The paramagnetic relaxation rates R_{1p} for the different concentrations of Mn have been obtained, as before, by subtracting the rate

Table 5.1.: Results of both 45 and 7 MHz fitting procedures

Measurements	BPP				Mean-Field Theory			
	E_a(eV)	τ_{Do}(s)	$T_{1e}T$(s.K)	$(T_{1d})_{min}$(ms)	E_a(eV)	τ_{Do}(s)	$T_{1e}T$(s.K)	$(T_{1d})_{min}$(ms)
T_1 at 7 MHz	0.496	$0.36\ 10^{-12}$	68.5	3.23	0.539	$0.96\ 10^{-13}$	70.1	3.23
T_2 at 7 MHz	0.498	$0.42\ 10^{-12}$	-	-	0.543	$1.05\ 10^{-13}$	-	-
T_1 at 45 MHz	0.495	$0.33\ 10^{-12}$	69.3	20.61	0.535	$0.99\ 10^{-13}$	71.5	20.59

Table 5.2.: Values of $\tau_i T$ obtained from $(R_{1p})_{max}$

Concentration of Mn	Temperature of $(R_{1p})_{max}$ (K)	$\tau_i T$ (s.K)	$\tau_i T/C$(%)	References
150 ppm	295	$1.8\ 10^{-10}$	$1.2\ 10^{-8}$	This work
500 ppm	323	$1.0\ 10^{-9}$	$2.0\ 10^{-8}$	This work
1%	378	$1.67\ 10^{-8}$	$1.67\ 10^{-8}$	This work
1.5%	-	$2.5\ 10^{-8}$	$1.67\ 10^{-8}$	Seymour (1982)

obtained for the pure sample from the observed rates i.e. $\frac{1}{T_{1p}} = \frac{1}{T_1} - \frac{1}{(T_1)_{pure}}$. Fig. 5.4. shows the resulting paramagnetic relaxation rates $R_{1p} = \frac{1}{T_{1p}}$ plotted against the reciprocal temperature for the various concentrations of Mn. R_{1p} is only obtained from the 45 MHz T_1 measurements for the reasons given earlier.

The main features observed in the case of $Y_{(1-y)}\ Gd_y\ H_{1.98}$ can again be seen here. The principal difference, however, is the shift of the temperature of $(R_{1p})_{max}$ to higher temperatures with increasing concentration of Mn^{2+}. For temperatures below $\sim$ 230 K, the values of R_{1p} for the 150 ppm and 500 ppm samples are subject to large error due to the small difference between the observed relaxation times and that of the pure sample. Thus a rigorous analysis of the data in this range of temperature is not possible for these concentrations of Mn, but it should be pointed out that the temperatures and, less reliably the values of $(R_{1p})_{max}$ can be determined. For reasons which are discussed in section 4.1.c. we can confidently assume that the interaction giving rise to paramagnetic relaxation is the dipolar coupling between the magnetic moment of the Mn^{2+} ions and the protons. With this assumption the rate R_{1p} goes through a maximum when $\tau_D \sim 1/n_1(a_o)$ where $n_1(a_o) = \frac{C_1}{a_o^6}$ and where C_1 is given by equation (2.43). The temperatures for which R_{1p} goes through a maximum are lower than that for $Y_{(1-y)}\ Gd_y\ H_{1.98}$. This suggests that Mn^{2+} in $Ti\ H_{1.74}$ has a shorter electronic relaxation time τ_i than Gd^{3+} in $YH_{1.98}$.

We have seen that for YH_2, the rate R_{1p} is proportional to the concentration of magnetic ions. Here, however, it can be seen that this is not the case, suggesting either that the Mn^{2+} ions are not randomly distributed or that hydrogens tend to avoid the vicinity

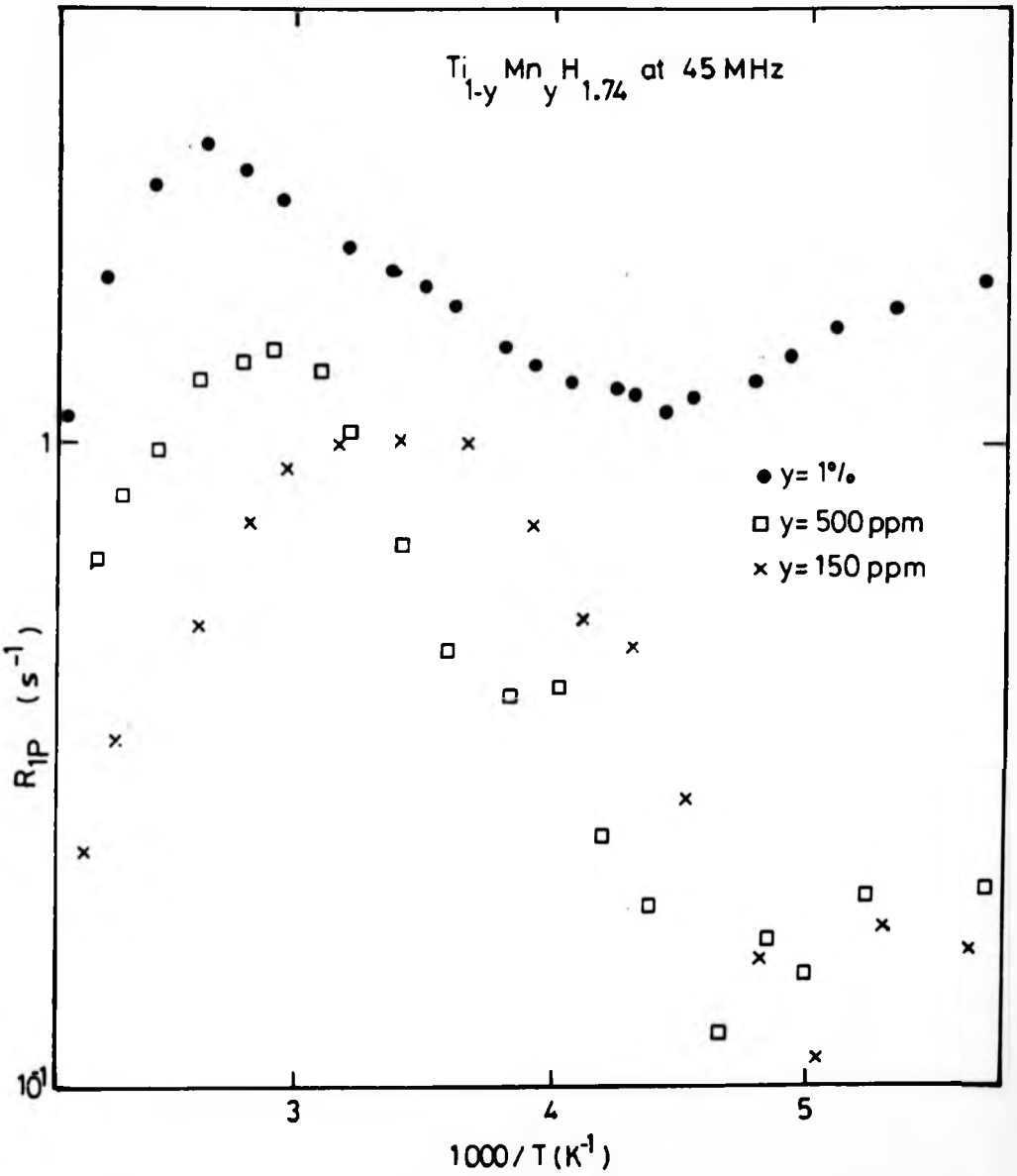

Fig. 5.4: Proton paramagnetic contribution R_{1p} to the total relaxation rate as a function of temperature in $TiH_{1.74}$ + Mn.

of Mn perhaps due to lattice strains introduced by the presence of Mn or large repulsive interactions. In view of the scatter of the data for temperatures below that of $(R_{1p})_{max}$ we first concentrate the discussion on temperatures at which the maxima in R_{1p} occur, which are reliable.

5.4. The shift of the temperature of $(R_{1p})_{max}$ with Mn concentration

The maximum is obtained when $\tau_D = 1/n_1(a_o)$ where

$$n_1(a_o) = \frac{2}{5} \frac{\gamma_p^2 \gamma_n^2 \hbar^2 J(J+1)}{a_o^6} \left| \frac{\tau_i}{1+\omega_o^2\tau_i^2} + \frac{7}{3} \frac{\tau_i}{1+\omega_e^2\tau_i^2} \right| \qquad (5.3)$$

since the terms in the pre-factor are constant (it has been assumed that g=2) the only variable is τ_i and we now consider the variation of this parameter. The linewidth of Mn in the γ phase of titanium hydride doped with 1.5% Mn has been measured using ESR (Seymour 1982). The half width at half maximum, assuming that the line is life time broadened, yields $\tau_i = 85\ 10^{-12}$ s at 295 K. This gives rise to a value of $\tau_i T = 2.5\ 10^{-8}$ sK. Here it has been assumed that $\Delta\omega = bT$ when in reality $\Delta\omega = a+bT$ (Barnes 1981) where a is proportional to the density of states at the Fermi level and the Curie-Weiss temperature (this accounts for the 'slowing' of relaxation near to a magnetic phase transition). The ordering temperature in $PdH_{0.7}$ + 3% Mn is $\sim$ 2 K (Burger et McLachlan 1973) and if we assume that the ordering temperature is similar in $Ti_{(1-y)}\ Mn_y\ H_x$, to first order, the term "a" may be neglected and the line width is just given by $\Delta\omega \sim \frac{1}{\tau_i}$. However, the value of $\tau_i T$ deduced from the ESR measurement should be regarded as a lower limit.

Using this value of $\tau_i T$ we obtain b = 7.8 Å and β = 7.1 Å, compared to R = 8.06 Å, 21.89 Å and 32.70 Å for 1%, 500 and 150 ppm

Mn^{2+} respectively. Thus, although the condition β, $b < R$ is only strictly fulfilled for the low concentration samples, it is not unreasonable to proceed in assuming that this condition is realised also for the 1% Mn sample, validating the applicability of the theory of paramagnetic impurity relaxation effects to this system. From equation (5.3) we can see that, in order to reproduce the experimental shift of the temperature of $(R_{1p})_{max}$ to higher temperatures as the concentration of Mn is increased, the value of $\tau_i T$ must increase with increasing Mn concentration. In order to be able to quantify this observation we first discuss the theory of the electronic relaxation time of the impurity ion, in a metal.

5.4.a. The behaviour of τ_i in "bottleneck regime"

The solution of coupled phenomenological equations of the Bloch form, which include relaxation of the local moment system to the conduction electrons at a rate δ_{ie}, relaxation of the conduction electrons to the lattice at a rate δ_{eL} and relaxation of the conduction electrons towards the magnetic ions (Overhauser process) at a rate δ_{ei} leads to an expression for the linewidth as a function of the relaxation rates which may be written as (Cottet et al 1968)

$$\Delta H = \frac{(\delta_{ei} + \delta_{eL})\delta_{ei} + (\gamma_e \lambda \chi_i H_o)^2}{(\delta_{ei} + \delta_{eL})^2 + (\gamma_e \lambda \chi_i H_o)^2} \frac{\delta_{eL}}{\delta_{ei}} \Delta H_K \qquad (5.4)$$

where γ_e is the gyromagnetic ratio (the same value for the conduction electron and local moments is generally assumed); λ, the molecular field constant, H_o the applied magnetic field, χ_i the local moment susceptibility and ΔH_K the unbottlenecked linewidth. The rates δ_{ei} and δ_{ie} may be expressed in terms of the exchange interaction parameter as (Barnes (1978), Taylor (1975))

Mn^{2+} respectively. Thus, although the condition β, $b < R$ is only strictly fulfilled for the low concentration samples, it is not unreasonable to proceed in assuming that this condition is realised also for the 1% Mn sample, validating the applicability of the theory of paramagnetic impurity relaxation effects to this system. From equation (5.3) we can see that, in order to reproduce the experimental shift of the temperature of $(R_{1p})_{max}$ to higher temperatures as the concentration of Mn is increased, the value of $\tau_i T$ must increase with increasing Mn concentration. In order to be able to quantify this observation we first discuss the theory of the electronic relaxation time of the impurity ion, in a metal.

5.4.a. The behaviour of τ_i in "bottleneck regime"

The solution of coupled phenomenological equations of the Bloch form, which include relaxation of the local moment system to the conduction electrons at a rate δ_{ie}, relaxation of the conduction electrons to the lattice at a rate δ_{eL} and relaxation of the conduction electrons towards the magnetic ions (Overhauser process) at a rate δ_{ei} leads to an expression for the linewidth as a function of the relaxation rates which may be written as (Cottet et al 1968)

$$\Delta H = \frac{(\delta_{ei} + \delta_{eL})\delta_{ei} + (\gamma_e \lambda \chi_i H_o)^2}{(\delta_{ei} + \delta_{eL})^2 + (\gamma_e \lambda \chi_i H_o)^2} \frac{\delta_{eL}}{\delta_{ei}} \Delta H_K \qquad (5.4)$$

where γ_e is the gyromagnetic ratio (the same value for the conduction electron and local moments is generally assumed); λ, the molecular field constant, H_o the applied magnetic field, χ_i the local moment susceptibility and ΔH_K the unbottlenecked linewidth. The rates δ_{ei} and δ_{ie} may be expressed in terms of the exchange interaction parameter as (Barnes (1978), Taylor (1975))

$$\frac{\delta_{ie}}{\gamma_e T} = \frac{\Delta H_K}{T} = \frac{\pi k}{g\mu_B} [J_{ie}\ N(E_F)]^2$$

$$\delta_{ei} = \frac{2\pi}{3\hbar} J_{ie}^2\ N(E_F)\ S(S+1)N$$

while

$$\chi_e = 2\mu_B^2\ N(E_F)$$

$$\chi_i = \frac{g^2\mu_B^2 S(S+1)N}{3KT}$$

where $N(E_F)$ is the density of states at the Fermi surface and N is the concentration of paramagnetic impurities (of spin S) per cm^3. From these results, we can consider the two following opposite situations:

(i) When the conduction electron are in good thermal contact with the lattice ($\delta_{eL} >> \delta_{ei}$), expression (5.4) reduces to

$$\Delta H = \Delta H_K \tag{5.9}$$

(ii) When $\delta_{eL} << \delta_{ei}$, the conduction electrons and impurities are in thermal equilibrium before relaxing to the lattice. This characterises the "bottleneck regime", where the line-width is given by

$$\gamma\Delta H = \frac{\delta_{ie}}{\delta_{ei}} \delta_{eL} \tag{5.10}$$

and since from the expressions above $\frac{\delta_{ie}}{\delta_{ei}} = \frac{3}{2} \frac{N(E_F)kT}{S(S+1)N}$ we note that the linewidth in this limit is inversely proportional to the concentration of magnetic ions (δ_{eL} is independent of the impurity concentration Barnes (1981)). Thus finally we obtain

$$\tau_i T = \frac{T}{\gamma\Delta H} = \frac{2}{3} \frac{S(S+1)N}{N(E_F)\ k\ \delta_{eL}} \tag{5.11}$$

The bottleneck may be pictured in a very simple way. In order to maintain equilibrium with the lattice the local moment attempts to couple some of its energy to the lattice via the conduction electrons. When the conduction electron relaxation time is small enough, the limiting factor is the rate at which the local moment can transfer energy to the conduction electrons. At the other extreme when the conduction electron relaxation rate is low, energy is piled up in the conduction-electron spin system and the linewidth is that of the coupled system. In the bottleneck regime since $\tau_i T$ depends on δ_{eL} its temperature dependence will be that of $1/\delta_{eL}$. Assuming that the exchange of energy between the conduction electron spins and the lattice (phonons) occurs on account of the spin-orbit interaction (i.e. the coupling between the lattice vibrations and the motion of the electrons is so strong that even weak spin-orbit coupling is sufficient to produce a highly effective relaxation mechanism), Elliot (1954) showed that $\delta_{eL} = \frac{(\Delta g)^2}{d\tau_R}$ where Δg is the difference between the conduction electrons g value and that for the free electron (i.e. g=2). Here τ_R is the collision time of the conduction electrons which may be approximated as proportional to the electrical conductivity of the metal. Thus since d is independent of temperature for $T > \theta_D$, $\delta_{eL} \propto T$. However, as indicated by Barnes (1981) a large contribution, which often dominates δ_{eL}, arises from spin-orbit scattering from defects and should be temperature independent (Rettori et al 1974). In view of the latter effect, it is probably reasonable to follow other authors and take δ_{eL} to be constant for $Ti_{(1-y)}\ Mn_y\ H_{1.74}$. This is justified by the fact that Alquie et al (1976) observed a linear increase of the linewidth with increasing temperature for $Pd_{(1-y)}\ Mn_y\ H_{0.7}$ which is a bottlenecked system.

5.4.b. Dependence of τ_i on Mn concentration

Taking J = S = $^5/_2$ and $a_o = \frac{a\sqrt{3}}{4} = 1.92 \times 10^{-8}$ cm and noting that $\omega_e\tau_i >> 1$ and $\omega_o\tau_i << 1$ in the range of temperatures where the maxima are observed (i.e. $\tau_i T = 2.5\ 10^{-8}$ sK), equation (5.3) reduces to

$$\eta_1(a_o) = 1.67\ 10^{16}\ \tau_i\ s^{-1} \qquad (5.12)$$

Thus from the temperature of the maximum using the condition $\tau_D = 1/\eta_1(a_o)$ it is possible to deduce that.

$$\tau_i T = \frac{T_{max}}{1.67\ 10^{16}\ \tau_D(T_{max})} \qquad (5.13)$$

where T_{max} is the temperature of the maximum. The calculations have been performed using $\tau_D = \tau_{D_o} \exp(E_a/kT) = 0.33\ 10^{-12} \exp\ (0.495\ (eV)/kT)$ as given in table 5.1, and the results are shown in table 5.2. Fig. 5.5. shows clearly that $\tau_i T$ is proportional to the concentration within experimental error (i.e. the error on the temperature of the maximum). Since the proportionality with concentration is achieved for values of N ranging over two decades we may confidently conclude that we are dealing with a bottlenecked system. This may be compared with the conclusions reported by Alquie et al (1976) who deduced from ESR measurements that $Pd_{(1-y)}\ Mn_y\ H_{0.7}$ is bottlenecked. From the slope of the straight line $\tau_i T$ versus concentration of impurities. We have seen earlier that for $\tau_D << \frac{1}{\eta_1(a_o)}$ the rate may be expressed as $R_{1p} = \frac{4\pi}{3} N a_o^3 \eta_1(a_o)$. From this relation an approximate value of the rate may be obtained at the maximum. Since $\omega_e\tau_i >> 1$ and $\omega_o\tau_i << 1$ we have $(R_{1p})_{max} \sim 5.0\ 10^{-7}\ N\ (\tau_i)_{max}$, where $(\tau_i)_{max}$ is the value of τ_i for the temperature of the maximum. Furthermore, since $\tau_i T = 1.64\ 10^{-8}\ c$ and $N = \frac{4c}{a^3}$ we have $(R_{1p})_{max} \propto c^2$. Therefore the value of the

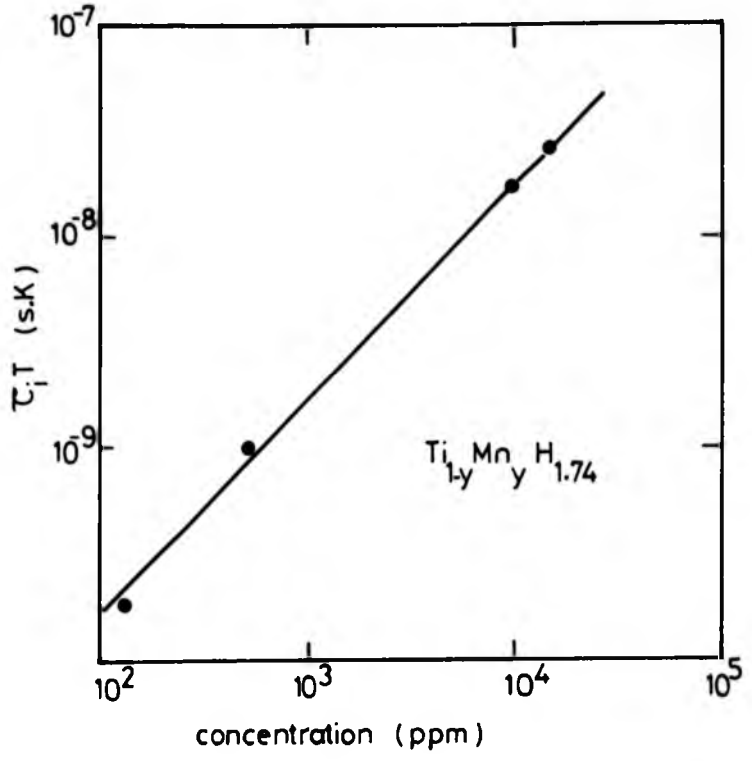

Fig. 5.5: Variation of $\tau_i T$ as obtained from equation (5.13), with the manganese concentration.

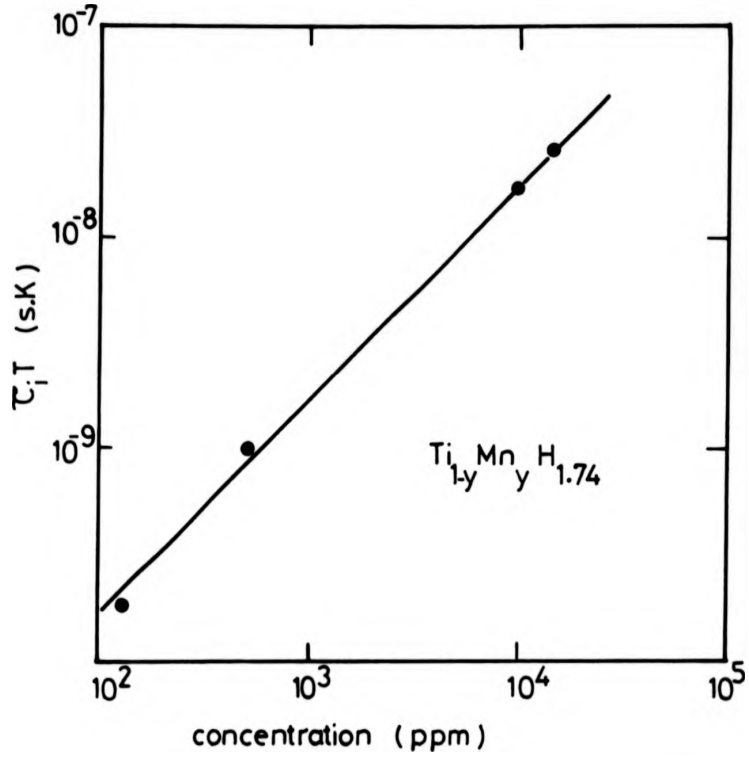

Fig. 5.5: Variation of $\tau_i T$ as obtained from equation (5.13), with the manganese concentration.

rate R_{1p} at the maximum should be proportional to the square of the concentration. It should be noted that the proportionality to c^2 holds for the limit $\tau_D << \frac{1}{n_1(a_o)}$ where $\omega_e\tau_i >> 1$, that is for the range of temperatures which are above that of $(R_{ip})_{max}$. For the range of temperatures below that of $(R_{1p})_{max}$ it has been seen that $R_{1p} \propto N\, D^{3/4}\, C_1^{1/4}$, thus within the limits $\omega_e\tau_i >> 1$ and $\omega_o\tau_i << 1$ we should have $R_{1p} \propto C^{5/4}$. Unfortunately for reasons given above the accuracy of R_{1p} at low temperature is not good enough to be able to check on this effect, but we may conclude from the data given in fig. 4.3 that the quadratic dependence of R_{1p} on Mn concentration at and above the temperature of $(R_{1p})_{max}$ is not shown experimentally. This suggests, as discussed earlier, that either the Mn ions are not randomly distributed or that hydrogens avoid the vicinity of the paramagnetic ions.

5.5. Temperature dependence of R_{1p} below T_{max}

We look first at the temperature of the transition from the spin-diffusion to slow-atomic-diffusion regimes. We have seen in Chapter II that this transition occurs when $D_s \sim D_a$ which is equivalent to $T_{2RL} \simeq \tau_D$ where D_s and D_a are the spin and atomic diffusion coefficients respectively and T_{2RL} is the value of T_2 in the rigid lattice region. The value of D_s is calculated from the expression $D_s = 0.15\, \frac{\gamma_n^2 \hbar}{a_1}$ given by Lowe and Gade (1968) and the value of D_a is deduced from the work of Bustard et al (1979) who performed direct measurements of the diffusion coefficient in $TiH_{1.70}$. As a check, the condition $T_{2RL} = \tau_D$ is also considered and since we do not have a measured value of T_{2RL}, this value is deduced from the value obtained for $YH_{1.98}$

$$\text{i.e. } \frac{T_{2RL}(TiH_{1.74})}{T_{2RL}(YH_{1.98})} = \frac{\beta_Y}{\beta_{Ti}} \frac{a_1^3 Ti}{a_{1Y}^3} = \frac{1.98}{1.74} \left[\frac{2.21}{2.60}\right]^3 = 0.701$$

rate R_{1p} at the maximum should be proportional to the square of the concentration. It should be noted that the proportionality to c^2 holds for the limit $\tau_D << \frac{1}{\eta_1(a_o)}$ where $\omega_e\tau_i >> 1$, that is for the range of temperatures which are above that of $(R_{1p})_{max}$. For the range of temperatures below that of $(R_{1p})_{max}$ it has been seen that $R_{1p} \propto N\, D^{3/4}\, C_i^{1/4}$, thus within the limits $\omega_e\tau_i >> 1$ and $\omega_o\tau_i << 1$ we should have $R_{1p} \propto C^{5/4}$. Unfortunately for reasons given above the accuracy of R_{1p} at low temperature is not good enough to be able to check on this effect, but we may conclude from the data given in fig. 4.3 that the quadratic dependence of R_{1p} on Mn concentration at and above the temperature of $(R_{1p})_{max}$ is not shown experimentally. This suggests, as discussed earlier, that either the Mn ions are not randomly distributed or that hydrogens avoid the vicinity of the paramagnetic ions.

5.5. Temperature dependence of R_{1p} below T_{max}

We look first at the temperature of the transition from the spin-diffusion to slow-atomic-diffusion regimes. We have seen in Chapter II that this transition occurs when $D_s \sim D_a$ which is equivalent to $T_{2RL} = \tau_D$ where D_s and D_a are the spin and atomic diffusion coefficients respectively and T_{2RL} is the value of T_2 in the rigid lattice region. The value of D_s is calculated from the expression $D_s = 0.15\, \frac{\gamma_n^2 \hbar}{a_1}$ given by Lowe and Gade (1968) and the value of D_a is deduced from the work of Bustard et al (1979) who performed direct measurements of the diffusion coefficient in $TiH_{1.70}$. As a check, the condition $T_{2RL} = \tau_D$ is also considered and since we do not have a measured value of T_{2RL}, this value is deduced from the value obtained for $YH_{1.98}$

$$\text{i.e. } \frac{T_{2RL}(TiH_{1.74})}{T_{2RL}(YH_{1.98})} = \frac{\beta_Y}{\beta_{Ti}} \frac{a_1^3 Ti}{a_{1Y}^3} = \frac{1.98}{1.74} \left[\frac{2.21}{2.60}\right]^3 = 0.701$$

where β_Y and β_{Ti} are the fraction of T sites occupied and a_{1Y} and a_{1Ti} are the lattice parameters of the sc lattice formed by the tetrahedral sites for Y and Ti respectively. This yields a value of T_{2RL} for $TiH_{1.74}$ of 8.4 μs compared with 12 μs for $YH_{1.98}$ (this is consistent with the shorter F.I.D. observed at low temperature in $TiH_{1.74}$ compared to that observed for $YH_{1.98}$). From the above conditions the transition temperature can be calculated. The condition $D_a \sim D_s$ gives T_c = 337 K while the condition $T_{2RL} = \tau_D$ gives T_c = 330 K. The two temperatures are in very good agreement but as can be seen in fig. 5.3, where the transition temperature is estimated to be $250 \geq T_c \geq 230$ for the sample doped with 1% Mn, the agreement with experiment is poor. However, before drawing any conclusions from this result let us consider the temperature dependence of R_{1p} in the slow atomic diffusion regime. The slow atomic diffusion regime which is described by equation (2.51) is limited at low temperature by the condition $D_s \sim D_a$ and at high temperature by the condition $\tau_D \sim 1/\eta_1(a_o)$. In this regime $R_{1p} \propto C_1^{1/4} D_a^{3/4}$ and since $C_1 \propto T^{-1}$, assuming a Korringa relation for $\tau_i T$, the relaxation rate will be dominated by the temperature dependence of $D_a^{3/4}$ which is thermally activated. Thus in this regime we expect R_{1p} to be characterised by an activation energy $E_a' = 3/4\ E_a$, where E_a is the activation energy characterising the diffusion process i.e. 0.495 eV as deduced from the T_1 data using an exponential correlation function (see table 5.1). In view of the poor reliability of the data in this regime for the samples containing 150 and 500 ppm of Mn, only the sample doped with 1% is discussed here. The slope of Ln R_{1p} as a function of $1/T$ gives E_a' = 0.06 eV which when corrected for the $(\frac{1}{T})^{1/4}$ temperature dependence of $C_1^{1/4}$ yields $E_a' \sim 0.08$ eV corresponding to $E_a \sim 0.11$ eV. This seems to indicate that the hydrogen diffusion

in the vicinity of the impurity is much faster than that in the bulk (as observed in pure $TiH_{1.74}$), and that this very low activation energy may be the result of a large repulsive interaction between the Mn^{2+} ions and the hydrogen atoms. This is consistent with the non-linear dependence of R_{1p} on Mn concentration and the low observed transition temperature between the spin diffusion and slow atomic diffusion regimes discussed above. In fact from the condition $\tau_D \sim T_{2RL}$ at T_c, it can be seen qualitatively that the latter will be reduced if a faster τ_D than that deduced for the pure sample is used.

In view of the very similar activation energy and transition temperature T_c deduced from data reported for $TiH_{1.94}$ and $TiH_{1.57}$ doped with 510 ppm Mn (Seymour 1982), the fact that our low concentration measurements seem to be characterised by a larger activation energy than that deduced for the 1% Mn sample may be attributed to the larger error in this range of temperatures (slow atomic diffusion) due to residual impurities present in the pure sample (see section 5.3). Thus we conclude that the deduced activation energy ($E_a \sim 0.11$ eV) and the preexponential dwell time in the vicinity of the Mn ion are independent of Mn concentration. Hence the conclusions drawn in the previous section with regard to bottlenecking are still valid since the only parameters changing with Mn concentration, in equation (5.13), are the temperature of $(R_{1p})_{max}$ and τ_i. From the evidences presented above the value of τ_D (T_{max}) is certainly different than deduced for the pure sample. This would result in different values of $\tau_i T$ than those deduced earlier but the Mn concentration dependence of $\tau_i T$ is still very much present and the deductions made earlier with regard bottlenecking are still valid. This is corroborated by the fact that the relaxation of Mn^{2+} ions in transition metals is usually bottlenecked compared to rare earth ions (e.g. Gd^{3+} in $YH_{1.98}$). This may be

understood as due to, if we compare this effect to the specific case of $YH_{1.98}$ + Gd^{3+}

(i) the stronger coupling of d conduction electrons with the d local moment of Mn^{2+} resulting in larger value of δ_{ei} for Mn^{2+} than for Gd^{3+}.

(ii) the fact that the main mechanism involved in the conduction electron-lattice relaxation is due to spin orbit coupling which increases with the atomic number resulting in more effective relaxation for heavier element i.e. as one goes from Y to Ti, δ_{eL} is expected to decrease.

We now turn to the hydrogen concentration dependence of the relaxation rate R_{1p}.

5.6. Hydrogen concentration dependence of R_{1p}

Our measurements were aimed at the investigation of the Mn concentration dependence of the observed relaxation times T_1 and T_2, thus only samples having a fixed amount of hydrogen have been studied. However, our data may be compared with R_{1p} data deduced from T_1 measurements for $TiH_{1.57}$, $TiH_{1.38}$ (Barnes 1983) and $TiH_{1.98}$ (Seymour 1982) doped with 510 ppm Mn. Unfortunately these samples were not prepared from the same Ti metal as that here and the evidence based on the values of $T_{1e}T$ deduced from T_1 measurement for the undoped samples of the above references, suggests that their starting metal was of much higher purity. Therefore definite conclusions cannot be drawn from quantitative comparisons and only the qualitative aspects will be considered here.

The values of $(R_{1p})_{max}$ are 4.6 s^{-1} (T = 370 K), 1.1 s^{-1} (T = 312 K) and 0.45 s^{-1} (330 < T < 310 K) for $TiH_{1.94}$, Ti $H_{1.57}$ and $TiH_{1.38}$ doped

with 510 ppm Mn respectively. These are to be compared to our value $(R_{1p})_{max}$ = 1.45 s^{-1} for $T_iH_{1.74}$ + 500 ppm Mn at T = 323 K. It can be seen that the values of $(R_{1p})_{max}$ and the temperature at which R_{1p} goes through a maximum increase with increasing hydrogen content for the fixed ∿ 500 ppm Mn concentration. The value of $(R_{1p})_{max}$ is proportional to $n_1(a_o)$ (i.e. $(R_{1p})_{max} \sim \frac{4\pi}{3} N a_o^3 n_1(a_o)$) and is thus expected to be dependent on the value of $\tau_i T$ on hydrogen concentration let us concentrate first on the variation of the density of states at the Fermi energy as a function of hydrogen content for titanium hydride.

In titanium hydride, Frisch and Forman (1968) have found that the titanium Knight shift is positive (+ 0.26%) and independent of hydrogen concentration. As discussed in chapter II, the Knight shift is the result of three contributions (see section 2.2.b.) - the contact term which depends on the s-density of states at E_F, the electron orbital interaction which involves an average over all occupied states and the core polarisation contribution which depends on the d density of states at the Fermi energy. The first two contributions result in a positive Knight shift while the third generally gives a negative Knight shift. The band calculations of Gupta (1979) for Ti H_2 indicate clearly that the density of states at the Fermi energy is dominated by d-electrons and hence the contribution from the s-electrons may be neglected with respect to the other contributions. Furthermore the fact that the Ti Knight shift is independent of the hydrogen concentration indicates that the main contribution to the Knight shift arises from the orbital term since it involves averages over all occupied states which make the Knight shift less sensitive to changes of hydrogen concentration. This contribution gives the positive Knight shift observed. Assuming that this is the case, the Ti electronic relaxation rate should also be

dominated by the orbital contribution and will be given by

$$(T_{1e}T)^{-1}_{Ti} = \frac{4\pi}{\hbar} (N_d(E_F)\ A_{hf})^2\ k \qquad (5.14)$$

where k is Boltzmann constant and A_{hf} the hyperfine interaction constant. Thus $(T_{1e}T)^{-1}_{Ti}$ should be proportional to the square of the d density of states of the Fermi energy. It should be noted that even if the core polarisation term contribute to $(T_{1e}T)^{-1}_{Ti}$, the proportionality to $(N_d(E_F))^2$ is still true. NMR measurements (Korn (1983), Goring et al (1981), Bowman et al (1981)), indicate that the proton relaxation rate due to the conduction electron increases with increasing hydrogen concentration. Since the proton rate is dominated by the core polarisation contribution which is proportional to $[N_d(E_F)]^2$, the Ti electronic relaxation rate is also expected to increase with increasing hydrogen content. Now with the assumption that the presence of Mn does not drastically change the shape of the d band at the Fermi level and does not alter the position of the Fermi level, we may express $\tau_i T$ in terms of $(T_{1e}T)_{Ti}$ in both the absence and presence of bottlenecking in the paramagnetic ion spin relaxation.

(i) in the absence of bottlenecking $\delta_{eL} >> \delta_{ei}$ and equation (5.4) reduces to $\Delta H = \Delta H_K$. Thus from equations (5.5) and (5.14), $(\tau_i T)^{-1} \alpha (T_{1e}T)^{-1}_{Ti}$ and $(\tau_i T)^{-1}$ is expected to increase with hydrogen concentration.

(ii) In the presence of bottlenecking $\delta_{eL} << \delta_{ei}$ and we obtain $(\tau_i T)^{-1} \alpha (T_{1e}T)^{-\frac{1}{2}}_{Ti}$. Thus in this case as well $(\tau_i T)^{-1}$ is expected to increase with hydrogen concentration but to a lesser extent than in the first case.

Therefore in both cases the value of the rate R_{1p} at the maximum is expected to decrease with increasing hydrogen concentration (i.e. $(R_{1p})_{max} \alpha \tau_i$) contrary to the experimental observations. The only

explanation for the observed increase in the value of $(R_{1p})_{max}$ for a fixed amount of Mn is that hydrogens avoid the vicinity of Mn^{2+} ions (anti-trapping). The theory developed in section 2.2.c.2 relied on the fact that the proton are randomly distributed however if this condition is not fulfilled the distribution of hydrogen around the impurity must be taken into account. This may be achieved by introducing a probability factor $\underline{p}$ in the final expression of the relaxation rate R_{1p}. It can be seen intuitively, assuming that the non-random distribution of H around Mn^{2+} is the result of repulsive interactions, that the probability factor is related to the vacancy concentration (i.e. $\underline{p}$ = 0 for 100% vacancies and $\underline{p}$=1 for 0% vacancy) and thus the rate (R_{1p}) is expected to increase with decreasing vacancy concentration (i.e. increasing hydrogen concentration) as is observed experimentally. For the same reasons the shortest distance of approach to a paramagnetic ion, a_o, is likely to be reduced and the condition $\tau_D \sim \frac{1}{n_1(a_o)}$ or $\beta = a_o$ is obtained for higher temperatures. Thus the temperature of the maximum is expected to increase with increasing hydrogen concentration as observed experimentally.

Since the same conclusions may be drawn from both the interpretation of the Mn and hydrogen concentration data we assert that, due to a large repulsive interaction, hydrogen avoids the vicinity of Mn ions (anti-trapping). Furthermore, the Mn concentration-dependence data suggests that $Ti_{(1-y)}\ Mn_y\ H_{1.74}$ is a bottlenecked system. This is not surprising in view of the fact that **S**-state Mn^{2+} resonances are usually very strongly bottlenecked (Barnes 1981).

It is interesting to note the T_1 data of Pope et al (1981) which shows clear subsidiary minima, for $TiH_{1.98}$, $Zr\ H_{1.96}$ and HfH_x with x = 1.91, x = 1.78, x = 1.70 and x = 1.58, at the temperature T ~ 300 K.

explanation for the observed increase in the value of $(R_{1p})_{max}$ for a fixed amount of Mn is that hydrogens avoid the vicinity of Mn^{2+} ions (anti-trapping). The theory developed in section 2.2.c.2 relied on the fact that the proton are randomly distributed however if this condition is not fulfilled the distribution of hydrogen around the impurity must be taken into account. This may be achieved by introducing a probability factor p in the final expression of the relaxation rate R_{1p}. It can be seen intuitively, assuming that the non-random distribution of H around Mn^{2+} is the result of repulsive interactions, that the probability factor is related to the vacancy concentration (i.e. $p = 0$ for 100% vacancies and $p=1$ for 0% vacancy) and thus the rate (R_{1p}) is expected to increase with decreasing vacancy concentration (i.e. increasing hydrogen concentration) as is observed experimentally. For the same reasons the shortest distance of approach to a paramagnetic ion, a_o, is likely to be reduced and the condition $\tau_D \sim \frac{1}{n_1(a_o)}$ or $\beta = a_o$ is obtained for higher temperatures. Thus the temperature of the maximum is expected to increase with increasing hydrogen concentration as observed experimentally.

Since the same conclusions may be drawn from both the interpretation of the Mn and hydrogen concentration data we assert that, due to a large repulsive interaction, hydrogen avoids the vicinity of Mn ions (anti-trapping). Furthermore, the Mn concentration-dependence data suggests that $Ti_{(1-y)}\ Mn_y\ H_{1.74}$ is a bottlenecked system. This is not surprising in view of the fact that S-state Mn^{2+} resonances are usually very strongly bottlenecked (Barnes 1981).

It is interesting to note the T_1 data of Pope et al (1981) which shows clear subsidiary minima, for $TiH_{1.98}$, $Zr\ H_{1.96}$ and HfH_x with $x = 1.91$, $x = 1.78$, $x = 1.70$ and $x = 1.58$, at the temperature $T \sim 300$ K.

This has been interpreted as due to large changes in the density of states in this range of temperatures. This is to be compared to our results which show the same feature but due to paramagnetic impurities. It is thought likely their results also reflect the unsuspected presence of paramagnetic impurities since it has been seen here that only 150 ppm of Mn in $TiH_{1.74}$ produces an observable effect on the measured T_1. It is interesting also to note that $T_{1\rho}$ is not affected to the same extent as T_1 and in view of what has been said in the previous chapter this is expected when the subsidiary minimum is attributed to paramagnetic impurities. We believe therefore that their interpretation in terms of density of states changes may be in error.

REFERENCES

Alquie, G., A. Kreisler, J. P. Burger: J. Less-common Metals, 49, 97, (1976).

Barnes, R. G. (Private communication).

Barnes, S. E : Advances in Physics, 30, 801 (1981).

Beaudry, B. J : (Private communication).

Belhoul, M., G. A. Styles, E. F. W. Seymour, R. G. Barnes: to be published.

Bowman, R. C.,Jr., W. K. Rhim: Phys. Rev.,B24, 2232 (1981).

Burger, J. P., P. S. McLachlan: Solid State Commun., 13, 1563 (1973).

Bustard, L. D., R. M. Cotts, E. F. W. Seymour: Z. Fur. Phys. Chem.,115, 247 (1979).

Cottet, H., P. Donze, J. Dupraz, B. Giovannini, M. Peter: Z. Angew. Phys., 24, 249 (1968).

Doolan, K. R., P. P. Narang, I. M. Pope: J. Phys. F, 10, 2073 (1980).

Elliot, R. J: Phys. Rev., 96, 266 (1954).

Frisch, R. C., R. A. Forman: J. Chem. Phys.,48, 5187 (1968).

Goring, R., R. Lucas, K. Bohmhammel: J. Phys. C., 14, 5675 (1981).

Gupta, M: Solid State Commun., 29, 47 (1979).

Korn, C., D. Zamir: J. Phys. Chem. Solids, 31, 489 (1970).

Korn, C: Phys. Rev., B17, 1707 (1978).

Korn, C: Phys. Rev., B , (1983).

Pope, J. M., P. P. Narang, K. R. Doolan: J. Phys. Chem. Solids, 42, 519 (1981).

Rettori, C., H. M. Kim, E. P. Chock, D. Davidov: Phys. Rev., B10, 1826 (1974).

Seymour, E. F. W. (Private communication).

Taylor, R. H: Advances in Physics, 24, 681 (1975).

Yafet, Y, V. Jaccarino: Phys. Rev., 133, A1630 (1964).

CHAPTER VI: PALLADIUM AND PALLADIUM YTTRIUM HYDRIDES

Alloying palladium with a few percent of rare earth metal not only increases the mechanical stability due to suppression of the α/β miscibility gaps below room temperature (Wise et al 1975), but it has been shown also to increase the rate at which hydrogen is able to permeate through a membrane of the alloy (Hughes and Harris, 1978). Since the permeability is proportional to the diffusion coefficient, in view of the fact that the lattice parameter increases by several percent on alloying, one may be led to the conclusion that the larger permeability in the alloy is the result of an increase in the bulk diffusion coefficient. More recently it has been reported that the presence of short range order (SRO) has large effects on the diffusion parameters in these alloys (Hughes et al 1980).

Proton spin lattice relaxation measurements coupled with direct diffusion coefficient measurements not only allow the derivation of the diffusion parameters under equilibrium condition, but should give information on the state of the alloy.

6.1. Experimental results

In order to investigate these effects both spin lattice relaxation time T_1 and direct diffusion coefficient measurements were performed in $(Pd_{0.92}Y_{0.08})\ H_{0.51}$ at 7 MHz. To serve as reference for the observations on the alloy, measurements were also made in a pure palladium hydride. To that effect the spin lattice relaxation time was measured for $Pd\ H_{0.54}$ at 7 MHz.

Fig. 6.1. shows T_1 for $(Pd_{0.92}Y_{0.08})H_{0.51}$ and Pd $H_{0.54}$ as a function of the reciprocal temperature at an operating frequency of 7 MHz. T_1 goes through a minimum at 215 K in both samples with $(T_1)_{min}$ = 11.8 ms for $(Pd_{0.92}\ Y_{0.08})\ H_{0.51}$ and $(T_1)_{min}$ = 12.9 ms for Pd $H_{0.54}$. Due to the suppression of the miscibility gap the former sample is single β phase while the latter is likely to be a mixture of α and β phases, but most of the observed signal is provided by the hydrogen in the β phase of composition about Pd $H_{0.64}$.

The most striking feature of the results is that the temperatures of the minima are the same, which if attributed to proton dipole-dipole interactions, indicates that the diffusion coefficients at these temperatures are the same. This seems surprising if we consider the shapes of the minima which are characterised by quite different activation energies. The results of the diffusion coefficient measurements in the range of temperature 273 to 343 K and at 7 MHz are shown in fig. 6.2. The temperature range of the measurements was limited at low temperatures by the resolution of the technique used and at high temperatures by the high hydrogen equilibrium pressure (i.e. several atmospheres) in the pyrex sample container. The linear behaviour of Ln D versus 1000/T indicates that the diffusion coefficient follows an Arrhenius relation, as expected.

6.2. Discussion of the experimental results

We have seen in Chapters IV and V that very small amount of paramagnetic impurities can have a drastic effect on the observed relaxation times. This may lead to broader or asymmetric minima resulting in uncertainties in the values of the diffusion parameters. For these reasons the diffusion coefficient data which is not affected by the presence of paramagnetic impurities is discussed first.

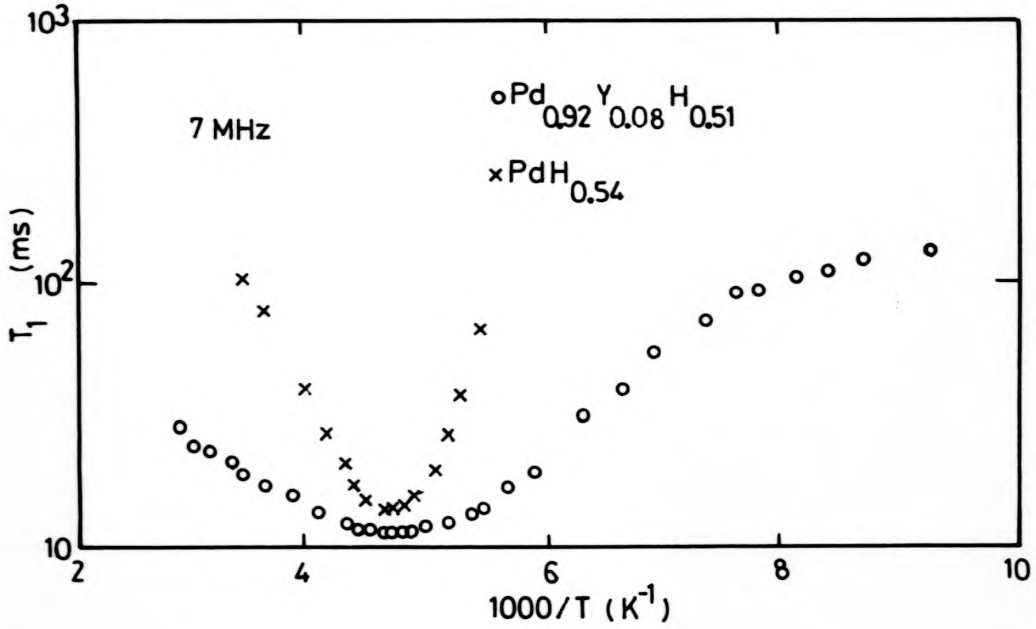

Fig. 6.1: Spin-lattice relaxation time as a function of the reciprocal temperature in $PdH_{0.54}$ and $[Pd_{0.92}Y_{0.08}]H_{0.51}$.

6.2.a. Diffusion coefficient results

The data have been fitted to an Arrhenius relation resulting in: $D = 6.47 \times 10^{-3} \exp\left(-\frac{0.26\ (eV)}{kT}\right)\ cm^2\ s^{-1}$. The activation energy obtained is higher than that obtained in palladium hydride i.e. $E_a = 0.228$ eV (Cornell and Seymour (1975), Davis et al (1976)). This is in accordance with the ideas of Buchold et al (1976), who suggested that the increase in activation energy as the solute concentration is increased, may be attributed to a local arrangement of conduction electrons around the solute atoms and hence around the hydrogens (screening model). The value of D at infinite temperature when allowing for the site-blocking factor $(1-\alpha)$ where α is the concentration of hydrogen, yields a value $\frac{D_o}{(1-\alpha)} = 13.2 \times 10^{-2}\ cm^2\ s^{-1}$. This value is larger by a factor of 4.4 than the corresponding value for palladium hydride which is $3 \times 10^{-3}\ cm^2\ s^{-1}$ (Völkl and Alefeld 1978). This confirms the increase in permeability in $Pd_{0.92}\ Y_{0.08}$ compared to that in Pd at high temperature.

Physical and mechanical property measurements (Brooks et al 1976) made on $Pd_{0.92}\ Y_{0.08}$ show that this alloy exhibits extensive short-range order (SRO). Short-range order implies a distribution of atoms where the number of A-A or A-B bonds is increased in comparison with a random distribution but where the concentration of the different atoms is the same on all sublattices. For instance one might imagine a material made up of a random distribution of small submicroregions of variable degree of order including the possibility of long range order. A major driving force for the ordering process in this alloy is the partial relief of the strain energy associated with the large atomic mismatch of the component atoms i.e. the nominal size factor is 31% for the Pd Y alloy (Hughes et al 1980). Furthermore Loebich

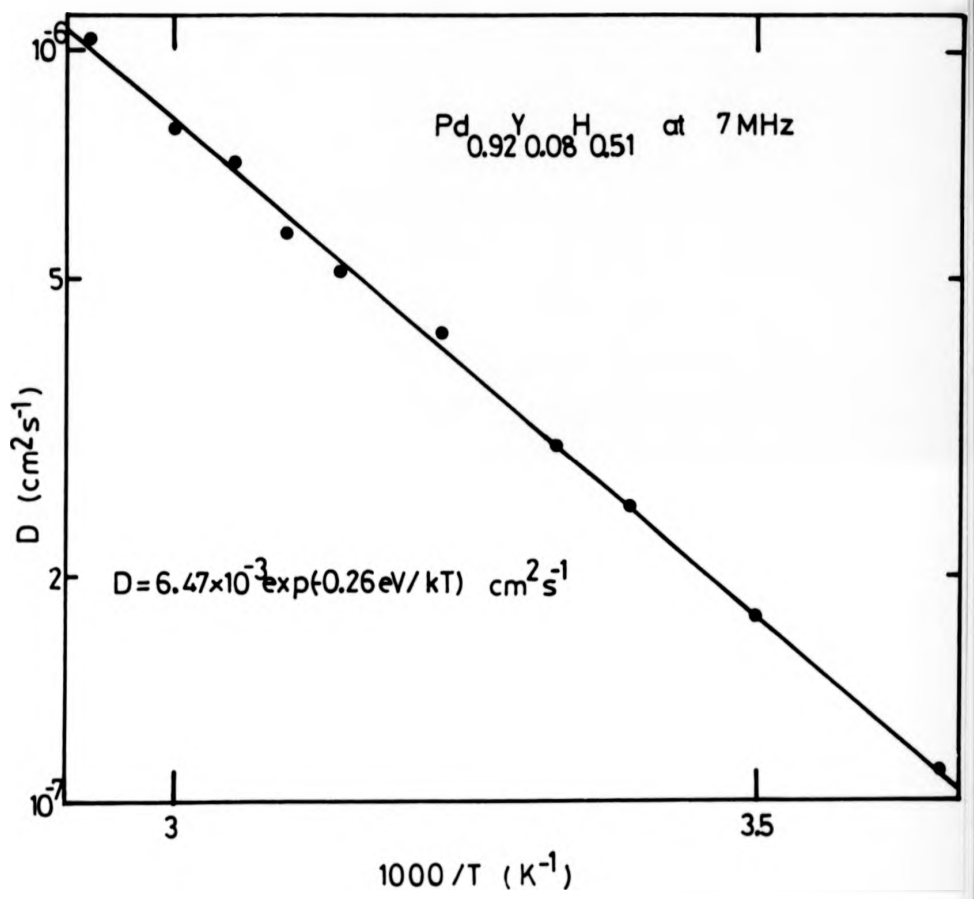

Fig. 6.2: Diffusion coefficient as a function of the reciprocal temperature. The solid line is the least squares fit to LnD versus 1/T.

and Raub (1973) who studied the phase diagram of PdY indicate that this alloy crystallises with the CuAu structure in the very stable Pd_3Y phase. This, when combined with the fact that the valency of yttrium is 3 as deduced from magnetic susceptibilty measurements (Harris and Norman 1968), suggests that the short-range ordered PdY sample can be thought as a Pd matrix with ordered Pd_3Y submicro-regions. This is confirmed by the observation that the linear variation of lattice spacing with composition extrapolates to the lattice spacing of the fully ordered Pd_3Y phase (Hirst et al 1976) i.e. a = 4.02 Å (Loebich and Raub 1973). Thus if one assumes that hydrogens avoid the ordered submicroregions (i.e. Pd_3Y), an Arrhenius relation for the proton diffusion characterised by an activation energy E_a = 0.228 eV (similar to that in pure palladium hydride) is expected for the ordered sample and an activated diffusion process with E_a > 0.228 eV is expected in the fully disordered alloy. Indeed this is observed experimentally. Hughes et al (1980), who deduced the activation energy for hydrogen diffusion from permeability and solubility measurements, report an increase in E_a from 0.226 eV to 0.315 eV as the sample undergoes the transition from ordered to disordered state which occurs at T $\sim$ 610 K. When the sample is quenched from T > 610 K the same high activation energy is obtained at low temperatures. This is to be contrasted to $Pd_{0.83}Ag_{0.17}$ which does not show SRO and has a single activation energy, $E_a \sim 0.28$ eV, for hydrogen diffusion. This may be understood since the nominal size factor is only 5% in palladium silver. Buchold et al (1976) show that the activation energy for hydrogen diffusion increases with silver content in PdAg. Assuming that the same effect occurs in the present alloy (as suggested by the result discussed above), we may deduce an approximate value of the fraction of yttrium and palladium which form the ordered Pd_3Y phase. If we assume a

linear increase in E_a with yttrium concentration (justified to some extent because of the low yttrium concentration) we find that 2.8% of the yttrium and thus 8.4% of the palladium form the Pd_3Y compound i.e. $[(Pd_{0.836}Y_{0.052}) + 2.8\%\ (Pd_3Y)]\ H_{0.51}$ which is equivalent to a $(Pd_{0.94}\ Y_{0.06})\ H_{0.58}$ sample if we assume that hydrogen avoid the Pd_3Y regions. This result will be used in the following section.

6.2.b. Relaxation time results

The observed minimum for $(Pd_{0.92}\ Y_{0.08})H_{0.51}$ is shallower than the corresponding minimum for $PdH_{0.54}$. If we assumed that the shape of the minimum is governed entirely by T_{1d}, this would suggest that the activation energy for hydrogen diffusion is much smaller in $(Pd_{0.92}\ Y_{0.08})H_{0.51}$ than in $Pd\ H_{0.54}$. The results obtained from the analysis of the T_1 data assuming that $\frac{1}{T_1} = \frac{1}{T_{1d}} + \frac{1}{T_{1e}}$ are shown in fig. 6.3 which illustrates the fitting procedure and yields $\tau_D = 1.4 \times 10^{-10} \exp\left(\frac{0.092\ eV}{KT}\right)$ s using the value $T_{1e}T = 84$ s.K. as given by Davis et al (1976) or $\tau_D = 0.9 \times 10^{-10} \exp\left(\frac{0.104\ eV}{KT}\right)$ s and $T_{1e}T = 15$ s.K. when the latter is treated as a fitting parameter. The values of the activation energy is smaller by a factor ~ 2.6 than that deduced from direct diffusion coefficient measurements. Chang et al (1981) report on activation energy $E_a = 0.20$ eV in $LaNi_5$ as deduced from low temperature T_1 and $T_{1\rho}$ measurements (i.e. $\omega_o\tau_c >> 1$ and $\omega_1\tau_c >>$ respectively) compared to $E_a = 0.42$ eV deduced from direct diffusion coefficient measurements. They interpreted this discrepancy as due to an anomalous spectral density function. Analysis of their data using a frequency temperature superposition technique (Jones et al 1980) to fit an empirical spectral density function of the form $J(\omega,\tau_c) = A(\tau_c)\ B(\Omega)\ F(\omega\tau_c)$, allowed them to obtain good agreement with the latter value of E_a (i.e. $E_a = 0.41$ eV). However,

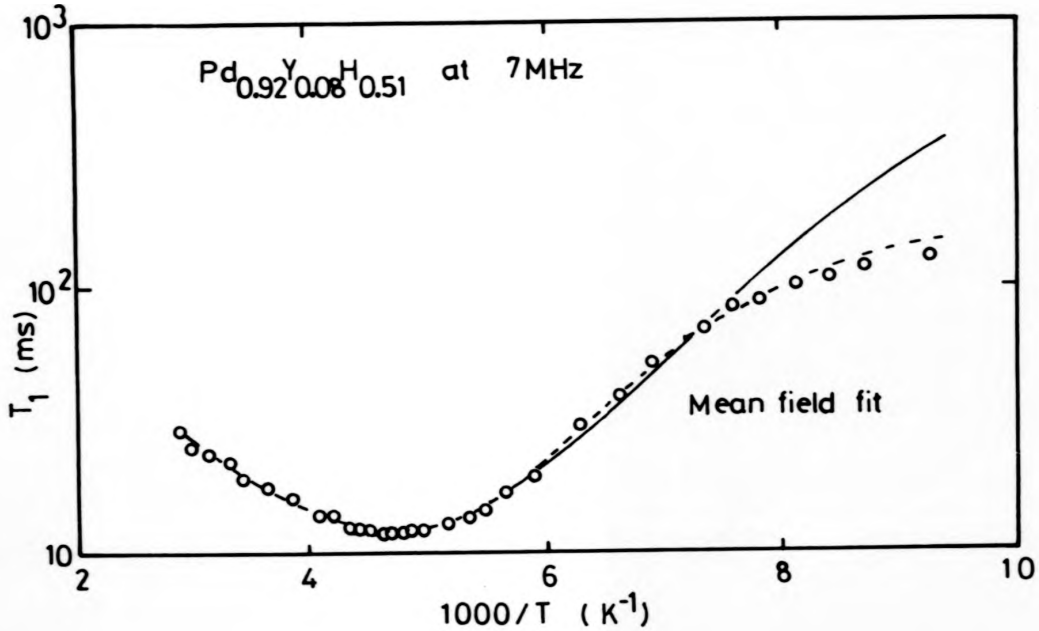

Fig. 6.3: Results of the fitting procedure. The full curve is obtained using $T_{1e}T$ = 84 s.k. while the broken line is obtained when $T_{1e}T$ is treated as a fitting parameter.

it is interesting to note that $LaNi_5$ is subject to decomposition when hydriding, and forms ferromagnetic Ni and La $(OH)_3$. Thus we suspect that the asymmetric T_1 and $T_{1\rho}$ minima result from the presence of magnetic impurities in their sample. Similarly, in the present measurements we think that the low activation energy deduced from the analysis of T_1 results from the extra contribution to T_1 due to the presence of paramagnetic impurities in the sample. Since susceptibility data (Harris and Norman 1968) on palladium-yttrium solid solutions indicate that Pd_3Y is non-magnetic, we suspect that the impurities have been introduced to the sample during the alloying process (i.e. it is very difficult to produce yttrium free of rare earth impurities). A detailed analysis of the impurity content of the sample is not available and it is, therefore impossible to estimate quantitatively the paramagnetic contribution, but we should be able to assess the T_{1d} contribution, using the values of activation energy and pre-exponential term derived from the direct diffusion coefficient measurements.

First let us investigate if the observed minimum can be associated with that due to dipole-dipole interactions. Assuming that this is the case we can deduce, for the temperature of $(T_1)_{min}$, a value of the diffusion coefficient and compare it to the value of D_a, extrapolated to this temperature, obtained from the direct diffusion coefficient measurements. Using the results of Barton and Sholl (1980) which predict, for an f.c.c. lattice, that T_1 goes through a minimum when $\omega_o\tau_D = 0.95$, we deduce $\tau_D = 2.16 \times 10^{-8}$ s at T = 215 K. The diffusion coefficient can be calculated from the expression $D = f_T \frac{\langle \ell \rangle^2}{6\tau_D}$ where f_T is the auto-correlation factor and $\langle \ell \rangle$ is the mean jump distance. Davis et al (1976) have shown

from T_1 coupled with diffusion coefficient measurements for palladium hydride, that the hydrogen atoms jump between nearest neighbour octahedral sites and we assume that the same applies to the palladium yttrium hydride system. Using the value of the lattice parameter a = 4.08 Å, reported by Wise et al (1975) for the concentration $(Pd_{0.94} Y_{0.06}) H_{0.58}$ as deduced in the previous section for the disordered regions, we obtain $\langle \ell \rangle$ = 2.88 Å, and using the value of f_T = 0.90 calculated from the expression given by Sankey and Fedders (1977) (see section 4.2.e: for a f.c.c. lattice A = 0.245 and B = 0.030), we are able to deduce D (215 K) = 5.8 x 10^{-9} cm^2 s^{-1}. This value is in good agreement with the value D = 5.5 x 10^{-9} cm^2 s^{-1} deduced from the measured diffusion coefficient for T = 215 K. We therefore conclude that the temperature of the observed minimum is at least partly due to proton dipole-dipole interactions. This is confirmed by the value of $(T_1)_{min}$ deduced from mean-field theory, which gives $(2\alpha T_{1d})^{-1}_{min}$ = 152 where $\alpha = \frac{\gamma^4 \hbar^2 I(I+1)c}{5b^6 \omega_o}$ with c = fraction of hydrogen sites occupied and b = lattice constant, yielding $(T_1)_{min}$ = 13.5 ms.

We now calculate the contribution T_{1d} to the observed T_1. The results of the calculation are shown in fig. 6.4 which indicates $\left(\frac{1}{T_{1d}} + \frac{1}{T_{1e}}\right)^{-1}$ (full line) and T_{1p} (broken line). The shape of T_{1p}, particularly around the main observed minimum, should not be regarded as anomalous since its evaluation relies entirely on the calculated value of T_{1d} and T_{1e} which if overestimated would produce this effect. In fact the calculated value of $(T_{1d})_{min}$ = 11.3 ms compared to the experimental value $(T_{1d})_{min}$ = 12.8 ms for $Pd\ H_{0.54}$ indicates that the theory overestimates the value of the minimum. Thus, neglecting this anomaly we can see that T_1 is nearly entirely dominated by T_{1p}.

In conclusion the activation energy deduced from the direct diffusion coefficient measurement is in good agreement with that

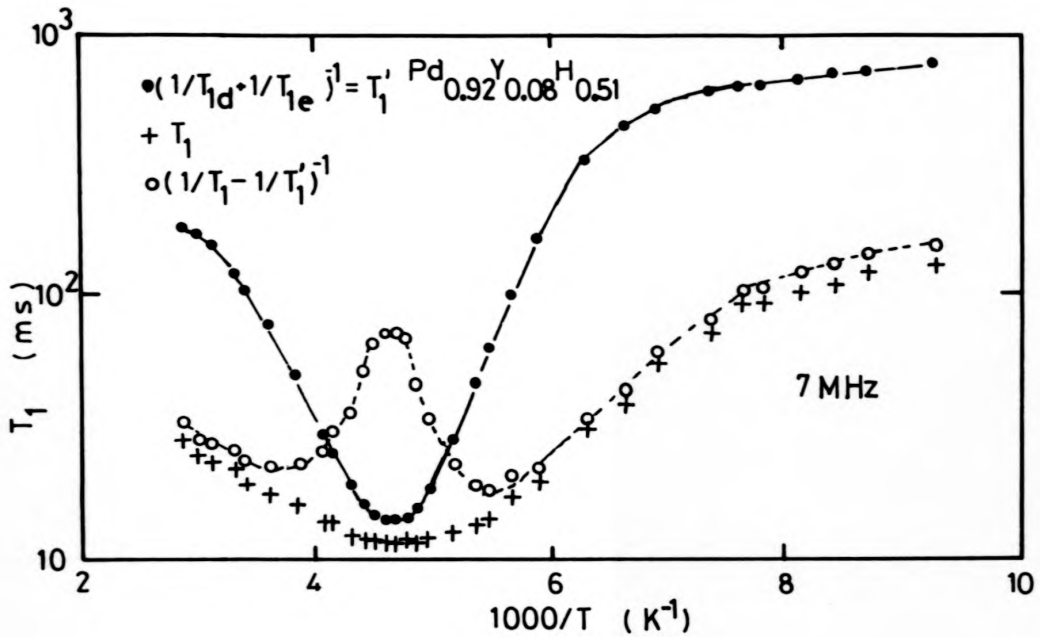

Fig. 6.4: Extra contribution to the observed T_1. T_{1d} and T_{1e} are calculated using the parameters described in the text.

deduced by Hughes et al (1980) and indicates that the sample is partially ordered. The anomalous behaviour of T_1 may be understood in terms of a paramagnetic contribution. This is confirmed by recent NMR measurements at 45 MHz performed on the same sample (Schone 1983) which indicate that the observed $(T_1)_{min} \simeq 12$ ms occurs at the same temperature T = 215 K as that measured at 7 MHz. Again we have an example which illustrates clearly the importance of paramagnetic effects on the observed relaxation times.

REFERENCES

Barton, W. A., C. A. Sholl: J. Phys. C, 13, 2579 (1980).

Brooks, J. W., M. H. Loretto, I. R. Harris: Met. Sci., 10, 397 (1976).

Buchold, H., G. Sicking, E. Wicke: J. Less-Common Met., 49, 25 (1976).

Chang, H., I. J. Lowe, R. J. Karlicek: in Nuclear and Electron Resonance Spectroscopies Applied to Materials Science, ed. by E. N. Kaufman and G. K. Shenoy,(North Holland, New York, 1981).

Cornell, D. A., E. F. W. Seymour: J. Less-Common Met., 39, 43 (1975).

Davis, P. P., E. F. W. Seymour, D. Zamir, W. David Williams, R. M. Cotts: J. Less-Common Met., 49, 159 (1976).

Harris, I. R., M. Norman: J. Less-Common Met., 15, 285 (1968).

Hughes, D. T., I. R. Harris: J. Less-Common Met., 61, P9 (1978).

Hughes, D. T., J. Evans, I. R. Harris: J. Less-Common Met., 74, 255 (1980).

Jones, T. C., T. K. Halstead, K. H. J. Buschow: J. Less-Common Met., 73, 209 (1980).

Loebich, D., E. Raub: J. Less-Common Met., 30, 47 (1973).

Schone, H. (Private communication 1983).

Völkl, J., G. Alefeld: Hydrogen in Metals I, ed. by G. Alefeld and J. Völkl (Springer Verlag, Berlin 1978).

Wise, M. L. H., J. P. G. Farr, I. R. Harris: J. Less-Common Met., 41, 115 (1975).

REFERENCES

Barton, W. A., C. A. Sholl: J. Phys. C, 13, 2579 (1980).

Brooks, J. W., M. H. Loretto, I. R. Harris: Met. Sci., 10, 397 (1976).

Buchold, H., G. Sicking, E. Wicke: J. Less-Common Met., 49, 25 (1976).

Chang, H., I. J. Lowe, R. J. Karlicek: in Nuclear and Electron Resonance Spectroscopies Applied to Materials Science, ed. by E. N. Kaufman and G. K. Shenoy,(North Holland, New York, 1981).

Cornell, D. A., E. F. W. Seymour: J. Less-Common Met., 39, 43 (1975).

Davis, P. P., E. F. W. Seymour, D. Zamir, W. David Williams, R. M. Cotts: J. Less-Common Met., 49, 159 (1976).

Harris, I. R., M. Norman: J. Less-Common Met., 15, 285 (1968).

Hughes, D. T., I. R. Harris: J. Less-Common Met., 61,P9 (1978).

Hughes, D. T., J. Evans, I. R. Harris: J. Less-Common Met., 74, 255 (1980).

Jones, T. C., T. K. Halstead, K. H. J. Buschow: J. Less-Common Met., 73, 209 (1980).

Loebich, D., E. Raub: J. Less-Common Met., 30, 47 (1973).

Schone, H. (Private communication 1983).

Völkl, J., G. Alefeld: Hydrogen in Metals I, ed. by G. Alefeld and J. Völkl (Springer Verlag, Berlin 1978).

Wise, M. L. H., J. P. G. Farr, I. R. Harris: J. Less-Common Met., 41, 115 (1975).

CHAPTER VII: CONCLUSIONS

The principal aim of this work has been to show the important effects that small amounts of paramagnetic impurities can have on the observed relaxation times and relaxation time measurements for a series of samples doped with controlled amounts of impurities have been reported. The coupling between the hydrogen nuclear spin and the local moment of the impurity is mainly dipolar and contributes an additional relaxation mechanism. The different specific regimes which arise from such an interaction have been most comprehensively documented in the investigation of yttrium-gadolinium dihydrides. This study has clearly shown that if the temperature dependent impurity induced contribution to the observed relaxation times is not taken into account, the parameters derived from the analysis of the observed relaxation times may lead to erroneous conclusions. It has been seen that when the paramagnetic contribution to the observed T_1 relaxation time is taken into account, the observed marked asymmetry of T_1 is completely removed. Therefore we conclude that a large part of the published data which shows either an asymmetric T_1 or the presence of a subsidiary minimum may require reinterpretation taking impurity effects into account.

Although this effect may be considered as a nuisance it has been shown for the case of titanium manganese dihydride that the study of the paramagentic relaxation times may open the door to new means of investigating the problems associated with trapping and anti-trapping. Furthermore the range of temperatures accessible in these measurements is about 2 orders of magnitude greater than that typically available in electron spin resonance studies.

Appendix 1

Calculation of the contact hyperfine constant A

The contact Hamiltonian is given by

$$H = \frac{16\pi}{3} \beta\gamma_n h \vec{I}.\vec{S}\, \delta(r)$$

where β is the Bohr magneton, γ_n is the nuclear gyromagnetic ratio, I is the nuclear spin and S is the electron spin. Since we are interested in the contact term at a hydrogen site (tetrahedral) arising from the overlap of the 4f electronic wavefunction of the Gd ion and the hydrogen nuclear spin, we have

$$E_i = \langle\psi|H|\psi\rangle = \sum_r \langle\psi|r\rangle\langle r|H|\psi\rangle$$

where $|\psi\rangle$ is the ket of the 4f wavefunction and $\langle\psi|r\rangle$ is the complex conjugate radial distribution of the 4f wavefunction. The only non vanishing element of this equation is given for, $r = r_H$, the distance between a Gd ion and a tetrahedral hydrogen, leading to

$$E_i = \frac{16\pi}{3} \beta\gamma h\, |\psi(r_H)|^2 I.S$$

where $A = \frac{16\pi}{3} \beta\gamma h|\psi(r_H)|^2$. is the contact constant.

Using the values of the radial 4f distribution function tabulated by Harman and Skillman and taking $r_H = 2.25\ 10^{-8}$ cm we obtain $|\psi(r_H)|^2 = 2.984 \times 10^{19}$ cm^{-3} giving $A = 124 \times 10^3$ rd s^{-1}. Such an interaction would produce a minimum in T_{1p} for (see section 2.2.c.1.)

$$\frac{1}{\tau_D^2} = \frac{1}{3} A^2 S(S+1)$$

which corresponds to $\tau_D \sim 2.2 \times 10^{-5}$ s (i.e. $S = \frac{7}{2}$). This value of τ_D would be obtained for a temperature much lower than that of the observed $(T_{1p})_{min}$, $T \cong 450$ K.

which corresponds to $\tau_D \sim 2.2 \times 10^{-5}$ s (i.e. $S = \frac{7}{2}$). This value of τ_D would be obtained for a temperature much lower than that of the observed $(T_{1p})_{min}$, $T \approx 450$ K.

Appendix 2

Spark source mass spectroscopic analysis for the yttrium metal used in the preparation of the series of $YH_{1.98}$ doped with Gd.

ANALYSIS (ATOMIC PPM)

SPARK SOURCE MASS SPECTROMETRIC ANALYSIS - ID: Y-12381B

MAJOR ELEMENT: Y

LI	<.000	BE	<.002	B	.07	NA	<.1	MG	.10	AL	3	SI	3	P	<.03
S	<.1	CL	3	K	<.04	CA	.10	TI	.80	V	<.03	CR	.5	MN	<.04
FE	10	CO	<.05	NI	3	CU	5	ZN	<.06	GA	<.06	GE	<.08	AS	<.02
SE	<.1	BR	<.05	RB	<2000	SR	<.1	ZR	<.3	NB	<.8	MO	<.8	RU	<.6
RH	<.1	PD	<.3	AG	<.09	CD	<.08	IN	<.03	SN	<.1	SB	<.05	TE	<.06
I	<.04	CS	<.004	BA	<.08	HF	<.8	TA	<.6	W	20	RE	<.4	OS	<.2
IR	<.09	PT	<.3	AU	<.07	HG	<.08	TL	<.06	PB	20	BI	<.04	TH	<.5
														U	<.2

RARE EARTH IMPURITIES

SC	K1	Y		LA	3	CE	2	PR	4.0	ND	<.6	SM	<.4	EU	<.2
GD	2.1	TB	4.5	DY	<.6	HO	<.2	ER	<.5	TM	<.1	YB	<.3	LU	<.3

REMARKS: Semiquantitative survey

Vacuum Fusion Results - Wt. ppm in ( )

O	834 (150)	N	25 (4)	H	704 (8)

Combustion			Absorption			
C	141 (11)	F	<14 (<3)	Fe	8 (4.7)

Appendix 3

Computer Programs

All the fitting programs used in this investigation were based on a set of subroutines most comprehensively described by Bevington (see Chapter III for reference) and his description should be consulted for a full definition of all the parameters which appear in the programmes. The variable names used are identical.

The main program first sets the parameter FLAMDA = 0.001 at the beginning of the fit and requires a starting value of the fitting parameters. These values should be as close as possible to the actual fitted parameters. The experimental values are read from a file on stream 3 and stored in the arrays Y(I) and X(I), respectively. The experimental values were either, T_1 and T, T_2 and T, $T_{1\rho}$ and T or M_z and τ depending on whether the results or for the last set of data the experimental T_1 and T_2 measurements were to be fitted. The main program is important in that it determines when the iterative procedure should be stopped. This is illustrated in statement 999 of the program listed. The DO loop is set to performed 50 iterations. In this loop the subroutine CURFIT is called. CURFIT is a program to make a least-squares fit to a function which need not be linear in its parameters. This subprogram returns the parameter CHISQR (least-square error) which is compared to a tolerance set in the loop. If the tolerance is met the iterations are stopped and the fitted parameters together with their errors (SIGMAA(I)) are listed on both stream 2 and 6. Stream 2 is connected to the VDU while stream 6 is connected to the line printer. It should be noted that the number of iterations required to meet the set tolerance is very much dependent on the choice of the

starting parameters. However, this number never exceeded 20 iterations, and if the fitted parameters are listed only after 50 iterations, the fitting procedure should be started again with a better choice of starting parameters.

The subroutine GPLOT which is called at the end of the program (very last statement before the STOP statement), requires a set of subroutines which are listed at the very end of the total program, and is used to plot the result of the fitting procedure on the VDU which is connected to a graphics board. The variables (Y(I), X(I)) are plotted in point mode (with a choice of 4 different symbols) and the fitted variables (YFIT(I), X(I)) are ploted in vector mode (full curve). An example of the program used to fit T_{1p} to Richard's expression (see Chapter II) is listed thereafter. In this program the function FUNCTN calculates the value of T_{1p} according to equation (2.51). The ratio of the fractional Bessel functions i.e. $I_{3/4}/I_{-3/4}$ is calculated, using a series expansion in the subprogram BESSEL.

```
C-----------------------------------------------------------------------
C  MAIN PROGRAM : .E.EP
C
C  PURPOSE
C     THIS  PROGRAM FIT TIP TO RICHARS ' EXPRESSION  .THE  FITTED
PARAMETERS
C     MUST FIRST BE ESTIMATED
C
C  SUBROUTINES AND FUNCTION SUBPROGRAMS REQUIRED
C    CHIFIT
C        EVALUATES THE PARAMETERS CORRESPONDING TO  BEST FIT
C
C-----------------------------------------------------------------------
      DIMENSION X(1000),SIGMAY(100),DELTAA(10),SIGMAA(10)
     1 ,YFIT(1000),S1(100),S2(100),Y(1000),A(10),FL(78)
      DIMENSION FR(78)
      DATA DASH,SPACE /'-',' '/
      WRITE(6,804)
      WRITE(2,804)
804   FORMAT(1H1,' RICHARDS FITTING TO TIPARA DATA VERSUS TEMPERATURE '
     1 /' DATA ARE ENTERED AS T1 T WITH FORMAT:F7.2,1X,F6.1 '/
     1 ' FITTING PROCEDURE: MINIMUM OF PARABOLLA (CHIFIT)'//)
      FLAMDA=0.001
      WRITE(2,250)
250   FORMAT(' MODE -DETERMINES METHOD OF WEIGHTING LEAST-SQUARES FIT'/
     1 8X,'+1 WEIGHT(I)=1./Y(I) (WEIGHT THE HIGH TEMP SIDE OF TIMIN)'/
     1 8X,'0  WEIGHT(I)=1.0     (NO WEIGHTING)'/
     1 8X,'-1 WIGHT(I)=1/Y(I)   (WEIGHT THE VALUES OF T1 AT THE MIN)'/)
      READ(1,8)MODE
      MODE=0
      WRITE(6,250)
      WRITE(6,251) MODE
251   FORMAT(/' METHOD OF WEIGHTING CHOOSEN :',I2//)
      WRITE(2,05)
05    FORMAT(' NUMBER OF POINTS ;FREE - ')
      READ(1,8)NPTS
      WRITE(2,800)
800   FORMAT(' FREQUENCY IN (MHZ) ; FREE - ')
      READ(1,8) WO
      DO 235 I=1,78
235   FR(I)=SPACE
      WRITE(2,236)
236   FORMAT(' COMMENTS :? ')
      READ(1,237)FR
237   FORMAT(78A1)
      WRITE(6,238)FR,WO
238   FORMAT(' COMMENTS: ',78A1/' FREQUENCY: ',F4.1,' MHZ')
      WRITE(2,700)
700   FORMAT(' NUMBERS OF PARAMETERS MUST BE 3 OR 4 ;(I1)- ')
      READ(1,701) NTERMS
701   FORMAT(I1)
      WRITE(2,500)
500   FORMAT(//' NOW GIVE VALUES OF STARTING PARAMETERS AS '
```

```
     1 'REQUIRED'/)
       WRITE(2,501)
501    FORMAT(' VALUE OF A(1) TAUI (SK):FREE - ')
       READ(1,*) TIMIN
       WRITE(2,503)
503    FORMAT(' VALUE OF A(2) TAUD0 (S):FREE- ')
       READ(1,*)EA1
       WRITE(2,505)
505    FORMAT(' VALUE OF THE AUTO CORRELA FACTOR :FREE - ')
       READ(1,*)TAUC01
       IF (NTERMS.EQ.3) GO TO 702
       WRITE(2,507)
507    FORMAT(' VALUE OF THE ACTIVATION ENERGY (EV):FREE ')
       READ(1,*)SK1
       A(4)=SK1
       GO TO 703
702    WRITE(2,509)
       WRITE(6,509)
509    FORMAT(/' HERE NUMBERS OF FLOATING PARAMETERS =3 '
     1  /'AND THE VALUE OF THE ACTIVATION ENERGY IS FIXED '/)
       A(4)=2.6E-08
703    DO 803 I=1,NPTS
       READ(3,802) Y(I),X(I)
802    FORMAT(F7.2,1X,F6.1)
       Y(I)=1000.0/Y(I)
803    CONTINUE
       NFREE=NPTS-NTERMS
       A(1)=TIMIN
       A(2)=EA1
       W0=W0*6.283E+06
       A(3)=TAUC01
       ARG=1.76E-08*W0
       DO 104 I=1,NTERMS
104    DELTAA(I)=A(I)/10.0
       WRITE(2,212)
212    FORMAT(' VALUE OF THE CONCENTRATION OF INPURITIES:(PPM)-FREE ')
       READ(1,*)CON
       DO 903 I=1,78
903    FL(I)=DASH
       WRITE(6,14)FL,FL
14     FORMAT(//78A1//21X,' CHIQR ',5X,' A(1) ',2X,' A(2) ',
     1 3X,' A(3)',3X,' A(4)'/78A1)
       CHISQR=0
       DO 11 L=1,50
       R=CHISQR
       CALL CURFIT(X,Y,SIGMAY,NPTS,NTERMS,MODE,A,DELTAA,
     1 SIGMAA,FLAMDA,YFIT,CHISQR,CON,ARG,W0)
       XTOL=1.E-15
       TOL=ABS((R-CHISQR)/CHISQR)
       IF(TOL.LE.XTOL) GO TO 12
       RL=CHISQR
13     M=L
       WRITE(2,16)M,CHISQR,A(1),A(2),A(3),A(4)
       WRITE(6,16)M,CHISQR,A(1),A(2),A(3),A(4)
16     FORMAT(/' AT ITERATION ',I2,2X,E9.3,3X,E9.3,3X,E9.3,3X,
```

```
     1 E9.3,2X,E9.3)
 11    CONTINUE
 12    IF (NTERMS .EQ. 3) SIGMAA(4)=0.0
       SIGMAA(3)=SQRT(SIGMAA(3))
       SIGMAA(1)=SQRT(SIGMAA(1))
       SIGMAA(2)=SQRT(SIGMAA(2))
       SIGMAA(4)=SQRT(SIGMAA(4))
       IF(NTERMS.EQ.3) SIGMAA(4)=0.0
       WRITE(6,440)
       WRITE(6,805)
       WRITE(2,805)
805    FORMAT(//20X,' PARAMETERS CORRESPONDING TO BEST FIT  '///)
       WRITE(2,806)A(1),SIGMAA(1),A(2),SIGMAA(2),A(3),SIGMAA(3),
     1 A(4),SIGMAA(4)
       WRITE(6,806)A(1),SIGMAA(1),A(2),SIGMAA(2),A(3),SIGMAA(3),
     1 A(4),SIGMAA(4)
806    FORMAT(///10X,' KORRINGA TAUI   = ',E9.3,' S-K ',5X,
     1 ' ERROR = ',E9.3/10X,' PREXPONETIAL (TAUDO) = ',E9.3,'SEC  ',
     1 5X,' ERROR = ',E9.3/10X,' CORR FACTOR ',E9.3,' S',
     1 5X,' ERROR = ',E9.3/10X,' ACTIVATION ENERGY      = ',E9.3,' EV ',
     1 5X,' ERROR = ',E9.3/)
440    FORMAT(///10X ' ACTUAL AND FITTED VALUES FOR BEST FIT '//)
       DO 951 I=1,NPTS
       Y(I)=1000./Y(I)
       YFIT(I)=1000./YFIT(I)
       WRITE(2,952)I,Y(I),I,X(I),I,YFIT(I)
       WRITE(6,952)I,Y(I),I,X(I),I,YFIT(I)
952    FORMAT(8X,' Y(',I3,')=',F7.2,3X,' X(',I3,')=',F6.1,3X,
     1 ' YFIT(',I3,')=',F7.2)
951    CONTINUE
       CALL GPLOT(NPTS,X,Y,YFIT)
       STOP
       END


C-----------------------------------------------------------------
C
C  SUBROUTINE CURFIT
C
C
C  PURPOSE
C    MAKE A LEAST-SQUARES FIT TO A NON LINEAR FUNCTION
C    WITH A LINEARISATION OF THE FITTING FUNCTION
C  USAGE
C    CALL CURFIT(,X,Y,SIGMAY,NPTS,NTERMS,MODE,A,DELTAA,SIGMAA,
C                FLAMDA,YFIT,CHISQ,R)
C
C  DESCRIPTION OF PARAMETERS
C    X     -ARRAY OF DATA POINTS FOR INDEPENDENT VARIABLE
C    Y     -ARRAY OF DATA POINTS FOR DEPENDENT VARIABLE
C    SIGMAY-ARRAY OF STANDARD DEVIATIONS FOR Y DATA POINTS
C    NPTS  -NUMBER OF PAIRS OF DATA POINTS
C    NTERMS-NUMBER OF PARAMETERS
C    MODE  -DETERMINES METHOD OF WEIGHTING LEAST-SQUARES FIT
C          +1 (INSTRUMENTAL) WEIGHT(I)=1./SIGMAY(I)**2
```

```
C           0 (NO WEIGHTING) WEIGHT(I)=1.
C          -1 (STATISTICAL)  WEIGHT(I)=1./Y(I)
C    A     -ARRAY OF PARAMETERS
C    DELTAA-ARRAY OF INCREMENTS FOR PARAMETERS A
C    SIGMAA-ARRAY OF STANDARD DEVIATIONS FOR PARAMETERS A
C    FLAMDA-PROPORTION OF GRADIENT SEARCH INCLUDED
C    YFIT  -ARRAY OF CALCULATED VALUES OF Y
C    CHISQ-REDUCED CHI SQUARE FOR FIT
C    R     -DIFFERENCE IN TWO SUCCESSIVE CHISQR TO BE COMPARED
C           TO THE TOLERANCE SET IN THE MAIN PROGRAM
C
C  SUBROUTINES AND FUNCTION SUBPROGRAMS REQUIRED
C    FUNCTN(X,I,A)
C       EVALUATES THE FITTING FUNCTION FOR ITH TERM
C    FCHISQ(Y,SIGMAY,NPTS,NFREE,MODE,YFIT)
C       EVALUATES REDUCED CHI SQUARE FOR FIT TO DATA
C    FDERIV(X,I,A,DELTAA,NTERMS,DERIV)
C       EVALUATES THE DERIVATIVES OF THE FITTING FUNCTION
C       FOR THE ITH TERM WITH RESPECT TO EACH PARAMETER
C    MATINV(ARRAY,NTERMS,DET)
C       INVERTS A SYMETRIC TWO DIMENSIONAL MATRIX OF DEGREE NTERMS
C       AND CALCULATES ITS DETERMINANT
C
C  COMMENTS
C    DIMENSION STATEMENT VALID FOR NTERMS UP TO 10
C    SET FLAMDA=0.001 AT BEGINING OF SEARCH
C    FOR NON ANALYTICAL EXPRESIONS OF THE DERIVATIVES WITH RESPECT
C      TO A USE SUBROUTINE FDER(X,I,A,DELTAA,NTERMS,DERIV) INSTEAD
C      OF FDERIV :
C   IMPORTANT: THE NUMBER OF PAIRS OF DATA MUST BE GREATER THAN THE
C              NUMBER OF PARAMETERS
C
C-----------------------------------------------------------------------

      SUBROUTINE CURFIT(X,Y,SIGMAY,NPTS,NTERMS,MODE,A,DELTAA,
     1 SIGMAA,FLAMDA,YFIT,CHISQR,CON,ARG,NO)
      DOUBLE PRECISION ARRAY,ALPHA,BETA
      DIMENSION Y(100),X(100),SIGMAY(100),A(10),DELTAA(10),SIGMAA(10),
     1 YFIT(100)
      DIMENSION WEIGHT(100),ALPHA(10,10),BETA(10),DERIV(10),
     1 ARRAY(10,10),B(10)
      NFREE=NPTS-NTERMS
      IF(NFREE)13,13,20
13    CHISQR=0.0
      GO TO 110
C
C     EVALUATE WEIGHTS
C
20    DO 30 I=1,NPTS
      IF(MODE)22,27,29
22    IF(Y(I))25,27,23
23    WEIGHT(I)=1./Y(I)
      GO TO 30
25    WEIGHT(I)=1./(-Y(I))
      GO TO 30
```

```
27     WEIGHT(I)=1.0
       GO TO 30
29     WEIGHT(I)=1./SIGMAY(I)**2
30     CONTINUE
C
C      EVALUATE ALPHA AND BETA MATRICES
C
       DO 34 J=1,NTERMS
       BETA(J)=0.
       DO 34 K=1,J
34     ALPHA(J,K)=0.
       DO 50 I=1,NPTS
       CALL FDER (X,I,A,DELTAA,NTERMS,DERIV,ARG,CON,WO)
       DO 46 J=1,NTERMS
      BETA(J)=BETA(J)+WEIGHT(I)*(Y(I)-FUNCTN(X,I,A,NTERMS,ARG,CON,WO))*
     1DERIV(J)
       DO 46 K=1,J
46     ALPHA(J,K)=ALPHA(J,K)+WEIGHT(I)*DERIV(J)*DERIV(K)
50     CONTINUE
       DO 53 J=1,NTERMS
       DO 53 K=1,J
53     ALPHA(K,J)=ALPHA(J,K)
C
C      EVALUATE CHI SQUARE AT STARTING POINT
C
       DO 62 I=1,NPTS
62     YFIT(I)=FUNCTN(X,I,A,NTERMS,ARG,CON,WO)
       CHISQ1=FCHISQ(Y,SIGMAY,NPTS,NFREE,MODE,YFIT,WO)
C
C      INVERT MODIFIED CURVATURE MATRIX TO FIND NEW PAREMETERS
C
71     DO 74 J=1,NTERMS
       DO 73 K=1,NTERMS
73     ARRAY(J,K)=ALPHA(J,K)/DSQRT(ALPHA(J,J)*ALPHA(K,K))
74     ARRAY(J,J)=1.+FLAMDA
       CALL MATINV(ARRAY,NTERMS,DET)
       DO 84 J=1,NTERMS
       B(J)=A(J)
       DO 84 K=1,NTERMS
84     B(J)=B(J)+BETA(K)*ARRAY(J,K)/DSQRT(ALPHA(J,J)*ALPHA(K,K))
C
C      IF CHI SQUARE INCREASED ,INCREASE FLAMDA AND TRY AGAIN
C
       DO 92 I=1,NPTS
92     YFIT(I)=FUNCTN(X,I,B,NTERMS,ARG,CON,WO)
       CHISQR=FCHISQ(Y,SIGMAY,NPTS,NFREE,MODE,YFIT,WO)
       R=CHISQ1-CHISQR
       IF(CHISQ1-CHISQR) 95,101,101
95     FLAMDA=10.*FLAMDA
       GO TO 71
C
C
C      EVALUATE PARAMETERS AND UNCERTAINTIES
C
C
```

```
101     DO 103 J=1,NTERMS
        A(J)=B(J)
        SIGMAA(J)=SNGL(ARRAY(J,J)/ALPHA(J,J))
103     SIGMAA(J)=ABS(SIGMAA(J))
        FLAMDA=FLAMDA/10.
110     RETURN
        END

C-------------------------------------------------------------
C
C  FUNCTION FCHISQ
C
C  PURPOSE
C    EVALUATE REDUCED CHI SQUARE FOR FIT TO DATA
C       FCHISQ=SUM((Y-YFIT)**2/SIGMAY**2)/NFREE
C
C  USAGE
C    RESULT=FCHISQ(Y,SIGMAY,NPTS,NFREE,MODE,YFIT)
C
C  DESCRIPTION OF PARAMETERS
C    Y      -ARRAY OF DATA POINTS
C    SIGMAY-ARRAY OF STANDARD DEVIATIONS FOR DATA POINTS
C    NPTS   -NUMBERS OF DATA POINTS
C    NFREE -NUMBER OF DEGREES OF FREEDOM
C    MODE   -DETERMINES METHOD OF WEIGHTING LEAST-SQUARES FIT
C           +1(INSTRUMENTAL) WEIGHT(I)=1./SIGMAY(I)**2
C            0(NO WEIGHTING) WEIGTH(I)=1.
C           -1(STATISTICAL)  WEIGHT(I)=1./Y(I)
C    YFIT   -ARRAY OF CALCULATED VALUES OF Y
C
C  SUBROUTINES AND FUNCTION SUBPROGRAMS REQUIRED
C    NONE
C
C-------------------------------------------------------------

        FUNCTION FCHISQ(Y,SIGMAY,NPTS,NFREE,MODE,YFIT,W0)
        DOUBLE PRECISION CHISQ,WEIGHT
        DIMENSION SIGMAY(100),Y(100),YFIT(100)
        CHISQ=0.
        IF(NFREE)13,13,20
13      FCHISQ=0.
        GO TO 40
C
C
C       ACCUMULATE CHI SQUARE
C
20      DO 30 I=1,NPTS
        IF (MODE) 22,27,29
22      IF (Y(I)) 25,27,23
23      WEIGHT=1./Y(I)
        GO TO 30
25      WEIGHT=1./(-Y(I))
        GO TO 30
27      WEIGHT=1.0
        GO TO 30
```

```
 29     WEIGHT=1./(SIGMAY(I)**2)
 30     CHISQ=CHISQ+WEIGHT*(Y(I)-YFIT(I))**2
 C
 C      DIVIDE BY NUMBER OF DEGREES OF FREEDOM
 C
        FREE=NFREE
        FCHISQ=CHISQ/FREE
 40     RETURN
        END
```

```
C-------------------------------------------------------------
C
C  SUBROUTINE MATINV
C
C  PURPOSE
C    INVERT A SYMMETRIC MATRIX AND CALCULATE ITS DETERMINANT
C
C  USAGE
C    CALL MATINV(ARRAY,NTERMS,DET)
C
C  DESCRIPTIONS OF PARAMETERS
C    ARRAY -INPUT MATRIX WHICH IS REPLACED BY ITS INVERSE
C    NTERMS-DEGREE OF MATRIX (ORDER OF DETERMINANT)
C    DET   -DETERMINANT OF INPUT MATRIX
C
C  SUBROUTINES AND FUNCTION SUBPROGRAMS REQUIRED
C    NONE
C
C  COMMENTS
C    DIMENSION STATEMENT VALID FOR NTERMS UP TO 10
C
C-------------------------------------------------------------
```

```
        SUBROUTINE MATINV(ARRAY,NTERMS,DET)
        DOUBLE PRECISION ARRAY,AMAX,SAVE
        DIMENSION ARRAY(10,10),IK(10),JK(10)
 10     DET=1.
 11     DO 100 K=1,NTERMS
 C
 C      FIND LARGEST ELEMENT ARRAY(I,J) IN REST OF MATRIX
 C
        AMAX=0.
 21     DO 30 I=K,NTERMS
        DO 30 J=K,NTERMS
 23     IF (DABS(AMAX)-DABS(ARRAY(I,J))) 24,24,30
 24     AMAX=ARRAY(I,J)
        IK(K)=I
        JK(K)=J
 30     CONTINUE
 C
 C      INTERCHANGE ROWS AND COLUMNS TO PUT AMAX IN ARRAY(K,K)
 C
 31     IF (AMAX) 41,32,41
```

```
32      DET=0.
        GO TO 140
41      I=IK(K)
        IF(I-K) 21,51,43
43      DO 50 J=1,NTERMS
        SAVE=ARRAY(K,J)
        ARRAY(K,J)=ARRAY(I,J)
50      ARRAY(I,J)=-SAVE
51      J=JK(K)
        IF(J-K) 21,61,53
53      DO 60 I=1,NTERMS
        SAVE=ARRAY(I,K)
        ARRAY(I,K)=ARRAY(I,J)
60      ARRAY(I,J)=-SAVE
C
C
C       ACCUMULATE ELEMENTS OF INVERSE MATRIX
C
61      DO 70 I=1,NTERMS
        IF(I-K) 63,70,63
63      ARRAY(I,K)=-ARRAY(I,K)/AMAX
70      CONTINUE
71      DO 80 I=1,NTERMS
        DO 80 J=1,NTERMS
        IF (I-K) 74,80,74
74      IF (J-K) 75,80,75
75      ARRAY(I,J)=ARRAY(I,J)+ARRAY(I,K)*ARRAY(K,J)
80      CONTINUE
81      DO 90 J=1,NTERMS
        IF(J-K) 83,90,83
83      ARRAY(K,J)=ARRAY(K,J)/AMAX
90      CONTINUE
        ARRAY(K,K)=1./AMAX
100     DET=DET*AMAX
C
C       RESTORE ORDERING OF MATRIX
C
101     DO 130 L=1,NTERMS
        K=NTERMS-L+1
        J=IK(K)
        IF (J-K) 111,111,105
105     DO 110 I=1,NTERMS
        SAVE=ARRAY(I,K)
        ARRAY(I,K)=-ARRAY(I,J)
110     ARRAY(I,J)=SAVE
111     I=JK(K)
        IF(I-K) 130,130,113
113     DO 120 J=1,NTERMS
        SAVE=ARRAY(K,J)
        ARRAY(K,J)=-ARRAY(I,J)
120     ARRAY(I,J)=SAVE
130     CONTINUE
140     RETURN
        END
C-------------------------------------------------------------
```

```
C   SUBROUTINE FDER
C
C    NTERMS-NUMBER OF PARAMETERS
C    DERIV -DERIVATIVES OF FUNCTION
C
C  SUBROUTINES AND FUNCTION SUBPROGRAMS REQUIRED
C    I,I,A)
C      EVALUATES THE FITTING FUNCTION FOR THE ITH TERM
C
C-----------------------------------------------------------------

       SUBROUTINE FDER(X,I,A,DELTAA,NTERMS,DERIV,ARG,CON,WO)
       DIMENSION X(100),A(4),DELTAA(4),DERIV(4)
       DO 18 J=1,NTERMS
       AJ=A(J)
       DELTA=DELTAA(J)
       A(J)=AJ+DELTA
       YFIT=FUNCTN(X,I,A,NTERMS,ARG,CON,WO)
       A(J)=AJ-DELTA
       DERIV(J)=(YFIT-FUNCTN(X,I,A,NTERMS,ARG,CON,WO))/(2.0DELTA)
18     A(J)=AJ
       RETURN
       END

C-----------------------------------------------------------------
   FUNCTION FUNCT

   USAGE
      CALCULATES TIP USING RICHARD'S EQUATION

   PARAMETERS
      X: TEMPERATURE
      A: FITTING PARAMETERS
      NTERMS: NUMBER OF FITTING PARAMETERS
      CON: CONCENTRATION OF IMPURITIES IN PPM
      WO: OPERATING FREQUENCY

   SUBPROGRAM REQUIRED
      FUNCTION BESSEL: CALCULATE THE RATIO OF FRACTIONAL
                       ORDER (I3/4/I-3/4)
C-----------------------------------------------------------------
      FUNCTION FUNCTN(X,I,A,NTERMS,ARG,CON,WO)
      DIMENSION A(10),X(100)
      DOUBLE PRECISION COTH1,COTH2,TOT,BRI,XB1,XB2
      WE=WO*6.283
      T=X(I)
      TOT=T/1.04E-07
      TAUI=SNGL(1/TOT)
      TAUD=0.426E-12*EXP(11604.82*0.431/T)
      DS=A(1)
      IF(NTERMS.EQ.3)A(4)=2.6E-08
      DA=2.6E-08*.02/(.6*TAUD)
      AMN=0.43*3.2E-08
      IF(DA.GT.DS)GO TO 100
      XB1=DBLE(1.14*ARG/T)
```

```
      XB2=DBLE(0.143*ARG/T)
      COTH1=1.14*(DEXP(XB1)+DEXP(-1*XB1))/(DEXP(XB1)-DEXP(-1*XB1))
      COTH2=0.143*(DEXP(XB2)+DEXP(-1*XB2))/(DEXP(XB2)-DEXP(-1*XB2))
      BRI=COTH1-COTH2
      BSQ=SNGL(BRI*BRI)
      DERI=SNGL(COTH2*COTH2-COTH1*COTH1+1.2857)
      AMUP=6.50E-20*SQRT(BSQ+(DERI*0.637*ATAN(523.6E+03*TAUI)))
      B=0.01766*(AMUP**0.25)
      D=DS
      BREAL=B
      GO TO 101
100   D=DA
      BREAL=AMN
101   RTA=1/TAU1+1/TAUD
      RTA=1/RTA
      R1=RTA/(1+(WO*RTA)**2)
      R2=7*RTA/(3*(1+(WE*RTA)**2))
      C=R1+R2
      BETA=((C/D)**0.25)*3.534E-08
      DELTA=(0.707*BETA/BREAL)**2
      R=DELTA
      RATIO=BESSEL(R)
      FUNCTN=0.605*1.0E+19*D*BETA*RATIO*COM/100
      RETURN
      END


C-------------------------------------------------------------
      FUNCTION BESSEL

      USAGE
          CALCULATE RATIO OF FRACTIONAL ODER BESSEL FNCTS

      PARAMETERS
          Z: DELTA

C-------------------------------------------------------------
      FUNCTION BESSEL(Z)
      DIMENSION BESS1(400),BESS2(400)
      DOUBLE PRECISION TOL,TAL,BESS1,BESS2
      DOUBLE PRECISION SUM1,SUM2
9     SUM1=1.0
      SUM2=1.0
      FAC=1.0
      B1=1.0
      B2=1.0
      TOL1=1.0E-08
      Z=Z/2
      PRE1=Z**(0.75)/0.91906
      PRE2=Z**(-0.75)/3.6256
      DO 3 M=1,400
      B1=B1*(M+0.75)
      B2=B2*(M-0.75)
      FAC=FAC*M
      L=2*M
```

```
      POWER=Z**L
      SUM1=SUM1+(POWER/(B1*FAC))
      SUM2=SUM2+(POWER/(B2*FAC))
      BESS1(M)=PRE1*SUM1
      BESS2(M)=PRE2*SUM2
      IF(M.EQ.1) GO TO 3
      M=M-1
      TOL=DABS(BESS1(M)-BESS1(N))
      TAL=DABS(BESS2(M)-BESS2(N))
      IF(TOL.LE.TOL1.AND.TAL.LE.TOL1) GO TO 10
3     CONTINUE
10    BESSEL=BESS1(M)/BESS2(M)
      RETURN
      END

C-------------------------------------------------------
    SUBROUTINE GPLOT

    USAGE
      SET OF SUBROUTINE USED TO PLOT GRAPHS ON VDU
C-------------------------------------------------------
      SUBROUTINE GPLOT(NPTS,X,Y,YFIT)
      DIMENSION IX(1000),IYFIT(1000),IY(1000),X(1000),Y(1000),YFIT(1000)
      DO 3 I=1,NPTS
      Y(I)=ALOG10(Y(I))
      X(I)=1000/X(I)
      YFIT(I)=ALOG10(YFIT(I))
      X(I+NPTS)=X(I)+0.01
      X(I+2*NPTS)=X(I)+0.02
      X(I+3*NPTS)=X(I)-0.01
      X(I+4*NPTS)=X(I)-0.02
      Y(I+NPTS)=Y(I)
      Y(I+2*NPTS)=Y(I)
      Y(I+3*NPTS)=Y(I)
      Y(I+4*NPTS)=Y(I)
      Y(I+5*NPTS)=Y(I)+0.01
      Y(I+6*NPTS)=Y(I)+0.02
      Y(I+7*NPTS)=Y(I)-0.01
      Y(I+8*NPTS)=Y(I)-0.02
      X(I+5*NPTS)=X(I)
      X(I+6*NPTS)=X(I)
      X(I+7*NPTS)=X(I)
      X(I+8*NPTS)=X(I)
3     CONTINUE
      N=9*NPTS
C Subroutine to plot (as points) N data points with values
C  X,Y with autoscaling and fully labelled axes. N<1001
      XMIN=1000000.0
      XMAX=-1000000.0
      YMIN=1000000.0
      YMAX=-1000000.0
      DO 1 I=1,N
      IF(X(I).GT.XMAX)XMAX=X(I)
      IF(X(I).LT.XMIN)XMIN=X(I)
      IF(Y(I).GT.YMAX)YMAX=Y(I)
```

```
      IF(Y(I).LT.YMIN)YMIN=Y(I)
1     CONTINUE
      DO 5 I=1,NPTS
      IF(YFIT(I).GT.YMAX)YMAX=YFIT(I)
      IF(YFIT(I).LT.YMIN)YMIN=YFIT(I)
5     CONTINUE
      CALL RANGE(XMIN,XMAX,STEPX)
      CALL RANGE(YMIN,YMAX,STEPY)
      CALL GRAFST(XMIN,XMAX,STEPX,YMIN,YMAX,STEPY)
      DO 2 I=1,N
      X1=101.0+(X(I)-XMIN)*900.0/(XMAX-XMIN)
      IX(I)=X1
      Y1=60.0+(Y(I)-YMIN)*650.0/(YMAX-YMIN)
2     IY(I)=Y1
      CALL POINT(IX,IY,N)
      DO 6 I=1,NPTS
      YF1=60.0+(YFIT(I)-YMIN)*650/(YMAX-YMIN)
      IYFIT(I)=YF1
6     CONTINUE
      CALL PLOT(IX,IYFIT,NPTS)
      RETURN
      END



      SUBROUTINE POINT(IX,IY,N)
C     SUBROUTINE TO PLOT N POINTS (POINT MODE),N X&Y COORDS IN FILE
C     N<1001; 0<IX<1024; 0<IY<780
C     TO CLEAR GRAPHIC DISPLAY PRESS FUNCT M
      DIMENSION IX(1000),IY(1000),IASCII(128),IBUFF(81)
      DO 100 I=1,128
100   IASCII(I)=(I-1)*16777216
C     N.B. IASCII = CHAR. +1
 1020 FORMAT(A1)
 1025 FORMAT(81A1)
C     CLEAR SCREEN
C     SET POINT MODE
      WRITE(2,1020)IASCII(27)
      IBUFF(1)=IASCII(29)
      K=1
      DO 1100 I=1,N
      IXH=0
      IXL=IX(I)
      IF (IXL.LT.32) GOTO 1060
 1056 IXL=IXL-32
      IXH=IXH+1
      IF (IXL.GE.32) GOTO 1056
 1060 IYH=0
      IYL=IY(I)
      IF (IYL.LT.32) GOTO 1070
 1066 IYL=IYL-32
      IYH=IYH+1
      IF (IYL.GE.32) GOTO 1066
 1070 IBUFF(K+1)=IASCII(33+IYH)
```